Analysing energy detector diversity receivers for spectrum sensing

An approximation based approach

Donagh Horgan
BE

NATIONAL UNIVERSITY OF IRELAND, CORK

School of Engineering

Department of Electrical and Electronic Engineering

Thesis submitted for the degree of
Doctor of Philosophy

16 January 2014

Supervisor: Dr. Colin C. Murphy
Head of Department/School: Prof. Nabeel A. Riza

Research supported by the Irish Research Council for Science, Education and Technology (IRCSET)

I, Donagh Horgan, certify that this thesis is my own work and I have not obtained a degree in this university or elsewhere on the basis of the work submitted in this thesis.

Donagh Horgan

Abstract

The analysis of energy detector systems is a well studied topic in the literature: numerous models have been derived describing the behaviour of single and multiple antenna architectures operating in a variety of radio environments. However, in many cases of interest, these models are not in a closed form and so their evaluation requires the use of numerical methods. In general, these are computationally expensive, which can cause difficulties in certain scenarios, such as in the optimisation of device parameters on low cost hardware. The problem becomes acute in situations where the signal to noise ratio is small and reliable detection is to be ensured or where the number of samples of the received signal is large. Furthermore, due to the analytic complexity of the models, further insight into the behaviour of various system parameters of interest is not readily apparent.

In this thesis, an approximation based approach is taken towards the analysis of such systems. By focusing on the situations where exact analyses become complicated, and making a small number of astute simplifications to the underlying mathematical models, it is possible to derive novel, accurate and compact descriptions of system behaviour. Approximations are derived for the analysis of energy detectors with single and multiple antennae operating on *additive white Gaussian noise* (AWGN) and independent and identically distributed Rayleigh, Nakagami-m and Rice channels; in the multiple antenna case, approximations are derived for systems with *maximal ratio combiner* (MRC), *equal gain combiner* (EGC) and *square law combiner* (SLC) diversity. In each case, error bounds are derived describing the maximum error resulting from the use of the approximations. In addition, it is demonstrated that the derived approximations require fewer computations of simple functions than any of the exact models available in the literature. Consequently, the regions of applicability of the approximations directly complement the regions of applicability of the available exact models. Further novel approximations for other system parameters of interest, such as sample complexity, minimum detectable signal to noise ratio and diversity gain, are also derived.

In the course of the analysis, a novel theorem describing the convergence of the chi square, noncentral chi square and gamma distributions towards the normal distribution is derived. The theorem describes a tight upper bound on the error resulting from the application of the central limit theorem to random variables of the aforementioned distributions and gives a much better description of the resulting error than existing Berry-Esseen type bounds. A second novel theorem, providing an upper bound on the maximum error resulting from the use of the central limit theorem to approximate the noncentral chi square distribution where the noncentrality parameter is a multiple of the number of degrees of freedom, is also derived.

Acknowledgements

The work in this thesis, the work that led to the work in this thesis and the work that didn't lead anywhere at all has occupied me for five years of my life. Five years is a long time. Enough for nine countries, four bedrooms and three (and counting) grey hairs; enough for all afternoon card games, pointless arguments and far too much tea; enough for rainy days, leaky shoes and wet socks; enough for four o'clock pints and afternoon starts; enough to make new friends and neglect old ones; enough to make up for it; enough for free time and none at all; enough for frustration and satisfaction; enough to write a thesis.

Things often don't work out quite the way you expect them to. Over the past few years, I've run into a few of what Flann O'Brien called insoluble pancakes, conundrums of inscrutable potentialities or, put more simply, snorters. Sometimes, problems can be quite difficult. Fortunately, I had an excellent support group: my supervisor, Colin, my fellow postgraduate students, Ralph, my friends outside of university (at home and abroad) and, of course, my family. Over the years, I've been reassured, consoled, hugged, teased and given a healthy dose of cynicism either in person, over the phone or by email. It made the worst days tolerable and the best unforgettable. Thanks for putting up with me. Unfortunately, there's only room for one name on the cover.

I've also had a lot of support from others in the last few years: the academic and administrative staff in my department, who made it a nice place to be; The Irish Research Council for Science, Education and Technology, who sponsored the work that led to this thesis; the Boole Centre for Research in Informatics, who let me use their compute cluster, and Brian Clayton, who didn't get mad when my code kept crashing it; the editors and reviewers from the various conferences and journals I've submitted papers to, who (mostly) criticised constructively; and Kevin McCarthy and Marco Chiani, who had the unenviable task of reading this thesis and examining me on it. Thanks for the suggestions (and also for finding what I hope was the last typo). I think it reads a lot better now.

Finally, I'd like to thank Monty, who never minded when I was in a grumpy mood and doesn't have the capacity to understand what an acknowledgement is. He's been curled in a ball on a rug by my feet the whole time I've been writing this.

"That's another thing we've learned from your Nation," said Mein Herr, *"map-making. But we've carried it much further than you. What do you consider the largest map that would be really useful?"*

"About six inches to the mile."

"Only six inches!" exclaimed Mein Herr. *"We very soon got to six yards to the mile. Then we tried a hundred yards to the mile. And then came the grandest idea of all! We actually made a map of the country, on the scale of a mile to the mile!"*

"Have you used it much?" I enquired.

"It has never been spread out, yet," said Mein Herr: *"the farmers objected: they said it would cover the whole country, and shut out the sunlight! So we now use the country itself, as its own map, and I assure you it does nearly as well."*

(An excerpt from *Sylvie and Bruno*, by Lewis Carroll)

Contents

Chapter 1

Introduction

1.1 The electromagnetic spectrum: a valuable natural resource

The electromagnetic spectrum is a valuable natural resource: without it, there could be no radio stations, no mobile phones, no wireless hotspots, no air traffic control, no GPS navigation and no emergency communications for police or rescue coordinators. In short, the world would be a very different and less convenient place to live in. It is fortunate, then, that there is an electromagnetic spectrum and that, to date, there has been enough of it to house all of these technologies and many more.

However, not all spectra are equal: signals transmitted at higher frequencies require more power than signals transmitted at lower frequencies to have the same broadcast range. A typical example of this is shown in Figure 1.1, where the range of a *digital television* (DTV) transmitter is contrasted with that of a Wi-Fi hotspot. The DTV transmitter broadcasts at a lower frequency than the Wi-Fi hotspot, which means that its signal has a larger physical range for a given transmit power. In this case, the choices of frequencies are appropriate as Wi-Fi users typically do not require a large transmission range. However, it is clear that the range of frequencies that can reach large geographic areas, within reasonable power constraints, is finite.

With the explosion of wireless technology in recent years, regulators have licensed more and more of this desirable range (a rough illustration is shown in Figure 1.2(a)), leaving an ever-decreasing allocation for new applications. In the United States, the *Federal Communications Commission* (FCC) and the *National Telecommunications and Information Administration* (NTIA) have reported that the majority of this range has been licensed [1–3]. In Europe, a similar survey by the *European Regulators Group* (ERG) found that four European Union member countries did not have the frequency resources available for additional 2G/3G mobile networks [4]. If unchecked, this spectrum shortage could have a severe negative impact on innovation, growth and competition.

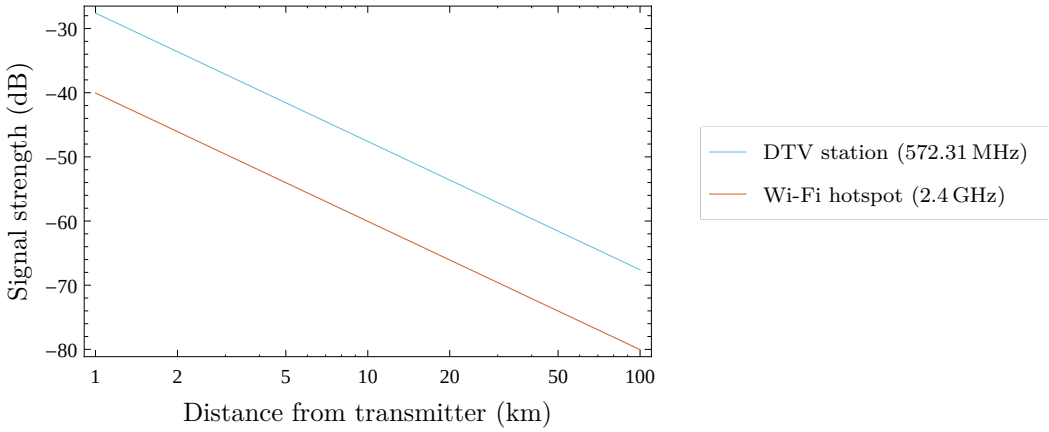

Figure 1.1: An illustration of the degradation in received signal power as a function of the receiver's distance from the transmitter. For simplicity, it is assumed that the signals are transmitted through free space.

Fortunately, the problem is not intractable: spectrum surveys have shown significant underusage of licensed bandwidth, depending on location and the time of day. In 2005, a forty six hour study conducted in Chicago, USA [5] found that the average spectrum occupancy — that is, the average amount of time a given channel is in use — varied from 0% to 70.9%, as can be seen in Figure 1.2(b). In 2007, a forty two hour survey [6] found that the average spectrum occupancy in Dublin, Ireland varied from 0.2% to 38.5%, as shown in Figure 1.2(c). A further study, conducted at a more rural location in Virginia in the United States in 2004 [7], found that the average spectrum occupancy there varied from 0% to 26.6%, as shown in Figure 1.2(d).

This widespread underuse has motivated the development of *dynamic spectrum access* (DSA) technologies which aim to identify spatially or temporally unused channels and exploit them for new applications, while preserving the *quality of service* (QoS) in existing wireless systems [8]. Consider the DTV transmission network shown in Figure 1.3(a). The range of the transmitter is shown in blue and the television indicates the physical location of a typical receiver. As everything lying beyond the range of the transmitter is spatially unoccupied spectrum, it can potentially be exploited for other uses by a DSA device, as shown in Figure 1.3(b).

However, there are many challenges to be met before spectrum can be liberated in this manner. If a DSA device is present within the range of the DTV transmitter, and determines that a transmission is present, it can identify the channel as being occupied and switch to a different, hopefully unoccupied, channel. However, mistakes can happen. For instance, if the DSA device were to determine that the channel was unoccupied, its subsequent transmissions might interfere with the reception of the DTV user, as shown in Figure 1.3(c). This is clearly an unacceptable outcome and poses a major technological and legal roadblock to the liberation of unused spectrum in general.

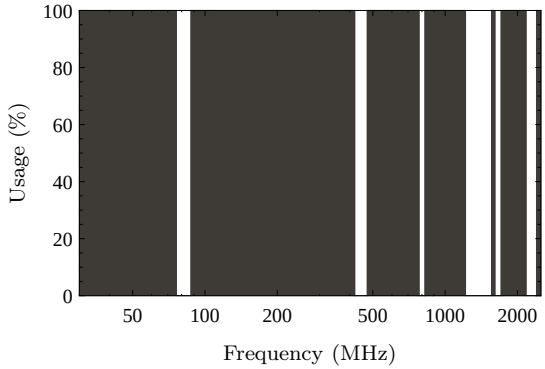

(a) Licensed bandwidth between 30 MHz and 2.5 GHz, according to the FCC [1]. For simplicity, only a few major services are illustrated: television, FM radio, aeronautical and maritime radio, mobile telephony, GPS and Wi-Fi.

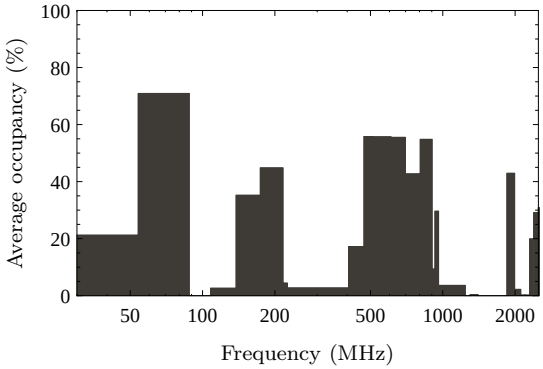

(b) Average spectrum occupancy in licensed bands between 30 MHz and 2.5 GHz, as measured in Chicago, USA in 2005 [5].

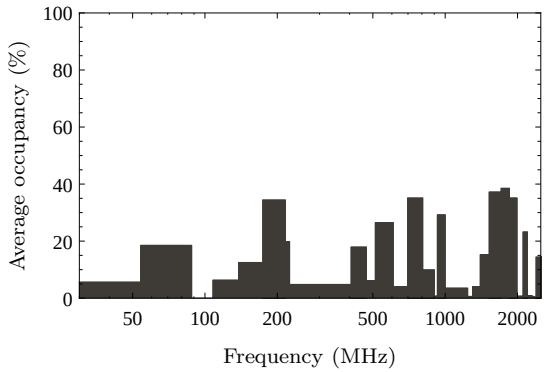

(c) Average spectrum occupancy in licensed bands between 30 MHz and 2.5 GHz, as measured in Dublin, Ireland in 2007 [6].

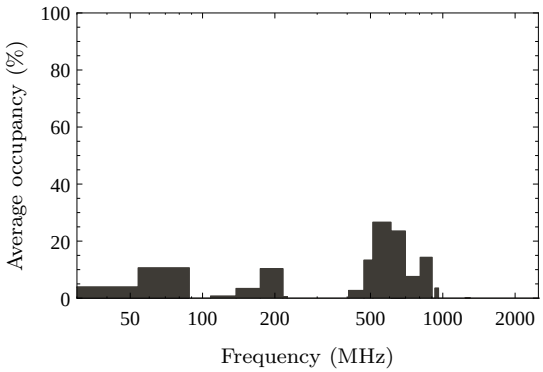

(d) Average spectrum occupancy in licensed bands between 30 MHz and 2.5 GHz, as measured in Virginia, USA in 2004 [7].

Figure 1.2: Various spectrum sensing and dynamic spectrum access scenarios.

Therefore, it must be ensured that the process by which unused channels are identified, known as spectrum sensing, is as reliable as possible.

Yet, there is a natural trade off between the reliability of the spectrum sensing process and the cost or power consumption of the device implementing it. Spectrum sensors operate by observing channels for a period of time, after which their observations are analysed for certain statistical properties from which the presence or absence of an existing user can be inferred. Ideally, spectrum sensors should always correctly identify whether a channel is occupied. However, this is usually quite difficult to guarantee due to time varying noise interference, which can obscure the presence of weak signals, and environmental factors such as ionospheric scattering and shadowing, which can attenuate the received signal power. Generally, if reliability is to be ensured in such cases, then either the channel must be observed for a long period of time, a large

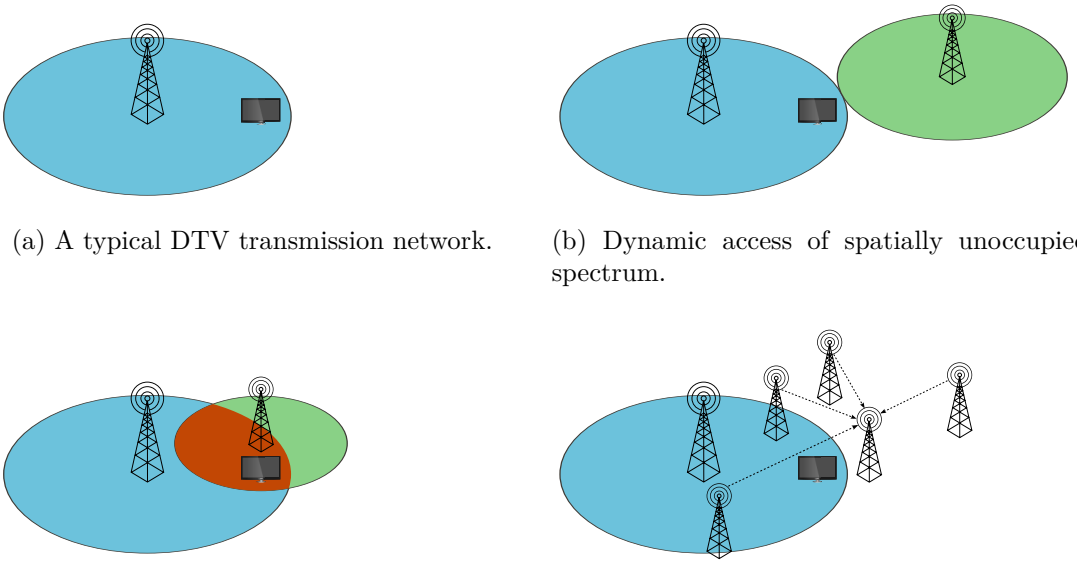

(a) A typical DTV transmission network.

(b) Dynamic access of spatially unoccupied spectrum.

(c) Interference with licensed transmissions.

(d) Cooperative spectrum sensing.

Figure 1.3: Spectrum licensing and occupancy measurements from various locations.

number of computations must be carried out, or both. Consequently, constraints on device cost, power consumption and sensing time directly affect the reliability of the sensing process.

The work in this thesis concerns a particular sensing technique, known as *energy detection*, which is typically not computationally intensive [9] but is also less reliable [10] than other sensing techniques. However, it has been shown that, if the energy detector is equipped with multiple antennae, then its reliability can be improved significantly using various signal processing techniques [11]. The multiple antenna energy detection paradigm also lends itself well to cooperative spectrum sensing, where neighbouring DSA devices share sensing information to ensure a lower overall probability of interference, as shown in Figure 1.3(d). Conveniently, this approach lowers the cost of the individual sensors involved as each does not need to perform as well as a single sensor would to achieve the same degree of reliability.

However, the mathematical models describing the behaviour of single and multiple antenna energy detector devices can become complicated in many situations, especially in everyday scenarios such as the sensing of channels in urban or rural environments. As a result, further insights into their behaviour are not readily apparent and complicated numerical computations are necessary to evaluate their reliability in even the simplest of circumstances. In later chapters, this problem is addressed by replacing these complicated behavioural descriptions with simpler ones, enabling new insights into the behaviour of energy detector systems and the fast and accurate computation of reliability measures.

1.2 Thesis outline

The remainder of this document is organised as follows:

- **Chapter 2** gives a broad overview of the spectrum sensing process, radio channel models, various spectrum sensing and multiple antenna techniques.
- **Chapter 3** addresses some issues specific to energy detection, such as signal quantisation and parameter uncertainty, summarises related work and discusses the advantages and disadvantages of the mathematical models available in the literature.
- **Chapter 4** discusses existing approximations for the analysis of energy detectors operating on channels with constant signal power (e.g. AWGN channels) and proposes novel approximations for the analysis of energy detectors with multiple antennae operating in such environments. A novel bound on the convergence of the chi square and noncentral chi square distributions to the normal distribution is also derived.
- **Chapter 5** develops novel closed form approximations for the analysis of energy detectors operating on indoor and outdoor mobile channels and ionospheric links (e.g. Nakagami-m and Rayleigh channels). The bound on the convergence of the chi square distribution to the normal distribution, developed in Chapter 4, is extended to the case of the convergence of the gamma distribution to the normal distribution.
- **Chapter 6** develops novel approximations for the analysis of energy detectors operating in urban and suburban radio environments (e.g. Rice and Rayleigh channels). A novel bound on the convergence of the noncentral chi square distribution to the normal distribution, where the noncentrality parameter is a multiple of the number of degrees of freedom, is also provided.
- **Chapter 7** concludes the thesis, summarising the contributions made and suggesting future research directions.
- **Appendix A** contains proofs of the theorems and lemmas stated in Chapters 4, 5 and 6.
- After Appendix A, there is some further information about the notation, abbreviations and references used throughout this work.

1.3 List of basic assumptions

Later in this work, a number of assumptions are made in order to simplify the mathematical analysis. In most cases, the effects of these assumptions will be accounted

for by error bounds, which can be used to determine the maximum effect of a given assumption on the outcome of the calculation in question. However, a number of assumptions are also made without an effort to quantify their effects. These assumptions are *basic* assumptions, necessary so that attention can be focused on the problem at hand, and therefore define the scope of this work.

One example is the effect of signal quantisation: all digital systems require that analogue signals be quantised before being processed, and the difference between the quantised signal and its analogue original may be substantial or negligible, depending on the design of the quantiser. However, such effects can generally be accounted for at a later point in time, through an appropriate modification of the underlying model.

The following is a list of assumptions, accompanied by justifying arguments, that will be relied upon throughout this thesis:

- **Interference:** Typically, spectrum sensors operate on channels where only licensed transmissions may occur. However, it is possible that other transmissions might also be present, resulting from leakage from adjacent channels or from malicious users. In this thesis, only the scenario where the spectrum sensor operates on a channel which is either unoccupied or is occupied solely by a licensed user and is unaffected by spectral leakage from adjacent channels is considered.
- **Correlated noise:** In practice, when analogue signals are sampled at the receiver, they are filtered, which can lead to correlation between samples of the signal which are separated in time. However, the effect of this correlation is related to the transfer function of the filter, which can usually be measured [12]. Consequently, pre-whitening techniques, such as that proposed by Zeng and Liang [12, Appendix A], can be used to decorrelate the samples. Therefore, in this thesis, it is assumed that samples of white noise signals are either naturally uncorrelated or can be decorrelated using an appropriate pre-whitening technique.
- **Flat and frequency selective fading:** The work in this thesis primarily concerns spectrum sensing with energy detectors, which are typically used for the detection of signals in relatively narrowband channels [13], and so are unaffected by *frequency selective fading* [14, p. 18]. Consequently, only the effects of *flat fading* will be considered in this thesis.
- **Slow and fast fading:** Depending on the coherence time of the channel, the amount of fading can either be constant or fluctuate significantly throughout the observation period [14, p. 18]. If the fading is constant, then it can be described using a standard *slow fading* model while, if it fluctuates, then a *fast fading* model, which describes the correlation between samples taken at different times, may be more appropriate. In this thesis, approximations are derived which describe the performance of energy detectors in a simpler manner than specific exact expres-

sions available in the literature. As these expressions assume a slow fading model, a similar assumption is made throughout the course of this work. If necessary, the approximation based method may be extended to the case of fast fading at a later time through a suitable generalisation.

- **Signal quantisation:** For simplicity of analysis, it is assumed that the quantisation of the received signal has a sufficiently large resolution so that the resulting quantisation errors are negligible.
- **Parameter uncertainty:** In practice, the calculation of performance metrics depends on prior knowledge of certain parameters, such as the magnitude of the noise power and, if appropriate, the value of the fading parameter. In all cases, it is assumed that the receiver has perfect knowledge of these parameters or, at worst, relies on an estimator which guarantees an arbitrarily good approximation given sufficient observation time. Further justification for this assumption in the case of noise power estimation is given in Section 3.1.2.
- **Antenna correlation:** In multiple antenna systems, it is usually assumed that the signals observed on each antenna are independent of one another. However, in certain circumstances, this assumption is not true and the correlation between the observed signals must be taken into account. This mostly occurs under frequency selective fading and in scenarios where there is insufficient spacing between the antennae [14, p. 389]. As the effects of frequency selective fading are not considered this thesis, this leaves just the latter scenario. However, Brennan [15] found that an antenna separation of thirty to fifty wavelengths is sufficient to guarantee a small correlation coefficient and Aalo [16] concludes that this can be sufficiently small so that it can be ignored in certain cases (these are discussed in more detail in Section 2.4.1). Consequently, for the remainder of this thesis, it is assumed that either the signals observed on different antennae are uncorrelated or, at worst, if they are correlated, the effect of this correlation on the overall performance of the system is negligible.
- **Signal corruption:** In cooperative systems, observations from individual sensors are transmitted either to neighbouring nodes or to a master node. As these observations are transmitted through wireless channels, they are prone to corruption due to various channel effects. However, it has been shown that such corruption typically does not affect the transmission of uncompressed decisions very severely and that, where it does, optimised channel aware coding can be use to mitigate the effect [17]. Consequently, for the remainder of this thesis, it is assumed that the effect of corruption is negligible, either due to the perfect transmission of the decision or the use of optimised coding schemes.

1.4 List of peer reviewed publications

The following papers were written and/or published during the course of the work that led to this thesis:

1. Donagh Horgan and Colin C. Murphy. On the convergence of the chi square and noncentral chi square distributions to the normal distribution. *IEEE Communications Letters*, 17(12):2233–2236, December 2013. ISSN 1089-7798. doi: 10.1109/LCOMM.2013.111113.131879. URL `http://ieeexplore.ieee.org/xpl/articleDetails.jsp?arnumber=6663749`.

2. Donagh Horgan and Colin C. Murphy. Fast and accurate approximations for the analysis of energy detection in Nakagami-m channels. *IEEE Communications Letters*, 17(1):83–86, January 2013. ISSN 1089-7798. doi: 10.1109/LCOMM.2012.111612.121964. URL `http://ieeexplore.ieee.org/xpls/abs_all.jsp?arnumber=6355939`.

3. Donagh Horgan and Colin C. Murphy. Implementation issues for optimized hard decision energy detector-based cooperative spectrum sensing. In *Proceedings of the 4th International Conference on Cognitive Radio and Advanced Spectrum Management (CogART)*, Barcelona, Spain, 2011. ACM. ISBN 978-1-4503-0912-7. doi: 10.1145/2093256.2093264. URL `http://doi.acm.org/10.1145/2093256.2093264`.

4. Donagh Horgan and Colin C. Murphy. Performance limits of cooperative energy detection in fading environments. In *Proceedings of the 4th International Conference on Cognitive Radio and Advanced Spectrum Management (CogART)*, Barcelona, Spain, 2011. ACM. ISBN 978-1-4503-0912-7. doi: 10.1145/2093256.2093274. URL `http://doi.acm.org/10.1145/2093256.2093274`.

5. Donagh Horgan and Colin C. Murphy. Voting rule optimisation for double threshold energy detector-based cognitive radio networks. In *Proceedings of the 4th International Conference on Signal Processing and Communication Systems (ICSPCS)*, page 1–8, Gold Coast, Australia, 2010. doi: 10.1109/ICSPCS.2010.5709679. URL `http://ieeexplore.ieee.org/xpls/abs_all.jsp?arnumber=5709679`.

Chapter 2

Background material

In the later chapters of this thesis, specific aspects of a particular spectrum sensor — namely, the *energy detector* — are explored. However, without a broad discussion of its merits and demerits, and comparisons with various competing technologies, this focus may seem unjustified, and so the primary intention of this chapter is to provide some context for the work that follows it.

A secondary intention is to provide a brief introduction to the notions of *cooperative spectrum sensing* and *diversity reception*, which will be built on in later chapters. In particular, aspects related to information sharing, such as *compression*, *corruption* and *correlation*, are discussed and further justification is provided for some of the assumptions stated in Chapter 1.

2.1 Mathematical models and spectrum sensing

Rosenblueth and Wiener [23] wrote that *no substantial part of the universe is so simple that it can be grasped and controlled without abstraction.* Indeed, they stated that the ideal abstraction is one which agrees with the universe in its entirety, but noted that there is an inherent contradiction in this idea: that any one capable of creating such a model would immediately find it of no use, because they would have already grasped the nature of the entire universe. The notion is a philosophical one, but has far-reaching implications. The perfect model, which describes the problem precisely, is so complex — as complex, in fact, as the original problem — that, in all likelihood, it cannot be realised.

We are left, then, with partial models, imperfect descriptions of the universe; but this is by no means a negative outcome. Partial models are, by definition, simpler than the ideal model, and simpler models are easier to comprehend and easier to use. As complex a system as an aeroplane may seem, it is necessarily a series of simplified

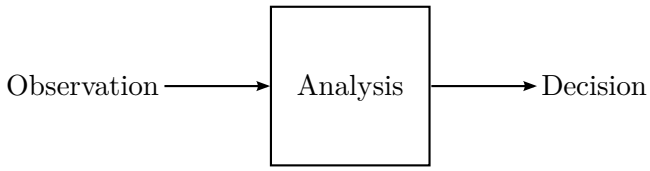

Figure 2.1: An illustration of an abstract decision making process.

abstractions of reality which, through the application of engineering methods, result in a flying machine.

The notion of simplified and complex models will become a recurring theme throughout this thesis: reality is modelled with mathematics, complicated models are replaced with simpler ones and, in many situations, it will be shown that, what at first may appear to be complex, fundamentally is not. However, it must be ensured that the generality lost through such simplifications is accounted for. While an overly complex model may be difficult to use, an overly simplified one is of no use at all, and so it is important to strike the right balance.

2.1.1 Observation, analysis, decision

The relationship between the physical task of spectrum sensing and the abstract mathematical models which feature throughout this work may not seem obvious at first, but is not difficult to understand. A spectrum sensor works by first observing some property of a channel and, then, deciding whether this channel is occupied or not. Abstractly, this can be thought of as a decision making process: data is observed, analysed and, then, a decision is made. An illustration of this kind of abstract system is shown in Figure 2.1.

Logically, the form of analysis that is used must depend on the kind of observation that is made. For instance, one might choose to observe a property which is constant, regardless of the occupancy of the channel, but this does not make sense: if the observed property does not change with the channel occupancy, how can the system make an accurate decision? Therefore, a property which varies with the occupancy of the channel must be chosen.

Often, such properties can vary with time, but are distributed according to a probability distribution, which itself does not vary with time. For instance, if the instantaneous power content of an unoccupied channel is measured, as in Figure 2.2, one might expect to see moderate variations in the measurements, from one moment to the next, because the noise interference is time-varying. However, if the *distribution* of the power of the noise interference were examined, it would be found that its mean value does *not* vary with time, and that its higher order moments, such as variance, behave similarly. As a result, the *average* power content of the channel is constant, but the *instantaneous*

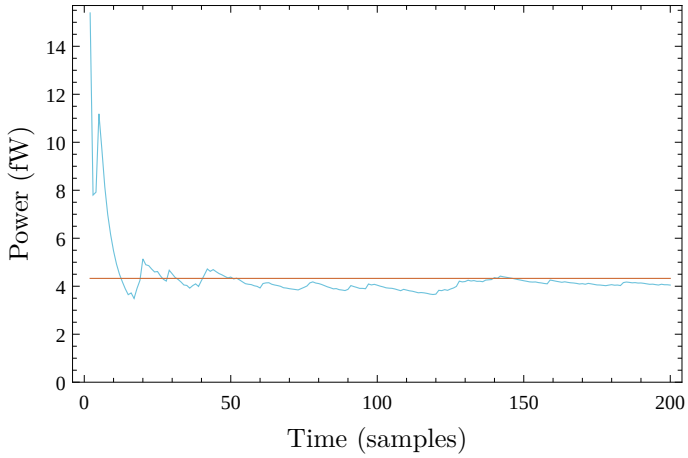

Figure 2.2: A plot of the instantaneous (blue) and average (red) noise power in an unoccupied channel.

power content is not. Observed properties that demonstrate this kind of statistical invariance are known as *stationary processes*.

Strictly speaking, a process is stationary only if the joint distribution of any set of its samples does not depend on time [24, p. 518]. However, such strict requirements do not need to be imposed on the observation. Instead, it is only required that the observed property is *wide sense stationary*, which is to say that its mean value and autocorrelation do not vary with time. By definition, then, any process that is stationary is also wide sense stationary. In the example given in Figure 2.2, the time-varying noise is a wide sense stationary process because its mean value is zero, and its average power, which is given by its autocorrelation function evaluated at zero time offset, is constant with respect to time.

Thus, if a property of the channel is observed, which varies with its occupancy and is wide sense stationary with respect to time, then the observations of this property will follow a certain probability distribution when the channel is occupied and a different probability distribution when it is unoccupied. Therefore, it can be determined whether the channel is occupied or not by checking to see if the observation belongs to one distribution or the other. To do this, one can use a *hypothesis test* or, in particular, because the decision making model has just two outcomes — either the channel is occupied, or it is not — a *binary hypothesis test*.

2.1.2 The binary hypothesis test

The binary hypothesis test works by determining which of two hypotheses are true: initially, the *null hypothesis* is assumed to be true, and the test then decides whether to accept this assumption, or reject it in favour of the *alternative hypothesis*. By convention, the null hypothesis is associated with the channel being unoccupied and

the alternative hypothesis with the channel being occupied [24, p. 444].

Each hypothesis can be viewed as a collection of events, where each event corresponds to a possible observation from the channel. By this definition, each collection is the set of all possible observations under a given hypothesis. Therefore, the set of all possible observations, known as the *observation space*, is given by

$$\Omega = H_0 \cup H_1, \tag{2.1}$$

where, by convention, H_0 denotes the set of events corresponding to the null hypothesis, H_1 denotes the set of events corresponding to the alternative hypothesis, and Ω denotes the observation space and is the complement of the empty set, $\varnothing$, that is $\Omega^c = \varnothing$. An example of an observation space can be seen in Figure 2.3.

The test itself is performed by deciding whether an observation is significantly different from the null hypothesis. To specify a decision rule, the observation space is partitioned into an *acceptance region* and a *rejection region*. If the observed event lies in the acceptance region, then the null hypothesis is accepted; otherwise, it is rejected. Therefore, the decision rule is

$$D = \begin{cases} H_0, & \text{if } x \in R^c, \\ H_1, & \text{if } x \in R, \end{cases} \tag{2.2}$$

where D denotes the outcome of the test and represents the accepted hypothesis, x denotes the observed event, R denotes the set of events in the rejection region, and R^c denotes the complement of R and is equivalent to the set of events in the acceptance region.

In the example of a partitioned observation space shown in Figure 2.3, the null hypothesis and the alternative hypothesis overlap, so that $H_0 \cap H_1 \neq \varnothing$. This means that an event observed from $H_0 \cap H_1$ could be a member of either H_0 or H_1. Thus, depending on the position of the decision boundary, it is possible to reject the null hypothesis when it is true, or to accept it when it is false. These are known as *Type I* and *Type II* errors, respectively.

In spectrum sensing, a Type I error is called a *false alarm* event, and corresponds to the case where a channel is incorrectly identified as occupied; Type II errors are known as *missed detection* events, and correspond to situations where the channel is mistakenly labelled as unoccupied. False alarm events cause DSA devices to ignore unused spectrum, while missed detection events can lead to interference with licensed transmissions. Therefore, the reliability of the decision making model can be specified by its probabilities of false alarm and missed detection.

Calculating the values of these probabilities is not difficult. By the previous definition, false alarms occur when the null hypothesis is incorrectly rejected. Mathematically,

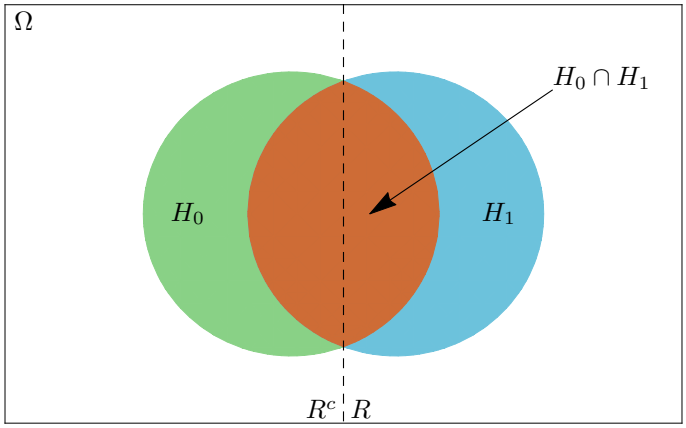

Figure 2.3: An example of an observation space, Ω. The null hypothesis is represented by the green area, while the alternative hypothesis is represented by the blue area, and their intersection is shown in red. The decision boundary is represented by the dashed line, with the rejection region, R, to its right and the acceptance region, R^c, to its left.

this can be expressed as

$$P_f = P[D = H_1|H_0], \tag{2.3}$$

where P_f denotes the probability of a false alarm. Assuming that the observation, x, follows a certain probability distribution when the channel is unoccupied, as in Figure 2.4, the probability of false alarm can be written as

$$\begin{aligned} P_f &= P[x \geq \lambda|H_0] \\ &= \int_{\lambda}^{\infty} f(x|H_0)dx, \end{aligned} \tag{2.4}$$

where λ is the decision threshold and represents the decision boundary in Figure 2.3, and $f(x|H_0)$ is the *probability density function* (PDF) of the distribution of x when the null hypothesis is true, as shown in Figure 2.4.

The probability of identifying an unoccupied channel, known as the *probability of acquisition*, is closely related to the probability of false alarm, as

$$\begin{aligned} P_a &= P[D = H_0|H_0] \\ &= P[x < \lambda|H_0] \\ &= \int_{-\infty}^{\lambda} f(x|H_0)dx \\ &= 1 - P_f, \end{aligned} \tag{2.5}$$

where P_a denotes the probability of acquisition, and the simplification follows from the fact that, because $f(x|H_0)$ is a probability density function, $\int_{-\infty}^{\infty} f(x|H_0)dx = 1$.

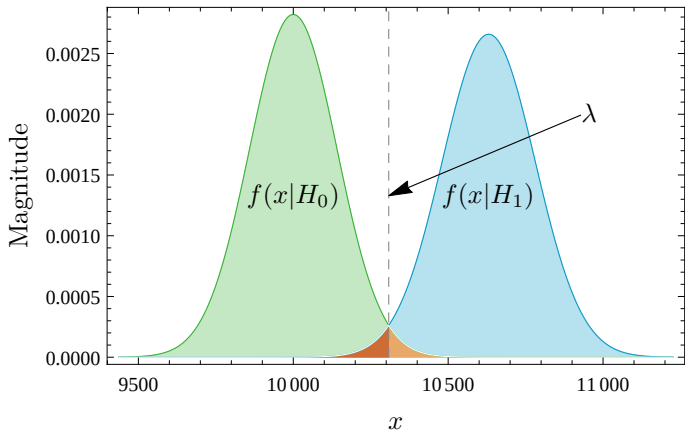

Figure 2.4: A plot of the probability density functions of an observed property, x, in an unoccupied channel (green) and in an occupied channel (blue). The decision threshold, λ, is given by the dashed line, and the areas corresponding to the probabilities of false alarm and missed detection are highlighted in orange and red, respectively.

Similarly, the probability of a missed detection can be calculated by

$$\begin{aligned} P_m &= P[D = H_0 \mid H_1] \\ &= P[x < \lambda | H_1] \\ &= \int_{-\infty}^{\lambda} f(x|H_1)dx, \end{aligned} \tag{2.6}$$

where P_m denotes the probability of a missed detection and $f(x|H_1)$ is the PDF of the distribution of x when the null hypothesis is false.

Finally, the probability of identifying an occupied channel, known as the *probability of detection*, can be calculated as

$$\begin{aligned} P_d &= P[D = H_1 | H_1] \\ &= P[x \geq \lambda | H_1] \\ &= \int_{\lambda}^{\infty} f(x|H_1)dx \\ &= 1 - P_m, \end{aligned} \tag{2.7}$$

where P_d denotes the probability of detection, and the simplification follows from the fact that $\int_{-\infty}^{\infty} f(x|H_1)dx = 1$.

2.1.3 How to make a good decision

From Figure 2.4, it is easy to see how the position of the decision threshold affects the probabilities of false alarm and missed detection. However, without any criteria to inform the choice, the value of λ is arbitrary, and may lead to unacceptably large probabilities of error. It is important, then, that there is some method for controlling

the error of the decision making process.

Fortunately, this is a well known problem and has a simple solution. According to the Neyman-Pearson lemma, the *likelihood ratio test* (LRT) given by

$$D = \begin{cases} H_0, & \text{if } \Lambda(x) < \kappa, \\ H_1, & \text{if } \Lambda(x) \geq \kappa, \end{cases} \tag{2.8}$$

where κ represents the decision threshold and $\Lambda(x) = \dfrac{f(x|H_1)}{f(x|H_0)}$ is the likelihood ratio, chosen so that

$$P_f = \int_{\Lambda(x)\geq\kappa} f(x|H_0)dx \triangleq \alpha, \tag{2.9}$$

where $\Lambda(x) \geq \kappa$ denotes the set of values in the rejection region, i.e. $R = \{x : \Lambda(x) \geq \kappa\}$, is the most powerful binary hypothesis test of size α [24, p. 446].

Put more simply, for some $0 \leq \alpha \leq 1$, letting $P_f = \alpha$ and using (2.4) and (2.9) to calculate λ, then the resulting probability of missed detection[1] will a minimum for that particular value of P_f. This ensures some control over the reliability of the decision making system.

2.2 Channel models

The task of spectrum sensing has now been related to an abstract mathematical model, which allows the reliability of the sensing process to be calculated. Before considering particular detector architectures, though, some consideration must first be given to the representation of radio signals in the model. As signals propagate through free space, they can be affected by a number of environmental factors, such as the Doppler shift, and thermal noise at the front end of the receiver. These effects, which can diminish the ability of spectrum sensors to detect signals in occupied channels, are often accounted for through the use of mathematical models of the propagation environment, commonly referred to as *channel models*. In their seminal book on the subject, Simon and Alouini list fifteen channel models alone [14], and there are a great many more, describing the large variety of phenomena that can affect a signal during its propagation.

In this brief review, three particular classes of channel model are considered: the first describes the effects of time-varying noise interference on the received signal; the second describes the fluctuation in received signal power due to the constructive and destructive interference of delayed, reflected, scattered and diffracted signal components, the effects of which are collectively known as *multipath fading*; and the last is used to model

[1] On a practical note, if the resulting probability of missed detection is too large, then α can be increased until the desired value is given by (2.6).

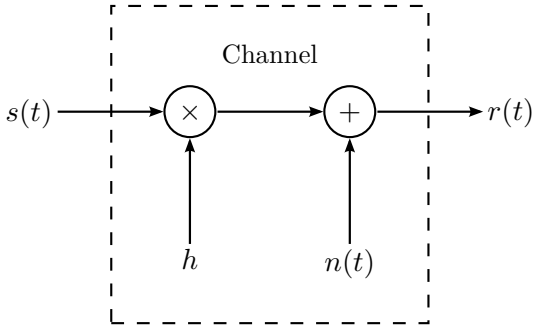

Figure 2.5: A generalised model of a transmission channel.

physical obstacles to signal propagation, such as buildings and mountains, the effects of which are known as *shadowing* or *shadow fading*.

Each of these channel models can be described using the generalised channel model shown in Figure 2.5, where the transmitted signal is denoted by $s(t)$ and the received signal by $r(t)$. As can be seen, the relationship between the transmitted and received signals is

$$r(t) = hs(t) + n(t), \tag{2.10}$$

where the channel gain, h, modulates the amplitude and phase of the transmitted signal, and the noise interference, $n(t)$, is additive.

It is also assumed that the generalised transmission channel is *frequency non-selective* or, in other words, that the channel response is constant with respect to frequency, so that each spectral component of the transmitted signal is affected by the same amplitude gain and phase delay. This is always the case in narrowband systems [14, p. 19] and is consistent with the assumption stated in Section 1.3 earlier.

2.2.1 The additive white Gaussian noise channel model

The *additive white Gaussian noise* (AWGN) channel is a basic mathematical model for communication channels in which the transmitted signal is affected by a random time-varying noise signal. The AWGN channel is a good model for thermal noise generated by receiver front ends [25, p. 106] and, while it does not take into account the effects of multipath fading or shadowing, it is useful for analysing the basic operation of a communications system before taking these other effects into account[2].

In the case of the AWGN channel, the noise interference is modelled as a time-varying quantity, $n(t)$, with amplitude distributed according to a Gaussian distribution with

[2]In this sense, the AWGN channel can be thought of as a very simplified abstraction of signal propagation, while the models discussed later are more sophisticated abstractions of the same physical process.

zero mean and variance, σ^2, that is

$$n(t) \sim \mathcal{N}(0, \sigma^2). \tag{2.11}$$

The *power spectral density* of the noise interference, $S_n(f)$, is constant[3], so that the noise power, P_n, is given [24, p. 580] by

$$\begin{aligned} P_n = \sigma^2 &= \mathbb{E}[n^2(t)] \\ &= \int_{-W}^{W} S_n(f) df \\ &= \int_{-W}^{W} \frac{N_0}{2} df \\ &= N_0 W, \end{aligned} \tag{2.12}$$

where $S_n(f) = \frac{N_0}{2}$, $2W$ is the bandwidth of the filter at the receiver front end and N_0 is the one-sided power spectral density of the noise interference which, for thermal noise, is usually calculated as

$$N_0 = k_B T_{sys}, \tag{2.13}$$

where $k_B \approx 1.381 \times 10^{-23}\,\mathrm{J\,K^{-1}}$ is the Boltzmann constant and T_{sys} is the temperature of the system, measured in Kelvin [26, p. 69].

The *signal to noise ratio* (SNR) at the receiver, γ, is given by

$$\gamma = h^2 \frac{P_s}{P_n}, \tag{2.14}$$

where P_s represents the power of the transmitted signal, and h is constant [14, p. 20].

2.2.2 The Rayleigh channel model

The *Rayleigh* channel model is a fading channel model, which is often used to describe propagation where there is no *line of sight* (LOS) from the receiver to the transmitter, such as in mobile links, ionospheric and tropospheric scattering, and ship to ship radio links [14, p. 22].

Like the AWGN channel, the Rayleigh channel is affected by additive white Gaussian noise, and so the noise interference is modelled as in (2.11). Unlike the AWGN channel, however, the channel response of the Rayleigh model varies with time. The Rayleigh channel model accounts for this fluctuation by modelling the channel response as a Rayleigh distributed random variable. Consequently, the signal to noise ratio at

[3] A constant power spectral density is often referred to as being *white* because it contains all frequencies in equal measure, just as white light does. This, along with the additive effect of $n(t)$ on $r(t)$, and the Gaussian distribution of its amplitude, is what gives the model its name.

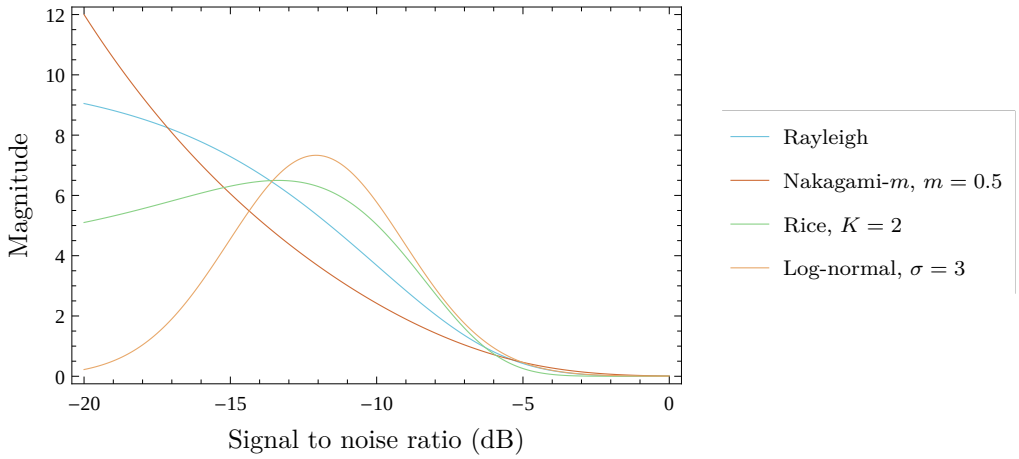

Figure 2.6: A plot of the PDFs of the signal to noise ratio for different fading channel models. In each case, the average signal to noise ratio is $-12\,\mathrm{dB}$.

the receiver, given by (2.14), follows an exponential distribution [14, p. 22], and its probability density function is given by

$$f_{Ray}(x) = \begin{cases} 0, & x < 0, \\ \frac{1}{\bar{\gamma}} e^{-\frac{x}{\bar{\gamma}}}, & x \geq 0, \end{cases} \tag{2.15}$$

where $f_{Ray}(x)$ is the PDF of the signal to noise ratio under Rayleigh fading and $\bar{\gamma}$ is the *average* signal to noise ratio at the receiver, given by

$$\bar{\gamma} = \mathbb{E}[h^2] \frac{P_s}{P_n}. \tag{2.16}$$

An illustration of the probability density function of the signal to noise ratio under Rayleigh fading is shown in Figure 2.6.

2.2.3 The Nakagami-m channel model

The *Nakagami-m* channel model is a general multipath fading model, and is often used to describe fading in both indoor and outdoor mobile radio links as well as in ionospheric radio links [14, p. 25]. It includes both the AWGN channel model and the Rayleigh channel model as special cases.

Like the AWGN and Rayleigh channels, the Nakagami-m channel models the time-varying noise interference as additive, white and Gaussian-distributed, and so $n(t)$ is given by (2.11). However, the channel response is modelled as a Nakagami-m distributed random variable. Consequently, the signal to noise ratio follows a gamma

distribution, with shape parameter, m, and scale parameter, $\frac{m}{\bar{\gamma}}$, that is

$$f_{Nak}(x) = \begin{cases} 0, & x < 0, \\ \left(\frac{m}{\bar{\gamma}}\right)^m \frac{x^{m-1}}{\Gamma(m)} e^{-\frac{mx}{\bar{\gamma}}}, & x \geq 0, \end{cases} \tag{2.17}$$

where $f_{Nak}(x)$ is the probability density function of the signal to noise ratio under Nakagami-m fading, $\bar{\gamma}$ is given by (2.16), and m is called the *fading parameter* and measures the severity of the effect of the multipath fading [14, p. 24].

Smaller values of m indicate more severe fading, while larger values indicate less severe fading. By definition, $m \in [\frac{1}{2}, \infty)$, and so the worst case fading occurs when $m = \frac{1}{2}$, and the best case occurs as $m \to \infty$ and is equivalent to the AWGN channel. When $m = 1$, (2.17) reduces to (2.15), and the Nakagami-m channel is equivalent to the Rayleigh channel [14, p. 25].

An illustration of the probability density function of the signal to noise ratio under Nakagami-m fading, with $m = \frac{1}{2}$, is shown in Figure 2.6.

2.2.4 The Rice channel model

The *Rice* channel, also known as the *Ricean*, *Rician* or *Nakagami-n* channel, is a further general model describing the effects of multipath fading. Typically, the Rice channel model is used to describe scenarios where one line of sight signal component dominates over many weaker components, and finds most use in the analysis of urban and suburban mobile radio links, pico-cellular indoor radio links, satellite links and ship to ship radio links [14, p. 24]. Like the Nakagami-m channel, the Rice channel includes the AWGN channel and the Rayleigh channel as special cases.

As before, the Rice channel incorporates an AWGN model for $n(t)$, as in (2.11). However, its channel response is modelled as a Rice distributed random variable, and so the signal to noise ratio follows a scaled noncentral chi square distribution with two degrees of freedom and noncentrality parameter equal to $2K$, that is

$$f_{Rice}(x) = \begin{cases} 0, & x < 0, \\ \left(\frac{K+1}{\bar{\gamma}}\right) e^{-K-\frac{(K+1)x}{\bar{\gamma}}} I_0\left(2\sqrt{\frac{K(K+1)x}{\bar{\gamma}}}\right), & x \geq 0, \end{cases} \tag{2.18}$$

where $f_{Rice}(x)$ is the probability density function of the signal to noise ratio under Rice fading, $\bar{\gamma}$ is again given by (2.16), $I_0(z)$ represents the zeroth order modified Bessel function of the first kind, and K is known as the *Rice factor* and measures the severity of the effect of the multipath fading [14, p. 23].

The Rice factor is defined in a similar manner to the Nakagami-m fading parameter: smaller values of K indicate more severe fading, while larger values indicate less severe

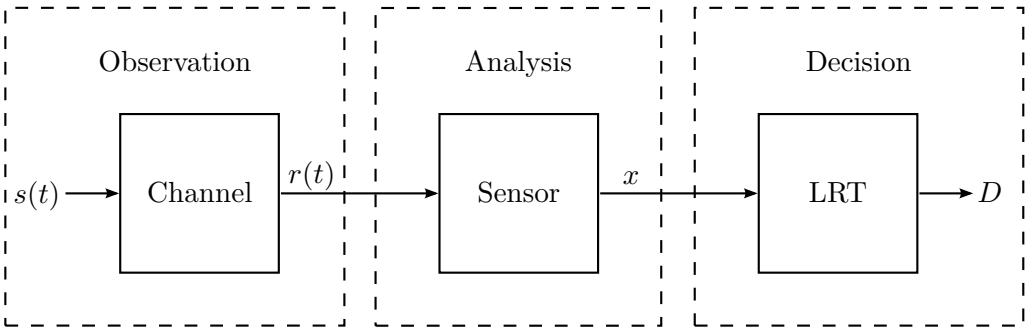

Figure 2.7: An abstract model of the spectrum sensing process.

fading. By definition, $K \in [0, \infty)$, and so the most severe fading occurs when $K = 0$ and the least severe fading occurs as $K \to \infty$. When $K = 0$, (2.18) reduces to (2.15), and so is equivalent to the Rayleigh channel; as $K \to \infty$, $f_{Rice}(x)$ tends to an impulse, and so is equivalent to the AWGN channel.

An illustration of the probability density function of the signal to noise ratio under Rice fading, with $K = 2$, is shown in Figure 2.6.

2.2.5 The log-normal channel model

The last model to be considered is the *log-normal* channel model, which is generally considered to be the best model for describing shadow fading [14, p. 32]. As before, the log-normal channel incorporates an AWGN model for $n(t)$, as in (2.11); its channel response is such that the signal to noise ratio is distributed according to

$$f_{LN}(x) = \begin{cases} 0, & x < 0, \\ \dfrac{\xi}{\sqrt{2\pi}\sigma x} \exp\left[-\dfrac{(10\log_{10} x - \mu)^2}{2\sigma^2}\right], & x \geq 0, \end{cases} \tag{2.19}$$

where $f_{LN}(x)$ is the probability density function of the signal to noise ratio under log-normal fading, $\xi = \frac{10}{\ln 10}$, and μ and σ are the mean and standard deviation of $10\log_{10} x$, respectively [14, p. 32].

An illustration of the probability density function of the signal to noise ratio under log-normal fading, with $\sigma = 3$, is shown in Figure 2.6.

2.3 Spectrum sensing techniques

In Section 2.1, an abstract model, describing the spectrum sensing process, was introduced, a more developed version of which is shown in Figure 2.7. So far, two components of the model have been discussed: the observation, which depends on the channel model used, and the decision, which is the outcome of a likelihood ratio test.

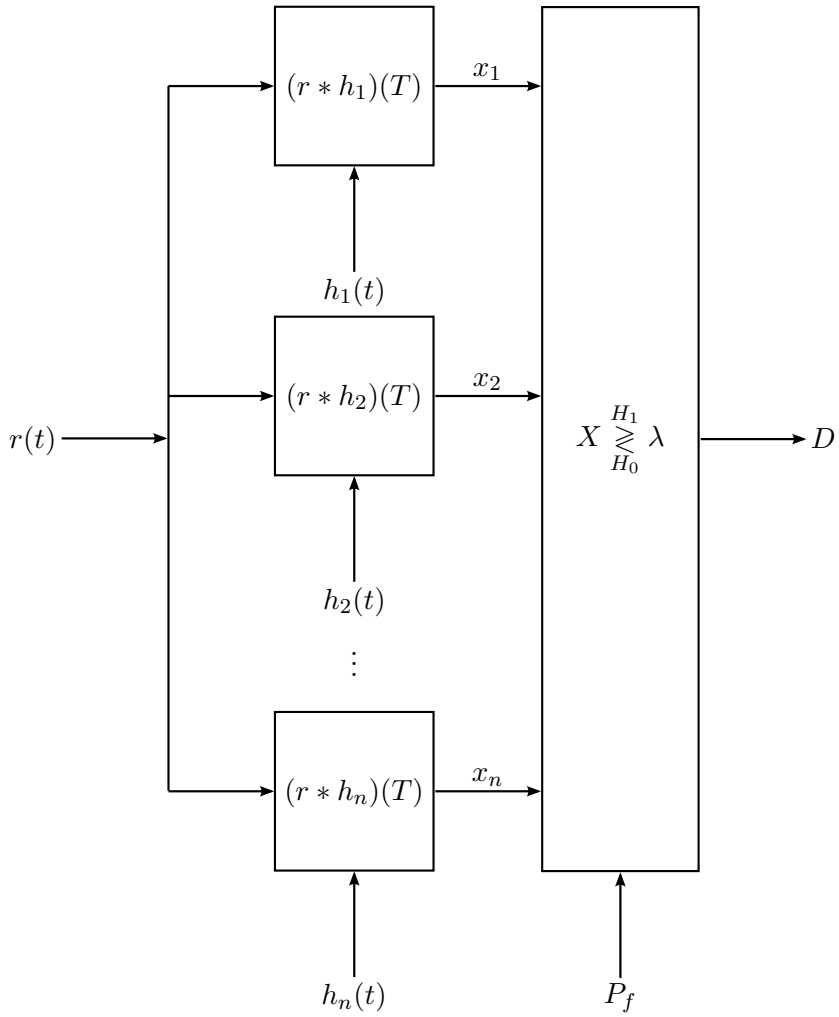

Figure 2.8: A matched filter detector.

The final component of the model, which translates the observations into decisions, is the sensing architecture.

In Section 2.2, it was discussed how different channel models can be used to model different signal propagation environments. In the same way, different sensing architectures are appropriate for use in different scenarios. Accordingly, in this section, several different sensing architectures are reviewed and where and how they are best used is discussed. In the following subsections, the sensing architectures are referred to using the general term *detector*, as both the analysis and decision components are implemented in the same system.

2.3.1 The matched filter detector

If the values of transmission parameters such as bandwidth, modulation type and phase delay are available, then it is well known that the optimum receiver for signals transmitted through AWGN channels is the *matched filter detector*, in the sense that it

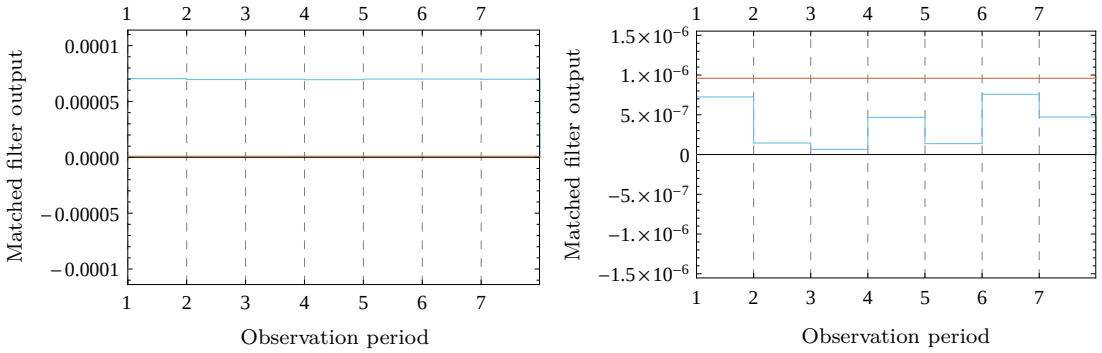

(a) The output of a matched filter detector (blue) when the channel is occupied. The decision threshold, λ, is shown in red.

(b) The output of a matched filter detector (blue) when the channel is unoccupied. The decision threshold, λ, is shown in red.

Figure 2.9: Matched filter outputs and decision thresholds for occupied and unoccupied channel scenarios.

minimises the probability of making an incorrect decision about the occupancy of the channel. Figure 2.8 shows a matched filter detector for a transmission system with n possible signals, where the signals $h_1(t), h_2(t), \dots h_n(t)$ are *matched* to the transmitted signal set, $s_1(t), s_2(t) \dots s_n(t)$, as

$$h_i(t) = s_i(T - t), \quad 1 \leq i \leq n, \tag{2.20}$$

where T is the length of the symbol period of the transmitted signal.

As can be seen, the test statistics, $x_1, x_2, \dots x_n$, are formed by convolving the received signal, $r(t)$, with each of the matched signals and sampling the output at $t = T$. Using the probability of false alarm to set the threshold, as in (2.4), a likelihood ratio test is then performed to determine whether the channel is occupied or not. If any or, equivalently, if the largest of the test statistics exceed the threshold, the channel is declared occupied. Therefore, the decision rule is

$$D = \begin{cases} H_0, & X < \lambda, \\ H_1, & X \geq \lambda, \end{cases} \tag{2.21}$$

where $X = \max(x_1, x_2, \dots x_n)$.

Figure 2.9(a) illustrates some typical matched filter detector outputs for an occupied channel. Seven distinct observation periods are illustrated. In each case, it is clear that the matched filter detector outputs exceed the decision threshold and so, using (2.21), the detector correctly decides that the channel is occupied. Similarly, in Figure 2.9(b), the outputs of the matched filter detector are illustrated for an unoccupied channel. As can be seen, in each of the observation periods, the maximum test statistic does not exceed the decision threshold, and so the detector correctly concludes that the channel is unoccupied.

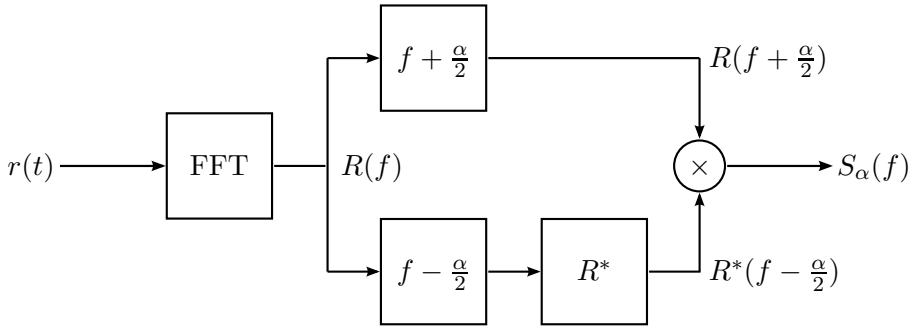

Figure 2.10: A spectral correlation function generator.

While the matched filter detector may appear to be an effective spectrum sensor, it requires full knowledge of the structure of any possible transmission as well as accurate estimates of various transmission parameters, such as phase delay, and so it cannot be used in situations where signals with unknown parameters must be detected. Consequently, it is not a suitable candidate technology for spectrum sensing. Furthermore, if such parameters are known, the matched filter detector requires local copies of each possible transmission in order to generate the test statistics. Therefore, in situations where the number of signals is large, or where many different types of signals must be detected, the matched filter detector requires a large amount of memory, high processing power, or both. This motivates the consideration of other technologies for spectrum sensing.

2.3.2 The cyclostationary feature detector

One popular alternative to the matched filter detector is the *cyclostationary feature detector*, first introduced by William A. Gardner in 1988 [27]. The cyclostationary feature detector does not require local copies of the transmitted signal and works well in situations where the signal to noise ratio is low. Consequently, it requires less information about transmitted signals than the matched filter detector, but can offer similar levels of performance. However, it too requires knowledge of certain transmission parameters which may not be available in practice (e.g. phase delay or the location of individual cyclostationary features) in order to operate effectively.

The concept behind the cyclostationary feature detector is relatively simple: in general, transmitted signals are embedded with periodic features such as pulse trains (e.g. *pulse width modulation* (PWM) signals), cyclic prefixes (e.g. *orthogonal frequency-division multiplexing* (OFDM) signals) and frequency hopping sequences (e.g. Bluetooth signals) in order for the receiver to estimate certain transmission parameters, to avoid inter-symbol interference or to prevent eavesdropping [28]. The cyclostationary feature detector works by exploiting such features in order to determine whether the channel is occupied or not.

In the frequency domain, the periodic features of the received signal are referred to as its cyclic features, and are represented using the *spectral correlation function*, $S_\alpha(f)$, of the received signal, defined as

$$S_\alpha(f) = R(f + \tfrac{\alpha}{2})R^*(f - \tfrac{\alpha}{2}), \tag{2.22}$$

where $R(f)$ is the Fourier transform of the received signal, f is the frequency of the received signal, and α is the cyclic frequency offset[4], a discrete quantity which refers to the location of a periodic feature. An example implementation, where $R(f)$ is calculated using a *fast Fourier transform* (FFT), is shown in Figure 2.10.

Being a function of both f and α, the spectral correlation function is a two dimensional quantity. When $\alpha = 0$, it reduces to the power spectral density of the signal:

$$\begin{aligned} S_0(f) &= R(f)R^*(f) \\ &= |R(f)|^2 \\ &= S(f), \end{aligned} \tag{2.23}$$

where $S(f)$ is the power spectral density — that is, the power per unit frequency — of the received signal. When $\alpha \neq 0$, then the spectral correlation function represents the *cyclic spectral density* of the received signal at offsets of $\pm\frac{\alpha}{2}$Hz from the carrier frequency. The advantage of computing the cyclic spectral density is that cyclic features of the transmitted signal, which do not appear in the power spectral density, are readily observed at certain offset frequencies in the cyclic spectral density. If present, these features are a good indicator that a channel may be occupied.

Figures 2.11(a) and 2.11(c) illustrate the power spectral density and spectral correlation function, respectively, of *binary phase shift keying* (BPSK) data transmitted through an AWGN channel. As the signal to noise ratio is large, the periodic feature at $(\frac{f}{f_s}, \frac{\alpha}{f_s}) = (0.5, 0.8)$, and the peaks of the real and imaginary components of the power spectral density at $(\frac{f}{f_s}, \frac{\alpha}{f_s}) = (0.1, 0)$ and $(\frac{f}{f_s}, \frac{\alpha}{f_s}) = (0.9, 0)$, respectively, are not difficult to see. When the signal to noise ratio is smaller, as illustrated in Figures 2.11(b) and 2.11(d), then the magnitudes of these features become smaller, but it is still possible to use the information to make a decision about the state of the channel.

The cyclostationary feature detector does this by computing a test statistic equal to the sum of the energy contained in each cyclic spectral density:

$$x = \int_{-\infty}^{\infty} \left(\sum_\alpha S_\alpha(f) \right) \, df. \tag{2.24}$$

[4]This α, representing the cyclic frequency offset, should not be confused with the α which represents the target probability of false alarm in the likelihood ratio test, defined in (2.9). This potentially confusing notation is adopted out of necessity, as both quantities are commonly denoted as α. Future references to α will make explicit which of the two meanings is intended.

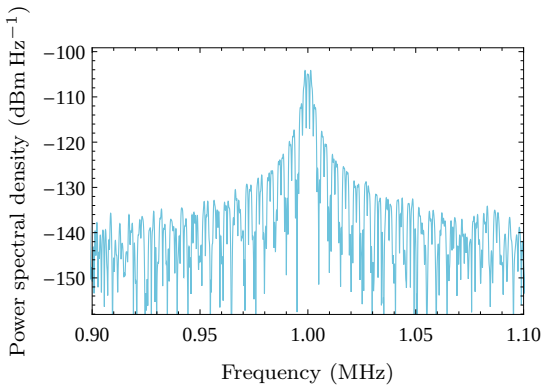

(a) Power spectral density of a BPSK signal in AWGN, with a signal to noise ratio of 10 dB.

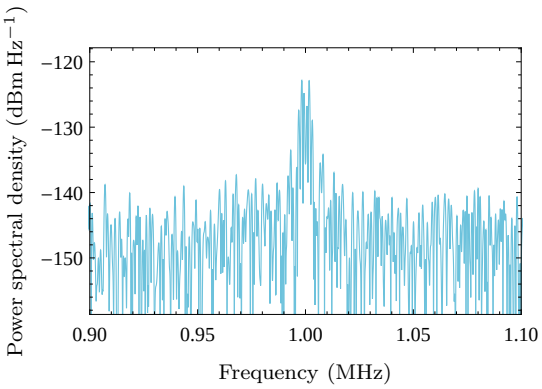

(b) Power spectral density of a BPSK signal in AWGN, with a signal to noise ratio of −10 dB.

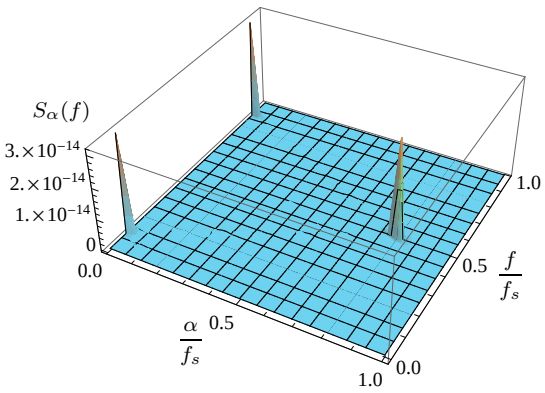

(c) Spectral correlation function of a BPSK signal in AWGN, with a signal to noise ratio of 10 dB. For convenience, f and α have been normalised to the sample frequency, f_s.

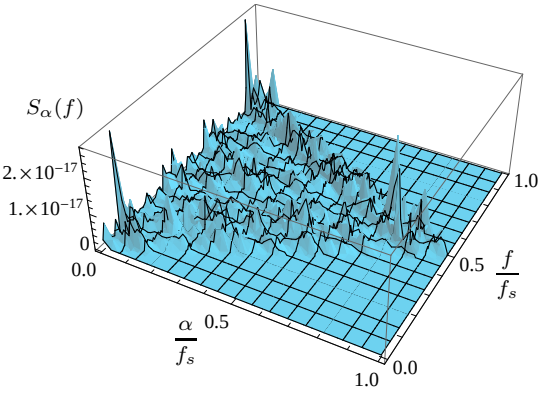

(d) Spectral correlation function of a BPSK signal in AWGN, with a signal to noise ratio of −10 dB. For convenience, f and α have been normalised to the sample frequency, f_s.

Figure 2.11: Power spectral densities and spectral correlation functions of BPSK signals in AWGN with different signal to noise ratios.

The likelihood ratio test is then used to determine the state of the channel. An illustration of such a detector is shown in Figure 2.12.

Unfortunately, the design has several drawbacks. For instance, when the signal to noise ratio is small, as in Figure 2.11(d), the discretisation of the frequency and cyclic frequency — necessary to compute the spectral correlation function — can often lead to quantisation noise. If such noise is present, it becomes much more difficult to reliably determine whether the channel is occupied or not. High resolution sampling is often required to overcome the effect. Derakhshani et al. found that the computation of the test statistic in such situations is both time consuming and computationally expensive [29]. Similarly, Turunen et al. found that the large number of points required by the FFT operation was to blame for the high power consumption of their *field programmable gate array* (FPGA) implementation of the detector. Derakhshani et al. also presented a simplified implementation of the detector, which offered reduced complexity, but required knowledge of the cyclic frequency offsets of the features for each of the signal

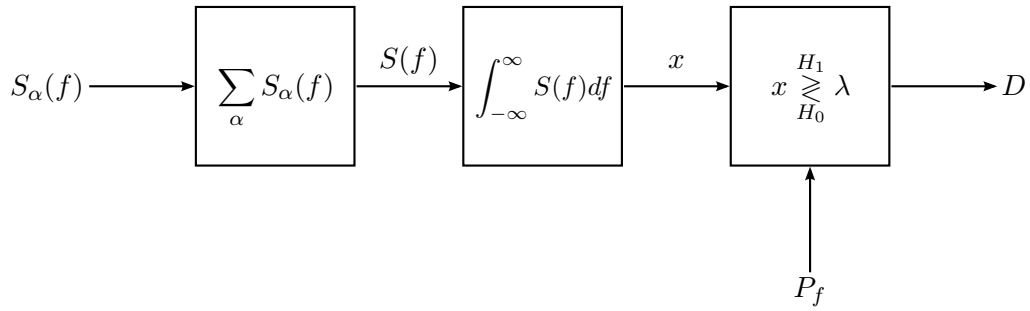

Figure 2.12: A cyclostationary feature detector.

types to be detected.

Furthermore, depending on the signal type, the spectral correlation may not be strong. In order to reduce the computational complexity of the detector, Fehske et al. proposed a neural network-based solution but found that the detector performance was poor for signals with low cyclic spectral correlations, such as *quadrature phase shift keying* (QPSK) [31]. Cyclic features are also known to be diminished by multipath fading. This has implications for both existing and new transmission technologies because the only way to compensate for the effects of the fading is to alter the profile of the transmitted signals [32]. However, this is generally not an option in the case of existing technologies, where international standards have been set and are not easily changed. For new systems, where standards are still in development, such changes may be contemplated, but the cost of altering the signal profile must also be considered. For instance, Sutton et al. [32] compensated for the effect of Rayleigh fading by embedding additional cyclic features in the transmitted signal but concluded that, while their method is an effective way to overcome multipath fading, the additional features required increased transmission bandwidth.

In summary, then, the cyclostationary feature detector, in the form presented in Figure 2.12, is a flexible spectrum sensing solution, capable of robust detection, even at low signal to noise ratios, but only if certain transmission parameters are known or can be estimated accurately. Consequently, it is not feasible as a generally applicable spectrum sensing solution. Even if such parameters could be estimated, the high performance of the cyclostationary feature detector comes at the cost of high power consumption, increased computational requirements and longer processing times. While simplified implementations are available, in general, they require some additional knowledge of the transmitted signal, and so are even less generally applicable than the standard cyclostationary feature detector. Furthermore, the detector is not suited to sensing signals with low spectral correlations, or legacy transmissions affected by multipath fading. Thus, a more generally applicable, and computationally inexpensive, technique must be considered.

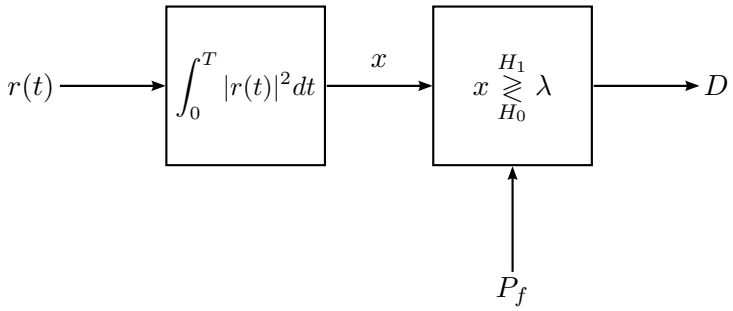

Figure 2.13: An energy detector.

2.3.3 The energy detector

The energy detector, also known as the *radiometer*, is a popular sensing technology which has been in use since the 1950s, but was most comprehensively analysed by Urkowitz in 1967 [13]. Like the cyclostationary feature detector, the energy detector does not require local copies of the transmitted signal set, instead forming its test statistic entirely from samples of the received signal. However, as will be shown, this simplicity comes at the cost of performance.

Figure 2.13 shows an illustration of a typical energy detector. As can be seen, the test statistic is computed as

$$x = \int_0^T |r(t)|^2 dt, \tag{2.25}$$

where T is the length of the observed signal, measured in seconds. Clearly, the test statistic is equal to the energy of the received signal[5]; it is this property that gives the detector its name.

Some typical energy detector outputs are shown in Figures 2.14(a) and 2.14(b). As can be seen, when the channel is occupied, the test statistic exceeds the threshold at the end of the observation period, and so the detector correctly deduces the state of the channel. Similarly, when the channel is unoccupied, the test statistic does not exceed the threshold and so the detector correctly concludes that the channel is not in use. However, in this case, had an observation period of 50 µs, rather than 700 µs, been used, the test statistic would have exceeded the threshold and the channel would have incorrectly been identified as being occupied — a false alarm event.

Like the previous sensing technologies, the energy detector has some drawbacks. For

[5]As an aside, from the definition in (2.24), the test statistic of the energy detector is equal to the test statistic of the cyclostationary feature detector when only $\alpha = 0$ is considered, that is

$$x = \int_{-\infty}^{\infty} S_0(f) df. \tag{2.26}$$

Therefore, the energy detector can be viewed as a specialisation of the cyclostationary feature detector which, unlike the simplified implementation by Derakhshani et al., does *not* require any additional information about the transmitted signals.

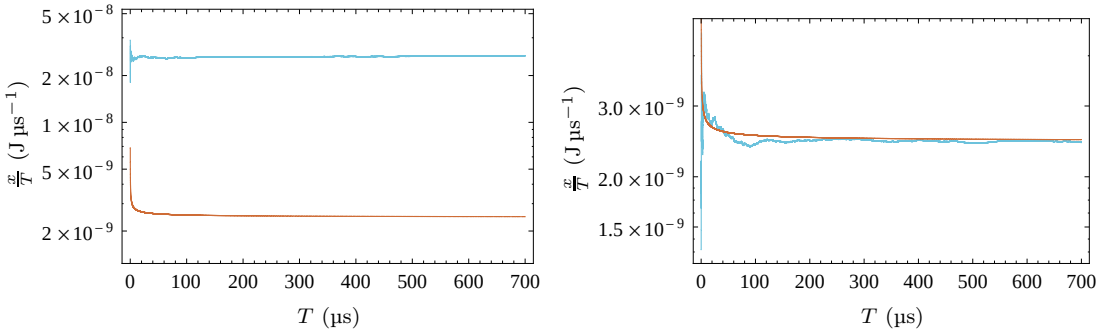

(a) An illustration of the normalised test statistic (blue) as a function of the observation time for an occupied channel. The normalised decision threshold, $\frac{\lambda}{T}$, is shown in red.

(b) An illustration of the normalised test statistic (blue) as a function of the observation time for an unoccupied channel. The normalised decision threshold, $\frac{\lambda}{T}$, is shown in red.

Figure 2.14: Typical energy detector outputs and decision thresholds for occupied and unoccupied channels.

instance, it cannot be used for the detection of spread spectrum or frequency hopping signals [28]. Perhaps its greatest deficiency, however, is its detection time in comparison to the matched filter. Tang showed that the energy detector requires $O(\frac{1}{\gamma^2})$ samples of the received signal for given probabilities of false alarm and missed detection, while the matched filter detector requires just $O(\frac{1}{\gamma})$ samples for the same error probabilities [10]. Essentially, this means that the energy detector requires much more time to detect signals with low signal to noise ratios than the matched filter, assuming equal sampling rates. An illustration of the problem is given in Figure 2.15.

2.3.4 Other sensing techniques

The detailed descriptions of the sensing techniques in the previous subsections were motivated by their widespread appearance in spectrum sensing literature. In fact, in their popular 2004 review, Cabric et al. describe *only* these techniques [28]. Yücek and Arslan, however, take a more balanced approach, also giving consideration to several other, less popular techniques [9]. While a fully exhaustive list would be a digression, for balance, some alternatives to the previously discussed techniques are listed here:

- Waveform sensing has been proposed as an alternative to matched filter detection. Fundamentally, the two are very similar. However, instead of using filters matched to the whole of the transmitted signal, the waveform sensor uses filters matched only to a portion of the transmitted signal, usually a preamble, pilot signal or synchronisation code [9]. Consequently, waveform processing requires less knowledge of the transmitted signal than matched filter detection, but still requires some knowledge of the transmitted signal, and so has limited applicability.

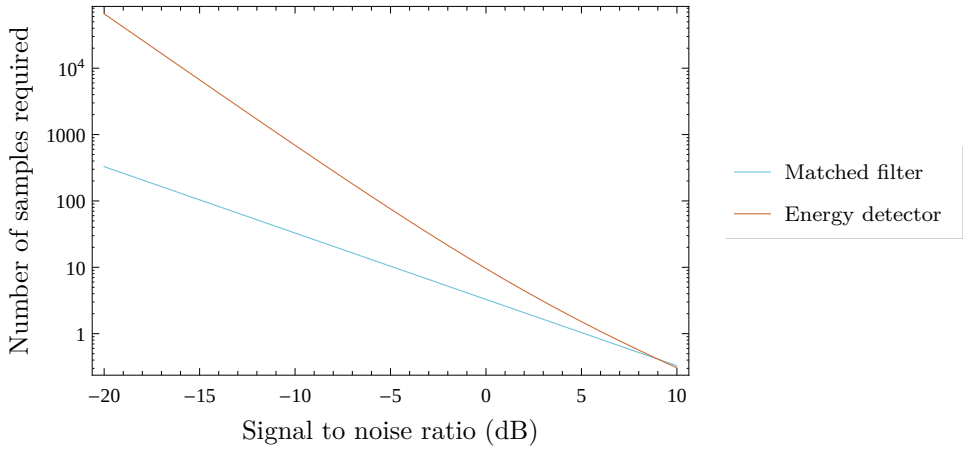

Figure 2.15: A log-linear plot of the number of samples required to ensure that $P_f = P_m = 0.1$ at different signal to noise ratios.

- The multi-taper method has been proposed as a possible alternative to energy detection [33]. This technique involves the use of filters to window different sub-bands of the channel under investigation in order to compute an accurate estimate of its power spectral density. However, this accuracy comes at the cost of increased processing power as each additional window function requires a Fourier transform operation.
- Wavelet-based sensing has also been investigated [34], but is generally considered useful for wideband sensing problems only, and requires large numbers of samples to be accurate.

2.4 Cooperative sensing and diversity reception

In a given situation, the question of which spectrum sensing technique is best is a trade off between cost and performance: if detection time is a priority, then the matched filter or waveform detectors may be an appropriate choice, but only if the transmitted signal structure is known, at least in part; if the only information known about the signal is that it has periodic features, then the cyclostationary feature detector may be a better choice, but only if the signal is not affected by fading, and then at the cost of increased processing power; or, if no information is known, then the energy detector or the multi-taper method may be best, but at the cost of increased detection time, and of increased processing requirements in the latter case. In short, there is no one right answer.

However, some conclusions can be drawn. The energy detector is by far the least computationally expensive solution and, while it cannot be used to detect spread spectrum or frequency hopping signals (for these, the cyclostationary feature detector appears

to be the most appropriate), it can detect any other type of deterministic signal [13], and so it is the most generally applicable of the sensing techniques discussed previously. The biggest drawback of the energy detector appears to be the large detection time it requires to ensure that low power transmissions are not present in the channel. However, as will be seen, this is not as big a problem as it seems and so, for the remainder of this review, the discussion is limited to energy detection, specifically to certain techniques which can be used decrease its sensing time. Broadly speaking, this can be achieved in one of two ways: using *cooperative sensing*[6], or through *diversity reception*. Accordingly, these concepts are briefly reviewed next.

2.4.1 Cooperative sensing

Cooperative sensing is a popular approach for increasing the performance of geographically distributed sensor networks. The key idea is to combine independent observations from different sensors in order to improve their overall performance. Cooperative sensing was first used in the 1980s to improve distributed radar detection [35] but, more recently, it has developed a following in the spectrum sensing community as a simple, but effective, way of increasing the performance of spectrum sensors [9, 21, 28].

Cooperative sensing comes in two flavours: centralised and decentralised. In centralised cooperation, a base station or master node, known as the *fusion centre*, coordinates the operation of the network. Instead of making a local decision, each node transmits its observation to the fusion centre, where the observations are combined, and an overall decision about the state of the channel is made, as in Figure 2.16. The overall decision is then transmitted to the individual sensors and, if the channel is unoccupied, the fusion centre allocates transmit slots and data rates to maximise usage of the free channel. Figure 2.17 illustrates a typical centralised network scenario, where the total sensing time is reduced by increasing the number of cooperating energy detectors.

However, this level of coordination can lead to a prohibitive communication overhead, particularly when the number of participating nodes is large [20]. In decentralised cooperation, individual nodes still share observations, but directly with neighbouring nodes instead of through a fusion centre. Individual nodes then make their own decision about the state of the channel, as in Figure 2.18. While decentralised cooperation requires less communication between nodes, and therefore less bandwidth, it is also

[6]To be fair, cooperative sensing can be applied to other technologies, but the benefits are limited. For instance, Derakhshani et al. [29] reduced the high computational cost of their cyclostationary feature detector by distributing the generation of the spectral correlation function across a network of sensors: each sensor generated the spectral correlation function for a specific value of α, and the results were then combined and further processed at a master node to reach an overall decision about the state of the channel. However, Derakhshani et al. found that, for given probabilities of error, the detection time in their distributed implementation was slightly *greater* than in their single node implementation, due to the simplifications required to adapt the algorithm to work in a distributed fashion. In the following discussion, it will be shown that cooperative energy detection requires no such simplifications, and always *decreases* the required detection time.

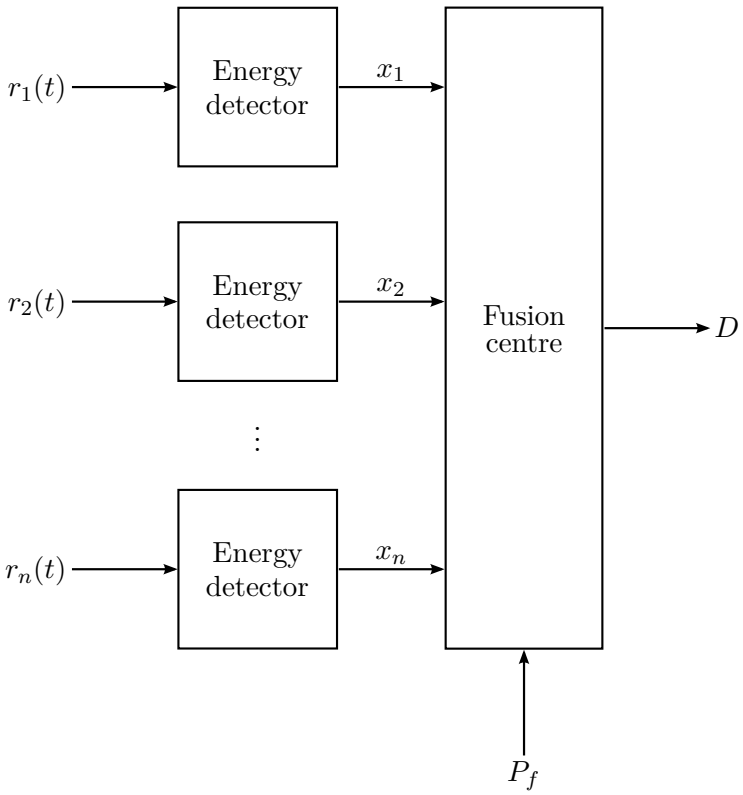

Figure 2.16: A centralised cooperative energy detector network.

known to achieve lower capacity on average [28]. For the remainder of this work, only the centralised form of cooperation is considered.

In both centralised and decentralised cooperation, a control channel is required to share information between nodes. However, it is a matter of debate how such channels should be implemented [28]. It has been proposed that the control channels could be *ultra wideband* (UWB) spread spectrum channels, in order to minimise interference with primary users, or that dedicated control bands could be established, but the latter proposal seems somewhat defeatist given the aim of dynamic spectrum access. In any case, control channels will almost certainly have limited bandwidth which, in turn, will impose restrictions on the level of cooperation between nodes.

One solution is for each node to compress its observation before transmission, at the cost of increased error probabilities. However, if large numbers of nodes cooperate, then the compression loss can be mitigated somewhat [20]. Another solution is to censor observations from specific nodes. For instance, in a network with ten cooperating nodes, just five nodes might transmit their observation to the fusion centre, with the criteria for choosing which nodes self-censor, and which transmit, linked to the confidence each node has in its observation [36]. It is also worth noting that compression and censoring are not mutually exclusive, and can be combined to further reduce communication overhead [22].

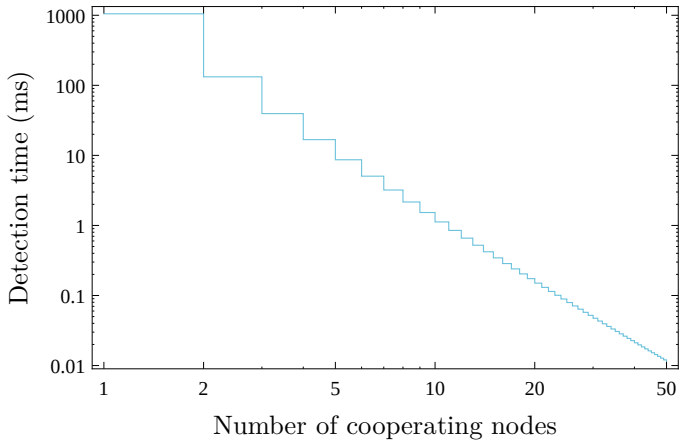

Figure 2.17: A log-log plot of sensing time as a function of network size for an idealised network of cooperating energy detectors operating on an AWGN channel.

Another important aspect of cooperative sensing is the independence, or otherwise, of the observations at each node. If the cooperating nodes are far enough apart, then it might be expected that their observations will be uncorrelated. However, if the nodes are close, then the correlation between their decisions must be taken into account when calculating performance metrics. For instance, Drakopoulos and Lee considered the effect of correlation on centralised cooperative networks where each node compresses its observation to just 1 bit, and found that the performance of a network of any size tends towards that of a single detector when the value of the average correlation between nodes tends towards unity [37].

Brennan [15] provides some insight into the level of correlation that might be found in multipath fading environments, stating that an antenna separation of thirty to fifty wavelengths is sufficient to reduce the correlation coefficient to less than 0.3, and a separation of ten to fifteen wavelengths is sufficient to reduce the correlation coefficient to less than 0.6. Grisdale et al. [38] analysed the effect of correlation on the performance of receivers operating on Rayleigh channels, showing that its effects are negligible in the case where the average correlation between nodes is less than 0.6. Aalo [16] is more conservative, stating that the effect of correlation on dual antenna devices should only be disregarded when the average correlation is less than a third. Still, as Brennan showed, this can be achieved through moderately spaced antennae.

Ghasemi and Sousa, in their analysis of the effects of correlation in log-normal shadowed environments, define a model for the average correlation between nodes, ρ, as

$$\rho = e^{-ad}, \tag{2.27}$$

where d is the average distance between neighbouring nodes, and $a \in \mathbb{R}^+$ and is a constant whose value depends on the environment [39]. Using experimental data, Gudmundson found that $a \approx 0.12$ in urban environments and $a \approx 0.002$ is rural envi-

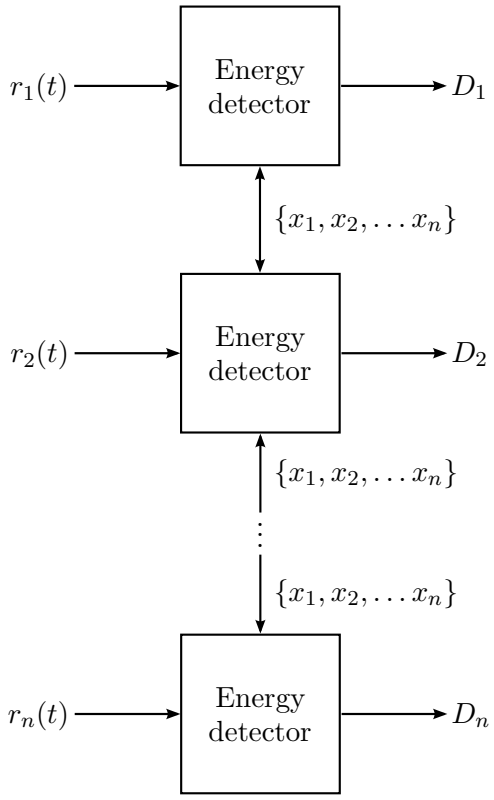

Figure 2.18: A decentralised cooperative energy detector network.

ronments [40]. The model is illustrated in Figure 2.19. As can be seen, the distance between nodes required for small values of ρ in the urban model are not large, although this distance increases significantly in the suburban model.

Thus, in multipath fading environments, an antenna separation on the order of tens of times the signal wavelength can mitigate the effects of correlation while, in shadowed environments, the spacing between nodes required to mitigate correlation effects is greater. As the later work in this thesis concerns multipath fading only, the effects of correlation are not considered further, and it is instead assumed that either all observations are uncorrelated or that the effect of any correlation present is negligible or can be mitigated through appropriate antenna separation.

The final aspect of cooperative sensing to be discussed is the imperfect nature of the control channel. Chaudhari et al. have showed that errors from the corruption of signals transmitted through control channels can have a significant effect of the performance of cooperative networks using both compressed and uncompressed observations [17]. The authors demonstrate that compressed observations are much more sensitive to the effects of corruption than uncompressed observations, but conclude that optimised channel aware coding can be used to mitigate these effects in both cases. As the work in this thesis relates to the transmission of uncompressed observations only, for the remainder of this work, it is assumed that observations transmitted between nodes are free from corruption and that, otherwise, optimised channel aware coding is used and

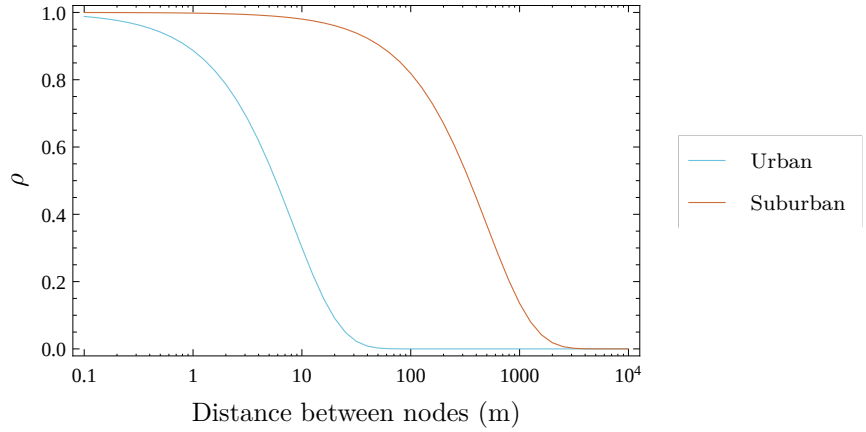

Figure 2.19: A log-linear plot of the shadowed correlation model proposed by Ghasemi and Sousa.

entirely mitigates the effects.

2.4.2 Diversity reception

Diversity reception is a technique, similar to cooperative sensing, used to improve the performance of spectrum sensors. The aim of diversity reception is to combine two or more versions of the same information-bearing signal, each of which is known as a *branch*, in order to increase the signal to noise ratio at the receiver. While generally used to model individual detectors with multiple antennae, diversity reception can also be used to model cooperative sensing networks.

There are many forms of diversity reception, of varying complexity, and even hybrid forms. Simon and Alouini list eight different forms [14], while Stüber lists an additional three [41]. In this work, three specific varieties are considered: the *maximal ratio combiner* (MRC), the *equal gain combiner* (EGC) and the *square law combiner* (SLC), which are the most commonly used, and most generally applicable, models found in the spectrum sensing literature.

2.4.2.1 The maximal ratio combiner

The maximal ratio combiner is a diversity receiver architecture which finds most use in situations where the channel gain and phase delay are known or can be measured, or estimated, accurately [14]. Typically, this information is not available in spectrum sensing scenarios and so the maximal ratio combiner is, in general, an infeasible spectrum sensing solution. Nevertheless, it is known to be the optimum diversity receiver, in the sense that it maximises the signal to noise ratio at its output [14, p. 317]. Consequently, the performance of the maximal ratio combiner is an upper bound on the

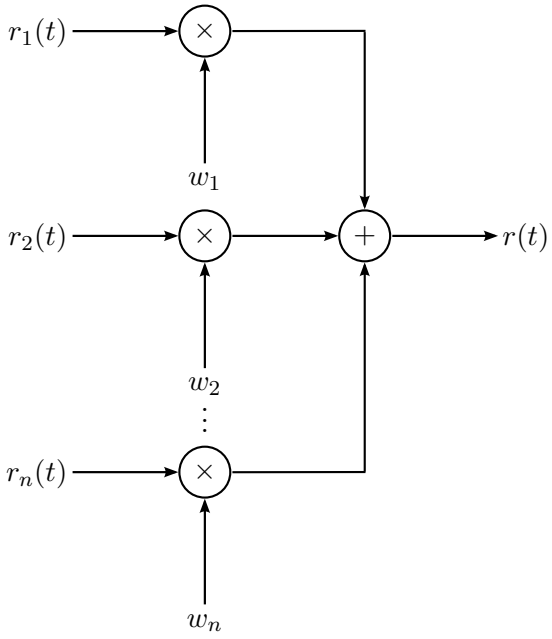

Figure 2.20: A maximal ratio combiner / equal gain combiner.

performance of *any* diversity reception scheme, and so the technique is worthy of further consideration for theoretical purposes.

An illustration of a maximal ratio combiner architecture with n branches is given in Figure 2.20. As can be seen, the received signals on each branch, $r_1(t), r_2(t), \ldots r_n(t)$, are weighted according the functions $w_1, w_2, \ldots w_n$ and summed together to produce a combined received signal, $r(t)$, which is then processed by the energy detector in the usual way.

For the maximal ratio combiner, the weight functions are given by

$$w_i = h_i, \tag{2.28}$$

where h_i is the channel response of the signal received on the i^{th} branch.

2.4.2.2 The equal gain combiner

While the maximal ratio combiner is the optimum diversity receiver, it is not a feasible solution for spectrum sensing. However, the equal gain combiner requires no information about the channel gains and phase delays on each branch and so is a more feasible sensing solution. The equal gain combiner has a similar architecture to the maximal ratio combiner, as shown in Figure 2.20, with the exception that all of its weight functions are equal to one, that is

$$w_1 = w_2 = \ldots = w_n = 1. \tag{2.29}$$

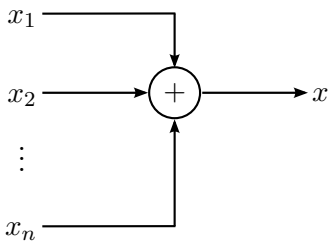

Figure 2.21: A square law combiner.

2.4.2.3 The square law combiner

The maximal ratio combiner and equal gain combiner architectures are intended to be used when the detector has direct access to the received signal on each of the branches. However, this is not always the case. For instance, in the centralised cooperative sensing system in Figure 2.16, the fusion centre has access to the test statistics generated at each node, but not the received signals themselves. In this case, bandwidth constraints prevent each node from forwarding an exact copy of its received signal to the fusion centre, and so a different form of diversity architecture must be considered: the square law combiner.

A typical square law combiner is illustrated in Figure 2.21. As can be seen, the square law combiner simply sums together the received test statistics, that is

$$x = \sum_{i=1}^{n} x_i, \tag{2.30}$$

where x is the test statistic at the output of the combiner.

Like the equal gain combiner, the square law combiner requires no knowledge of the phase delays on each branch, making it a feasible technology for spectrum sensing. In fact, the square law combiner is quite similar to the equal gain combiner, the key difference being that, in the case of the square law combiner, the combining operation is performed after the test statistics have been generated[7]. Consequently, the square law combiner can perform worse than the maximal ratio combiner and the equal gain combiner. However, as will be seen later, in many cases, the difference is not very large. Indeed, Ma et al. [42] found that the square law combiner is near-optimum when the signal to noise ratio is high.

[7]The square law combiner is sometimes referred to as the *post-detection equal gain combiner*.

2.5 Summary

This chapter began by relating a literal description of the spectrum sensing process to an abstract decision making model. Then, under the assumptions that:

1. The property under observation changes with the occupancy of the channel, and
2. The property under observation is a wide sense stationary process,

the binary hypothesis was applied to characterise its performance, and the Neyman-Pearson lemma was used to show that the probability of making an incorrect decision can be controlled using the likelihood ratio test.

Five different mathematical models for describing the propagation of transmitted signals through real world environments were considered: the AWGN model, which is used to describe time-varying noise interference; the Rayleigh, Nakagami-m and Rice models, which are used to describe multipath fading; and the log-normal model, which is used to describe shadow fading. While the log-normal model was discussed for the sake of completeness, from this point forward, only the other four channel models will be considered and, of those, mainly just the three multipath fading models.

Several spectrum sensing architectures were also reviewed, and it was found that which technique is best very much depends on the intended application: if detection time is critical, then the matched filter detector is best, but requires knowledge of the transmitted signal scheme; if only limited knowledge is available, then the cyclostationary feature detector is an appropriate choice, but requires high processing power; if cost is critical, then the energy detector is best.

Of all the technologies considered in this chapter, the energy detector is by far the simplest and the most generally applicable. Its main drawback is the detection time required to sense the channel reliably. However, as discussed earlier, this can be overcome through the use of cooperative sensing and diversity reception techniques. A more in depth review of material relating specifically to the energy detector is given in the next chapter.

Chapter 3

A survey of related work

While the previous chapter gave a broad overview of various spectrum sensing techniques, the intention of this chapter is to provide a rigorous survey of material relating specifically to the energy detector. In particular, exact formulations for the decision probabilities of energy detector diversity receivers operating on AWGN channels are derived, and approaches taken by other researchers to extend this analysis to multipath fading channels are reviewed. The chapter concludes with a critical assessment of these approaches, which motivates the decision to consider approximation based approaches in the coming chapters.

3.1 Some brief notes on model non-idealities

The previous chapter presented material relating to detector architectures in a very general way. However, in doing so, some details, which affect all the architectures considered previously, were omitted. Thus, before discussing energy detector diversity receivers in more detail, some non-idealities, which have not yet been accounted for in the system model, must be addressed.

3.1.1 Signal sampling

The idealised detectors presented in the last chapter assumed that the received signal, $r(t)$, is an analogue quantity. However, in reality, the system processing the received signal will be digital, and so the signal must be sampled at discrete time intervals.

Urkowitz first considered the effect of sampling on the energy detector, and showed that its test statistic, defined in (2.25), has the discrete time approximation

$$x \approx \frac{1}{2W} \sum_{j=0}^{M-1} \left| r\left(\tfrac{j}{2W}\right) \right|^2, \tag{3.1}$$

where M is the total number of samples of the received signal and is equal to the time bandwidth product, that is

$$M = 2TW, \tag{3.2}$$

and $r\left(\frac{j}{2W}\right)$ refers to the j^{th} discrete sample of the received signal, so that the first sample occurs at time $t = 0$ and the last sample occurs at time $t = T - \frac{1}{2W}$ [13].

Urkowitz also showed that the error resulting from the approximation in (3.1) becomes negligible as M becomes large. Thus, the digital system becomes equivalent to its analogue counterpart as the number of samples increases.

3.1.2 Noise power uncertainty

In the last chapter, the average noise power, σ^2, was related to the system temperature, T_{sys}, using (2.13). However, this relation does not take into account the change in the average value, also known as the *drift*, of the noise power that can occur as T_{sys} varies over time. If the drift is significant, estimates of the noise power may become inaccurate and so any decision made based on them will become less reliable. Noise power drift can also occur as a result of time-varying antenna gain, initial calibration errors and *radio frequency* (RF) interference from other users [43].

Sonnenschein and Fishman first considered the theoretical implications of noise power uncertainty and demonstrated that it severely reduced the reliability of the energy detector [44, 45]. More recently, Tandra and Sahai showed that matched filter detectors [46] and cyclostationary feature detectors [47] also become less reliable when the noise power estimate is inaccurate, although the effect is not quite as severe as in the case of the energy detector. Specifically, Tandra and Sahai state that, for a given level of noise power uncertainty, there is a minimum value of signal to noise ratio below which detection cannot occur for all three detector types. In the case of the energy detector, the minimum detectable signal to noise ratio, γ_{min}, known as the *SNR wall*, is given by

$$\gamma_{min} = \frac{\rho^2 - 1}{\rho}, \tag{3.3}$$

where ρ is the measure of uncertainty in the noise power estimate, such that the estimated noise power, $\hat{\sigma}^2$, is contained in the interval $[\frac{1}{\rho}\sigma^2, \rho\sigma^2]$. By this definition, $1 < \rho < \infty$.

For given probabilities of false alarm and missed detection, this kind of noise uncertainty increases the number of samples required so that $M \to \infty$ as $\gamma \to \gamma_{min}$, as can be seen in Figure 3.1, where the initialism ENP denotes *estimated noise power* and is discussed later. Thus, for $\gamma < \gamma_{min}$ an infinitely large number of samples is required and reliable

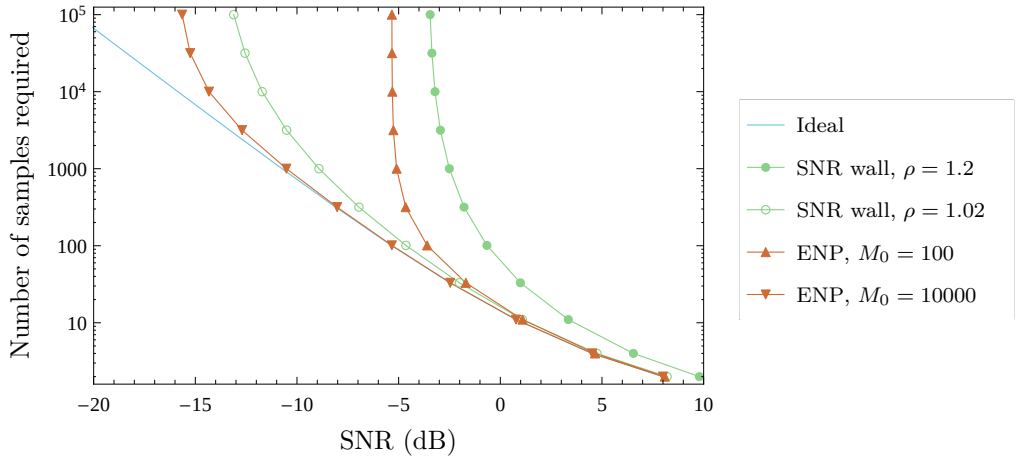

Figure 3.1: A logarithmic plot of the number of samples required to guarantee that $P_f = P_m = 0.1$ as a function of the average signal to noise ratio at the receiver for different noise power uncertainty scenarios.

detection is impossible.

However, there are a number of problems with this model. Firstly, Tandra and Sahai assume that the value of ρ can be arbitrarily large, which is not the case in practice. In laboratory tests, Hill and Felstead [48] found that σ^2 varied on the order of $\pm 0.05\%$ over the course of two minutes, typically a relatively long period of time in signal detection terms, which suggests that ρ may actually be bounded as $1 < \rho < 1.0005$. Furthermore, Mariani et al. found that Tandra and Sahai's model for noise uncertainty is overly pessimistic, because it does not take into account the *consistency*[1] of the noise power estimation process [43]. Specifically, they demonstrated that the SNR wall for energy detectors employing consistent noise power estimators is, at worst, that given in (3.3), and is more generally described by

$$\gamma_{min} = \frac{1 - Q^{-1}(P_f)\sqrt{\phi}}{1 - Q^{-1}(P_d)\sqrt{\phi}} - 1, \tag{3.4}$$

where $Q^{-1}(z)$ is the inverse of the Gaussian Q function [49, Equation 26.2.3], so that $x = Q^{-1}(Q(x))$, and ϕ measures the consistency of the noise power estimator technique.

Mariani et al. propose a modified energy detector, the *estimated noise power* (ENP) energy detector, which generates an estimate of the noise power, $\hat{\sigma}^2$, as

$$\hat{\sigma}^2 = \frac{1}{M_0} \sum_{j=0}^{M_0-1} \left| n\left(\tfrac{j}{2W}\right) \right|^2, \tag{3.5}$$

where M_0 is the number of samples used to generate the noise power estimate, and is related to the time bandwidth product in a similar fashion to (3.2), and $n\left(\frac{j}{2W}\right)$ refers

[1] A consistent estimator is one whose estimated value converges towards the true value over time such that, as the estimation time tends to infinity, the estimate becomes arbitrarily accurate.

to the j^{th} discrete sample of $n(t)$.

As (3.5) is a consistent estimator of σ^2, $\phi = \frac{1}{M_0}$ in (3.4), and so the SNR wall can be overcome by increasing the number of samples used in estimating the noise power [43]. Figure 3.1 shows two examples where such estimates can overcome moderate to severe values of ρ. Consequently, for the remainder of this thesis, it is assumed that such an estimation technique is used to generate an accurate value of $\hat{\sigma}^2$, so that there is a negligible difference between the estimated and actual values of noise power, that is

$$\hat{\sigma^2} \approx \sigma^2. \tag{3.6}$$

3.2 Energy detection in AWGN channels

A slight change in notation is now adopted to distinguish between the decision probabilities of different diversity architectures: henceforth, P_{f_X}, P_{a_X}, P_{d_X} and P_{m_X} will be used to denote the probabilities of false alarm, acquisition, detection and missed detection, respectively, for a diversity receiver of type X. As before, the following relationships hold

$$P_{a_X} = 1 - P_{f_X}, \tag{3.7}$$

$$P_{m_X} = 1 - P_{d_X}, \tag{3.8}$$

and, for consistency, $X = \text{ND}$ will be used to denote the *no diversity* (ND) case.

Also, for convenience, a normalised test statistic, $\hat{x}$, is defined as

$$\hat{x} = \frac{1}{\sigma^2} \sum_{j=0}^{M-1} \left| r\left(\tfrac{j}{2W}\right) \right|^2. \tag{3.9}$$

3.2.1 Receivers with no diversity

For energy detectors with no diversity, Urkowitz showed that $\hat{x}$ follows a chi square distribution with M degrees of freedom, when the channel is unoccupied, and a non-central chi square distribution with M degrees of freedom and non-centrality parameter $M\gamma_{_{ND}}$, when a signal is present; that is

$$\hat{x} \sim \begin{cases} \chi^2_M, & H_0, \\ \chi^2_M(M\gamma_{_{ND}}), & H_1, \end{cases} \tag{3.10}$$

where χ_k^2 represents the chi square distribution with k degrees of freedom, and $\chi_k^2(s)$ represents the noncentral chi square distribution with k degrees of freedom and non-centrality parameter s [13], and γ_{ND} denotes the signal to noise ratio at the input to the energy detector, and is given by (2.14).

Thus, the probabilities of false alarm and detection are given [50] by

$$P_{f_{ND}} = \frac{\Gamma\left(u, \frac{\lambda}{2}\right)}{\Gamma(u)}, \tag{3.11}$$

$$P_{d_{ND}}(\gamma_{ND}) = Q_u\left(\sqrt{M\gamma_{ND}}, \sqrt{\lambda}\right), \tag{3.12}$$

where $\Gamma(a, b)$ is the upper incomplete Gamma function, $\Gamma(a)$ is the Gamma function, $Q_m(a, b)$ is the Marcum Q_m function [51, Equation 1], $u = \frac{M}{2}$, and the relationship between the probability of detection and the signal to noise ratio has been emphasised for later convenience.

3.2.2 Receivers with MRC diversity

In maximal ratio combiner systems, the received signals on each branch are weighted and combined, as in Figure 2.20, to form a new received signal, $r(t)$, which is given by

$$\begin{aligned} r(t) &= \sum_{i=1}^{n} w_i r_i(t) \\ &= \sum_{i=1}^{n} h_i(h_i s(t) + n_i(t)) \\ &= \sum_{i=1}^{n} h_i^2 s(t) + \sum_{i=1}^{n} h_i n_i(t), \end{aligned} \tag{3.13}$$

where the weight functions, $w_1, w_2 \ldots w_n$, are those specified in (2.28).

The received signal can be thought of as having been transmitted through a channel, that is

$$r(t) = gs(t) + n(t) \tag{3.14}$$

where $g = \sum_{i=1}^{n} h_i^2$ represents the channel gain and $n(t) = \sum_{i=1}^{n} h_i n_i(t)$ represents the time-varying noise interference.

Noting that $\mathbb{E}[n(t)] = 0$, the power contained in $n(t)$ is given by

$$\begin{aligned}
\mathbb{E}[n^2(t)] &= \mathbb{E}\left[\left(\sum_{i=1}^{n} h_i n_i(t)\right)^2\right] \\
&= \mathbb{E}[h_1^2 n_1^2(t) + h_1 h_2 n_1(t) n_2(t) + \ldots + h_n^2 n_n^2(t)] \\
&= \mathbb{E}[h_1^2 n_1^2(t)] + \mathbb{E}[h_1 h_2 n_1(t) n_2(t)] + \ldots + \mathbb{E}[h_n^2 n_n^2(t)] \\
&= h_1^2\,\mathbb{E}[n_1^2(t)] + h_2^2\,\mathbb{E}[n_2^2(t)] + \ldots + h_n^2\,\mathbb{E}[n_n^2(t)] \\
&= \sum_{i=1}^{n} h_i^2\,\mathbb{E}[n_i^2(t)] \\
&= g\sigma^2. \qquad (3.15)
\end{aligned}$$

Thus, the signal to noise ratio at the output of the MRC combiner, γ_{MRC}, is given by

$$\begin{aligned}
\gamma_{MRC} &= \frac{g^2 P_s}{\mathbb{E}[n^2(t)]} \\
&= \frac{g P_s}{\sigma^2}. \qquad (3.16)
\end{aligned}$$

Using (2.14), (3.16) can be further simplified as

$$\gamma_{MRC} = \sum_{i=1}^{n} \gamma_i, \qquad (3.17)$$

where γ_i is the signal to noise ratio on the i^{th} branch of the receiver [52].

Thus, if $r(t)$ is sampled and input into an energy detector, as in (3.9), then the resulting normalised test statistic will be distributed according to

$$\hat{x} \sim \begin{cases} \chi_M^2, & H_0, \\ \chi_M^2(M\gamma_{MRC}), & H_1. \end{cases} \qquad (3.18)$$

Consequently, the decision probabilities will be as in (3.11) and (3.12), with γ_{MRC} replacing γ_{ND} in the latter case, as shown in Table 3.1 [52].

Table 3.1: Decision probabilities for various diversity receiver architectures operating on AWGN channels.

X	P_{f_X}	$P_{d_X}(\gamma_X)$
ND	$\frac{\Gamma\left(u,\frac{\lambda}{2}\right)}{\Gamma(u)}$	$Q_u\left(\sqrt{M\gamma_{ND}},\sqrt{\lambda}\right)$
MRC	$\frac{\Gamma\left(u,\frac{\lambda}{2}\right)}{\Gamma(u)}$	$Q_u\left(\sqrt{M\gamma_{MRC}},\sqrt{\lambda}\right)$
EGC	$\frac{\Gamma\left(u,\frac{\lambda}{2}\right)}{\Gamma(u)}$	$Q_u\left(\sqrt{M\gamma_{EGC}},\sqrt{\lambda}\right)$
SLC	$\frac{\Gamma\left(nu,\frac{\lambda}{2}\right)}{\Gamma(nu)}$	$Q_{nu}\left(\sqrt{M\gamma_{SLC}},\sqrt{\lambda}\right)$

3.2.3 Receivers with EGC diversity

In equal gain combiner systems, the received signals on each branch are once again combined, as in Figure 2.20, so that the signal at the combiner output is given by

$$\begin{aligned} r(t) &= \sum_{i=1}^{n} w_i r_i(t) \\ &= \sum_{i=1}^{n} (h_i s(t) + n_i(t)) \\ &= gs(t) + n(t), \end{aligned} \tag{3.19}$$

where $g = \sum_{i=1}^{n} h_i$ represents the channel gain, $n(t) = \sum_{i=1}^{n} n_i(t)$ is the time-varying noise interference at the output of the combiner, and the weight functions are specified in (2.29).

Again, noting that $\mathbb{E}[n(t)] = 0$, the average power of $n(t)$ is given by

$$\begin{aligned}\mathbb{E}[n^2(t)] &= \mathbb{E}\left[\left(\sum_{i=1}^{n} n_i(t)\right)^2\right] \\ &= \mathbb{E}[n_1^2(t) + n_1(t)n_2(t) + \ldots + n_n^2(t)] \\ &= \sum_{i=1}^{n} \mathbb{E}[n_i^2(t)] \\ &= n\sigma^2, \end{aligned} \tag{3.20}$$

and so the signal to noise ratio at the output of the combiner, γ_{EGC}, is given by

$$\begin{aligned}\gamma_{EGC} &= \frac{g^2 P_s}{\mathbb{E}[n^2(t)]} \\ &= \left(\frac{1}{\sqrt{n}} \sum_{i=1}^{n} h_i\right)^2 \frac{P_s}{\sigma^2}. \end{aligned} \tag{3.21}$$

Thus, if $r(t)$ is then sampled and input to an energy detector, the normalised test statistic is distributed [53] according to

$$\hat{x} \sim \begin{cases} \chi_M^2, & H_0, \\ \chi_M^2(M\gamma_{EGC}), & H_1. \end{cases} \tag{3.22}$$

Consequently, the decision probabilities are again as in (3.11) and (3.12), with γ_{EGC} replacing γ_{ND} in the latter case, as shown in Table 3.1.

3.2.4 Receivers with SLC diversity

In square law combiner systems, the test statistics from each branch are combined as in Figure 2.21. If the test statistics on each branch are normalised, as in (3.9), then the test statistic at the combiner output is given by

$$\hat{x} = \sum_{i=1}^{n} \hat{x}_i, \tag{3.23}$$

where $\hat{x}_i$ is the normalised test statistic on the i^{th} branch and is distributed according to

$$\hat{x}_i \sim \begin{cases} \chi_M^2, & H_0, \\ \chi_M^2(M\gamma_i), & H_1, \end{cases} \tag{3.24}$$

where γ_i is the signal to noise ratio on the i^{th} branch [13].

Therefore, $\hat{x}$ is the sum of n chi square distributed random variables when the channel

is unoccupied, and n noncentral chi square random variables when it is occupied, and so is distributed according to

$$\hat{x} \sim \begin{cases} \chi^2_{Mn}, & H_0, \\ \chi^2_{Mn}(M\gamma_{SLC}), & H_1, \end{cases} \tag{3.25}$$

where γ_{SLC} is the signal to noise ratio at the output of the combiner [50], and is given by

$$\gamma_{SLC} = \sum_{i=1}^{n} \gamma_i. \tag{3.26}$$

The resulting decision probabilities are given in Table 3.1.

3.3 Energy detection in multipath fading environments

3.3.1 A brief history of the state of the art

While Urkowitz presented a thorough analysis of the operation of the energy detector in AWGN channels in 1967, it wasn't until 2002, and the work of Kostylev, that attention turned to its analysis under other channel models. In fact, research interest in the topic appears to be directly related to a widespread increase in interest in dynamic spectrum access, as can be seen in Figure 3.2. As energy detection has emerged as a key enabling technology for spectrum sensing, this may not be very surprising, but it does serve to illustrate that the research area is relatively new, and that the community of researchers involved in it produce a relatively small number of publications each year. In fact, many of the contributions in this thesis rely on the advances made by these researchers. Thus, a concise history of the research in the area over the past decade is not only feasible, but critical to the understanding of the work in later chapters.

Kostylev [54] first derived exact expressions for the probability of detection of energy detectors operating in Rayleigh, Rice and Nakagami-m channels. However, many of his results required numerical integration or infinite summation to evaluate, and he did not consider diversity receivers. Digham et al. [11] later pointed out that there were both typographical and mathematical errors in Kostylev's work, and provided corrections, so it is not considered further, and is only mentioned as a matter of historical interest.

Digham et al. extended Kostylev's analysis to SLC systems with *independent and identically distributed* (i.i.d.) Rayleigh-faded branches [11], later refining their results and extending their analysis to include the effect of correlation between different branches [50]. However, the scope of their work was also limited. For instance, while the performance of SLC systems in Rayleigh faded channels was considered, the analysis was not extended to Nakagami-m and Rice channels. Furthermore, in the case of Rice fading

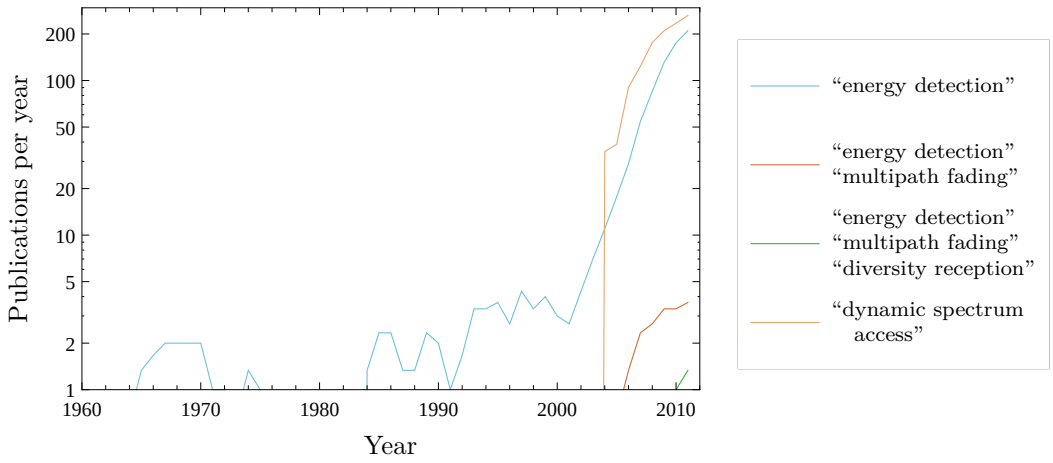

Figure 3.2: A logarithmic plot of the number of publications per year as a function of time, for the search phrases indicated in the legend. The figures were generated using IEEE Xplore, smoothed using a three year moving average filter, and are accurate as of September 29$^{\text{th}}$ 2013.

with no diversity, Digham et al. were only able to provide a closed form solution for the trivial case where $M = 2$.

Herath [55] extended Digham et al.'s work on SLC systems for the more general case of i.i.d. Nakagami-m fading, while Herath et al. [52] presented alternative formulations for the probability of detection of energy detectors with no diversity in Rayleigh, Nakagami-m and Rice channels. Herath et al. [52] were also the first to publish on the effect of i.i.d. Rayleigh and Nakagami-m fading on systems with MRC diversity, while Herath and Rajatheva [56] first considered the analysis of energy detectors with EGC diversity on i.i.d. Rayleigh and Nakagami-m channels.

In 2011, Annamalai et al. [57] developed new representations for the probability of detection of energy detectors with no diversity, MRC diversity and SLC diversity, in AWGN channels, and then derived new expressions for the probability of detection of these systems in independent and identically distributed Rayleigh, Nakagami-m and Rice channels. Olabiyi and Annamalai presented refinements of the work in later publications, providing alternative infinite series expressions [58, 59] and extending their analysis for composite Nakagami-m / log-normal channels [60].

Independently, Sun et al. considered the effects of i.i.d. Nakagami-m fading on energy detectors with no diversity, MRC diversity and SLC diversity [61], developing infinite series based expressions similar to Annamalai et al., while Sun supplemented these results with an analysis of the effect of Rice fading on energy detectors with no diversity in his Ph.D. thesis [62].

Several authors have also considered the case of *independent and non-identically distributed* (i.n.d.) and correlated channels. Annamalai et al. [57] considered the effect of i.n.d. Rayleigh, Nakagami-m and Rice fading on energy detectors with MRC and SLC

diversity, deriving further infinite series based expressions for the detection probabilities in each case. Similarly, Banjade et al. [63] consider the effects of correlated Rayleigh and Nakagami-m fading. However, while their analysis considers several different correlation models, it is limited to the analysis of energy detectors with SLC diversity only and requires the computation of high order residues, which may not be practical in many circumstances.

Finally, several authors have derived approximations for the decision probabilities in Rayleigh and Nakagami-m fading channels. Ghasemi and Sousa [64] first considered an approximation based technique for energy detectors with no diversity operating in Rayleigh faded channels, while López-Benítez and Casadevall [65] derived an alternative expression to Ghasemi and Sousa using an approximation they developed for the error function. Atapattu et al. derived a similar result, and extended the analysis to include Nakagami-m channels and SLC systems [66, 67]. The idea of approximation based techniques is returned to in later chapters; for now, consideration is given to exact expressions for the decision probabilities only.

3.3.2 General expressions for the decision probabilities

In Sections 2.2.3 and 2.2.4, it was discussed how the Rayleigh channel is a special case of both the Nakagami-m channel and the Rice channel. Consequently, to avoid repetition, henceforth, only formulations relating to the Nakagami-m and Rice channels will be presented. These can then be specialised to the Rayleigh channel using the appropriate simplification. Furthermore, henceforth, the notation $f_{X,Y}(x)$ shall be used to denote the probability density function of the signal to noise ratio at the input to the energy detector with diversity type X operating on a channel of type Y.

For the diversity type X, the probability of detection for an energy detector in a fading channel Y, $P_{d_{X,Y}}$, is given [11, 52] by its probability of detection in an AWGN channel averaged with respect to the probability density function of the signal to noise ratio at the input to the energy detector, that is

$$\begin{aligned} P_{d_{X,Y}} &= \mathbb{E}[P_{d_X}(\gamma_X)] \\ &= \int_{-\infty}^{\infty} P_{d_X}(x) f_{X,Y}(x) dx. \end{aligned} \tag{3.27}$$

Expressions for the probabilities of false alarm of diversity receivers operating on fading channels can be arrived at in a similar manner. However, regardless of the diversity type, the probability of false alarm does not depend on the signal to noise ratio (see Table 3.1), and so there is no variation under Nakagami-m and Rice fading, that is

$$P_{f_{X,Y}} = P_{f_X}, \tag{3.28}$$

where $P_{f_{X,Y}}$ denotes the probability of false alarm for an energy detector of diversity type X operating on a fading channel Y.

3.3.3 Receivers with no diversity

For receivers with no diversity, $f_{ND,Nak}(x)$ and $f_{ND,Rice}(x)$ are given by (2.17) and (2.18), respectively, that is

$$f_{ND,Nak}(x) = \begin{cases} 0, & x < 0, \\ \left(\frac{m}{\bar{\gamma}}\right)^m \frac{x^{m-1}}{\Gamma(m)} e^{-\frac{mx}{\bar{\gamma}}}, & x \geq 0, \end{cases} \tag{3.29}$$

$$f_{ND,Rice}(x) = \begin{cases} 0, & x < 0, \\ \left(\frac{K+1}{\bar{\gamma}}\right) e^{-K-\frac{(K+1)x}{\bar{\gamma}}} I_0\left(2\sqrt{\frac{K(K+1)x}{\bar{\gamma}}}\right), & x \geq 0. \end{cases} \tag{3.30}$$

Thus, $P_{d_{ND,Nak}}$ can be evaluated by substituting (3.12) and (3.29) into (3.27) and letting $\gamma_{ND} = x$, while $P_{d_{ND,Rice}}$ can be evaluated by substituting (3.12) and (3.30) into (3.27) and letting $\gamma_{ND} = x$.

A list of different formulations for $P_{d_{ND,Nak}}$ and $P_{d_{ND,Rice}}$, derived by the authors[2] discussed in Section 3.3.1, is given in Table 3.2, where ${}_1F_1(a;b;z)$ denotes the confluent hypergeometric function [68, Equation 13.2.2], $L_n(z)$ denotes the Laguerre polynomial of degree n [69, Equation 8.970], and the variables

$$\beta = \frac{m}{m + u\bar{\gamma}}, \tag{3.31}$$

$$\Omega = \frac{K+1}{K+1+u\bar{\gamma}}, \tag{3.32}$$

have been used to simplify the notation somewhat. Although there is some variation in the formulations, the equations listed in Table 3.2 are all equivalent methods for calculating $P_{d_{ND,Nak}}$ or $P_{d_{ND,Rice}}$, respectively.

3.3.4 Receivers with MRC diversity

For maximal ratio combiner systems, the signal to noise ratio at the output of the combiner is the sum of the signal to noise ratio on each branch, as in (3.17). Under

[2]While it is not usual to reproduce the work of others in this way, there are good reasons for doing so: firstly, because the later work in this thesis will draw comparisons with the exact formulations presented here, and so the tables will serve as a convenient reference; and also, because each of the authors discussed in Section 3.3.1 adopts a unique notation, and so a reproduction of their results here, in a standard notation, will help the reader to understand the key differences between the different formulations and facilitate the reproduction of results presented later in this thesis.

Source	$P_{d_{ND,Nak}}$	$P_{d_{ND,Rice}}$
Annamalai et al. [57–59]	$1-\beta^m\sum_{k=0}^{\infty}\frac{\Gamma(k+m)}{\Gamma(m)k!}\left(1-\frac{\Gamma(k+u,\frac{\lambda}{2})}{\Gamma(k+u)}\right)(1-\beta)^k$	$1-e^{-K(1-\Omega)}\,\Omega\sum_{k=0}^{\infty}k!\left(1-\frac{\Gamma(k+u,\frac{\lambda}{2})}{\Gamma(k+u)}\right)(1-\Omega)^k\sum_{i=0}^{k}\left(\frac{1}{(i!)^2(k-i)!}\right)(K\Omega)^i$
Digham et al. [11, 50]	$e^{-\frac{\lambda\beta}{2m}}\beta^{m-1}L_{m-1}\left(-\frac{\lambda}{2}(1-\beta)\right)$ $+e^{-\frac{\lambda\beta}{2m}}(1-\beta)\sum_{k=0}^{m-2}\beta^k L_i\left(-\frac{\lambda}{2}(1-\beta)\right)$ $+e^{-\frac{\lambda}{2}}\beta^m\sum_{k=1}^{u-1}\frac{\left(\frac{\lambda}{2}\right)^k}{k!}\,{}_1F_1\left(m;k+1;\frac{\lambda}{2}(1-\beta)\right)$	$Q_1\left(\sqrt{2K(1-\Omega)},\sqrt{\lambda\Omega}\right)$, for two samples (i.e. $M=2$) only
Herath et al. [52, 55]	$1-e^{-\frac{\lambda}{2}}\beta^m\sum_{k=u}^{\infty}\frac{\left(\frac{\lambda}{2}\right)^k}{k!}\,{}_1F_1\left(m;k+1;\frac{\lambda}{2}(1-\beta)\right)$	$e^{-K(1-\Omega)-\frac{\lambda}{2}}\,\Omega\sum_{k=1}^{\infty}\frac{(K(1-\Omega)\Omega)^{k-1}}{(k-1)!}\left(\frac{1}{(k-1)!}\frac{d^{k-1}}{dz^{k-1}}\left[\frac{e^{\frac{\lambda}{2}z}}{(1-z)z^{u-1}}\right]\Big\|_{z=1-\Omega}\right.$ $\left.+\frac{1}{(u-2)!}\frac{d^{u-2}}{dz^{u-2}}\left[\frac{e^{\frac{\lambda}{2}z}}{(1-z)(z-(1-\Omega))^k}\right]\Big\|_{z=0}\right)$
Sun et al. [61, 62]	$1-e^{-\frac{\lambda}{2}}\beta^m\sum_{k=u}^{\infty}\frac{\left(\frac{\lambda}{2}\right)^k}{k!}\sum_{l=0}^{k-u}\frac{\Gamma(l+m)}{\Gamma(m)l!}(1-\beta)^l$	$1-e^{-K-\frac{\lambda}{2}}\,\Omega\sum_{k=u}^{\infty}\frac{\left(\frac{\lambda}{2}\right)^k}{k!}\sum_{l=0}^{k-u}(1-\Omega)^l\,{}_1F_1\left(l+1;1;K\Omega\right)$

Table 3.2: Probabilities of detection for energy detectors with no diversity operating on Nakagami-m and Rice channels. The equations can be specialised to Rayleigh fading by letting $m=1$ in $P_{d_{ND,Nak}}$ or $K=0$ in $P_{d_{ND,Rice}}$.

i.i.d. Nakagami-m fading, the signal to noise ratio on each branch follows a gamma distribution with shape parameter, m, and scale parameter, $\frac{\bar{\gamma}}{m}$, as in (3.29). Thus, the signal to noise ratio at the combiner output is the sum of n such gamma distributed random variables, and so follows a gamma distribution [70] with shape parameter, mn, and scale parameter, $\frac{\bar{\gamma}}{m}$. Consequently, its probability density function, $f_{MRC,Nak}(x)$, is given by

$$f_{MRC,Nak}(x) = \begin{cases} 0, & x < 0, \\ \left(\frac{m}{\bar{\gamma}}\right)^{mn} \frac{x^{mn-1}}{\Gamma(mn)} e^{-\frac{mx}{\bar{\gamma}}}, & x \geq 0. \end{cases} \tag{3.33}$$

The probability density function of the signal to noise ratio at the output of the combiner under i.i.d. Rice fading is derived in a different manner. Recalling (3.16), the signal to noise ratio at the combiner output is related to the sum of the squares of the channel responses on each branch. As discussed in Section 2.2.4, these responses are modelled as Rice distributed random variables. Thus, the signal to noise ratio at the output of the combiner depends on the sum of the squares of n i.i.d. Rice distributed random variables, and so follows a scaled noncentral chi square distribution with $2n$ degrees of freedom and noncentrality parameter equal to $2Kn$ [71]. Consequently, its probability density function, $f_{MRC,Rice}(x)$, is given by

$$f_{MRC,Rice}(x) = \begin{cases} 0, & x < 0, \\ \left(\frac{K+1}{\bar{\gamma}}\right)^{\frac{n+1}{2}} \left(\frac{x}{Kn}\right)^{\frac{n-1}{2}} e^{-Kn-\frac{(K+1)x}{\bar{\gamma}}} I_{n-1}\left(2\sqrt{\frac{Kn(K+1)x}{\bar{\gamma}}}\right), & x \geq 0. \end{cases} \tag{3.34}$$

A list of different formulations for $P_{d_{MRC,Nak}}$ and $P_{d_{MRC,Rice}}$, derived by the authors discussed in Section 3.3.1, is given in Table 3.3.

3.3.5 Receivers with EGC diversity

In equal gain combiner systems, the signal to noise ratio at the combiner output is given by (3.21), and depends on the sum of the channel gains, h_i. Thus, under i.i.d. Nakagami-m or Rice fading, the signal to noise ratio at the output of the combiner depends on the sum of n i.i.d. Nakagami-m or Rice distributed random variables, respectively. However, the distributions of the sums of such variables are known to be difficult to evaluate [14, 41, 71–73].

Dharmawansa et al. [74] and Rahman and Harada [75] derived exact expressions for the probability density function of γ_{EGC} under Nakagami-m fading but in forms which, in practice, require truncation and are difficult to evaluate when $n > 2$. Herath used Dharmawansa et al.'s formulation to derive a formulation for $P_{d_{EGC,Nak}}$, but noted that the complexity of his solution increased sharply with the number of diversity branches,

Source	$P_{d_{MRC,Nak}}$	$P_{d_{MRC,Rice}}$
Annamalai et al. [57–59]	$1-\beta^{mn}\sum_{k=0}^{\infty}\frac{\Gamma(k+mn)}{\Gamma(mn)k!}\left(1-\frac{\Gamma(k+u,\frac{\lambda}{2})}{\Gamma(k+u)}\right)(1-\beta)^k$	$1-e^{-Kn(1-\Omega)}\,\Omega^n\sum_{k=0}^{\infty}\left(1-\frac{\Gamma(k+u,\frac{\lambda}{2})}{\Gamma(k+u)}\right)(1-\Omega)^k \times\sum_{i=0}^{k}\frac{\Gamma(k+n)}{i!(k-i)!\Gamma(n+i)}(Kn\Omega)^i$
Herath et al. [52, 55]	$1-e^{-\frac{\lambda}{2}}\beta^{mn}\sum_{k=u}^{\infty}\frac{\left(\frac{\lambda}{2}\right)^k}{k!}\,{}_1F_1\left(mn;k+1;\frac{\lambda}{2}(1-\beta)\right)$	$e^{-Kn(1-\Omega)-\frac{\lambda}{2}}\,\Omega^n\sum_{k=1}^{\infty}\frac{(Kn(1-\Omega)\Omega)^{k-1}}{(k-1)!} \times\left(\frac{1}{(k+n-2)!}\frac{d^{k+n-2}}{dz^{k+n-2}}\left[\frac{e^{\frac{\lambda}{2}z}}{(1-z)z^{u-n}}\right]\Big\|_{z=1-\Omega} +\frac{1}{(u-n-1)!}\frac{d^{u-n-1}}{dz^{u-n-1}}\left[\frac{e^{\frac{\lambda}{2}z}}{(1-z)(z-(1-\Omega))^{k+n-1}}\right]\Big\|_{z=0}\right)$
Sun et al. [61, 62]	$1-\beta^{mn}\sum_{k=0}^{\infty}\frac{\Gamma(k+mn)}{\Gamma(mn)k!}\left(1-\frac{\Gamma(k+u,\frac{\lambda}{2})}{\Gamma(k+u)}\right)(1-\beta)^k$	-

Table 3.3: Decision probabilities for energy detectors with MRC diversity operating on Nakagami-m and Rice channels. The equations can be specialised to Rayleigh fading by letting $m=1$ in $P_{d_{MRC,Nak}}$ or $K=0$ in $P_{d_{MRC,Rice}}$. As Digham et al. did not consider MRC systems under Nakagami-m and Rice fading, and Sun et al. did not consider MRC systems under Rice fading, no results are listed in these cases.

and that computing the truncation points for $n > 3$ is a difficult problem [55]. Herath's formulations for $n = 2$ and $n = 3$ are reproduced in Table 3.4.

However, the problem is not intractable. Nakagami [72] proposed an approximation for the sum of i.i.d. Nakagami-m random variables, which models the signal to noise ratio at the EGC output as a gamma distributed random variable, with shape parameter, mn, and scale parameter, $\frac{\omega\bar{\gamma}}{mn}$, so that the exact probability density function, $f_{EGC,Nak}(x)$, can be closely approximated as

$$f_{EGC,Nak}(x) \approx \hat{f}_{EGC,Nak}(x) = \begin{cases} 0, & x < 0, \\ \left(\frac{mn}{\omega\bar{\gamma}}\right)^{mn} \frac{x^{mn-1}}{\Gamma(mn)} e^{-\frac{mnx}{\omega\bar{\gamma}}}, & x \geq 0, \end{cases} \tag{3.35}$$

where

$$\omega = 1 + \frac{n-1}{m}\left(\frac{\Gamma(m+\frac{1}{2})}{\Gamma(m)}\right)^2. \tag{3.36}$$

Plots of the exact and approximate probability density functions for different parameter sets are shown in Figure 3.3(a). As can be seen, the proposed approximation is quite accurate in many scenarios of interest. Dharmawansa et al. have also found that Nakagami's approximation is quite accurate across a wide range of values [74].

To the best of the author's knowledge at the time of writing, no exact closed form representation for the probability density function of the sum of i.i.d. Rice distributed random variables is available in the literature. Abu-Dayya and Beaulieu derived an exact infinite series representation [76], but Hu and Beaulieu note that its computation is difficult due to its inherent complexity [71]. However, Hu and Beaulieu and López-Salcedo [73] have derived approximations which were found to be accurate across a wide range of values. Both approximations rely on look up tables of fitted constants, which must be calculated in advance using a numerical method. Of these, Hu and Beaulieu's approximation depends on the smallest number of fitted constants and is particularly suited to the method of integration used in later chapters, proposing that the probability density function of the signal to noise ratio at the combiner output can be closely approximated by a scaled noncentral chi square distribution with $2n$ degrees of freedom and a noncentrality parameter equal to $\frac{2Kn}{a}$. Thus, the PDF of the signal to noise ratio at the output of an equal gain combiner, $f_{EGC,Rice}(x)$, can be approximated as

$$\hat{f}_{EGC,Rice}(x) = \begin{cases} 0, & x < 0, \\ \left(\frac{K+1}{b\bar{\gamma}}\right)^{\frac{n+1}{2}} \left(\frac{ax}{Kn}\right)^{\frac{n-1}{2}} e^{-\frac{Kn}{a}-\frac{(K+1)x}{b\bar{\gamma}}} I_{n-1}\left(2\sqrt{\frac{Kn(K+1)x}{ab\bar{\gamma}}}\right), & x \geq 0, \end{cases} \tag{3.37}$$

where a and b are constants and are given in Table 3.5. Plots of the exact and approximate probability density functions for different parameter sets are shown in Figure

Source	$P_{d_{EGC,Nak}}$
Herath et al. [56]	$1-e^{-\frac{\lambda}{2}}\sum_{k=u}^{\infty}\frac{\left(\frac{\lambda}{2}\right)^k}{k!}\sum_{l=0}^{\infty}\left(\frac{2m}{2m+\bar{\gamma}}\right)^{2m+l}\left(\frac{1}{2^{4m+l-2}}\right)\left(\frac{\Gamma(\frac{1}{2})\Gamma^2(2m+l)}{\Gamma(l+1)\Gamma^2(m)\Gamma(2m+l+\frac{1}{2})}\right)$ $\times\ {}_1F_1\left(2m+l;k+1;\frac{\lambda}{2}\left(\frac{\bar{\gamma}}{2m+\bar{\gamma}}\right)\right)$, for $n=2$ only
	$1-e^{-\frac{\lambda}{2}}\sum_{k=u}^{\infty}\frac{\left(\frac{\lambda}{2}\right)^k}{k!}\sum_{l=0}^{\infty}\sum_{p=0}^{\infty}\left(\frac{3m}{3m+\bar{\gamma}}\right)^{3m+l+p}\left(\frac{1}{2^{4m+l+p-3}}\right)\left(\frac{\Gamma(\frac{1}{2})\Gamma(2m+l)\Gamma(2m+p)\Gamma(3m+l)\Gamma(3m+l+\frac{1}{2})\Gamma(4m+2l+p)}{\Gamma(l+1)\Gamma(p+1)\Gamma^3(m)\Gamma(2m+l+\frac{1}{2})\Gamma(3m+l+p+\frac{1}{2})\Gamma(6m+2l)}\right)$ $\times\ {}_1F_1\left(3m+l+p;k+1;\frac{\lambda}{2}\left(\frac{\bar{\gamma}}{3m+\bar{\gamma}}\right)\right)$, for $n=3$ only

Table 3.4: Decision probabilities for energy detectors with EGC diversity operating on Nakagami-m channels. The equations can be specialised to Rayleigh fading by letting $m=1$.

Table 3.5: Values of the constants a and b.

		n						
		2	3	4	5	6	7	8
$K = 1\,\text{dB}$	a	1.32278	1.37013	1.41124	1.43405	1.45500	1.46733	1.46425
	b	1.02794	1.02880	1.03355	1.03485	1.03701	1.03788	1.03528
$K = 3\,\text{dB}$	a	1.22281	1.25660	1.27920	1.29307	1.30535	1.31207	1.30927
	b	1.03172	1.03520	1.03919	1.04069	1.04269	1.04319	1.04019
$K = 5\,\text{dB}$	a	1.15570	1.17752	1.19070	1.19954	1.20586	1.21157	1.21857
	b	1.03379	1.03731	1.03967	1.04143	1.04261	1.04379	1.04556
$K = 7\,\text{dB}$	a	1.10170	1.11704	1.12438	1.13027	1.13544	1.13766	1.13470
	b	1.02660	1.03082	1.03293	1.03434	1.03575	1.03646	1.03575

3.3(b). As can be seen, the approximation is quite accurate in many cases, although it becomes less accurate outside the range of values of K for which a and b are available. In such cases, the values of the constants must be extrapolated from the available data points, which can lead to less accurate results. Still, the approximation is a convenient one and will be useful in Chapter 6.

3.3.6 Receivers with SLC diversity

In square law combiner systems, the signal to noise ratio at the output of the combiner is simply the sum of the signal to noise ratios on each branch, as in (3.26). Thus, the signal to noise ratio at the combiner output in SLC systems follows the same distribution as the signal to noise ratio at the combiner output in MRC systems, and so $f_{_{SLC,Nak}}(x)$ and $f_{_{SLC,Rice}}(x)$ are given by (3.33) and (3.34), respectively.

A list of different formulations for $P_{d_{SLC,Nak}}$ and $P_{d_{SLC,Rice}}$, derived by the authors discussed in Section 3.3.1, is given in Table 3.6.

3.4 Discussion

In this chapter, the operation of the energy detector in AWGN and multipath fading channels was discussed. In the AWGN case, Urkowitz's analysis was used to derive expressions for the decision probabilities of different diversity receivers; in the case of multipath fading channels, expressions for the probability density function of the signal to noise ratio at the combiner output for each diversity and fading channel type were derived and alternative expressions for the decision probabilities available in the literature were tabulated. It is worth giving some further consideration to these expressions.

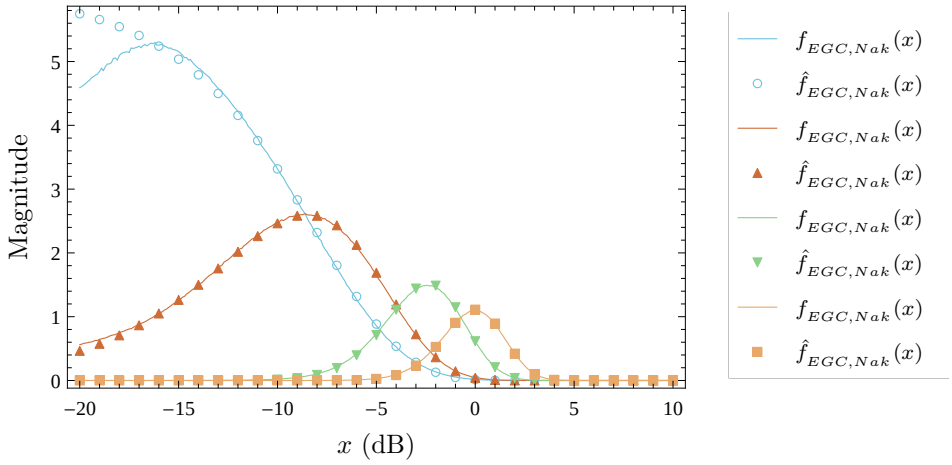

(a) Plots of $f_{EGC,Nak}(x)$ and $\hat{f}_{EGC,Nak}(x)$ for the scenarios where $\bar{\gamma} = -10$dB, $m = \frac{1}{2}$, $n = 2$ (blue), $\bar{\gamma} = -8$dB, $m = 1$, $n = 2$ (red), $\bar{\gamma} = -6$dB, $m = 2$, $n = 3$ (green), and $\bar{\gamma} = -4$dB, $m = 3$, $n = 3$ (orange).

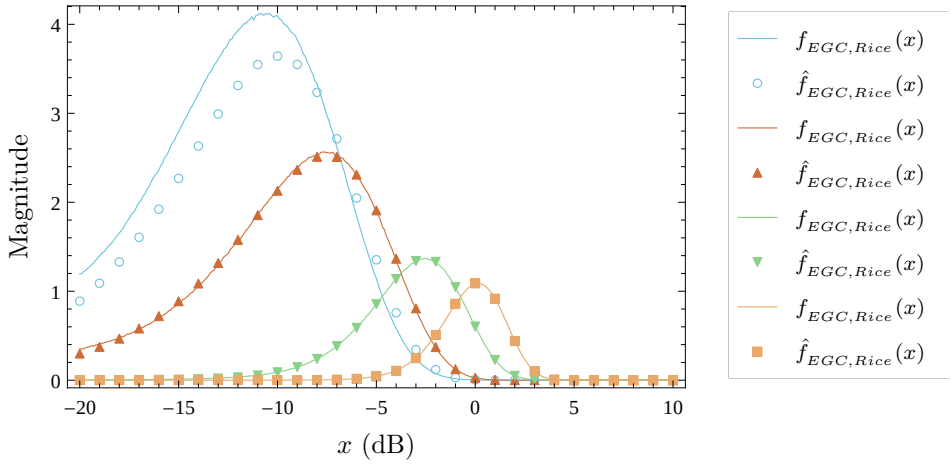

(b) Plots of $f_{EGC,Rice}(x)$ and $\hat{f}_{EGC,Rice}(x)$ for the scenarios where $\bar{\gamma} = -10$dB, $K = 0$, $n = 2$ (blue), $\bar{\gamma} = -8$dB, $K = 1$, $n = 2$ (red), $\bar{\gamma} = -6$dB, $K = 2$, $n = 3$ (green), and $\bar{\gamma} = -4$dB, $K = 5$, $n = 3$ (orange).

Figure 3.3: Plots of the exact and approximate probability density functions of the signal to noise ratio at the output of an equal gain combiner in Nakagami-m and Rice channels.

The motivation for deriving exact expressions for the decision probabilities in multipath fading channels is two-fold: firstly, to avoid having to use expensive numerical integration techniques to evaluate the general integral in (3.27) and, secondly, to provide some deeper insight into the operation of diversity systems under multipath fading conditions. Indeed, Digham et al.'s primary criticism of Kostylev's work was that it lacked closed form results [11].

However, most of the expressions discussed in this chapter are not closed form results. For instance, in Table 3.2, six of the formulations involve the summation of infinite series. In these cases, the probability of detection must be computed either by numerical summation or by truncating the infinite series and summing the remainder. However, if the series is truncated, then the position of the truncation point itself must be calculated using a numerical method [55, 57, 62].

Furthermore, while Digham et al.'s expression for $P_{d_{ND,Nak}}$ is not in the form of an infinite series, it does feature a series requiring $u-2$ terms to be computed. Recalling that $u = \frac{M}{2}$, and that M is often large, as in Figure 2.15, this formulation potentially requires tens of thousands of terms to be evaluated.

The truncated infinite series approach has the same drawback. Figure 3.4(a) shows the values of the truncation point required to give a maximum absolute error of 10^{-6} when calculating $P_{d_{ND,Nak}}$, that is

$$\begin{aligned} \epsilon^{T}_{X,Y} &= \mid P_{d_{X,Y}} - P^{T}_{d_{X,Y}} \mid \\ &\leq 10^{-6}, \end{aligned} \tag{3.38}$$

where $\epsilon^{T}_{X,Y}$ denotes the absolute truncation error[3] for diversity type X and channel type Y, and $P^{T}_{d_{X,Y}}$ is the truncated version of the infinite series formulation $P_{d_{X,Y}}$. As can be seen, for small numbers of samples, the truncation point is quite small, but increases rapidly as M becomes larger. The truncation points for $P_{d_{MRC,Nak}}$ demonstrate similar behaviour, as can be seen in Figure 3.4(b), while the problem becomes worse for SLC systems, as shown in Figure 3.4(c). Figure 3.4(d) demonstrates that a similar trend exists for Annamalai et al.'s formulations for $P_{d_{ND,Rice}}$, $P_{d_{MRC,Rice}}$ and $P_{d_{SLC,Rice}}$. In short, for the values of M likely to be encountered in real world scenarios, all these infinite series require large numbers of terms to be computed.

[3]Ideally, the truncation error should describe the difference between the precise value of the infinite series and its truncated counterpart. However, computational limitations prevent this and so the infinite series itself is subject to some truncation. Using numerical methods, it is possible to ensure that the error resulting from this truncation is very small, allowing the accurate calculation of (3.38). Consequently, throughout the remainder of this work, wherever the precise value of a fading channel detection probability is specified, it should be taken to be its true value within a tolerance of 10^{-10}. The tolerance of other numerical calculations used in this work (e.g. infinite series, infinite integrals and root finding methods) is subject to a similar warning. Unless otherwise specified, such calculations should be understood to have been computed using Mathematica 9, with a `$MachinePrecision` value of $53\log_{10} 2$ and default `AccuracyGoal` and `PrecisionGoal` values.

Source	$P_{d_{SLC,Nak}}$	$P_{d_{SLC,Rice}}$
Annamalai et al. [57–59]	$1-\beta^{mn}\sum_{k=0}^{\infty}\frac{\Gamma(k+mn)}{\Gamma(mn)k!}\left(1-\frac{\Gamma(k+nu,\frac{\lambda}{2})}{\Gamma(k+nu)}\right)(1-\beta)^k$	$1-e^{-Kn(1-\Omega)}\,\Omega^n\sum_{k=0}^{\infty}\left(1-\frac{\Gamma(k+nu,\frac{\lambda}{2})}{\Gamma(k+nu)}\right)(1-\Omega)^k \times\sum_{i=0}^{k}\frac{\Gamma(k+n)}{i!(k-i)!\Gamma(n+i)}(Kn\Omega)^i$
Herath et al. [52, 55]	$1-e^{-\frac{\lambda}{2}}\beta^{mn}\sum_{k=nu}^{\infty}\frac{\left(\frac{\lambda}{2}\right)^k}{k!}\,{}_1F_1\left(mn;k+1;\frac{\lambda}{2}(1-\beta)\right)$	-
Sun et al. [61, 62]	$1-\beta^{mn}\sum_{k=0}^{\infty}\frac{\Gamma(k+mn)}{\Gamma(mn)k!}\left(1-\frac{\Gamma(k+nu,\frac{\lambda}{2})}{\Gamma(k+nu)}\right)(1-\beta)^k$	-

Table 3.6: Decision probabilities for energy detectors with SLC diversity operating on Nakagami-m and Rice channels. The equations can be specialised to Rayleigh fading by letting $m=1$ in $P_{d_{SLC,Nak}}$ or $K=0$ in $P_{d_{SLC,Rice}}$. As Digham et al. did not consider SLC systems under Nakagami-m and Rice fading, and Herath et al. and Sun et al. did not consider SLC systems under Rice fading, no results are listed in these cases.

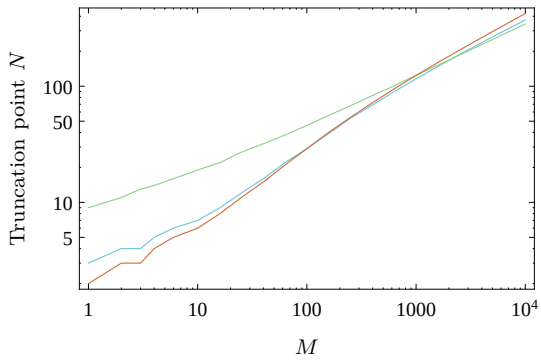

(a) A log-log plot of the truncation point required for Annamalai et al.'s (blue), Sun et al.'s (red) and Herath et al.'s (green) formulations for $P_{d_{ND,Nak}}$ with $m = 2$ and $\bar{\gamma} = -10\,\text{dB}$.

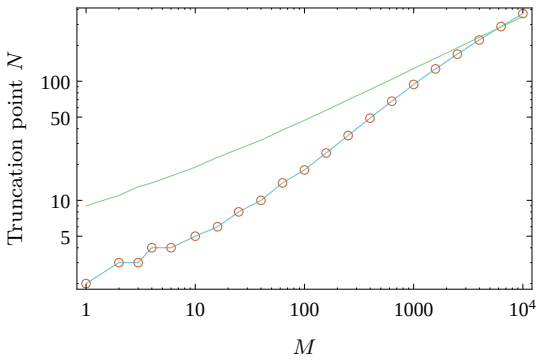

(b) A log-log plot of the truncation point required for Annamalai et al.'s (blue), Sun et al.'s (red circles) and Herath et al.'s (green) formulations for $P_{d_{MRC,Nak}}$ with $m = 1$, $n = 3$ and $\bar{\gamma} = -18\,\text{dB}$.

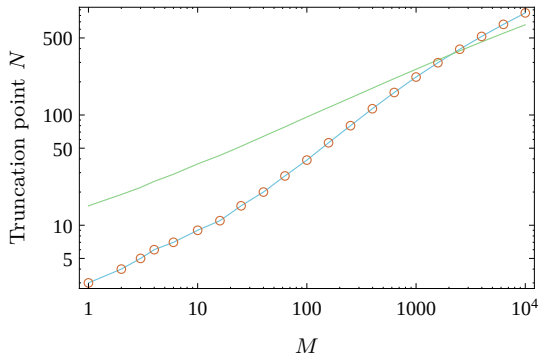

(c) A log-log plot of the truncation point required for Annamalai et al.'s (blue), Sun et al.'s (red circles) and Herath et al.'s (green) formulations for $P_{d_{SLC,Nak}}$ with $m = 1$, $n = 5$ and $\bar{\gamma} = -15\,\text{dB}$.

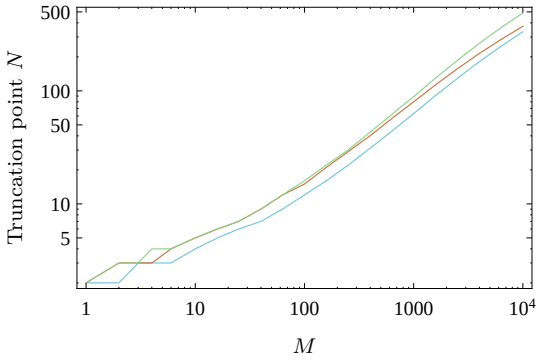

(d) A log-log plot of the truncation point required for Annamalai et al.'s formulations for $P_{d_{ND,Rice}}$ (blue), $P_{d_{MRC,Rice}}$ (red) and $P_{d_{SLC,Rice}}$ (green) with $K = 5$, $n = 2$ and $\bar{\gamma} = -16\,\text{dB}$.

Figure 3.4: Log-log plots of the truncation point required to give $\epsilon^T_{X,Y} \leq 10^{-6}$ as functions of the number of samples, M. In each case, $P_{f_X} = 0.1$. From Tables 3.3 and 3.6, Sun et al.'s formulations for $P_{d_{MRC,Nak}}$ and $P_{d_{SLC,Nak}}$ are equivalent to Annamalai et al.'s, and so the truncation points are the same in these cases.

Furthermore, Herath's formulations for $P_{d_{ND,Rice}}$ and $P_{d_{MRC,Rice}}$ require high order differentiation, on the order of $u - 1$ and $u - n - 1$, respectively. These can be computed either numerically or symbolically. However, high order numerical derivatives can be susceptible to error due to floating point arithmetic [77, p. 226], and symbolic computation is only possible on computers with large amounts of memory [78, p. 10]. For the large values of u likely to be encountered in practice, neither method appears practical at present.

As a further drawback, most of the formulations considered in this chapter are so complicated that they do not readily enable astute system designs. For instance, if

the number of samples required to meet a specified probability of detection is to be calculated, in the manner of Figure 2.15, currently, this can only be done using a numerical method. Similarly, if the minimum signal to noise ratio detectable by the system is to be calculated, once again, a numerical method is required. In short, the lack of closed forms prevents the equations from being inverted easily and, thus, prevents tractable analysis of the behaviour of the system.

In fact, in many cases, the formulations are just restatements of the integral average given in (3.27). Consider the *probability mass function* (PMF) of the negative binomial distribution, $f(s; r, p)$, given by

$$f(s; r, p) = \frac{\Gamma(s + r)}{\Gamma(r)s!}(1 - p)^r p^s. \tag{3.39}$$

It can be shown that Annamalai et al.'s formulation for $P_{d_{ND,Nak}}$ is simply a discrete average over $f(k; m, 1 - \beta)$, while their formulation for $P_{d_{ND,Rice}}$ is simply a discrete average over $f(1; k, \Omega)$. As the formulations for each channel type are equivalent, it is not surprising to see elements of the same negative binomial PMFs in the other formulations for $P_{d_{ND,Nak}}$, and that a similar pattern holds for the MRC and SLC formulations in Tables 3.3 and 3.6.

Yet, none of this should be surprising. Analysing the effects of signal propagation is a complicated problem, and complicated problems often have complicated solutions. As Rosenblueth and Wiener [23] wrote: *the best material model for a cat is another, or preferably the same, cat.* If the exact values of the decision probabilities of diversity receivers in fading channels must be calculated, then there is an associated cost which must be accepted. The choice of numerical integration, numerical summation or series truncation is arbitrary, but a choice must be made.

However, Rosenblueth and Wiener also wrote that *no substantial part of the universe is so simple that it can be grasped and controlled without abstraction.* Thus, if a deep understanding of a particular aspect of a complicated system is to be gained, the model of that system must first be simplified appropriately.

These two points cannot be overstated. There is a fundamental trade off between simplicity and generality, and it is often misunderstood. Digham et al. criticised Kostylev for the lack of simplicity in his results, but subsequent efforts have been similarly flawed. While simple, exact and closed form representations may exist, if so, they have eluded discovery thus far, and may continue to do so for quite some time. Consequently, the remainder of this thesis concentrates on reducing the complexity of the exact mathematical models described in this chapter in an effort to derive simple yet accurate approximate representations for the decision probabilities of energy detector diversity receivers.

Chapter 4

AWGN channel analysis: an approximation-based approach

In this chapter, central limit theorem approximations for the distribution functions of chi square and noncentral chi square random variables are discussed. In order to quantify the resulting error, Berry-Esseen type bounds are considered, but are found to be too loose for many practical applications. Consequently, a novel method for the quantification of the error resulting from the use of the central limit theorem is proposed. Novel approximations for the decision probabilities of energy detector diversity receivers are then derived and the resulting error is quantified. Subsequently, some example uses of these approximations are given and it is shown that further simple and useful approximations for the analysis of other system parameters are readily obtainable.

4.1 Motivation

Energy detection is a broad topic, and has many applications. In the context of this thesis, however, its intended use is spectrum sensing, and so there is a particular emphasis on reliability at low signal to noise ratios. In fact, for digital television signals, the IEEE 802.22 standard for cognitive radio-based *wireless regional area networks* (WRANs) [79, 80] specifies a sensor sensitivity of $-116\,\mathrm{dBm}$ which, for a receiver with a noise figure of $11\,\mathrm{dB}$, operating on a $6\,\mathrm{MHz}$ channel[1], is equivalent to an absolute signal to noise ratio of $-21\,\mathrm{dB}$. At such low signal to noise ratios, large numbers of samples are required in order to make reliable decisions (see, for example, Figure 2.15). Thus, the question naturally suggests itself: in the context of dynamic spectrum access, can the usual model of energy detection be simplified in a way that enables further tractable analysis, but sacrifices little in the way of accuracy?

[1] As digital television broadcasting allows for channel bandwidths of up to $8\,\mathrm{MHz}$, it is possible that even smaller signal to noise ratios may need to be detected.

In short, the answer is yes. In 1967, Urkowitz proposed central limit theorem approximations for the decision probabilities of energy detectors with no diversity [13]. There are two advantages to using such approximations. Firstly, the Gaussian Q function can be used to calculate both decision probabilities, and so one can avoid having to calculate the regularised incomplete gamma function, which is known to be more difficult to compute than the Gaussian Q function [81], and the Marcum Q_m function, which is known to be difficult to evaluate in general [82–85]. The second advantage lies in the form of the Gaussian Q function, which lends itself well to further manipulation, allowing the analysis of other system parameters of interest [see, for instance, 46].

However, Urkowitz never published a quantification of the error resulting from his approximations and, to the best of the author's knowledge at the time of writing, no such quantification is available in the literature. As noted in Chapter 2, overly complicated models are difficult to use, but overly simplified models are of no use at all. Thus, before Urkowitz's approximations can be relied upon, the resulting error must be quantified.

Therefore, the aims of this chapter are threefold:

1. To quantify the error resulting from Urkowitz's approximations for the decision probabilities of energy detectors with no diversity.
2. To extend Urkowitz's approximations to energy detectors with MRC, EGC and SLC diversity.
3. To derive further simple approximations for the analysis of other system parameters of interest.

4.2 Sums of i.i.d. chi square and noncentral chi square random variables

Urkowitz's approximations for the decision probabilities of energy detectors with no diversity rely on central limit theorem [24, p. 370] approximations for the distribution of the test statistic under the null and alternative hypotheses. Consequently, the error resulting from their use depends on the error resulting from the use of the central limit theorem. Recalling (3.9), the test statistic for energy detectors with no diversity follows a chi square distribution when the channel is unoccupied and a noncentral chi square distribution otherwise. Thus, in this section, central limit theorem approximations for these distributions are discussed.

> **Central limit theorem:** Let $Y_1, Y_2, \ldots$ be a sequence of i.i.d. random variables with finite mean, μ, and finite variance, σ^2. Now, let S_n be the sum of n such

random variables, that is

$$S_n = \sum_{i=1}^{n} Y_i. \tag{4.1}$$

If Z_n is a zero mean, unit variance random variable defined by

$$Z_n = \frac{S_n - n\mu}{\sigma\sqrt{n}}, \tag{4.2}$$

then

$$\lim_{n\to\infty} P[Z_n > z] = Q\left(z\right), \tag{4.3}$$

where $Q(x)$ is the Gaussian Q function [49, Equation 26.2.3].

Consider a noncentral chi square distributed random variable, $\chi_k^2(s)$, with k degrees of freedom and noncentrality parameter s. It is well known that $\chi_k^2(s)$ has the form

$$\chi_k^2(s) = \sum_{i=1}^{k} X_i^2, \tag{4.4}$$

where $X_1, X_2, \ldots X_k$ are i.i.d. Gaussian distributed random variables with finite common mean, $\mu = \sqrt{\frac{s}{k}}$, and unit variance [26, p. 45-46]. As (4.4) is in the same form as (4.1), the central limit theorem can be applied to show that

$$\lim_{k\to\infty} P\left[\frac{\chi_k^2(s) - k\,\mathbb{E}[X_i^2]}{\sqrt{k\,\mathrm{Var}[X_i^2]}} > x\right] = Q\left(x\right), \tag{4.5}$$

where $\mathrm{Var}[X]$ denotes the variance of the random variable X.

The expected value and variance of X_i^2 are given [26, p. 48], respectively, by

$$\mathbb{E}[X_i^2] = 1 + \frac{s}{k}, \tag{4.6}$$

$$\mathrm{Var}[X_i^2] = 2\left(1 + 2\frac{s}{k}\right), \tag{4.7}$$

and so (4.5) can be simplified to

$$\lim_{k\to\infty} P\left[\frac{\chi_k^2(s) - (k+s)}{\sqrt{2(k+2s)}} > x\right] = Q\left(x\right). \tag{4.8}$$

In many scenarios, the number of degrees of freedom is finite, but (4.8) can still be

used to approximate the distribution of $\chi_k^2(s)$ as k becomes large, that is

$$P\left[\frac{\chi_k^2(s)-(k+s)}{\sqrt{2(k+2s)}} > x\right] \approx Q(x)$$
$$\implies P[\chi_k^2(s) > z] \approx Q\left(\frac{z-(k+s)}{\sqrt{2(k+2s)}}\right), \tag{4.9}$$

where $z \triangleq \sqrt{2(k+2s)}x + k + s$. It should be noted that, for finite k and s, it is always possible to choose a value of x so that $z = z_0$ for some $z_0 \in \mathbb{R}_0^+$. Consequently, the value of z in (4.9) is arbitrary as long as k and s are finite.

As the complementary *cumulative distribution function* (CDF) of the noncentral chi square distribution is given [26, p. 47] by

$$P[\chi_k^2(s) > x] = \begin{cases} 1, & x \le 0, \\ Q_\nu(\sqrt{s}, \sqrt{x}), & x > 0, \end{cases} \tag{4.10}$$

the error resulting from the use of (4.9), $\epsilon_{CLT}(k,s,x)$, can be written as

$$\epsilon_{CLT}(k,s,x) = \begin{cases} 1 - Q\left(\frac{x-(k+s)}{\sqrt{2(k+2s)}}\right), & x \le 0, \\ Q_\nu(\sqrt{s}, \sqrt{x}) - Q\left(\frac{x-(k+s)}{\sqrt{2(k+2s)}}\right), & x > 0, \end{cases} \tag{4.11}$$

where, for convenience, $\nu = \frac{k}{2}$.

While (4.11) precisely describes the error[2] resulting from the use of the central limit theorem, both the exact and approximate probabilities must be calculated in order to evaluate it, and deeper insight into the behaviour of the error with varying k, s and x is not readily apparent. However, a more intuitive result can be obtained.

Berry [86] and Esseen [87] derived a bound for the error resulting from the application of the central limit theorem to sums of i.i.d. random variables of any distribution, often referred to as the *Berry-Esseen theorem*. As the theorem is quite general, it can often overestimate the error by a large amount. However, it has recently been much improved upon by Korolev and Shevtsova [88]. Thus, to the best of the author's knowledge at the time of writing, the tightest Berry-Esseen type bound for the sum of the i.i.d. random variables $Y_1, Y_2, \ldots, Y_n$ is given by

$$\left| P\left[\sum_{i=1}^{n} Y_i > z\right] - Q\left(\frac{z - n\,\mathbb{E}[Y_i]}{\sqrt{n\,\mathrm{Var}[Y_i]}}\right)\right| \le \frac{0.33477(\beta + 0.429)}{\sqrt{n}}, \tag{4.12}$$

[2] In practice, x will not be less than zero and so (4.11) could be simplified further. However, for completeness, both cases are considered here.

where β is a function of the distribution of $Y_1, Y_2, \ldots, Y_n$, and is given by

$$\beta = \mathbb{E}\left[\left|\frac{Y_i - \mathbb{E}[Y_i]}{\sqrt{\mathrm{Var}[Y_i]}}\right|^3\right]. \tag{4.13}$$

In the case of noncentral chi square random variables, using (4.6) and (4.7), β can be written as

$$\beta = \mathbb{E}\left[\left|\frac{Y_i - (1+\frac{s}{k})}{\sqrt{2\,(1+2\frac{s}{k})}}\right|^3\right]. \tag{4.14}$$

To the best of the author's knowledge at the time of writing, the expectation in (4.14) has no closed form and so must be calculated using a numerical method.

The maximum absolute error, $\max_x |\epsilon_{CLT}(k,s,x)|$, and the Berry-Esseen bound given by (4.12), are illustrated for different values of s in Figure 4.1. While the Berry-Esseen bounds describe the rate of decrease quite well, they consistently overestimate the magnitude of the error by a large amount. This is a consequence of the generality of the Berry-Esseen theorem, which applies to sums of i.i.d. random variables of *any* distribution. Once again, abstraction has come at the cost of accuracy: the model oversimplifies the problem and important detail is lost. However, if noncentral chi square distributed random variables are considered in isolation, rather than random variables of any distribution, then it is possible to derive a novel tighter bound, which is stated here as a theorem and is proved in Appendix A.1.

Theorem 4.1: For chi square and noncentral chi square random variables, the maximum absolute error resulting from the use of the central limit theorem, $\max_{s,x} |\epsilon_{CLT}(k,s,x)|$, with respect to both the noncentrality parameter, s, and the location parameter, x, is given by

$$\max_{s,x} |\epsilon_{CLT}(k,s,x)| = \max\left(Q\left(\sqrt{\tfrac{k}{2}}\right), \epsilon_\infty(k)\right), \tag{4.15}$$

where

$$\epsilon_\infty(k) \approx \frac{1}{\sqrt{9\pi k}}, \tag{4.16}$$

as k becomes large.

The bound given in (4.15) is also shown in Figure 4.1. As can be seen, the bound is quite accurate over the entire range of values of k and is a much more accurate estimate of the actual error than any of the Berry-Esseen bounds. Consequently, from this point forward, (4.15) is used to model the maximum error resulting from the use of the central limit theorem to approximate the distribution of chi square and noncentral chi square

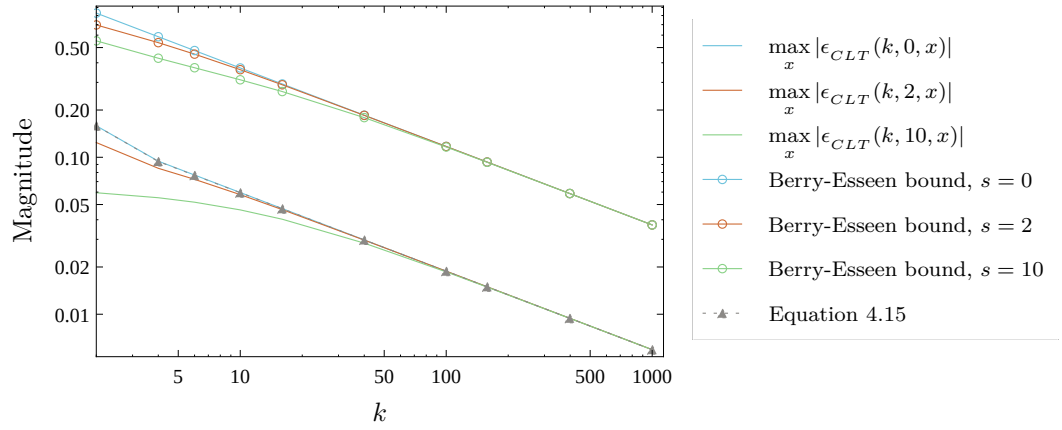

Figure 4.1: A log-log plot of the maximum absolute error, Berry-Esseen bounds and the bound given in Theorem 4.1, as functions of k, for different values of s. The maximum absolute error and Berry-Esseen bounds were calculated using numerical method based implementations of (4.11) and (4.12), respectively, while the proposed bound was computed directly using (4.15).

random variables.

It is interesting to note that, provided $k \geq 4$, (4.15) can be simplified to

$$\max_{s,x} |\epsilon_{CLT}(k,s,x)| \approx \frac{1}{\sqrt{9\pi k}}, \tag{4.17}$$

as $\frac{1}{\sqrt{9\pi k}} \geq Q\left(\sqrt{\frac{k}{2}}\right)$ for $k \geq 4$. Thus, in many scenarios of interest, (4.17) can be used instead of (4.15) to model the error resulting from the application of the central limit theorem.

4.3 Novel approximations for the decision probabilities

Using (4.9), and the values of k and s given in (3.10), (3.18), (3.22) and (3.25), the decision probabilities of energy detector diversity receivers can be approximated as shown[3] in Table 4.1, where the notations $\hat{P}_{f_X}$ and $\hat{P}_{d_X}(\gamma_X)$ denote the approximate probabilities of false alarm and detection, respectively, for the diversity type X.

The associated approximation error, $\epsilon_{CLT,X}(\gamma_X)$, is given by

$$\epsilon_{CLT,X}(\gamma_X) = P_{d_X}(\gamma_X) - \hat{P}_{d_X}(\gamma_X), \tag{4.18}$$

[3]The approximations for receivers with no diversity are equivalent to those proposed by Urkowitz. However, the error bound is novel.

Table 4.1: Approximate decision probabilities, and their associated error bounds, for energy detector diversity receivers operating on AWGN channels.

X	$\hat{P}_{f_X}$	$\hat{P}_{d_X}(\gamma_X)$	$\max\lvert\epsilon_{CLT,X}\rvert$
ND	$Q\left(\frac{\lambda - M}{\sqrt{2M}}\right)$	$Q\left(\frac{\lambda - M(1+\gamma_{ND})}{\sqrt{2M(1+2\gamma_{ND})}}\right)$	$\frac{1}{\sqrt{9\pi M}}$
MRC	$Q\left(\frac{\lambda - M}{\sqrt{2M}}\right)$	$Q\left(\frac{\lambda - M(1+\gamma_{MRC})}{\sqrt{2M(1+2\gamma_{MRC})}}\right)$	$\frac{1}{\sqrt{9\pi M}}$
EGC	$Q\left(\frac{\lambda - M}{\sqrt{2M}}\right)$	$Q\left(\frac{\lambda - M(1+\gamma_{EGC})}{\sqrt{2M(1+2\gamma_{EGC})}}\right)$	$\frac{1}{\sqrt{9\pi M}}$
SLC	$Q\left(\frac{\lambda - Mn}{\sqrt{2Mn}}\right)$	$Q\left(\frac{\lambda - M(n+\gamma_{SLC})}{\sqrt{2M(n+2\gamma_{SLC})}}\right)$	$\frac{1}{\sqrt{9\pi Mn}}$

for the approximation for the probability of detection, and

$$\epsilon_{CLT,X}(0) = P_{f_X} - \hat{P}_{f_X}, \tag{4.19}$$

for the approximation for the probability of false alarm, as $P_{f_X} = P_{d_X}(0)$ and $\hat{P}_{f_X} = \hat{P}_{d_X}(0)$.

As (4.18) and (4.19) are in the same form as (4.11), the error resulting from their use can be bounded using Theorem 4.1. However, in most spectrum sensing scenarios, $M \gg 4$, as channels must be sensed at very small signal to noise ratios (recall Figure 2.15). In such situations, the error can be more simply bounded using (4.17), as shown in Table 4.1, where

$$\max\lvert\epsilon_{CLT,X}\rvert \geq \lvert\epsilon_{CLT,X}(\gamma_X)\rvert, \quad \forall\ \gamma_X \geq 0, M \geq 4. \tag{4.20}$$

The bounds in Table 4.1 are useful in many scenarios. For instance, they can be used to show that 354 samples are required to ensure that $\max\lvert\epsilon_{CLT,ND}\rvert \leq 0.01$. This can clearly be seen in Figures 4.2(a) and 4.2(b), where the exact and approximate decision probabilities, and the resulting approximation error, have been plotted for $M = 354$ and $\hat{P}_{f_{ND}} = 0.2$. Similar results, also illustrated in Figures 4.2(a) and 4.2(b), can be

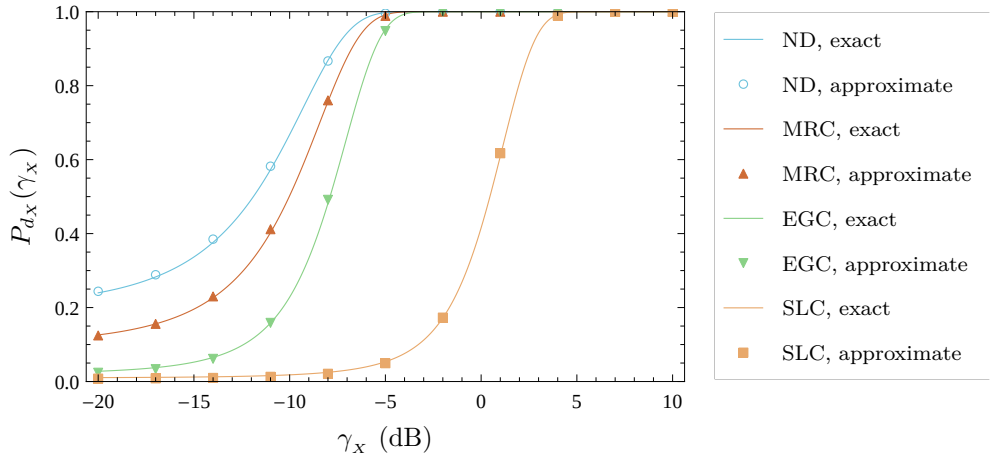

(a) A plot of the exact and approximate probabilities of detection, as functions of γ_X, for the specified diversity types.

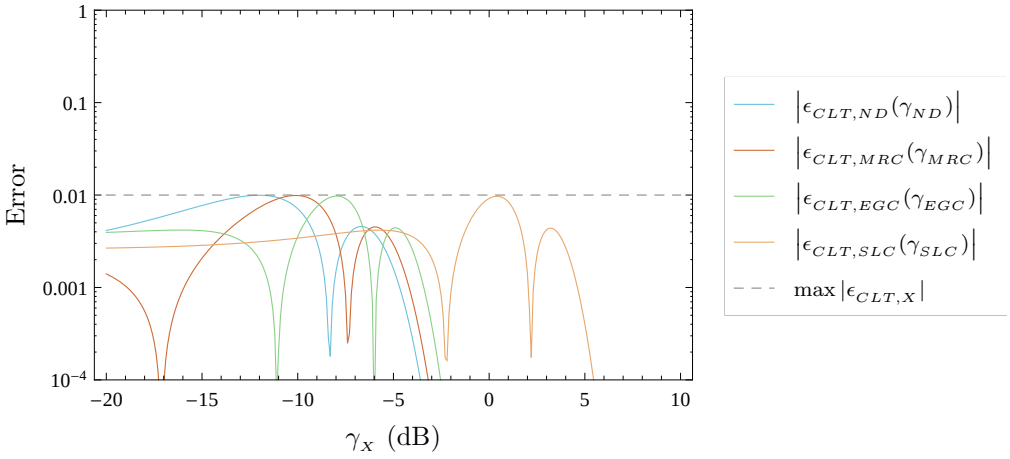

(b) A log-linear plot of the approximation error, and its bound, for the trends shown in Figure 4.2(a). In each case, $\max|\epsilon_{CLT,X}| = 0.01$.

Figure 4.2: Plots of the exact and approximate probabilities of detection, and the resulting approximation errors, for different diversity systems. The blue trends correspond to the case where $M = 354$ and $\hat{P}_{f_{ND}} = 0.2$, the red trends to $n = 3$, $M = 354$ and $\hat{P}_{f_{MRC}} = 0.1$, the green trends to $n = 3$, $M = 354$ and $\hat{P}_{f_{EGC}} = 0.02$, and the orange trends to $n = 6$, $M = 59$ and $\hat{P}_{f_{SLC}} = 0.01$.

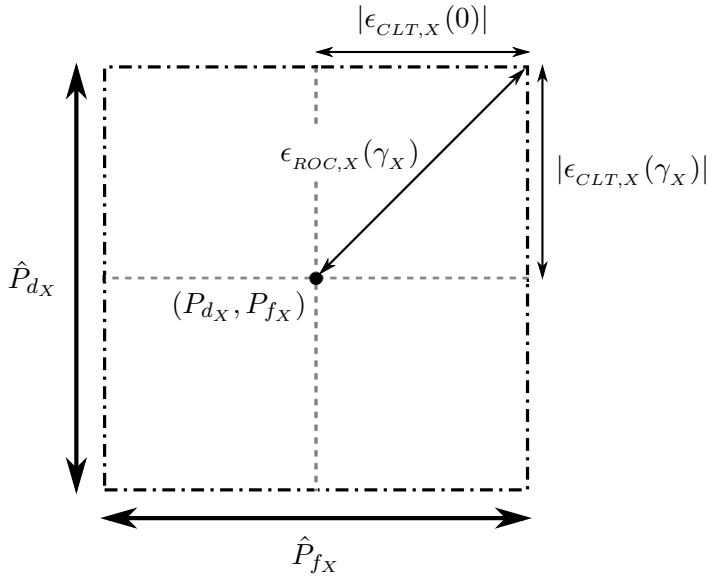

Figure 4.3: Two dimensional error resulting from the use of approximations for both decision probabilities.

shown for the other diversity types.

While the error resulting from the use of either $\hat{P}_{f_X}$ or $\hat{P}_{d_X}(\gamma_X)$ is easy to quantify using the bounds in Table 4.1, extra care must be taken if both approximate decision probabilities are used simultaneously. Figure 4.3 illustrates the problem in more detail: given a decision probability pair, (P_{f_X}, P_{d_X}), and an approximate decision probability pair, $(\hat{P}_{f_X}, \hat{P}_{d_X})$, the Euclidean distance between the two, $\epsilon_{ROC}(\gamma_X)$, is given by

$$\epsilon_{ROC,X}(\gamma_X) = \sqrt{\epsilon^2_{CLT,X}(\gamma_X) + \epsilon^2_{CLT,X}(0)}. \tag{4.21}$$

Typically, $\epsilon_{ROC}(\gamma_X)$ must be calculated numerically. However, using Theorem 4.1, it is not difficult to show that

$$\max|\epsilon_{ROC,X}| \leq \sqrt{2}\ \max|\epsilon_{CLT,X}|, \tag{4.22}$$

where $\max|\epsilon_{ROC,X}| \geq \epsilon_{ROC,X}(\gamma_X)\ \forall\ \gamma_X$. Consequently, if both approximate decision probabilities are used, then larger numbers of samples are required in order to guarantee the same maximum approximation error.

For instance, using the formulae given in Table 4.1, the receiver operating characteristics of the systems specified in Figure 4.2 can be plotted as shown in Figures 4.4(a) and 4.4(b). However, as can be seen, the resulting two dimensional error, $\epsilon_{ROC,X}(\gamma_X)$, is greater than 0.01 in each case. Using (4.22), it can be shown that the numbers of

samples required to ensure that $\max|\epsilon_{ROC,X}| \leq \epsilon_0 = 0.01$ is given by

$$\begin{aligned}
\max|\epsilon_{ROC,ND}| \leq\ & \max|\epsilon_{ROC,MRC}| = \max|\epsilon_{ROC,EGC}| \\
& \leq \sqrt{\frac{2}{9\pi M}} \leq \epsilon_0 \\
\implies M & \geq \frac{2}{9\pi(\epsilon_0)^2} \\
& \geq 707.34 \\
\therefore M & = 708,
\end{aligned}$$

$$\begin{aligned}
\max|\epsilon_{ROC,SLC}| & \leq \sqrt{\frac{2}{9\pi Mn}} \leq \epsilon_0 \\
\implies M & \geq \frac{2}{9\pi n(\epsilon_0)^2} \\
& \geq 117.89 \\
\therefore M & = 118.
\end{aligned}$$

Using these numbers of samples and plotting the receiver operating characteristics and the approximation errors for each diversity type, as in Figures 4.5(a) and 4.5(b), it can seen that the maximum error does not exceed 0.01 in each case.

4.4 Novel approximations for other system parameters

While the approximations given in Table 4.1 are useful in their own right, they also enable the tractable analysis of other system parameters, if the approximation error resulting from the use of the central limit theorem is not large. Thus, the complicated interaction between varying decision probabilities, numbers of samples, diversity branches and signal to noise ratio can be better understood and more easily manipulated.

4.4.1 Sample complexity

Consider the approximations for the decision probabilities for SLC diversity systems given in Table 4.1: inverting the Gaussian Q function and rearranging, it can be shown that

$$\lambda = \sqrt{2Mn}Q^{-1}(\hat{P}_{f_{SLC}}) + Mn, \tag{4.23}$$

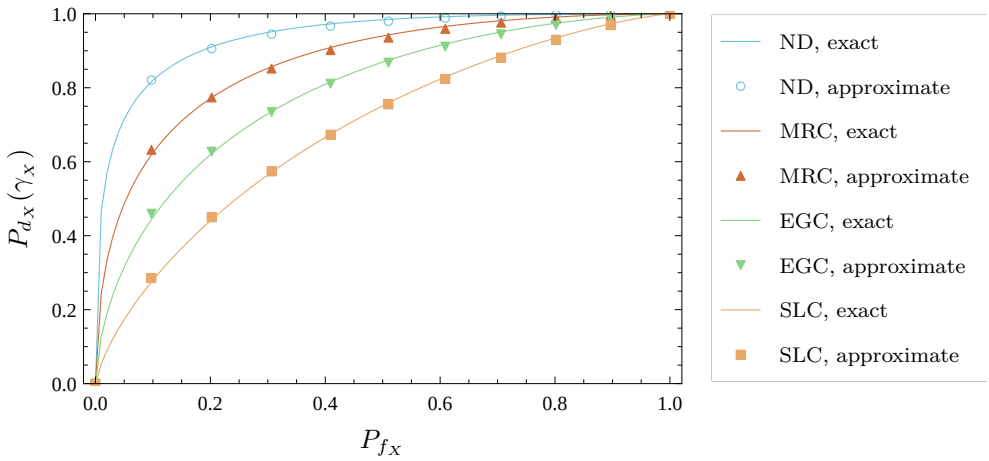

(a) Exact and approximate receiver operating characteristics, for the specified diversity types.

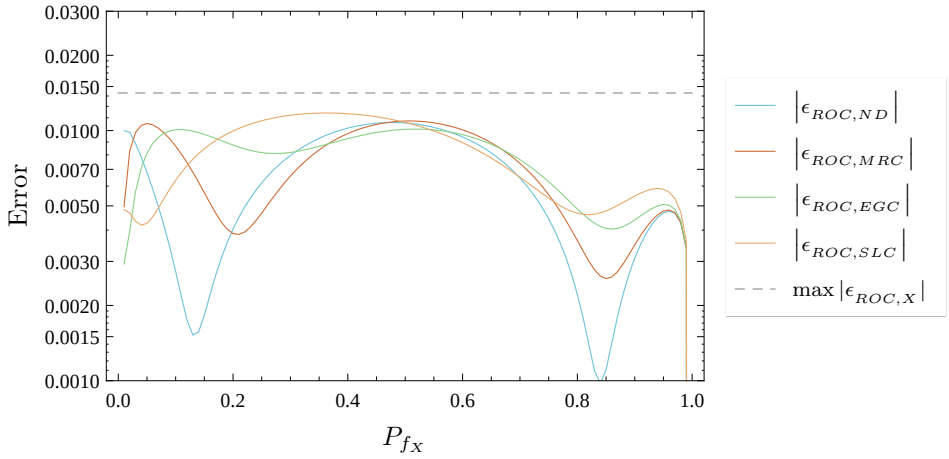

(b) A log-linear plot of the two dimensional approximation error, and its bound, for the trends shown in Figure 4.4(a). In each case, $\max|\epsilon_{ROC,X}| = 0.014$.

Figure 4.4: Receiver operating characteristics and approximation errors for different energy detector systems. The blue trends correspond to the case where $M = 354$ and $\gamma_{ND} = -7.5$dB, the red trends to $n = 3$, $M = 354$ and $\gamma_{MRC} = -9$dB, the green trends to $n = 3$, $M = 354$ and $\gamma_{EGC} = -10.5$dB, and the orange trends to $n = 6$, $M = 59$ and $\gamma_{SLC} = -5$dB.

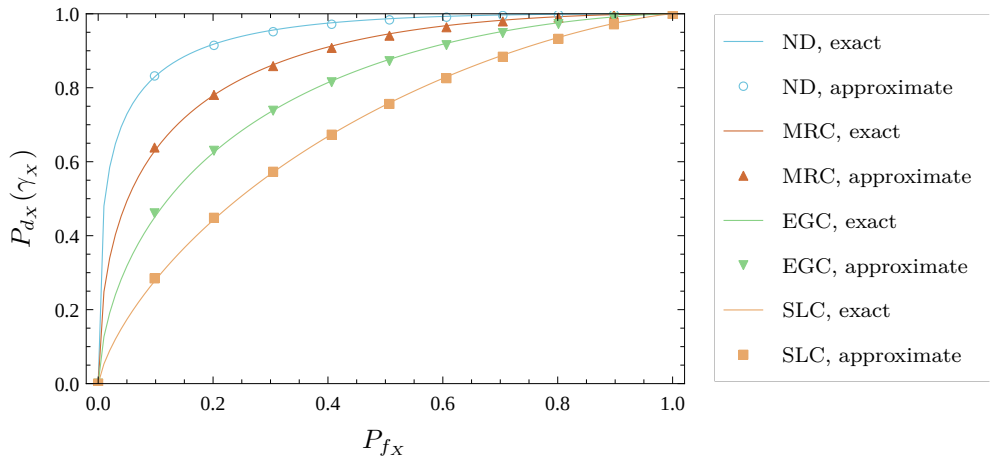

(a) Exact and approximate receiver operating characteristics, for the specified diversity types.

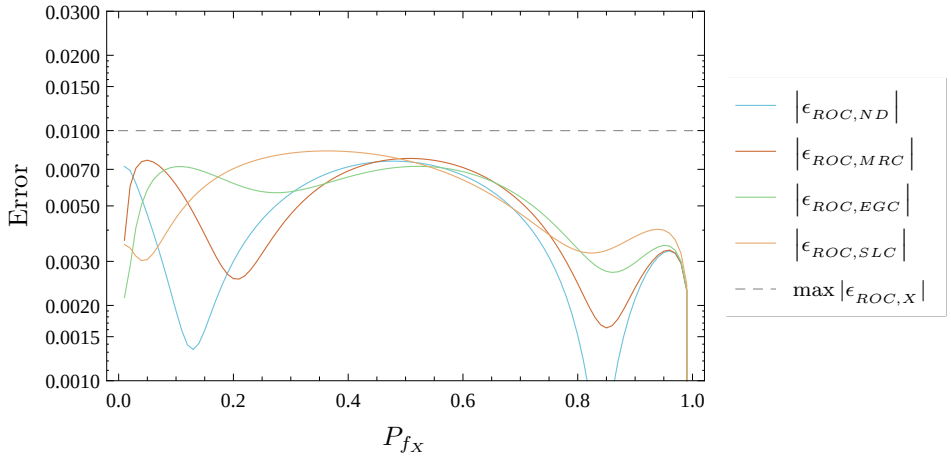

(b) A log-linear plot of the two dimensional approximation error, and its bound, for the trends shown in Figure 4.5(a). In each case, $\max|\epsilon_{ROC,X}| = 0.01$.

Figure 4.5: Receiver operating characteristics and approximation errors for different energy detector systems. The blue trends correspond to $M = 708$ and $\gamma_{ND} = -9$dB, the red trends to $n = 3$, $M = 708$ and $\gamma_{MRC} = -10.5$dB, the green trends to $n = 3$, $M = 708$ and $\gamma_{EGC} = -12$dB, and the orange trends to $n = 6$, $M = 118$ and $\gamma_{SLC} = -6.5$dB.

and

$$\lambda = \sqrt{2M(n+2\gamma_{SLC})}Q^{-1}(\hat{P}_{d_{SLC}}) + M(n+\gamma_{SLC}). \tag{4.24}$$

Equating (4.23) and (4.24) gives an equation independent of the decision threshold, λ, that is

$$\sqrt{2Mn}Q^{-1}(\hat{P}_{f_{SLC}}) + Mn = \sqrt{2M(n+2\gamma_{SLC})}Q^{-1}(\hat{P}_{d_{SLC}}) + M(n+\gamma_{SLC}), \tag{4.25}$$

which can itself be rearranged to give the number of samples, M, as a function of the other system variables:

$$M = \frac{2}{n}\left(\frac{Q^{-1}(\hat{P}_{f_{SLC}}) - \sqrt{1+\frac{2}{n}\gamma_{SLC}}Q^{-1}(\hat{P}_{d_{SLC}})}{\frac{1}{n}\gamma_{SLC}}\right)^2. \tag{4.26}$$

Noting the definition of γ_{SLC} in (3.26), it can be shown that

$$\begin{aligned}\frac{1}{n}\gamma_{SLC} &= \frac{1}{n}\sum_{i=1}^{n}\gamma_i \\ &= \gamma^*_{SLC},\end{aligned} \tag{4.27}$$

where γ^*_{SLC} is the average signal to noise ratio per diversity branch[4].

Using (4.27), (4.26) can be simplified to

$$M = \frac{2}{n}\left(\frac{Q^{-1}(\hat{P}_{f_{SLC}}) - \sqrt{1+2\gamma^*_{SLC}}Q^{-1}(\hat{P}_{d_{SLC}})}{\gamma^*_{SLC}}\right)^2 \triangleq \hat{M}_{SLC} \approx M_{SLC}, \tag{4.28}$$

where M_{SLC} denotes the sample complexity for SLC diversity, that is the number of samples required to meet the specified decision probabilities at a given signal to noise ratio, and the change in notation is intended to emphasise that, in this case, the number of samples is a function of the other system variables rather than an arbitrary value, as before. It should be noted that the approximation in (4.28) is only accurate if the associated approximation error, given in Table 4.1, is not large as

$$P_{f_X} - \max|\epsilon_{CLT,X}| \leq \hat{P}_{f_X} \leq P_{f_X} + \max|\epsilon_{CLT,X}|, \tag{4.29}$$

$$P_{d_X}(\gamma_X) - \max|\epsilon_{CLT,X}| \leq \hat{P}_{d_X}(\gamma_X) \leq P_{d_X}(\gamma_X) + \max|\epsilon_{CLT,X}|. \tag{4.30}$$

[4]The use of the superscript star notation here is intended to avoid confusion with the earlier overbar notation, which is used to denote the average signal to noise ratio with respect to both the number of branches and the random fluctuation of the channel gain with time (i.e. multipath fading).

Table 4.2: Sample complexities of various diversity receiver architectures operating on AWGN channels. These equations are accurate only if the approximation errors, given in Table 4.1, are not large.

X	$\hat{M}_X$
ND	$2\left(\frac{Q^{-1}(\hat{P}_{f_{ND}}) - \sqrt{1+2\gamma_{ND}}Q^{-1}(\hat{P}_{d_{ND}})}{\gamma^*_{ND}}\right)^2$
MRC	$\frac{2}{n^2}\left(\frac{Q^{-1}(\hat{P}_{f_{MRC}}) - \sqrt{1+2n\gamma^*_{MRC}}Q^{-1}(\hat{P}_{d_{MRC}})}{\gamma^*_{MRC}}\right)^2$
EGC	$\frac{2}{n^2}\left(\frac{Q^{-1}(\hat{P}_{f_{EGC}}) - \sqrt{1+2n\gamma^*_{EGC}}Q^{-1}(\hat{P}_{d_{EGC}})}{\gamma^*_{EGC}}\right)^2$
SLC	$\frac{2}{n}\left(\frac{Q^{-1}(\hat{P}_{f_{SLC}}) - \sqrt{1+2\gamma^*_{SLC}}Q^{-1}(\hat{P}_{d_{SLC}})}{\gamma^*_{SLC}}\right)^2$

The sample complexities for the other diversity types[5] can be derived in a similar manner and are given in Table 4.2, where $\hat{M}_X$ denotes the sample complexity for the diversity type X, $\gamma^*_{ND} = \gamma_{ND}$ for convenience, γ^*_{MRC} denotes the average signal to noise ratio per branch in an MRC system and is given by

$$\begin{aligned}\gamma^*_{MRC} &= \frac{1}{n}\gamma_{MRC} \\ &= \frac{1}{n}\sum_{i=1}^{n}\gamma_i,\end{aligned} \tag{4.31}$$

and γ^*_{EGC} is defined as

$$\begin{aligned}\gamma^*_{EGC} &= \frac{1}{n}\gamma_{EGC} \\ &= \left(\frac{1}{n}\sum_{i=1}^{n}h_i\right)^2\frac{P_s}{\sigma^2} \\ &= \bar{h}^2\frac{P_s}{\sigma^2},\end{aligned} \tag{4.32}$$

where $\bar{h}$ is the average value of the channel gain per diversity branch. Figure 4.6 illus-

[5]The approximation for the sample complexity in the no diversity case is equivalent to that derived by Tandra and Sahai [46, Equation 5]. However, the sample complexities for the other diversity types are, to the best of the author's knowledge at the time of writing, novel contributions.

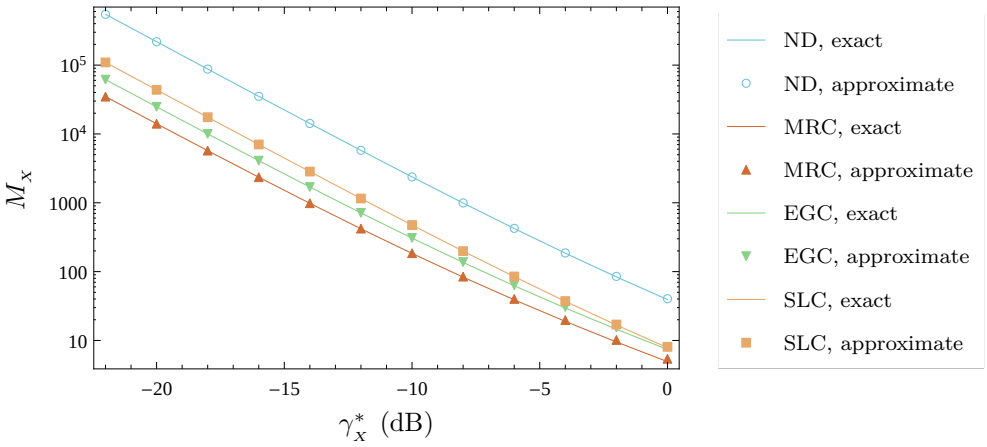

Figure 4.6: A log-linear plot of the sample complexity for different energy detector architectures as a function of the signal to noise ratio per branch, γ_X^*. For MRC diversity, $n = 4$; for EGC diversity, $n = 3$; and, for SLC diversity, $n = 5$. In each case $P_{f_X} = P_{m_X} = 0.05$.

trates the exact (calculated numerically) and approximate (calculated using Table 4.2) sample complexities for each diversity type. As can be seen, the derived approximations are quite accurate in each case.

The approximations in Table 4.2 have some interesting properties. For instance, the sample complexity of MRC and EGC systems is inversely proportional to the square of the number of diversity branches, while in the case of SLC diversity, the sample complexity is inversely proportional to just the number of diversity branches. Thus, the rate at which the sample complexity decreases with increasing numbers of diversity branches is much greater for MRC and EGC systems than for SLC systems.

It is also interesting to note that, for each diversity type, the sample complexity is approximately inversely proportional to the square of the signal to noise ratio. For instance, in the case of receivers with MRC diversity, if γ_{MRC}^* is small, then $\sqrt{1 + 2n\gamma_{MRC}^*} \approx 1$, and so

$$\begin{aligned} \hat{M}_{MRC} &\approx \frac{k}{(\gamma_{MRC}^*)^2} \\ 10\log_{10}\hat{M}_{MRC} &\approx -20\log_{10}\gamma_{MRC}^* + 10\log_{10}k \\ \hat{M}_{MRC,dB} &\approx -2\gamma_{MRC,dB}^* + 10\log_{10}k, \end{aligned} \tag{4.33}$$

where $k = 2\left(\frac{Q^{-1}(\hat{P}_{f_{MRC}}) - Q^{-1}(\hat{P}_{d_{MRC}})}{n}\right)^2$, and is constant for given values of $\hat{P}_{f_{MRC}}$, $\hat{P}_{d_{MRC}}$ and n, $\hat{M}_{MRC,dB} = 10\log_{10}\hat{M}_{MRC}$ and $\gamma_{MRC,dB}^* = 10\log_{10}\gamma_{MRC}^*$. Thus, the relationship between $\hat{M}_{MRC,dB}$ and $\gamma_{MRC,dB}^*$ is an approximately linear one, and the effect of fluctuating signal to noise ratio becomes trivial to visualise and quantify. Similar relations can be shown to hold for systems with EGC, SLC and no diversity.

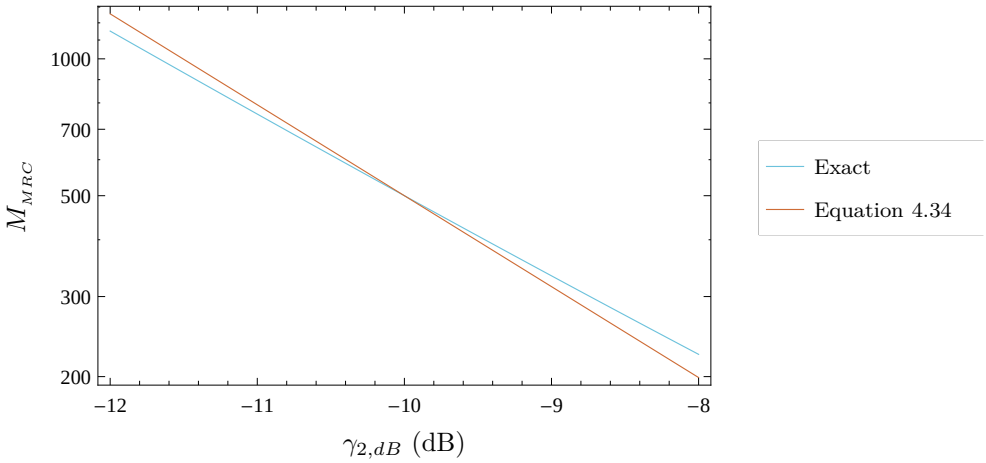

Figure 4.7: A log-linear plot of the exact and approximate sample complexities of an energy detector with three branch MRC diversity.

Using (4.33), and letting M_1 and M_2 represent the sample complexities at the signal to noise ratios $\gamma_{1,dB}$ and $\gamma_{2,dB}$, measured in decibels, respectively, it can be shown that

$$\begin{aligned} 10\log_{10} M_2 &\approx -2\gamma_{2,dB} + 10\log_{10} k \\ \underline{10\log_{10} M_1 &\approx -2\gamma_{1,dB} + 10\log_{10} k} \\ \implies 10\log_{10} M_2 - 10\log_{10} M_1 &\approx 2(\gamma_{1,dB} - \gamma_{2,dB}), \end{aligned}$$

$$\therefore M_2 \approx M_1 \times 10^{\left(\frac{\gamma_{1,dB}-\gamma_{2,dB}}{5}\right)}. \tag{4.34}$$

Figure 4.7 illustrates the accuracy and usefulness of (4.34) in approximating the sample complexity over a wide range of signal to noise ratios without the use of complicated numerical methods. If a single data point, $(M_1, \gamma_{1,dB})$, is known, then the sample complexity at different signal to noise ratios can be extrapolated from it. In the case of the data shown in Figure 4.7, the fact 500 samples are required in order to ensure certain probabilities of false alarm and missed detection when $\gamma^*_{MRC} = -10\,\text{dB}$ was used.

4.4.2 Minimum signal to noise ratio

A further quantity of interest is the minimum signal to noise ratio detectable by the system. For a given diversity type, this can be found by rearranging the appropriate formula in Table 4.2 and solving for γ_X. However, the resulting expressions can be complicated, and simpler, yet accurate, approximations are obtainable, if the minimum to noise ratio is sufficiently small.

For instance, in the no diversity case, letting $\sqrt{1+2\gamma_{ND}} \approx 1$, the sample complexity

Table 4.3: Approximations for the minimum signal to noise ratios of various diversity receiver architectures operating on AWGN channels. These equations are accurate only if the approximation errors, given in Table 4.1, are not large and $\gamma_{min,X}$ is small.

X	$\hat{\gamma}_{min,X}$
ND	$\sqrt{\frac{2}{M}}\left(Q^{-1}(\hat{P}_{f_{ND}}) - Q^{-1}(\hat{P}_{d_{ND}})\right)$
MRC	$\sqrt{\frac{2}{M}}\left(\frac{Q^{-1}(\hat{P}_{f_{MRC}}) - Q^{-1}(\hat{P}_{d_{MRC}})}{n}\right)$
EGC	$\sqrt{\frac{2}{M}}\left(\frac{Q^{-1}(\hat{P}_{f_{EGC}}) - Q^{-1}(\hat{P}_{d_{EGC}})}{n}\right)$
SLC	$\sqrt{\frac{2}{Mn}}\left(Q^{-1}(\hat{P}_{f_{SLC}}) - Q^{-1}(\hat{P}_{d_{SLC}})\right)$

can be rearranged to give

$$\gamma_{ND} \approx \sqrt{\frac{2}{M}}\left(Q^{-1}(\hat{P}_{f_{ND}}) - Q^{-1}(\hat{P}_{d_{ND}})\right) \triangleq \hat{\gamma}_{min,ND} \approx \gamma_{min,ND}, \tag{4.35}$$

where, for emphasis, the notation $\gamma_{min,X}$ denotes the minimum signal to noise ratio for the diversity type X. Again, (4.35) is valid only if the signal to noise ratio at the combiner output is small and the approximation error, given in Table 4.1, is not large. Similar formulations can be shown to hold for the other diversity types. A complete list is given in Table 4.3.

The approximation in (4.35) is useful because it avoids the need for complicated numerical methods. For instance, using (4.35), it is not difficult to show that the minimum signal to noise ratio required to ensure that the probabilities of false alarm and missed detection are no greater than 0.01 when 4000 samples are used is approximately $-9.83\,\text{dB}$. Using a numerical root finding method, it can be shown that the exact requirement is $-9.61\,\text{dB}$ — a difference of just $0.22\,\text{dB}$.

4.4.3 Diversity gain

The final quantity of interest is the number of diversity branches or cooperative nodes required to ensure certain performance criteria are met, which shall henceforth be referred to as the diversity gain. Again, for a given diversity type (with the exception

Table 4.4: Approximations for the diversity gain of different receivers operating on AWGN channels. These equations are only accurate if the approximation errors, given in Table 4.1, are not large and γ_X^* is small.

X	$\hat{n}_X$
MRC	$\left\lceil \sqrt{\frac{2}{M}} \left(\frac{Q^{-1}(\hat{P}_{f_{MRC}}) - Q^{-1}(\hat{P}_{d_{MRC}})}{\gamma^*_{MRC}} \right) \right\rceil$
EGC	$\left\lceil \sqrt{\frac{2}{M}} \left(\frac{Q^{-1}(\hat{P}_{f_{EGC}}) - Q^{-1}(\hat{P}_{d_{EGC}})}{\gamma^*_{EGC}} \right) \right\rceil$
SLC	$\left\lceil \frac{2}{M} \left(\frac{Q^{-1}(\hat{P}_{f_{SLC}}) - Q^{-1}(\hat{P}_{d_{SLC}})}{\gamma^*_{SLC}} \right)^2 \right\rceil$

of the no diversity case: here, $n = 1$), this may be found by solving the relevant formula in Table 4.2 for n, but the resulting expressions, while accurate, can be complicated. However, as before, if the signal to noise ratio is small, then simple, yet accurate, approximations can be obtained. These can be derived through direct manipulation of the formulae in Table 4.3, applying the ceiling function to ensure the specified criteria are met, and are listed in Table 4.4, where n_X denotes the diversity gain for the diversity type X and $\hat{n}_X \approx n_X$.

Again, the approximations in Table 4.4 are useful because they avoid the need for numerical routines. For instance, using numerical methods, it can be shown that six SLC branches are required to ensure probabilities of false alarm and missed detection of 0.1 at a signal to noise ratio of -21 dB when 40000 samples are used. Using the approximation in Table 4.4, however, it can be shown that $\hat{n}_{SLC} = 6$, which agrees with the exact answer but does not require the use of numerical methods.

4.5 Discussion

In this chapter, a novel and accurate method for the quantification of the error resulting from the use of the central limit theorem to approximate the distribution functions of chi square and noncentral chi square random variables was proposed. Using this method, the error resulting from the use of Urkowitz's approximations for the decision probabilities of energy detectors with no diversity was quantified. Subsequently, approximations for the decision probabilities of energy detectors with MRC, EGC and SLC diversity were derived, and the resulting error was also quantified. Using the de-

rived error bounds, it is possible to quickly and accurately determine the regions of applicability of the derived approximations.

In addition to the approximations for the decision probabilities, simple and useful approximations for the analysis of sample complexity, minimum signal to noise ratio and diversity gain were also derived. The approximations for the sample complexities of the different diversity receivers were shown to be accurate provided the error resulting from the use of the central limit theorem in each case is not large, while the approximations for the minimum signal to noise ratio and diversity gain were shown to be accurate under the further condition that the signal to noise ratio at the combiner output is small. Such approximations are likely to be of significant use in both the design and analysis of spectrum sensing systems, and avoid the use of computationally expensive numerical methods in order to determine basic information about the operation of the systems.

For reliable spectrum sensing at low signal to noise ratios, the number of samples required is often large enough so that both $\max|\epsilon_{CLT,X}|$ and $\max|\epsilon_{ROC,X}|$ are small enough to be considered negligible for many applications, and so the approximations in this chapter can be used without risking large errors. For instance, if the required minimum SNR at the receiver is $-21\,\text{dB}$, as in the IEEE 802.22 specification discussed in Section 4.1, then approximately 2×10^5 samples are required to ensure that the probabilities of false alarm and missed detection do not exceed 0.1. At such large numbers of samples, $\max|\epsilon_{CLT,ND}| \approx 4 \times 10^{-4}$ and $\max|\epsilon_{ROC,ND}| \approx 6 \times 10^{-4}$ which, for many applications, are acceptably small.

However, while the assumption of large numbers of samples may be justified in the case of spectrum sensing, it is not true in general. For instance, if the required minimum SNR is $0\,\text{dB}$, then just ten samples are required to ensure that the probabilities of false alarm and missed detection do not exceed 0.1. In this case, $\max|\epsilon_{CLT,ND}| \approx 6 \times 10^{-2}$ and $\max|\epsilon_{ROC,ND}| \approx 9 \times 10^{-2}$, which are approximately 150 times greater than in the previous example. Of course, whether these errors are acceptable or not depends on the application, but system designers should exercise caution before relying on such approximations in general. The bounds given in Table 4.1 facilitate exactly this purpose.

Yet, many researchers do not quantify the approximation error resulting from the use of the central limit theorem [see, for example, 10, 13, 19–21, 43, 46, 64–67, 89–97], instead assuming that it is negligible for "large" numbers of samples, but without stating which numbers of samples should be considered large and which should be considered small. In the energy detection literature, the assumption can be traced back to Urkowitz, who stated that $M \geq 250$ is sufficient for the approximation error to be negligible for energy detectors with no diversity[6]. However, Quan et al. [91] and Kim et al. [93] go

[6]Using the relevant formula in Table 4.1, it is easy to show that $\max|\epsilon_{CLT,ND}| \approx 0.012$ when

further, stating that $M \geq 10$ is sufficient to give good accuracy[7] in many cases. These are clearly matters of opinion rather than fact: individual applications determine one's willingness or ability to tolerate error. The analysis in this chapter now enables system designers to make more informed decisions about whether such approximations are appropriate or not on a case by case basis.

The use of approximations has enabled more astute system design by replacing complicated descriptions of behaviour with simpler ones. Previously hidden, simple relationships, such as the one between the sample complexity and signal to noise ratio given in (4.33), have become apparent. Furthermore, by avoiding the use of complicated, multi-variable functions, such as the regularised incomplete gamma and Marcum Q_m functions, and instead relying on well known, single variable functions, such as the Gaussian Q function, real time optimisation and calibration of sensing systems is possible, either by inexpensive direct computation or using one dimensional look up tables. Given this level of success, it is worth considering whether approximations can be applied to similar effect in other situations. In particular, the analysis of energy detector systems operating on multipath fading channels is known to be complicated in general, requiring the use of computationally expensive numerical methods in order to evaluate basic reliability and performance measures. Consequently, in the remaining discussion, approximations are considered for the analysis of energy detector systems in such situations.

$M = 250$. Depending on the application, this may or may not be an acceptable degree of error.

[7] When $M = 10$, $\max |\epsilon_{CLT,ND}| \approx 0.06$.

Chapter 5

Multipath fading channel analysis I: Nakagami-m channels

In this chapter, approximations for the detection probabilities of energy detector diversity receivers operating on Nakagami-m channels are considered, with the aim of finding simpler yet accurate alternatives to the exact methods outlined in Chapter 3. In each case, error bounds are provided so that the regions of applicability of the approximations are well defined. Furthermore, as a central limit theorem approximation for sums of i.i.d. gamma random variables is used in the course of the analysis, a bound for the resulting error is derived.

The relationships between system parameters of interest are also explored and it is demonstrated that a very simple relationship exists between the sample complexity and average signal to noise ratio per branch, regardless of the type of diversity in use. Closed form approximations for the sample complexity and minimum signal to noise ratio are also derived, under the constraint that the product of the fading parameter and the number of diversity branches, mn, is large (e.g. $mn \geq 20$). An approximation for the diversity gain of SLC systems is derived under similar constraints.

5.1 Motivation

In Chapter 3, it was discussed how the exact expressions for the decision probabilities of energy detector diversity receivers operating on multipath fading channels currently available in the literature are problematic due to the large number of terms that must be computed in order to evaluate them. Now, a further problem emerges: using these exact expressions, is it possible to derive further expressions for the sample complexity, minimum signal to noise ratio or diversity gain in the manner of Section 4.4? Given

that the decision probabilities in Tables 3.2–3.6 are in the form of infinite series[1], this seems unlikely. However, the problem is not intractable.

In the previous chapter, it was shown that the use of approximations allowed the simple and accurate computation of the decision probabilities of energy detector diversity receivers operating on AWGN channels and enabled the derivation of further approximations for the sample complexity, minimum signal to noise ratio and diversity gain. This naturally begs the question: can approximate representations be used in a similar way to simplify the design and analysis of energy detector diversity receivers in multipath fading channels? Previous research on the matter certainly suggests so.

Ghasemi and Sousa [64, 98] derived approximate expressions for the sample complexity and minimum signal to noise ratio of receivers with no diversity operating on Rayleigh channels, where each receiver transmits a compressed decision to the fusion centre after performing the binary hypothesis test locally. Atapattu et al. [66, 67] derived approximations for the detection probabilities of energy detectors with no diversity and SLC diversity operating on Nakagami-m channels, for scenarios where the signal to noise ratio is small while, under similar constraints, and using a further approximation for the error function, López-Benítez and Casadevall derived an alternative approximation for the probability of detection of an energy detector with no diversity operating on a Rayleigh channel [65]. However, in all of these cases, the approximation error was not quantified and so the region of applicability of each approximation is unclear. Furthermore, Ghasemi and Sousa's approximations apply to a very specific form of cooperative spectrum sensing, while Atapattu et al.'s approximations require the computation of high order derivatives and so introduce numerical computation issues in practice. Finally, in all cases, the analysis applies only to receivers with no diversity or SLC diversity, and so is incomplete.

Therefore, the aims of this chapter are:

1. To derive accurate and computationally inexpensive approximations for the probability of detection of receivers with the diversity types considered so far.
2. To derive bounds on the error resulting from the use of these approximations, so that their regions of applicability are well defined.
3. To derive further approximations for the sample complexity, minimum signal to noise ratio and diversity gain, enabling a complete description of the sensor system.

[1] With the exception, of course, of Digham et al.'s expression for $P_{d_{ND,Rice}}$, but this is valid for $M = 2$ only.

5.2 Novel approximations for small signal to noise ratios

In a similar fashion to (3.27), the approximate probability of detection for a diversity receiver of type X operating in a multipath fading channel Y, $\hat{P}_{d_{X,Y}}$, can be calculated as

$$\begin{aligned}\hat{P}_{d_{X,Y}} &= \mathbb{E}[\hat{P}_{d_X}(\gamma_X)] \\ &= \int_{-\infty}^{\infty} \hat{P}_{d_X}(x)\ f_{X,Y}(x)\ dx. \end{aligned} \tag{5.1}$$

As the approximate probabilities of false alarm in Table 4.1 do not depend on the signal to noise ratio, the approximate probability of false alarm for a diversity receiver of type X operating in a multipath fading channel Y, $\hat{P}_{f_{X,Y}}$, is given by

$$\hat{P}_{f_{X,Y}} = \hat{P}_{f_X}. \tag{5.2}$$

It is convenient to write $\hat{P}_{d_X}(\gamma_X)$ in the general form

$$\hat{P}_{d_X}(\gamma_X) = Q\left(\frac{\lambda - M(N_X + \gamma_X)}{\sqrt{2M(N_X + 2\gamma_X)}}\right), \tag{5.3}$$

where

$$N_X = \begin{cases} n, & X = \text{SLC}, \\ 1, & \text{otherwise}. \end{cases} \tag{5.4}$$

Thus, the probability of detection for receivers with each of the diversity types considered so far can be represented using a single expression.

Using (5.3), (5.1) can be written as

$$\hat{P}_{d_{X,Y}} = \int_{-\infty}^{\infty} Q\left(\frac{\lambda - M(N_X + x)}{\sqrt{2M(N_X + 2x)}}\right) f_{X,Y}(x)\ dx. \tag{5.5}$$

However, to the best of the author's knowledge at the time of writing, for the diversity receivers and channel types considered in this work, (5.5) must be evaluated numerically, as the presence of the $2x$ term in the denominator of the argument to the Gaussian Q function makes symbolic evaluation difficult. However, the following approximation can be made:

$$\hat{P}_{d_X}(\gamma_X) \approx \tilde{P}_{d_X}(\gamma_X) = Q\left(\frac{\lambda - M(N_X + \gamma_X)}{\sqrt{2MN_X}}\right). \tag{5.6}$$

As (5.6) is arrived at by letting $N_X + 2\gamma_X \approx N_X$ in (5.3), it shall henceforth be referred to as the low SNR approximation. This is the same simplification used by

Atapattu et al. [66, 67] and López-Benítez and Casadevall [65, 95–97] in the derivation of their approximations, and so the error bounds derived later will equally apply to their work.

The error resulting from the use of the low SNR approximation, $\epsilon_{SNR,X}(\gamma_X)$, can be written as

$$\epsilon_{SNR,X}(\gamma_X) = \hat{P}_{d_X}(\gamma_X) - \tilde{P}_{d_X}(\gamma_X). \tag{5.7}$$

Substituting (5.6) into (5.1) leads to the further approximation

$$\begin{aligned} \hat{P}_{d_{X,Y}} \approx \tilde{P}_{d_{X,Y}} &= \mathbb{E}[\tilde{P}_{d_X}(\gamma_X)] \\ &= \int_{-\infty}^{\infty} \tilde{P}_{d_X}(x)\ f_{X,Y}(x)\ dx, \end{aligned} \tag{5.8}$$

which will be useful throughout the remainder of this chapter.

The error resulting from the use of (5.8), $\epsilon_{SNR,X,Y}$, can be written as

$$\begin{aligned} \epsilon_{SNR,X,Y} &= \hat{P}_{d_{X,Y}} - \tilde{P}_{d_{X,Y}} \\ &= \int_{-\infty}^{\infty} \left(\hat{P}_{d_X}(x) - \tilde{P}_{d_X}(x)\right) f_{X,Y}(x)\ dx \\ &= \int_{-\infty}^{\infty} \epsilon_{SNR,X}(x)\ f_{X,Y}(x)\ dx. \end{aligned} \tag{5.9}$$

Conveniently, for the channel types considered in this work, $f_{X,Y}(x)$ is often left skewed and so $\epsilon_{SNR,X,Y}$ is often small. In the following sections, error bounds for $\epsilon_{SNR,X,Y}$ are derived which show this more explicitly.

5.2.1 Receivers with no diversity

5.2.1.1 A novel approximation for the probability of detection

Using (5.8), and noting that $f_{ND,Nak}(x) = 0$ for $x < 0$, the probability of detection for an energy detector with no diversity operating on a Nakagami-m channel can be approximated as

$$P_{d_{ND,Nak}} \approx \tilde{P}_{d_{ND,Nak}} = \frac{1}{\Gamma(m)} \int_0^{\infty} Q\left(\frac{\lambda - M(1+x)}{\sqrt{2M}}\right) e^{-\frac{mx}{\bar{\gamma}}} \left(\frac{m}{\bar{\gamma}}\right)^m x^{m-1} dx. \tag{5.10}$$

In order to progress further, the following integral identity, which is proved in Appendix A.2, is required.

Lemma 5.1: Let

$$F_k(a,b,c) = \frac{1}{\Gamma(k)} \int_0^\infty Q(a-bx)\ e^{-cx} c^k x^{k-1} dx. \tag{5.11}$$

If $c > 0$, then for $k \geq 1$, $k \in \mathbb{N}^+$,

$$\begin{aligned} F_k(a,b,c) = Q(a) + \frac{1}{2}\exp\left[-\frac{\sqrt{2}c}{b}\left(\frac{a-\frac{c}{2b}}{\sqrt{2}}\right)\right] \\ \times \sum_{p=0}^{k-1}\left(\frac{\sqrt{2}c}{b}\right)^p \mathrm{i}^p \operatorname{erfc}\left[-\left(\frac{a-\frac{c}{b}}{\sqrt{2}}\right)\right], \end{aligned} \tag{5.12}$$

where $\mathrm{i}^n \operatorname{erfc}(z)$ is the n^{th} repeated integral of the complementary error function [68, Equation 7.18.2], and has the simple recursive relation [68, Equations 7.18.1 and 7.18.7]

$$\mathrm{i}^n \operatorname{erfc}(z) = \begin{cases} \frac{2}{\sqrt{\pi}} e^{-z^2}, & n = -1, \\ \operatorname{erfc}(z), & n = 0, \\ -\frac{z}{n}\mathrm{i}^{n-1}\operatorname{erfc}(z) + \frac{1}{2n}\mathrm{i}^{n-2}\operatorname{erfc}(z), & n \geq 1. \end{cases} \tag{5.13}$$

Using Lemma 5.1, (5.10) can be written as

$$\begin{aligned} \tilde{P}_{d_{ND,Nak}} &= F_m\left(\frac{\lambda - M}{\sqrt{2M}}, \sqrt{\frac{M}{2}}, \frac{m}{\bar{\gamma}}\right) \\ &= Q\left(\frac{\lambda - M}{\sqrt{2M}}\right) + \frac{1}{2}\exp\left[-\frac{\frac{2m}{\bar{\gamma}}}{\sqrt{M}}\left(\frac{\lambda - M - \frac{m}{\bar{\gamma}}}{2\sqrt{M}}\right)\right] \\ &\quad \times \sum_{p=0}^{m-1}\left(\frac{\frac{2m}{\bar{\gamma}}}{\sqrt{M}}\right)^p \mathrm{i}^p \operatorname{erfc}\left[-\left(\frac{\lambda - M - \frac{2m}{\bar{\gamma}}}{2\sqrt{M}}\right)\right]. \end{aligned} \tag{5.14}$$

Noting the definition of $\hat{P}_{f_{ND}}$ in Table 4.1, (5.14) can be further simplified to

$$\begin{aligned} \tilde{P}_{d_{ND,Nak}} = \hat{P}_{f_{ND}} + \frac{1}{2}\exp\left[-\frac{\frac{2m}{\bar{\gamma}}}{\sqrt{M}}\left(\frac{\lambda - M - \frac{m}{\bar{\gamma}}}{2\sqrt{M}}\right)\right] \\ \times \sum_{p=0}^{m-1}\left(\frac{\frac{2m}{\bar{\gamma}}}{\sqrt{M}}\right)^p \mathrm{i}^p \operatorname{erfc}\left[-\left(\frac{\lambda - M - \frac{2m}{\bar{\gamma}}}{2\sqrt{M}}\right)\right], \end{aligned} \tag{5.15}$$

which, as will be discussed in more detail later, requires a significantly smaller computational effort to evaluate than any of the formulations given in Table 3.2. As a consequence of Lemma 5.1, (5.15) is valid for $m \in \mathbb{N}^+$ only[2].

While the approximation given in (5.15) agrees numerically with the expression derived by Atapattu et al. [66, 67] (both formulations follow from (5.10)), there is a key differ-

[2]Approximations valid for $m \in \mathbb{R}^+$ are discussed in Section 5.3.

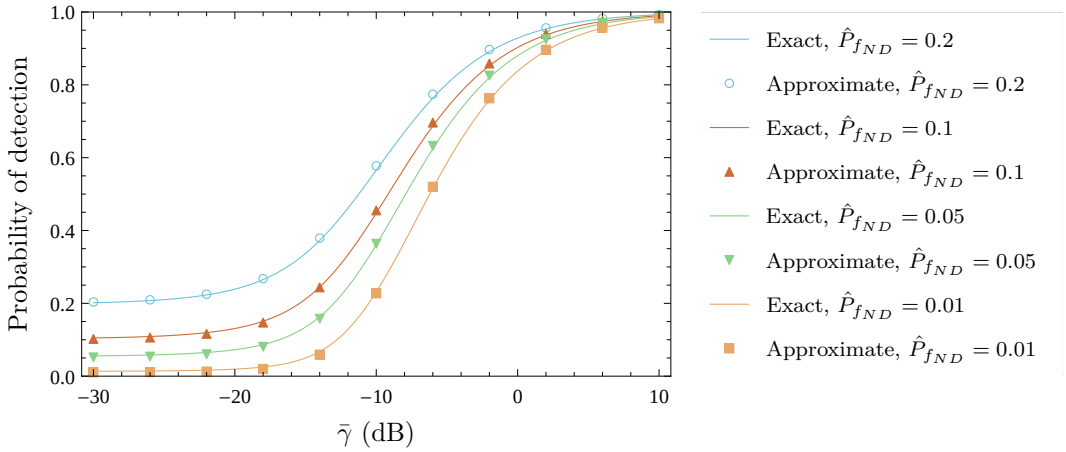

Figure 5.1: A plot of the exact and approximate probabilities of detection of an energy detector with no diversity operating on a Rayleigh faded channel. In each case, $M = 354$.

ence: the form presented by Atapattu et al. is similar to (A.40) and so differentiation (numeric or symbolic) must be performed in order to evaluate the result. This is a particular problem for large values of m, and even more so if numerical methods are employed. However, as the approximation given in (5.15) relies on the simple recursive relation in (5.13), no differentiation is required and the desired result is usually not difficult to compute (although the resulting symbolic expression may be verbose, if m is large). Thus, from a computational perspective, (5.15) is preferable to the method proposed by Atapattu et al., though the error resulting from the use of either is the same.

Using (5.15) and noting that, when $m = 1$, Nakagami-m fading is equivalent to Rayleigh fading, it can be shown that

$$\tilde{P}_{d_{ND,Ray}} = \hat{P}_{f_{ND}} + \exp\left[-\frac{\frac{2}{\bar{\gamma}}}{\sqrt{M}}\left(\frac{\lambda - M - \frac{1}{\bar{\gamma}}}{2\sqrt{M}}\right)\right]\left[-\left(\frac{\lambda - M - \frac{2}{\bar{\gamma}}}{\sqrt{2M}}\right)\right], \tag{5.16}$$

where, in the usual notation, $\tilde{P}_{d_{ND,Ray}}$ represents the approximate probability of detection for an energy detector with no diversity operating on a Rayleigh fading channel. Figure 5.1 illustrates the accuracy of (5.16), with $M = 354$, for different values of $\bar{\gamma}$ and $P_{f_{ND}}$.

It is interesting to note that the approximation in (5.16) is more concise than that derived by López-Benítez and Casadevall [65, Equation 21], though both rely on the central limit theorem and low SNR approximations. Furthermore, as (5.16) is arrived at without the use of the approximation for the error function employed by López-Benítez and Casadevall, it is also a more generally applicable approximation.

Finally, Atapattu et al. and López-Benítez and Casadevall did not quantify the sources

of error in their approximations. While the authors state that their approximations are valid for small signal to noise ratios, it is unclear exactly which signal to noise ratios should be considered small and which should be considered large, and so there is some ambiguity as to their regions of applicability.

5.2.1.2 Quantifying the approximation error

The total error resulting from the use of $\tilde{P}_{d_{X,Y}}$ to approximate $P_{d_{X,Y}}$, $\epsilon_{tot,X,Y}$, can be written as

$$\epsilon_{tot,X,Y} = P_{d_{X,Y}} - \tilde{P}_{d_{X,Y}}. \tag{5.17}$$

The absolute value of the total error can be bounded as

$$\begin{aligned} |\epsilon_{tot,X,Y}| &= |P_{d_{X,Y}} - \tilde{P}_{d_{X,Y}}| \\ &= |P_{d_{X,Y}} - \hat{P}_{d_{X,Y}} + \hat{P}_{d_{X,Y}} - \tilde{P}_{d_{X,Y}}| \\ &\leq |P_{d_{X,Y}} - \hat{P}_{d_{X,Y}}| + |\hat{P}_{d_{X,Y}} - \tilde{P}_{d_{X,Y}}| \\ &\leq |P_{d_{X,Y}} - \hat{P}_{d_{X,Y}}| + |\epsilon_{SNR,X,Y}|, \end{aligned} \tag{5.18}$$

where the definition of $\epsilon_{SNR,X,Y}$, given in (5.9), has been used to simplify the result. Using (3.27) and (5.1), $|P_{d_{X,Y}} - \hat{P}_{d_{X,Y}}|$ can expanded and bound as

$$\begin{aligned} |P_{d_{X,Y}} - \hat{P}_{d_{X,Y}}| &= \left| \int_{-\infty}^{\infty} (P_{d_X}(x) - \hat{P}_{d_X}(x))\ f_{X,Y}(x)\ dx \right| \\ &\leq \int_{-\infty}^{\infty} |P_{d_X}(x) - \hat{P}_{d_X}(x)|\ f_{X,Y}(x)\ dx \\ &\leq \int_{-\infty}^{\infty} |\epsilon_{CLT,X}(x)|\ f_{X,Y}(x)\ dx \\ &\leq \max |\epsilon_{CLT,X}| \int_{-\infty}^{\infty} f_{X,Y}(x)\ dx \\ &\leq \max |\epsilon_{CLT,X}|, \end{aligned} \tag{5.19}$$

where (4.20) has been used to simplify the result. Consequently, (5.18) simplifies to

$$|\epsilon_{tot,X,Y}| \leq \max |\epsilon_{CLT,X}| + |\epsilon_{SNR,X,Y}|. \tag{5.20}$$

Thus, the magnitude of the total approximation error is bounded by the sum of the maximum absolute error resulting from the use of the central limit theorem and the absolute error resulting from the use of the low SNR approximation. As the former quantity has already been bounded (recall Table 4.1), the following discussion concentrates on bounds for the latter.

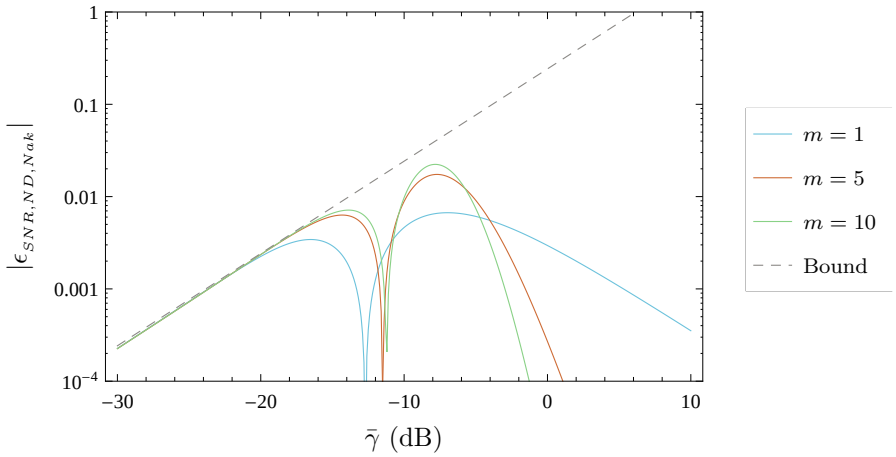

Figure 5.2: A log-linear plot of the error resulting from the low SNR approximation and the bound given in (5.22) for different values of m. In each case, $M = 508$ and $P_{f_{ND}} = 0.1$.

An asymptotic bound for small values of $\bar{\gamma}$

Before progressing, the following lemma, which is proved in Appendix A.3, is required.

> **Lemma 5.2:** For the diversity type X and channel type Y, the absolute value of the low SNR approximation error is bounded as
>
> $$|\epsilon_{SNR,X,Y}| \leq \frac{1}{\sqrt{2\pi e}} \cdot \frac{1}{N_X} \int_{-\infty}^{\infty} x \; f_{X,Y}(x) \; dx. \tag{5.21}$$

It is interesting to note that the integral in (5.21) is equivalent to the expected value of a random variable, Z. Accordingly, the integral in (5.21) will simplify to the mean of the distribution specified by $f_{X,Y}(x)$.

Therefore, for energy detectors with no diversity, the absolute value of the error resulting from the use of the low SNR approximation can be bounded as

$$|\epsilon_{SNR,ND,Nak}| \leq \frac{\bar{\gamma}}{\sqrt{2\pi e}}, \tag{5.22}$$

where the fact that the mean of the gamma distribution defined by $f_{ND,Nak}(x)$ is $\bar{\gamma}$ has been used to simplify the result. Thus, as $\bar{\gamma} \to 0$, $\epsilon_{SNR,ND,Nak} \to 0$. This can be seen quite clearly in Figure 5.2, where $|\epsilon_{SNR,ND,Nak}|$ has been calculated numerically for different values of m. Unfortunately, as can also be seen, the bound does not describe the error well when the signal to noise ratio is large. Thus, there is some motivation to consider bounds more suited to such situations.

A bound for the maximum error resulting from the low SNR approximation

Before progressing, the following lemma, which is proved in Appendix A.4, is required.

> **Lemma 5.3:** For the diversity type X and fading channel type Y, the absolute value of the low SNR approximation error is bounded as
>
> $$|\epsilon_{SNR,X,Y}| \lessapprox \frac{1}{\sqrt{MN_X\pi}} \max_x \left(x \; f_{X,Y}(x) \right), \tag{5.23}$$
>
> where the symbol $\lessapprox$ indicates that the left hand side of the equation is less than, or approximately equal to, the right hand side.

Using Lemma 5.3, $|\epsilon_{SNR,ND,Nak}|$ can be bounded as

$$|\epsilon_{SNR,ND,Nak}| \lessapprox \frac{1}{\sqrt{M\pi}} \max_x \left(x \; f_{ND,Nak}(x) \right). \tag{5.24}$$

From (3.29), it can be seen that $f_{ND,Nak}(x) = 0$ for $x \leq 0$ and $f_{ND,Nak}(x) \geq 0$ for $x > 0$. Consequently, $x \; f_{ND,Nak}(x)$ is maximised when $x > 0$. Under this condition, $x \; f_{ND,Nak}(x)$ can be written as

$$\begin{aligned} x \; f_{ND,Nak}(x) &= x \left(\frac{m}{\bar{\gamma}} \right)^m \frac{x^{m-1}}{\Gamma(m)} e^{-\frac{mx}{\bar{\gamma}}} \\ &= \bar{\gamma} \left[\left(\frac{m}{\bar{\gamma}} \right)^{m+1} \frac{x^m}{\Gamma(m+1)} e^{-\frac{mx}{\bar{\gamma}}} \right]. \end{aligned} \tag{5.25}$$

The term in the square brackets in (5.25) is equivalent to the probability density function of a gamma distributed random variable, with a shape parameter equal to $m+1$ and a scale parameter equal to $\frac{\bar{\gamma}}{m}$. As the gamma distribution is a unimodal distribution, its maximum value occurs at its mode, in this case when $x = \bar{\gamma}$. Using this, it is not difficult to show that

$$\begin{aligned} \max_x \left(x \; f_{ND,Nak}(x) \right) &= \bar{\gamma} \left[\left(\frac{m}{\bar{\gamma}} \right)^{m+1} \frac{x^m}{\Gamma(m+1)} e^{-\frac{mx}{\bar{\gamma}}} \right] \Bigg|_{x=\bar{\gamma}} \\ &= \frac{\left(\frac{m}{e}\right)^m}{\Gamma(m)}, \end{aligned} \tag{5.26}$$

and so (5.24) can be simplified to

$$|\epsilon_{SNR,ND,Nak}| \lessapprox \frac{\left(\frac{m}{e}\right)^m}{\sqrt{M\pi}\;\Gamma(m)}. \tag{5.27}$$

While (5.27) is a useful result, it is not particularly intuitive. However, Stirling's

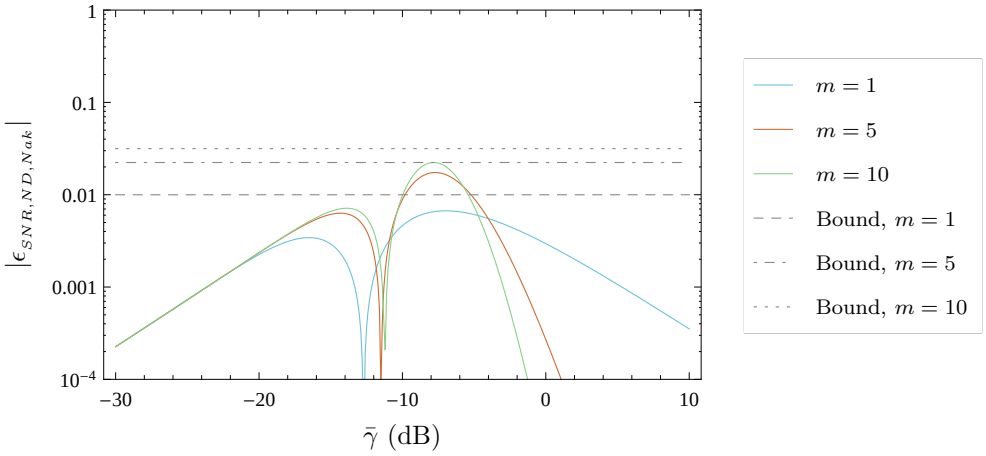

Figure 5.3: A log-linear plot of the error resulting from the use of the low SNR approximation and the bound given in (5.29) for different values of m. In each case, $M = 508$ and $P_{f_{ND}} = 0.1$.

approximation, in its inequality form [49, Equation 6.1.37], can be used to show that

$$\frac{\left(\frac{n}{e}\right)^n}{\Gamma(n)} < \sqrt{\frac{n}{2\pi}}, \tag{5.28}$$

to further simplify (5.27) to

$$|\epsilon_{SNR,ND,Nak}| \lessapprox \frac{1}{\pi}\sqrt{\frac{m}{2M}}, \tag{5.29}$$

the behaviour of which is more immediately clear than the bound given in (5.27). Figure 5.3 illustrates the bound given in (5.29) for different values of m.

One interesting feature of (5.29) is that the maximum error resulting from the low SNR approximation behaves similarly to the maximum error resulting from the use of the central limit theorem, in that it is inversely proportional to $\sqrt{M}$. Thus, for sufficiently large numbers of samples, the low SNR approximation error can be made arbitrarily small. Less conveniently, however, (5.29) also states that, as m becomes larger, the maximum value of the error increases, which can also be seen in Figure 5.3. Still, it should be noted that while such an increase can occur, its effect is not unbounded: recall from (A.79) that $|\epsilon_{SNR,ND,Nak}| \lessapprox \frac{1}{\sqrt{2\pi e}}$ and so, at worst, $|\epsilon_{SNR,ND,Nak}| \to \frac{1}{\sqrt{2\pi e}}$ as $m \to \infty$.

The derived bounds can be summarised using

$$\max|\epsilon_{SNR,ND,Nak}| = \min\left(\frac{\bar{\gamma}}{\sqrt{2\pi e}}, \frac{1}{\pi}\sqrt{\frac{m}{2M}}\right), \tag{5.30}$$

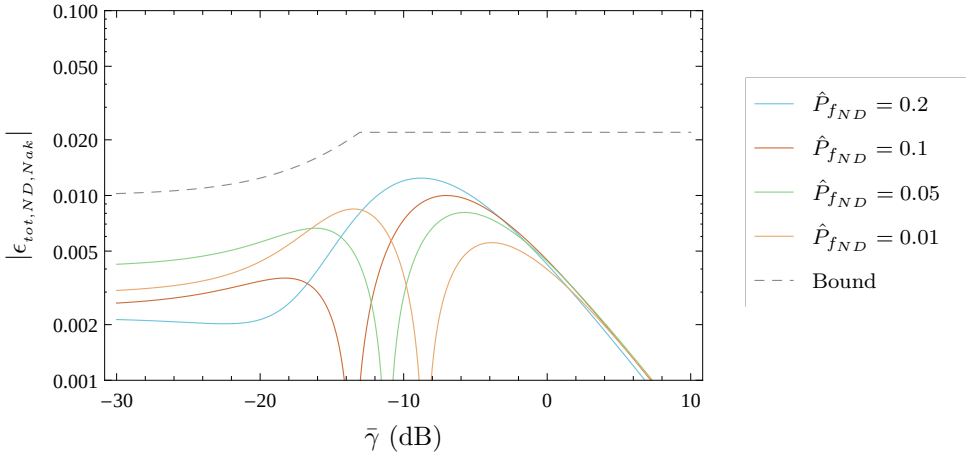

Figure 5.4: A log-linear plot of the approximation error resulting from the use of (5.16) for the conditions used to generate Figure 5.1. The value of the bound changes at approximately $\bar{\gamma} = -13\,\text{dB}$ because the value given by (5.22) becomes smaller than the value given by (5.29).

where, by definition, $\max|\epsilon_{SNR,ND,Nak}| \geq |\epsilon_{SNR,ND,Nak}|$. Consequently,

$$\max|\epsilon_{tot,ND,Nak}| \leq \max|\epsilon_{CLT,ND}| + \max|\epsilon_{SNR,ND,Nak}|, \tag{5.31}$$

where $\max|\epsilon_{tot,ND,Nak}| \geq |\epsilon_{tot,ND,Nak}|$.

Using (5.31) and the conditions used to generate Figure 5.1, it is not difficult to show that the approximation error resulting from the use of (5.16) can be bound as shown in Figure 5.4. As can be seen, the bound given by (5.31) describes the error well over the entire range of signal to noise ratios, particularly as the signal to noise ratio becomes small.

5.2.1.3 Novel approximations for other system parameters

While the approximation in (5.15) is a convenient way to calculate the probability of detection, there does not appear to be a simple method by which it can be manipulated to yield equations for quantities such as sample complexity or minimum signal to noise ratio in the manner of Section 4.4. Essentially, this is because $\tilde{P}_{d_{ND,Nak}}$ depends, in part, on a series with a variable number of terms. Even in the simplest case, where $m = 1$ and the series contains just one term, (5.15) gives an expression which is not readily invertible (see (5.16)). However, that is not to say that new insights cannot be gained.

Consider the formula for the probability of false alarm for energy detectors with no

diversity given in Table 4.1. By inverting the Q function, it can be shown that

$$Q^{-1}(\hat{P}_{f_{ND}}) = \frac{\lambda - M}{\sqrt{2M}}. \tag{5.32}$$

Using (5.32), (5.15) can be written as

$$\begin{aligned}\tilde{P}_{d_{ND,Nak}} = \hat{P}_{f_{ND}} + \frac{1}{2}\exp\left[-\frac{2m}{\sqrt{M\bar{\gamma}^2}}\left(\frac{Q^{-1}(\hat{P}_{f_{ND}})}{\sqrt{2}} - \frac{m}{2\sqrt{M\bar{\gamma}^2}}\right)\right] \\ \times \sum_{p=0}^{m-1}\left(\frac{2m}{\sqrt{M\bar{\gamma}^2}}\right)^p \mathrm{i}^p\,\mathrm{erfc}\left[-\left(\frac{Q^{-1}(\hat{P}_{f_{ND}})}{\sqrt{2}} - \frac{m}{\sqrt{M\bar{\gamma}^2}}\right)\right].\end{aligned} \tag{5.33}$$

Thus, $\tilde{P}_{d_{ND,Nak}}$ is a function of the parameters $\hat{P}_{f_{ND}}$, m, M and $\bar{\gamma}$ only.

Now, consider the case where $\tilde{P}_{d_{ND,Nak}}$, $\hat{P}_{f_{ND}}$ and m are constant. If M and $\bar{\gamma}$ are allowed to vary, then the product $k = M\bar{\gamma}^2$ must also be constant for equality to hold in (5.33). Therefore, if the sample complexity is known for a given value of $\bar{\gamma}$, the sample complexity at a different value of $\bar{\gamma}$ can easily be deduced.

To see this more clearly, let M_0 denote the number of samples required to meet some arbitrary pair of decision probabilities in a Nakagami-m channel with average signal to noise ratio $\bar{\gamma}_0$. Therefore,

$$k = M_0\bar{\gamma}_0^2. \tag{5.34}$$

Now, let M_1 denote the number of samples required to ensure that the same operating conditions are met in a similar Nakagami-m channel with average signal to noise ratio $\bar{\gamma}_1$. By the same logic as before,

$$k = M_1\bar{\gamma}_1^2, \tag{5.35}$$

and so

$$M_1 \approx M_0\left(\frac{\bar{\gamma}_0}{\bar{\gamma}_1}\right)^2, \tag{5.36}$$

where the approximation symbol is intended to emphasise that (5.36) is derived from (5.15) and so is only accurate when $\epsilon_{tot,ND,Nak}$ is small.

There are two noteworthy points regarding (5.36): firstly, that it describes precisely the same behaviour as (4.34), and so the product of the sample complexity and the square of the signal to noise ratio is approximately constant for AWGN, Rayleigh and Nakagami-m channels; and secondly, that it is difficult to see how it could have been deduced from any of the exact formulations available in the literature (see Table 3.2).

Furthermore, using (5.36) avoids the need for numerical methods when calculating the

sample complexity while still yielding good accuracy. For instance, given that precisely 4795310 samples are required in order to ensure that the probability of detection of an energy detector with no diversity, operating on a Rayleigh faded channel, is equal to 0.9 when its probability of false alarm is 0.1 and the average signal to noise ratio is $-21\,\text{dB}$, (5.36) can be used to show that approximately 30257 samples are required to ensure the same operating conditions at a single to noise ratio of $-10\,\text{dB}$. Using a more computationally intensive numerical root finding method, it can be shown that the exact number of samples required is 30640 — a difference of just 383 samples.

A further consequence of (5.36) is that the minimum signal to noise ratio, for a given number of samples, can easily be calculated if the minimum signal to noise ratio for a different (also given) number of samples is already known. This can be shown by rearranging (5.36) to give

$$\bar{\gamma_1} \approx \bar{\gamma_0}\sqrt{\frac{M_0}{M_1}}. \tag{5.37}$$

Again, it should be noted that (5.37) is only valid when the total approximation error is small.

The approximation in (5.37) is useful in approximating the change in the minimum signal to noise ratio of a receiver when the number of samples is adjusted. For instance, given that precisely 180290 samples are required in order to ensure that the minimum signal to noise ratio for an energy detector with no diversity operating on a Nakagami-m faded channel with $m = 3$ is $-14\,\text{dB}$, when the probability of missed detection is 0.01 and the probability of false alarm is 0.1, (5.37) can be used to show that doubling the number of samples will increase the minimum signal to noise ratio to approximately $-15.51\,\text{dB}$. Using a more computationally intensive numerical method, it can be shown that the exact answer is also $-15.51\,\text{dB}$.

5.2.1.4 Summary

In this subsection, an approximate representation for the probability of detection of an energy detector with no diversity operating on a Nakagami-m channel was derived under the assumption that the signal to noise ratio is small. The approximation has a novel, closed form and allows the accurate calculation of the probability of detection in many scenarios of interest. Unfortunately, it is valid for $m \in \mathbb{N}^+$ only, but some restriction of applicability is to be expected as abstraction often comes at the cost of generality. Despite this, the approximation was shown to be a useful, accurate and a convenient way by which to compute the probability of detection, even in situations where moderate to small numbers of samples are available (recall Figure 5.1).

It was shown that the total error resulting from the use of the approximation must be

less than or equal to the sum of the error resulting from the use of the central limit theorem and the error resulting from the use of the low SNR approximation. Two simple bounds for the latter quantity were derived, each having a distinct region of applicability. The first bound, given by (5.22), relates the low SNR approximation error to the average signal to noise ratio at the combiner output. This is most likely to be useful when dealing with practical spectrum sensing problems, where the required minimum signal to noise ratio is very small. However, as the bound tends to significantly overestimate the error as the signal to noise ratio increases, a second bound, given by (5.29), was also provided. This bound relates the low SNR approximation error to the fading parameter and number of samples, and so is likely to be of more general use than the previous bound, although it tends to significantly overestimate the approximation error when the signal to noise ratio is low and the number of samples is moderate. Thus, each bound has its own region of applicability, and so it is possible that one may employ either or both during the design or analysis of a sensor system.

As Atapattu et al.'s approximation for the detection probability of energy detectors with no diversity operating on Nakagami-m channels is numerically equivalent to (5.15), the bound given in (5.31) can also be used to quantify the error from its use. Similarly, it can be used to describe the error resulting from the use of the central limit theorem and low SNR approximation in López-Benítez and Casadevall's approximation for the probability of detection of an energy detector with no diversity operating on a Rayleigh channel. However, in the latter case, the authors also use an approximation for the Gaussian Q function, and so the total error resulting from the use of their approximation for the detection probability cannot be entirely bounded using (5.31).

As a further point of interest, it is noteworthy that, as the average signal to noise ratio becomes small, $\max|\epsilon_{tot,ND,Nak}| \to \max|\epsilon_{CLT,ND}|$. Thus, for receivers with sufficiently small sensitivities, the total approximation error is comparable in magnitude to the error resulting from the use of the central limit theorem. Therefore, for spectrum sensing type applications, where signals must be detected at low signal to noise ratios, the approximation given in (5.15) performs no worse than the approximations in Table 4.1. As the latter approximations have seen widespread use in the literature (those which apply to energy detection with no diversity, that is), it is reasonable to suggest that the new approximation is equally applicable.

Further approximations, for the sample complexity and minimum signal to noise ratio, were also considered. While it was found that the approximation in (5.15) is not well suited to functional inversion, and so closed form expressions are difficult to derive, it was possible to draw some novel insights into the behaviour of these quantities in certain scenarios of interest which, it appears, are not readily inferred from the exact expressions given in Table 3.2. In particular, it was shown that if the sample complexity at a given signal to noise ratio is known, then the sample complexity at a different signal to noise ratio can easily be inferred, or vice versa. This is likely to be of use in scenarios

where parameter adjustments must be made on the spectrum sensor device itself, and so computation time and/or power are constrained, or simply to save time when designing or analysing such systems.

Finally, it is interesting to note that, as the average signal to noise ratio becomes very large, the low SNR approximation error tends towards zero. This is to be expected since, by definition,

$$\begin{aligned} \lim_{\bar{\gamma}\to\infty} \hat{P}_{d_{ND,Nak}} = \lim_{\bar{\gamma}\to\infty} \tilde{P}_{d_{ND,Nak}} = 1 \\ \implies \lim_{\bar{\gamma}\to\infty} |\epsilon_{SNR,ND,Nak}| = 0. \end{aligned} \tag{5.38}$$

Yet, both derived bounds for the low SNR approximation error overestimate the actual error by a significant amount when the average signal to noise ratio is large (see Figures 5.2 and 5.3). However, the aim of this thesis is not the general analysis of energy detection (for this, the work discussed in Chapter 3 is more appropriate), but a simplified analysis of energy detection suitable for use in spectrum sensing applications. Therefore, the behaviour of energy detectors at large signal to noise ratios is not of particular interest and, while it is possible to derive a bound more appropriate for use when the average signal to noise ratio is large, to do so here would be a digression. With this in mind, it is worth considering how the analysis in this subsection can be extended to architectures employing MRC, EGC and SLC diversity.

5.2.2 Receivers with MRC diversity

For energy detectors employing a maximal ratio combiner, the probability of detection in Nakagami-m channels can be approximated by substituting (3.33) into (5.8) to give

$$\begin{aligned} P_{d_{MRC,Nak}} \approx \tilde{P}_{d_{MRC,Nak}} &= F_{mn}\left(\frac{\lambda - M}{\sqrt{2M}}, \sqrt{\frac{M}{2}}, \frac{m}{\bar{\gamma}}\right) \\ &= \hat{P}_{f_{MRC}} + \frac{1}{2}\exp\left[-\frac{\frac{2m}{\bar{\gamma}}}{\sqrt{M}}\left(\frac{\lambda - M - \frac{m}{\bar{\gamma}}}{2\sqrt{M}}\right)\right] \\ &\quad \times \sum_{p=0}^{mn-1}\left(\frac{\frac{2m}{\bar{\gamma}}}{\sqrt{M}}\right)^p \mathrm{i}^p \operatorname{erfc}\left[-\left(\frac{\lambda - M - \frac{2m}{\bar{\gamma}}}{2\sqrt{M}}\right)\right]. \end{aligned} \tag{5.39}$$

As a consequence of Lemma 5.1, (5.39) is valid for $mn \in \mathbb{N}^+$ only. Thus, in this case, non integer values of m are allowed as long as their product with the number of diversity branches, n, remains an integer.

In a similar manner to (5.31), the total approximation error, $\epsilon_{tot,MRC,Nak}$, can be

bounded as

$$\begin{aligned} \epsilon_{tot,MRC,Nak} &= P_{d_{MRC,Nak}} - \tilde{P}_{d_{MRC,Nak}} \\ \implies \max|\epsilon_{tot,MRC,Nak}| &\leq \max|\epsilon_{CLT,MRC}| + \max|\epsilon_{SNR,MRC,Nak}|. \end{aligned} \tag{5.40}$$

Using Lemma 5.2, it is possible to derive a bound for $|\epsilon_{SNR,MRC,Nak}|$ as a function of the average signal to noise ratio:

$$|\epsilon_{SNR,MRC,Nak}| \leq \frac{n\bar{\gamma}}{\sqrt{2\pi e}}, \tag{5.41}$$

where the fact that the mean of the gamma distribution defined by $f_{MRC,Nak}(x)$ is $n\bar{\gamma}$ has been used to simplify the result.

Using Lemma 5.3, $|\epsilon_{SNR,MRC,Nak}|$ can also be bound as

$$|\epsilon_{SNR,MRC,Nak}| \lessapprox \frac{1}{\sqrt{M\pi}} \max_x \left(x \ f_{MRC,Nak}(x) \right), \tag{5.42}$$

where, in a similar fashion to (5.27), it can be shown that

$$\begin{aligned} \max_x \left(x \ f_{MRC,Nak}(x) \right) &= n\bar{\gamma} \left[\left(\frac{m}{\bar{\gamma}} \right)^{mn+1} \frac{x^{mn}}{\Gamma(mn+1)} e^{-\frac{mx}{\bar{\gamma}}} \right] \Bigg|_{x=n\bar{\gamma}} \\ &= \frac{\left(\frac{mn}{e}\right)^{mn}}{\Gamma(mn)} \\ &< \sqrt{\frac{mn}{2\pi}}, \end{aligned} \tag{5.43}$$

and so (5.42) can be simplified to

$$|\epsilon_{SNR,MRC,Nak}| \lessapprox \frac{1}{\pi}\sqrt{\frac{mn}{2M}}. \tag{5.44}$$

As before, both bounds can be described using the single expression

$$\max|\epsilon_{SNR,MRC,Nak}| = \min\left(\frac{n\bar{\gamma}}{\sqrt{2\pi e}}, \frac{1}{\pi}\sqrt{\frac{mn}{2M}} \right). \tag{5.45}$$

Figure 5.5(a) illustrates the exact (calculated numerically) and approximate (calculated using (5.39)) probabilities of detection for a two branch MRC receiver operating on a Nakagami-m channel with $m = 1.5$ (i.e. $mn = 3$). Measuring the difference between the exact and approximate probabilities, it can easily be shown that the error is bounded by (5.40) over the entire range of values of signal to noise ratio, as shown in Figure 5.5(b).

As in the no diversity case, deriving a closed form solution for the sample complexity or minimum signal to noise ratio of the sensor system is a difficult problem. However,

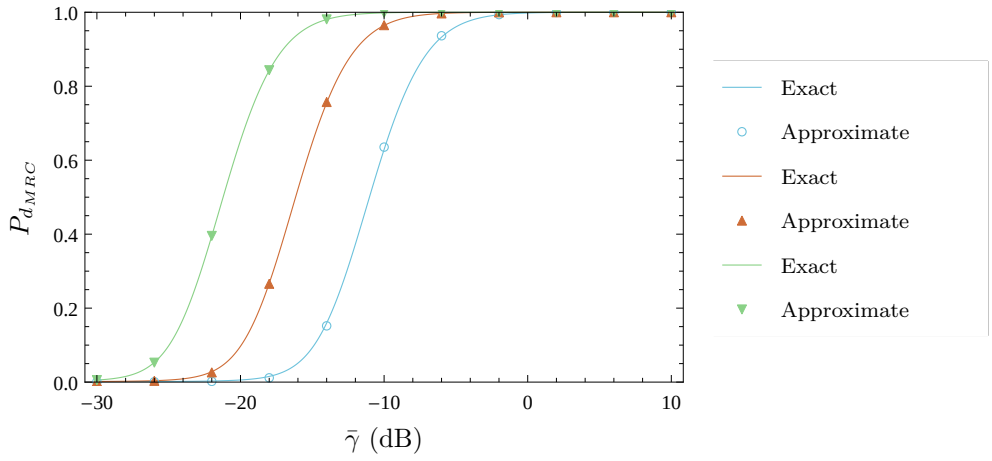

(a) A plot of the exact and approximate probabilities of detection.

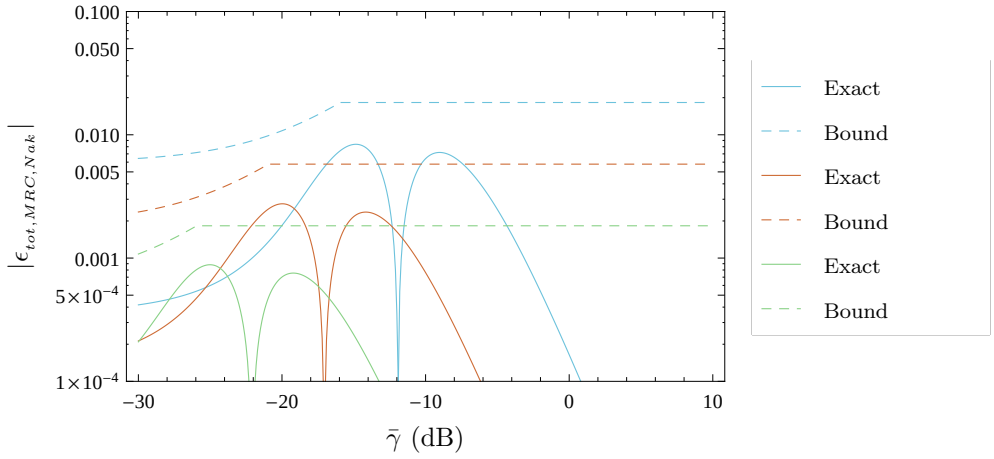

(b) A log-linear plot of the total approximation error, and its bound, for the trends shown in Figure 5.5(a).

Figure 5.5: Plots of the exact and approximate probabilities of detection, and the resulting approximation errors, for energy detectors with two branch MRC diversity operating on a Nakagami-m channel with $m = 1.5$. The blue trends correspond to $M = 1000$, the red trends to $M = 10000$ and the green trends to $M = 100000$. In each case, $P_{f_{MRC}} = 1 \times 10^{-3}$.

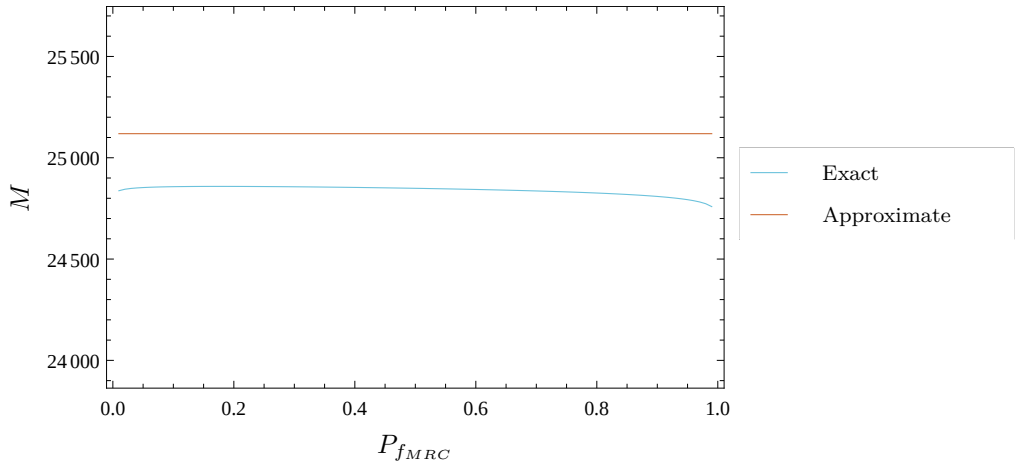

Figure 5.6: A plot of exact and approximate sample complexities as functions of the probability of false alarm.

in a similar fashion to (5.33), $\tilde{P}_{d_{MRC,Nak}}$ can be written in the form

$$\tilde{P}_{d_{MRC,Nak}} = \hat{P}_{f_{MRC}} + \frac{1}{2}\exp\left[-\frac{2m}{\sqrt{M\bar{\gamma}^2}}\left(\frac{Q^{-1}(\hat{P}_{f_{MRC}})}{\sqrt{2}} - \frac{m}{2\sqrt{M\bar{\gamma}^2}}\right)\right] \times \sum_{p=0}^{mn-1}\left(\frac{2m}{\sqrt{M\bar{\gamma}^2}}\right)^p \mathrm{i}^p \operatorname{erfc}\left[-\left(\frac{Q^{-1}(\hat{P}_{f_{MRC}})}{\sqrt{2}} - \frac{m}{\sqrt{M\bar{\gamma}^2}}\right)\right]. \quad (5.46)$$

Thus, it can be inferred that the sample complexity and minimum signal to noise ratio behave as in (5.36) and (5.37), respectively. Again, this is useful in many practical situations. For instance, if it is known that 10000 samples are required to ensure some arbitrary pair of decision probabilities for an energy detector with two branch MRC diversity in a Nakagami-m channel with $m = 1.5$ and an average signal to noise ratio of $-15\,\mathrm{dB}$, then (5.36) can be used to show that approximately 25119 samples are required to ensure the same decision probabilities are met for an energy detector with three branch MRC diversity operating on a Rayleigh channel with an average signal to noise ratio of $-17\,\mathrm{dB}$. This can be verified for arbitrary decision probabilities using a numerical method, as in Figure 5.6.

Unfortunately, it is not possible to use a method similar to (5.36) to analyse the effect of adding additional diversity branches to the sensor system. However, as can be seen in (5.46), the only effect of increasing n is to increase the number of terms in the series therein. This feature can be exploited to some advantage.

Consider an MRC sensor system with n_0 branches and detection probability P_{d_0} operating on a Nakagami-m channel, where $mn_0 \in \mathbb{N}^+$. If the number of branches changes to n_1, where $mn_1 \in \mathbb{N}^+$, and all other parameters remain constant, so that the resulting probability of detection is given by P_{d_1}, then, using (5.46), the resulting change in the

detection probability, $\delta P_d = P_{d_1} - P_{d_0}$, can be written as

$$\begin{aligned}\delta P_d = \ & \operatorname{sign}(n_1 - n_0)\frac{1}{2}\exp\left[-\frac{2m}{\sqrt{M\bar{\gamma}^2}}\left(\frac{Q^{-1}(\hat{P}_{f_{MRC}})}{\sqrt{2}} - \frac{m}{2\sqrt{M\bar{\gamma}^2}}\right)\right] \\ & \times \sum_{p=n_{min}}^{n_{max}} \left(\frac{2m}{\sqrt{M\bar{\gamma}^2}}\right)^p \mathrm{i}^p \operatorname{erfc}\left[-\left(\frac{Q^{-1}(\hat{P}_{f_{MRC}})}{\sqrt{2}} - \frac{m}{\sqrt{M\bar{\gamma}^2}}\right)\right], \end{aligned} \tag{5.47}$$

where $\operatorname{sign}(x) = \frac{x}{|x|}$ if $x \neq 0$ and is zero otherwise, $n_{min} = \min(mn_0, mn_1)$ and $n_{max} = \max(mn_0 - 1, mn_1 - 1)$. Thus, while an expression for the diversity gain is not directly available, the effect of modifying the number of branches in the system is not difficult to quantify, and so the former quantity can easily be calculated using a simple numerical method. It is again worth noting that it is difficult to see how (5.47) could have been inferred from any of the exact expressions given in Table 3.3.

The approximation in (5.47) can be used to determine the number of branches required to ensure certain operating conditions are met as different system parameters vary. For instance, if an energy detector with two branch MRC diversity operates on a Nakagami-m channel with $m = 2$, 29340 samples are sufficient to ensure that $P_{f_{MRC}} = 0.1$ and $P_{d_{MRC,Nak}} = 0.9$ at a signal to noise ratio of $-18\,\mathrm{dB}$. However, if it is required that $P_{d_{MRC,Nak}} \geq 0.99$, then the number of additional branches required must be computed using a numerical method. Using (5.47), it can easily be shown that

$$\delta P_d|_{n_0=2,n_1=3} = 0.08,$$

$$\delta P_d|_{n_0=3,n_1=4} = 0.015,$$

and so $P_{d_{MRC,Nak}} \approx 0.995$ when $n = 4$, which satisfies the criteria and agrees with the exact answer, which must be calculated numerically.

5.2.3 Receivers with EGC diversity

In equal gain combiner systems, the approximate probability of detection in Nakagami-m channels, $\tilde{P}_{d_{EGC,Nak}}$, can be calculated by substituting (3.35) into (5.8) to give

$$\begin{aligned}\tilde{P}_{d_{EGC,Nak}} &= F_{mn}\left(\frac{\lambda - M}{\sqrt{2M}}, \sqrt{\frac{M}{2}}, \frac{mn}{\omega\bar{\gamma}}\right) \\ &= \hat{P}_{f_{EGC}} + \frac{1}{2}\exp\left[-\frac{\frac{2mn}{\omega\bar{\gamma}}}{\sqrt{M}}\left(\frac{\lambda - M - \frac{mn}{\omega\bar{\gamma}}}{2\sqrt{M}}\right)\right] \\ &\quad \times \sum_{p=0}^{mn-1}\left(\frac{\frac{2mn}{\omega\bar{\gamma}}}{\sqrt{M}}\right)^p \mathrm{i}^p \operatorname{erfc}\left[-\left(\frac{\lambda - M - \frac{2mn}{\omega\bar{\gamma}}}{2\sqrt{M}}\right)\right]. \end{aligned} \tag{5.48}$$

which, again, as a consequence of Lemma 5.1, is valid for $mn \in \mathbb{N}^+$ only.

In deriving (5.48), Nakagami's approximation for the probability density function of the signal to noise ratio at the EGC output has been used (see (3.35)). Therefore, the total approximation error, $\epsilon_{tot,EGC,Nak}$, cannot be bounded as in (5.20). Instead, $\epsilon_{tot,EGC,Nak}$ can be bounded as

$$\begin{aligned}
\epsilon_{tot,EGC,Nak} &= \int_{-\infty}^{\infty} P_{d_{EGC}}(x) f_{EGC,Nak}(x)\ dx - \int_{-\infty}^{\infty} \tilde{P}_{d_{EGC}}(x) \hat{f}_{EGC,Nak}(x)\ dx \\
\implies |\epsilon_{tot,EGC,Nak}| &= \left| \int_{-\infty}^{\infty} \left(P_{d_{EGC}}(x) - \tilde{P}_{d_{EGC}}(x) \right) \hat{f}_{EGC,Nak}(x)\ dx \right. \\
&\qquad \left. + \int_{-\infty}^{\infty} P_{d_{EGC}}(x) \left(f_{EGC,Nak}(x) - \hat{f}_{EGC,Nak}(x) \right)\ dx \right| \\
&\leq \left| \int_{-\infty}^{\infty} \left(P_{d_{EGC}}(x) - \tilde{P}_{d_{EGC}}(x) \right) \hat{f}_{EGC,Nak}(x)\ dx \right| \\
&\qquad + \left| \int_{-\infty}^{\infty} P_{d_{EGC}}(x) \left(f_{EGC,Nak}(x) - \hat{f}_{EGC,Nak}(x) \right)\ dx \right| \\
&\leq \max |\epsilon_{CLT,EGC}| + |\epsilon_{SNR,EGC,Nak}| + |\epsilon_{PDF,EGC,Nak}|, \qquad (5.49)
\end{aligned}$$

where $|\epsilon_{PDF,EGC,Nak}|$ is given by

$$|\epsilon_{PDF,EGC,Nak}| = \left| \int_{-\infty}^{\infty} P_{d_{EGC}}(x) \left(f_{EGC,Nak}(x) - \hat{f}_{EGC,Nak}(x) \right)\ dx \right|. \qquad (5.50)$$

As before, using Lemma 5.2, $|\epsilon_{SNR,EGC,Nak}|$ can be bounded as

$$|\epsilon_{SNR,EGC,Nak}| \leq \frac{\omega\bar{\gamma}}{\sqrt{2\pi e}}, \qquad (5.51)$$

where the fact that the mean of the gamma distribution defined by $\hat{f}_{EGC,Nak}(x)$ is $\omega\bar{\gamma}$ has been used to simplify the result. Similarly, using Lemma 5.3, it can be shown that

$$|\epsilon_{SNR,EGC,Nak}| \lessapprox \frac{1}{\pi}\sqrt{\frac{mn}{2M}}, \qquad (5.52)$$

which, it is interesting to note, is equivalent to the bound for $|\epsilon_{SNR,MRC,Nak}|$ given in (5.44). Again, both bounds can be described using a single expression:

$$\max |\epsilon_{SNR,EGC,Nak}| = \min \left(\frac{\omega\bar{\gamma}}{\sqrt{2\pi e}}, \frac{1}{\pi}\sqrt{\frac{mn}{2M}} \right). \qquad (5.53)$$

Finally, using the second mean value theorem for infinite integrals [69, Equation 12.114], it can be shown that

$$|\epsilon_{PDF,EGC,Nak}| \leq \max |\epsilon_{PDF,EGC,Nak}| \triangleq \max_{\zeta} \left| \int_{\zeta}^{\infty} \left(f_{EGC,Nak}(x) - \hat{f}_{EGC,Nak}(x) \right)\ dx \right|. \qquad (5.54)$$

Consequently, it can be shown that

$$\max |\epsilon_{tot,EGC,Nak}| \leq \max |\epsilon_{CLT,EGC}| + \max |\epsilon_{SNR,EGC,Nak}| + \max |\epsilon_{PDF,EGC,Nak}|, \qquad (5.55)$$

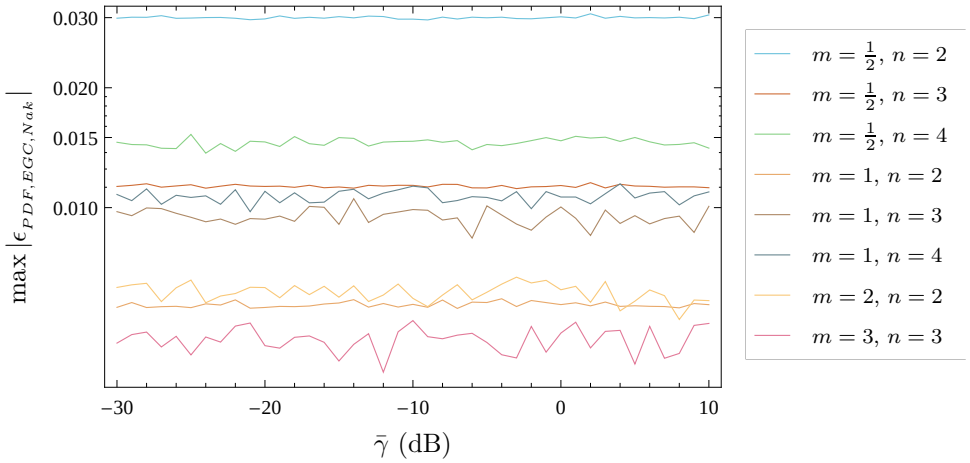

Figure 5.7: Plots of the bound on the error resulting from the use of Nakagami's approximation for the probability density function of the signal to noise ratio at the output of an equal gain combiner operating on a Nakagami-m channel. The trends become less smooth as the error becomes smaller due to the numerical method used to compute them.

where $\max|\epsilon_{tot,EGC,Nak}| \geq |\epsilon_{tot,EGC,Nak}|$.

As $f_{EGC,Nak}(x)$ is currently not available in closed form, (5.54) must be computed numerically. Figure 5.7 illustrates the bound for some typical values of m, n and $\bar{\gamma}$. As can be seen, the error is typically not large, and decreases as m and n increase. In particular, the worst case error occurs when $m = \frac{1}{2}$ and $n = 2$, and is approximately equal to 0.03 across the entire range of the signal to noise ratios considered. It is also worth noting that, while it appears that the error bound is constant for varying $\bar{\gamma}$, this is difficult to verify due to the lack of a closed form expression for $f_{EGC,Nak}(x)$.

While the error resulting from the use of Nakagami's approximation for the PDF of the signal to noise ratio at the output of an EGC system may be unacceptably large in some circumstances, it is worth noting that the only known exact method for the computation of $P_{d_{EGC,Nak}}$ is that of Herath and Rajatheva (see Table 3.4 for their expressions for $n = 2$ and $n = 3$). However, their method is a complicated one, and becomes even more so as n increases. Dharmawansa et al. noted that this difficulty arises from the need to compute nested infinite series, which are hard to evaluate in general, and whose number increases linearly with n. Thus, (5.48) offers a significantly simpler and, in many cases of interest, accurate alternative.

The accuracy of the approximation in (5.48) can be quantified using (5.49), as shown in Figures 5.8(a) and 5.8(b), where the exact probability of detection has been calculated using a numerical method. As can be seen, the derived approximation is quite accurate in each of the given scenarios.

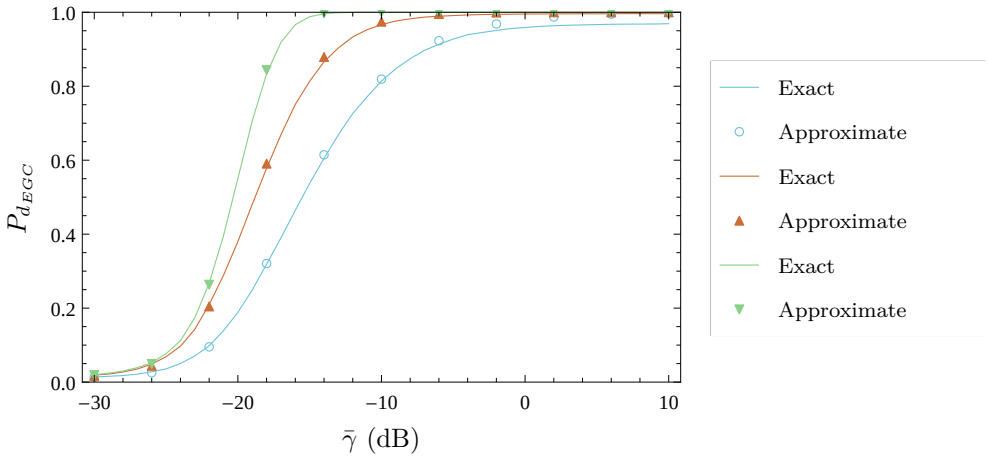

(a) A plot of the exact and approximate probabilities of detection.

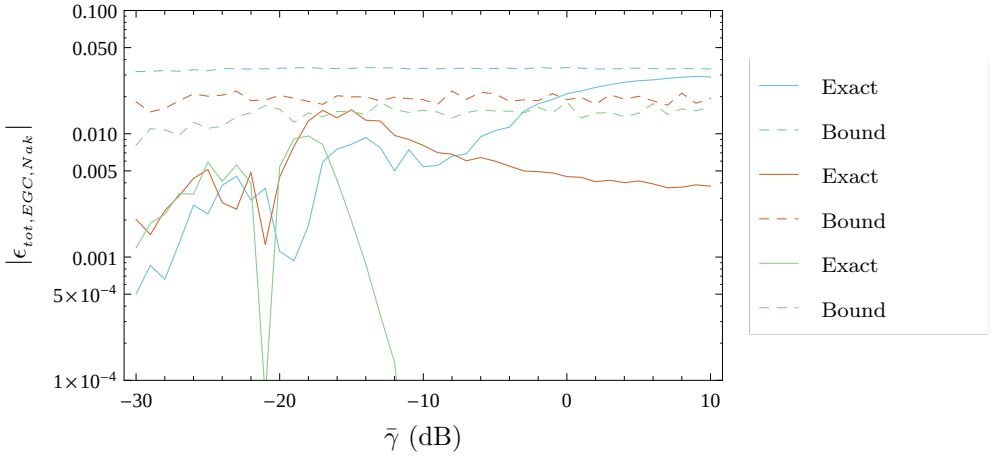

(b) A log-linear plot of the total approximation error, and its bound, for the trends shown in Figure 5.8(a). The numerical calculation of the exact detection probabilities has affected the smoothness of the trends.

Figure 5.8: Plots of the exact and approximate probabilities of detection, and the resulting approximation errors, for energy detectors with EGC diversity operating on Nakagami-m channels. The blue trends correspond to $m = \frac{1}{2}$ and $n = 2$, the red trends to $m = \frac{1}{2}$ and $n = 4$ and the green trends to $m = 1$, $n = 4$. In each case, $M = 10000$ and $P_{f_{EGC}} = 0.01$.

In a similar manner to (5.33), it can also be shown that

$$\tilde{P}_{d_{EGC,Nak}} = \hat{P}_{f_{EGC}} + \frac{1}{2}\exp\left[-\frac{\frac{2mn}{\omega}}{\sqrt{M\bar{\gamma}^2}}\left(\frac{Q^{-1}(\hat{P}_{f_{EGC}})}{\sqrt{2}} - \frac{\frac{mn}{\omega}}{2\sqrt{M\bar{\gamma}^2}}\right)\right] \times \sum_{p=0}^{mn-1}\left(\frac{\frac{2mn}{\omega}}{\sqrt{M\bar{\gamma}^2}}\right)^p \mathrm{i}^p\,\mathrm{erfc}\left[-\left(\frac{Q^{-1}(\hat{P}_{f_{EGC}})}{\sqrt{2}} - \frac{\frac{mn}{\omega}}{\sqrt{M\bar{\gamma}^2}}\right)\right], \quad (5.56)$$

and so it can again be inferred that $M\bar{\gamma}^2$ must remain constant for given values of $\tilde{P}_{d_{EGC,Nak}}$, $\hat{P}_{f_{EGC}}$, m and n (recall from (3.36) that ω is a function of both m and n). Thus, (5.36) and (5.37) also hold for EGC diversity receivers, if the total approximation error is not large.

It is also interesting to note that the sample complexity of MRC and EGC receivers can be related using (5.46) and (5.56). To see this, consider the scenario where an energy detector with MRC diversity uses $M = M_0$ samples and an energy detector with EGC diversity uses $M = M_1$ samples. If $\tilde{P}_{d_{MRC,Nak}} = \tilde{P}_{d_{EGC,Nak}}$ and $\hat{P}_{f_{MRC}} = \hat{P}_{f_{EGC}}$, it is not difficult to show that

$$\tilde{M}_{_{EGC,Nak}} \triangleq M_1 = \left(\frac{n}{\omega}\right)^2 M_0 \triangleq \left(\frac{n}{\omega}\right)^2 \tilde{M}_{_{MRC,Nak}}, \quad (5.57)$$

where $M_{_{X,Y}}$ denotes the sample complexity for an energy detector with diversity type X operating on the channel type Y and $\tilde{M}_{_{X,Y}} \approx M_{_{X,Y}}$ when the total approximation errors, given by (5.40) and (5.55), are small.

The approximation in (5.57) is useful when comparing the number of samples required to ensure certain decision probabilities are met for MRC and EGC architectures. For instance, if an energy detector with two branch MRC diversity requires precisely 164828 samples to ensure that $P_{d_{MRC,Nak}} = 0.99$ and $P_{f_{MRC}} = 0.01$ in a Nakagami-m channel with $\bar{\gamma} = -15\,\mathrm{dB}$ and $m = 1.5$, (5.57) can be used to show that an EGC receiver, with the same number of branches, operating on a similar channel, requires approximately 192886 samples to achieve the same decision probabilities. Using a numerical method, it can be shown that the precise number of samples required is 192148 — a difference of just 0.38%.

While the relationships between the number of samples and signal to noise ratio are not difficult to establish, the effect of altering the number of diversity branches cannot be quantified so simply as n affects both the number of terms, and their individual values, in the series in (5.56). Still, for EGC diversity, the number of branches is typically not large, and so it may be feasible to compute the quantity numerically through multiple evaluations of (5.56).

5.2.4 Receivers with SLC diversity

For square law combiner systems, the probability of detection in Nakagami-m channels can be approximated by substituting (3.33) into (5.8), recalling from (5.4) that $N_{_{SLC}} = n$, to give

$$\begin{aligned} P_{d_{SLC,Nak}} \approx \tilde{P}_{d_{SLC,Nak}} &= F_{mn}\left(\frac{\lambda - Mn}{\sqrt{2Mn}}, \sqrt{\frac{M}{2n}}, \frac{m}{\bar{\gamma}}\right) \\ &= \hat{P}_{f_{SLC}} + \frac{1}{2}\exp\left[-\frac{\frac{2mn}{\bar{\gamma}}}{\sqrt{Mn}}\left(\frac{\lambda - Mn - \frac{mn}{\bar{\gamma}}}{2\sqrt{Mn}}\right)\right] \\ &\quad \times \sum_{p=0}^{mn-1}\left(\frac{\frac{2mn}{\bar{\gamma}}}{\sqrt{Mn}}\right)^{p} \mathrm{i}^{p}\operatorname{erfc}\left[-\left(\frac{\lambda - Mn - \frac{2mn}{\bar{\gamma}}}{2\sqrt{Mn}}\right)\right], \end{aligned} \tag{5.58}$$

which, once again, as a consequence of Lemma 5.1, is valid for $mn \in \mathbb{N}^{+}$ only.

Atapattu et al. also derived an approximation for the detection probability of SLC receivers operating on Nakagami-m channels [66, Equation 6] but, unfortunately, there appears to be an error in their derivation (the authors average the detection probability of an SLC receiver over the distribution of the signal to noise ratio of a receiver with no diversity), and so the resulting expression is not meaningful. Correcting the mistake leads to a form similar to their approximation for the detection probability of receivers with no diversity operating on Nakagami-m channels [66, Equation 5], but requiring differentiation on the order of $mn - 1$, which may cause difficulty in practice. As the repeated integral of the complementary error function can be computed using the simple recursive relation in (5.13), the evaluation of (5.58) requires no differentiation and so is preferable from a computational perspective.

As $f_{_{SLC,Nak}}(x) = f_{_{MRC,Nak}}(x)$, the total approximation error, $\epsilon_{_{tot,SLC,Nak}}$, can be bounded as

$$|\epsilon_{_{tot,SLC,Nak}}| \leq \max|\epsilon_{_{CLT,SLC}}| + |\epsilon_{_{SNR,SLC,Nak}}|, \tag{5.59}$$

where, using Lemma 5.2, and recalling that $N_{_{SLC}} = n$, $|\epsilon_{_{SNR,SLC,Nak}}|$ can be bound as

$$|\epsilon_{_{SNR,SLC,Nak}}| \leq \frac{\bar{\gamma}}{\sqrt{2\pi e}}, \tag{5.60}$$

or, alternatively, using Lemma 5.3, as

$$|\epsilon_{_{SNR,SLC,Nak}}| \lessapprox \frac{1}{\pi}\sqrt{\frac{m}{2M}}. \tag{5.61}$$

Once again, both bounds can be summarised using the single expression

$$\max|\epsilon_{SNR,SLC,Nak}| = \min\left(\frac{\bar{\gamma}}{\sqrt{2\pi e}}, \frac{1}{\pi}\sqrt{\frac{m}{2M}}\right), \tag{5.62}$$

where $\max|\epsilon_{SNR,SLC,Nak}| \geq |\epsilon_{SNR,SLC,Nak}|$, and so

$$\max|\epsilon_{tot,SLC,Nak}| \leq \max|\epsilon_{CLT,SLC}| + \max|\epsilon_{SNR,SLC,Nak}|, \tag{5.63}$$

where $\max|\epsilon_{tot,SLC,Nak}| \geq |\epsilon_{tot,SLC,Nak}|$.

Figure 5.9(a) illustrates the exact (calculated using a numerical method) and approximate (calculated using (5.58)) probabilities of detection of energy detectors with SLC diversity, operating on Nakagami-m channels, for some typical scenarios. The errors resulting from the use of the approximations are shown in Figure 5.9(b). As can be seen, the errors are bounded quite well by (5.63) across the entire range of average signal to noise ratio values.

Noting the definition of $\hat{P}_{f_{SLC}}$ in Table 4.1, it can be shown that

$$\begin{aligned}\tilde{P}_{d_{SLC,Nak}} = \hat{P}_{f_{SLC}} + \frac{1}{2}\exp\left[-2m\sqrt{\frac{n}{M\bar{\gamma}^2}}\left(\frac{Q^{-1}(\hat{P}_{f_{SLC}})}{\sqrt{2}} - \frac{m}{2}\sqrt{\frac{n}{M\bar{\gamma}^2}}\right)\right] \\ \times \sum_{p=0}^{mn-1}\left(2m\sqrt{\frac{n}{M\bar{\gamma}^2}}\right)^p \mathrm{i}^p\,\mathrm{erfc}\left[-\left(\frac{Q^{-1}(\hat{P}_{f_{SLC}})}{\sqrt{2}} - m\sqrt{\frac{n}{M\bar{\gamma}^2}}\right)\right],\end{aligned} \tag{5.64}$$

from which it can, once again, be inferred that the sample complexity and minimum signal to noise ratio of SLC systems again behave as in (5.36) and (5.37), respectively.

In a similar manner to (5.57), the sample complexity of energy detectors with SLC diversity can be related to those of energy detectors with MRC and EGC diversity as

$$\hat{M}_{SLC,Nak} = n\hat{M}_{MRC,Nak}, \tag{5.65}$$

$$\hat{M}_{SLC,Nak} = \frac{\omega^2}{n}\hat{M}_{EGC,Nak}. \tag{5.66}$$

Thus, if the sample complexity is known for one architecture, the sample complexity for the other two can be approximated quite simply, as long as the associated approximation errors are not large.

The approximations in (5.65) and (5.66) are useful when comparing the number of samples required to ensure certain decision probabilities are met in MRC, EGC and SLC receivers operating on similar Nakagami-m channels. For instance, if it is known that an energy detector with two branch MRC diversity, operating on a Nakagami-m channel with $m = 0.5$, requires 1200130 samples to ensure a probability of detection of 0.9 and probability of false alarm of 0.1 at a signal to noise ratio of -21 dB, (5.36),

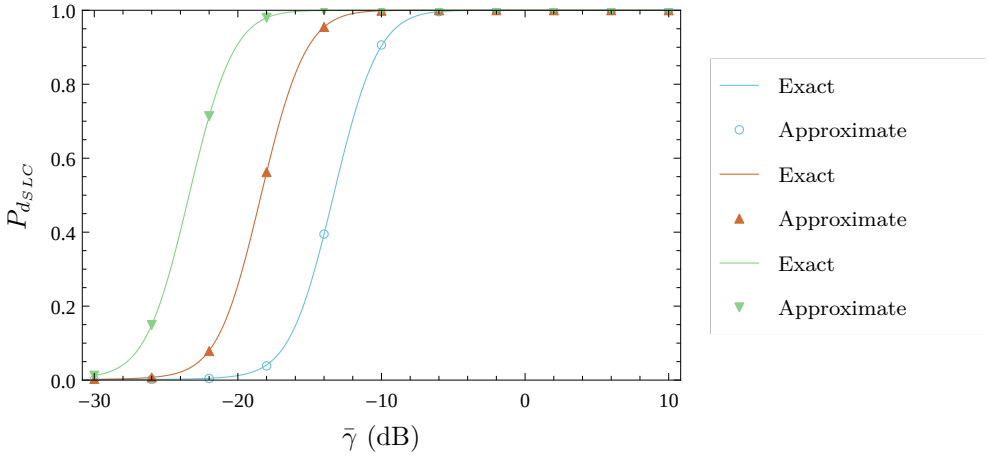

(a) A plot of the exact and approximate probabilities of detection.

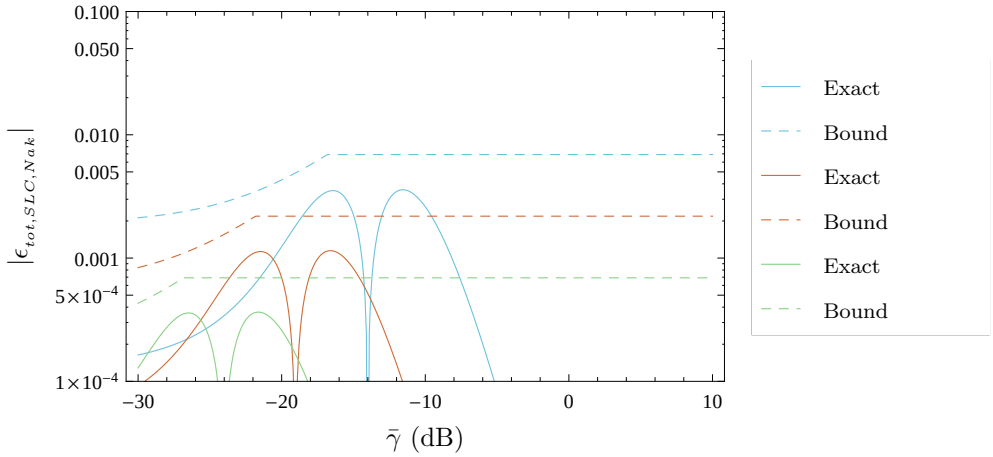

(b) A log-linear plot of the total approximation error, and its bound, for the trends shown in Figure 5.9(a).

Figure 5.9: Plots of the exact and approximate probabilities of detection, and the resulting approximation errors, for energy detectors with ten branch SLC diversity operating on a Nakagami-m channel with $m = 0.5$. The blue trends correspond to $M = 1000$, the red trends to $M = 10000$ and the green trends to $M = 100000$. In each case, $P_{f_{SLC}} = 0.001$.

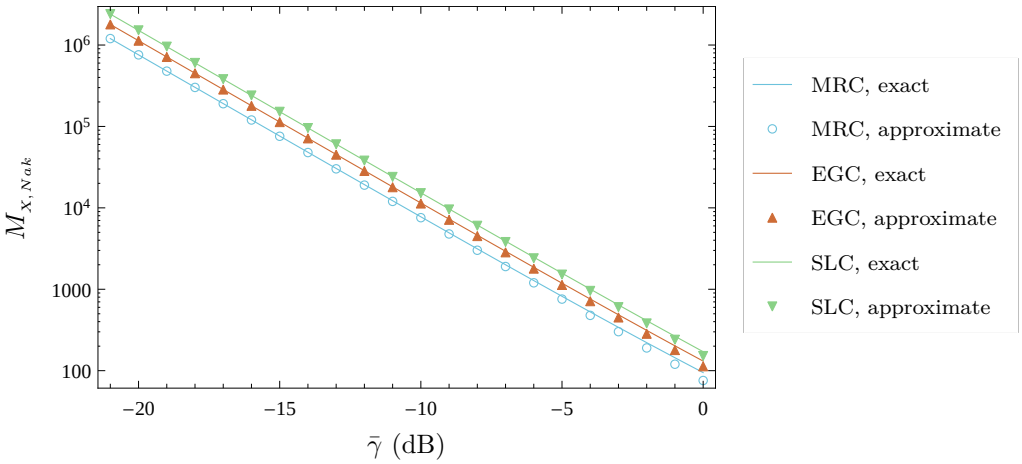

Figure 5.10: A log-linear plot of the number of samples required to ensure that $P_{f_X} = 0.1$ and $P_{d_{X,Nak}} = 0.9$ for the specified diversity receivers. In each case, $n = 2$.

(5.65) and (5.66) can be used to quickly calculate the numbers of samples required to ensure the same conditions are met across a wide range of signal to noise ratio values for MRC, EGC and SLC receivers, without the use of numerical methods, as shown in Figure 5.10. As can be seen, the approximations are quite accurate across the entire range of signal to noise ratio values, particularly as the signal to noise ratio becomes small.

As in the EGC case, the number of terms in the series in (5.64), as well as value of each term in the series, depends on n, and so no additional insight into the behaviour of the diversity gain of the system can be gained. Unlike EGC systems, however, square law combiners can often have large numbers of diversity branches. Consequently, it may not be convenient to calculate the diversity gain via multiple evaluations of (5.58). Thus, there is some motivation to consider alternative methods of approximating the diversity gain.

5.2.5 Discussion

5.2.5.1 Computational complexity

In Chapter 3, it was discussed how each of the exact expressions in Tables 3.2–3.6 contains an infinite series which must be truncated in order to be computed. However, as the truncation points increase with the number of samples, the evaluation of these exact expressions becomes complicated in many scenarios of interest. To address this problem, approximate representations were derived which allow the accurate computation of the probability of detection of energy detector diversity receivers operating on Nakagami-m channels in many situations and, in particular, when the number of samples is large. As each of the derived approximations involves the summation of a series

with mn terms[3], no truncation is required. Consequently, the derived approximations appear to be significantly less complicated than the available exact methods, avoiding the need to compute the truncation point as well as the computation of the truncated infinite series itself.

Yet, the previous analysis may have been somewhat disingenuous. In Figures 3.4(a)–3.4(c), the truncation points were calculated so that the error resulting from the truncation of the infinite series in each case was less than 10^{-6}. As the approximations derived in this chapter are only accurate to such a degree when the number of samples is very large, or the average signal to noise ratio is very small, a direct comparison may not be fair. However, letting the truncation error equal the maximum total approximation error in each case, the comparison becomes somewhat more balanced[4]. Still, even under these relaxed constraints, while the values of the required truncation points are smaller in general, their growth with increasing numbers of samples is still significant, as can be seen in Figures 5.11(a)–5.11(c), and large numbers of terms must still be computed when M is large. In fact, the available exact methods only require fewer terms to be summed than the derived approximate methods when the truncation error is large or the number of samples is small, scenarios which are not particularly relevant to spectrum sensing.

However, no concrete conclusions can be drawn from this: it has only been established that, in general, the exact methods involve the computation of more terms, while the approximate methods involve the computation of fewer. It is reasonable to suggest that, if the exact methods involve a large number of simple terms, while the approximate methods involve a small number of very complicated terms, then the exact methods may be less complicated overall. However, this is not the case. As can be seen in Tables 3.2–3.6, each of the exact methods consists of a weighted sum of incomplete gamma or confluent hypergeometric functions. Of these, the incomplete gamma function is known to be easier to compute to p decimal digits of precision [99], having a computational complexity on the order of $O(p)$ [81]. On the other hand, the formulae for the exact methods all involve weighted sums of the repeated integral of the complementary error function, which can be computed using the simple recursive relation given in (5.13). In fact, for an arbitrary integer order k, it is not difficult to see that $i^k \operatorname{erfc}(z)$ has the generic structure

$$i^k \operatorname{erfc}(z) = P(k-1, z)e^{-z^2} + P(k, z) \operatorname{erfc}(z), \tag{5.67}$$

where $P(n, x)$ represents some polynomial in x of order n. Therefore, weighted sums of the repeated integral of the complementary error function involve the computation of just one exponential function, one complementary error function and some polynomial

[3]This is a slight abuse of notation as $n = 1$ in the no diversity case.

[4]It is worth noting that the maximum total approximation error generally overestimates the actual error, and so this comparison is actually skewed in favour of the exact methods.

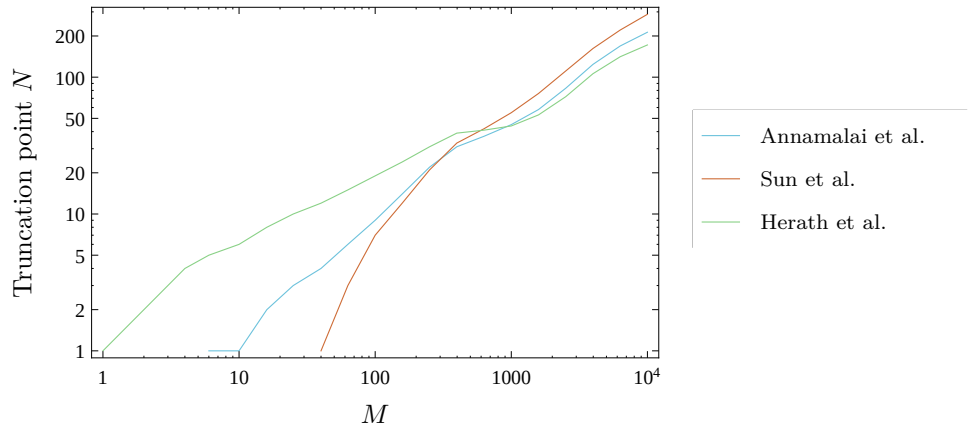

(a) Truncation points required for the same conditions as Figure 3.4(a).

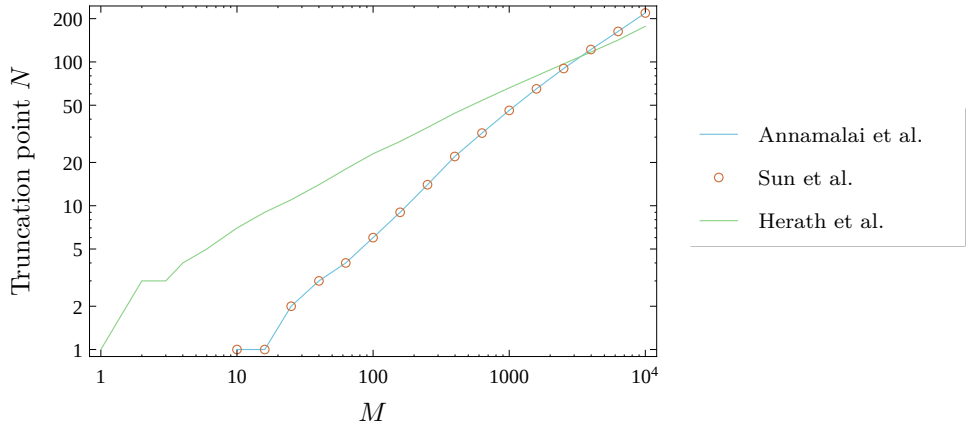

(b) Truncation points required for the same conditions as Figure 3.4(b).

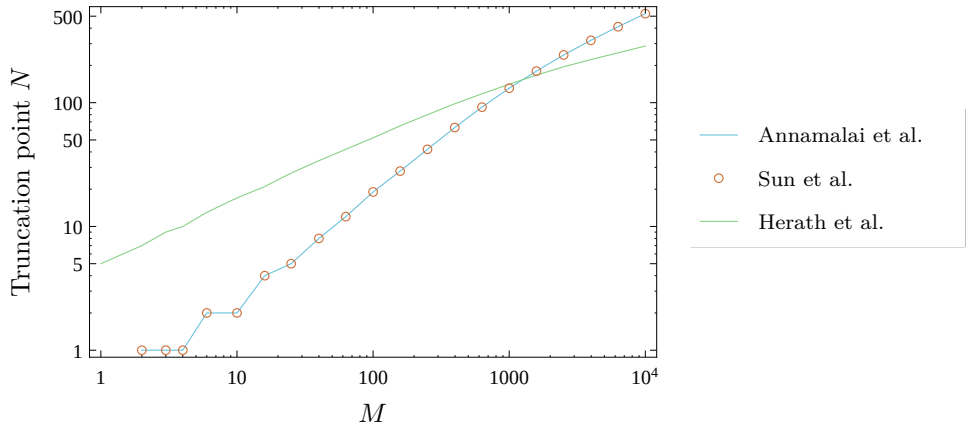

(c) Truncation points required for the same conditions as Figure 3.4(c).

Figure 5.11: Log-log plots of the truncation points required to give $\epsilon_{X,Y}^{T} \leq \max|\epsilon_{tot,X,Y}|$ as functions of the number of samples.

multiplications. Of these, the most computationally complex operation is the evaluation of the complementary error function, which has a comparable, although slightly smaller, computational complexity than the incomplete gamma function of $O(p^{\frac{2}{3}})$ [81]. Thus, for large M, the exact methods require, at best, the sum of a large number of incomplete gamma functions, while the approximate methods require the computation of just one complementary error function. Consequently, in many cases of interest, the approximate methods are significantly faster to compute than the exact methods. In fact, in CPU timing tests [19], the approximate methods were shown to be 100 to 100000 times faster than the exact methods while still yielding good accuracy.

Furthermore, on a practical note, if the decision probabilities are to be evaluated on the device itself (e.g. for calibration or optimisation purposes), and look up tables are used to reduce the number of computations required, then it is worth noting that the incomplete gamma function is a two variable function, while the error function is a single variable function, and so requires a smaller look up table. Therefore, if the resulting errors (truncation and approximation) are comparable in size, then the approximate methods derived in this chapter are preferable.

One caveat is that the approximations involve series with mn terms, and so the number of computations required becomes larger as m and n become large. Furthermore, if mn is large, then the repeated integral of the complementary error function of order mn must be computed and the associated polynomial terms (recall (5.67)) may become more computationally intensive to evaluate than the complementary error function. For instance, in the limit of $m \to \infty$, each expression should simplify to the probability of detection in an AWGN channel[5]. However, in this case, $mn \to \infty$, and the derived approximations become difficult to evaluate, as the upper limits on the series involved tend towards infinity. Thus, while the complexity of the approximate methods does not vary with increasing numbers of samples, it can grow significantly with increasing m and n, and so it must be concluded that their usefulness is limited to situations where the magnitude of mn is small to moderate. Still, in many cases of interest, mn is small to moderate, and so the derived approximations can usually be applied to quickly and accurately compute the desired result.

5.2.5.2 Accuracy / region of applicability

While the approximations derived in Chapter 4 relied only on the use of the central limit theorem, the approximations derived in this chapter required a further simplification: that for small signal to noise ratios, the detection probability for each diversity type could be approximated using (5.6). Two bounds for the error resulting from the use of this approximation were derived: the first related the error to the average signal

[5] As the low SNR approximation has been applied, the approximations should simplify to (5.6) rather than the formulae in Table 4.1.

to noise ratio per branch, while the second related it to the number of samples, the fading parameter and, in the case of MRC and EGC diversity, the number of diversity branches. By deriving two different bounds, it was possible to show that the derived approximations have a wide region of applicability: that is, that they are accurate for small signal to noise ratios, a case which is of particular interest in spectrum sensing, and that they are accurate when the number of samples is large, which is often the case when dealing with multipath fading channels. In particular, when the low SNR approximation error is small, the total approximation error is dominated by the error resulting from the use of the central limit theorem, and so the approximations derived in this chapter are comparable in accuracy to those derived in Chapter 4, of which those relating to energy detection with no diversity have seen widespread use in the literature. Thus, it seems reasonable to suggest that the approximations derived in this chapter are equally applicable in such situations.

In the case of EGC diversity, it was shown that the total approximation error also depended on the error resulting from the use of Nakagami's PDF approximation. A bound for this error was also derived, but it was found that numerical methods were required in order to compute it. Using such methods, the bound was computed for several parameter sets of interest (recall Figure 5.7), and it was shown that the resulting error is usually not large, and tends to decrease as m and n become large. The bound also appeared to be constant with respect to the average signal to noise ratio. However, these behaviours are difficult to verify analytically because the derived bound is not in a simple closed form. Still, as the only available exact method requires the computation of nested infinite summations, the number of which increases with n, the derived EGC approximation offers a simple, less computationally intensive and, in many cases of interest, accurate alternative.

5.2.5.3 Approximations for other system parameters

While it was not possible to derive closed form expressions for the sample complexity, minimum signal to noise ratio and diversity gain of diversity receivers operating on Nakagami-m channels in the manner of Chapter 4, the derived approximations enabled new insights into the behaviour of these quantities in certain situations of interest, which would be difficult to infer from any of the available exact formulations.

In the case of sample complexity and minimum signal to noise ratio, it was found that, when the number of samples is large and the signal to noise ratio is small, the product of the number of samples and the square of the signal to noise ratio is approximately constant. Thus, if the sample complexity for a given minimum signal to noise ratio is known, it is possible to quickly approximate the sample complexity for a different minimum signal to noise ratio, or vice-versa. Similarly, approximations were derived relating the sample complexity (and also, therefore, the minimum signal to noise ratio)

for each diversity type. Thus, if the sample complexity for a given diversity type, with n branches, operating on a given Nakagami-m channel, is known, then the sample complexity for a different diversity combiner, with n branches, operating on a similar channel, can be approximated quite easily. Combining both approximations enables the simple and accurate approximation of the sample complexity or minimum signal to noise ratio for diversity receivers based on known pairs of sample complexity and minimum signal to noise ratio (recall Figure 5.10). This is likely to be convenient for system simulation and design and real time parameter optimisation, where power, computation time and memory are limited.

Unfortunately, it was not possible to infer such simple relationships between the diversity gain and other system parameters. While, in the MRC case, it was possible to derive a formula to quantify the change in detection probability resulting from a change in the number of diversity branches in the system, similar relationships for EGC and SLC systems could not be found. As the number of diversity branches in EGC systems is usually not large, numerical computation of the diversity gain may be feasible in many cases. However, this is often not true of SLC systems, and so some further analysis is required in this area, as follows.

5.3 Novel approximations for small signal to noise ratios and large mn

From the discussion in Section 5.2.5, it is clear that, while the low SNR approximations are useful in many scenarios of interest, they also have some drawbacks. In short, these are:

1. They are only valid for $mn \in \mathbb{N}^+$ ($m \in \mathbb{N}^+$ in the no diversity case).
2. They become more computationally intensive to evaluate as mn becomes large.
3. The behaviours of the detection probabilities as m and n become large are not clear.
4. The diversity gain of SLC systems is difficult to quantify, particularly for large n.

As most of these problems arise when either m or n becomes large, these scenarios are of particular interest. However, central limit theorem approximations for the distribution of sums of i.i.d. gamma random variables must first be considered.

5.3.1 Sums of i.i.d. gamma random variables

Consider the gamma distributed random variable Y, with shape parameter η and scale parameter θ. It is well known that Y has the form of a sum of p i.i.d. gamma distributed

random variables, $Y_1, Y_2, \ldots, Y_p$, that is

$$Y = \sum_{i=1}^{p} Y_i, \tag{5.68}$$

where each of the Y_i follows a gamma distribution[6] with shape parameter $\frac{\eta}{p}$ and scale parameter θ. As (5.68) is in the same form as (4.1), the central limit theorem can be used to approximate the complementary CDF of Y, $P[Y > y]$, as

$$P[Y > y] \approx Q\left(\frac{y - p\,\mathbb{E}[Y_i]}{\sqrt{p\,\mathrm{Var}[Y_i]}}\right) = Q\left(\frac{\frac{y}{\theta} - \eta}{\sqrt{\eta}}\right), \tag{5.69}$$

where the fact that $\mathbb{E}[Y_i] = \frac{\eta\theta}{p}$ and $\mathrm{Var}[Y_i] = \frac{\eta\theta^2}{p}$ has been used to simplify the result.

Like the noncentral chi square distribution, the complementary CDF of the gamma distribution has a different representation when $y \leq 0$ than for $y > 0$, that is

$$P[Y > y] = \begin{cases} 1, & y \leq 0, \\ \dfrac{\Gamma(\eta, \frac{y}{\theta})}{\Gamma(\eta)}, & y > 0. \end{cases} \tag{5.70}$$

Thus, the error resulting from the use of (5.69), $\epsilon_{\Gamma}(\eta, \frac{y}{\theta})$, is given by

$$\epsilon_{\Gamma}\left(\eta, \frac{y}{\theta}\right) = \begin{cases} 1 - Q\left(\dfrac{\frac{y}{\theta} - \eta}{\sqrt{\eta}}\right), & y \leq 0, \\ \dfrac{\Gamma(\eta, \frac{y}{\theta})}{\Gamma(\eta)} - Q\left(\dfrac{\frac{y}{\theta} - \eta}{\sqrt{\eta}}\right), & y > 0. \end{cases} \tag{5.71}$$

As (5.71) is equivalent to (4.11) with $k = 2\eta$, $s = 0$ and $x = \frac{2y}{\theta}$, and $\theta > 0$ by definition, the error can be bounded, using Theorem 4.1, as

$$\max_{y} \left|\epsilon_{\Gamma}\left(\eta, \frac{y}{\theta}\right)\right| = \max_{z} \left|\epsilon_{\Gamma}\left(\eta, z\right)\right| = \max\left(Q\left(\sqrt{\eta}\right), \epsilon_{\Gamma,\infty}(\eta)\right), \tag{5.72}$$

where

$$\epsilon_{\Gamma,\infty}(\eta) \approx \frac{1}{\sqrt{18\pi\eta}}, \tag{5.73}$$

for large values of η. Figure 5.12 illustrates the maximum absolute error (calculated numerically), the Berry-Esseen bound (calculated using (4.12)) and the bound given in (5.72) for different values of η. As can be seen, the derived bound describes the resulting error much more accurately than the Berry-Esseen bound. Consequently, (5.72) can be used to quantify the error resulting from the use of central limit theorem approximations for gamma distributed random variables.

[6] This can readily be shown by comparing the characteristic functions of Y and Y_i [24, p. 164, 362].

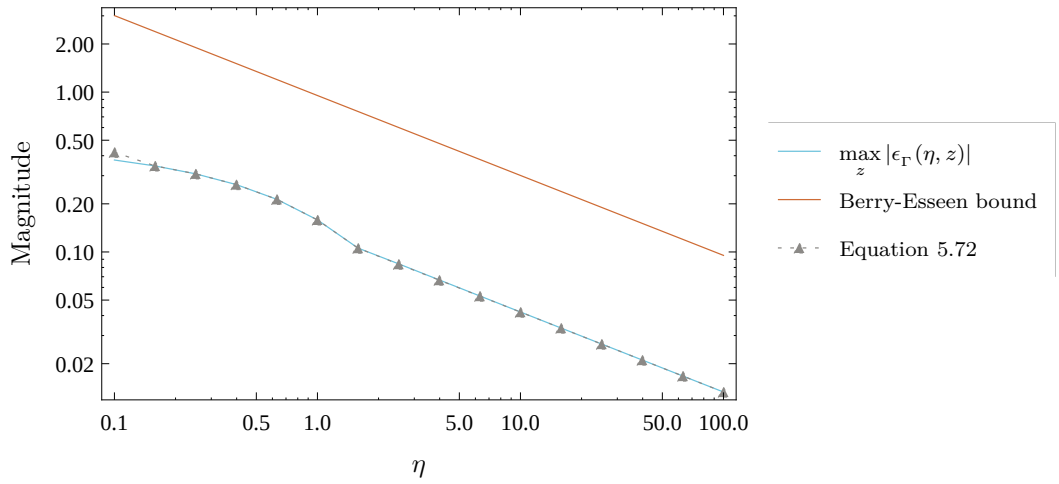

Figure 5.12: A log-log plot of the maximum absolute error, its Berry-Esseen bound and the bound given in (5.72) for different values of η.

5.3.2 Receivers with no diversity

5.3.2.1 A new approximation for the probability of detection

Using (5.69), the PDF of gamma distributed random variables can be approximated as

$$f(y) \approx \check{f}(y) = \frac{1}{\sqrt{2\pi\eta\theta}} \exp\left[-\left(\frac{\frac{y}{\theta}-\eta}{\sqrt{2\eta}}\right)^2\right]. \tag{5.74}$$

As the signal to noise ratio for energy detectors with no diversity follows a gamma distribution with shape parameter m and scale parameter $\frac{\bar{\gamma}}{m}$ (recall (3.29)), its PDF can be approximated, using (5.74), as

$$f_{ND,Nak}(x) \approx \check{f}_{ND,Nak}(x) = \frac{1}{\bar{\gamma}}\sqrt{\frac{m}{2\pi}} \exp\left[-\left(\frac{x-\bar{\gamma}}{\sqrt{\frac{2}{m}\bar{\gamma}}}\right)^2\right]. \tag{5.75}$$

Substituting (5.75) into (5.1), a further approximation for the probability of detection can be derived as

$$P_{d_{ND,Nak}} \approx \check{P}_{d_{ND,Nak}} = \frac{1}{\bar{\gamma}}\sqrt{\frac{m}{2\pi}} \int_{-\infty}^{\infty} Q\left(\frac{\lambda - M(1+x)}{\sqrt{2M}}\right) \exp\left[-\left(\frac{x-\bar{\gamma}}{\sqrt{\frac{2}{m}\bar{\gamma}}}\right)^2\right] dx. \tag{5.76}$$

In order to evaluate (5.76), the following integral identity is required, which is stated here in the form of a lemma and is proved in Appendix A.5.

Lemma 5.4: Let $G(q, r, s, t)$ define the integral

$$G(q,r,s,t) = \int_{-\infty}^{\infty} Q(q - rx) \exp\left[-\left(\frac{x-s}{t}\right)^2\right] dx. \tag{5.77}$$

Then, $G(q, r, s, t)$ has the closed form

$$G(q,r,s,t) = t\sqrt{\pi} Q\left(\frac{q - rs}{\sqrt{1 + \frac{r^2 t^2}{2}}}\right). \tag{5.78}$$

It is not difficult to show that (5.76) can be written as

$$\check{P}_{d_{ND,Nak}} = \frac{1}{\bar{\gamma}}\sqrt{\frac{m}{2\pi}} G\left(\frac{\lambda - M}{\sqrt{2M}}, \sqrt{\frac{M}{2}}, \bar{\gamma}, \sqrt{\frac{2}{m}}\bar{\gamma}\right), \tag{5.79}$$

and so Lemma 5.4 can be used to show that

$$\check{P}_{d_{ND,Nak}} = Q\left(\frac{\lambda - M(1+\bar{\gamma})}{\sqrt{2M\left(1 + \frac{M\bar{\gamma}^2}{2m}\right)}}\right). \tag{5.80}$$

As (5.80) is arrived at through the use of the central limit theorem approximation in (5.75), it shall henceforth be referred to as the large mn approximation[7]. Unlike the approximation given in (5.15), (5.80) is valid for $m \in \mathbb{R}^+$ as the use of Lemma 5.4 imposes no restrictions on the possible values of m. Figure 5.13(a) illustrates the exact (calculated numerically) and approximate (calculated using (5.80)) probabilities of detection for some typical sensing scenarios. As can be seen, the approximation is quite accurate over the entire range of signal to noise ratio values.

Finally, as discussed in Section 2.2.3, the Nakagami-m channel becomes an AWGN channel in the limit of $m \to \infty$. Therefore, one should expect that the detection probability in a Nakagami-m channel converges to the detection probability in an AWGN channel under the same constraints. While this is difficult to show using the low SNR approximation in (5.15), it is trivial to demonstrate using (5.80) as

$$\begin{aligned}\lim_{m\to\infty} \check{P}_{d_{ND,Nak}} &= \lim_{m\to\infty} Q\left(\frac{\lambda - M(1+\bar{\gamma})}{\sqrt{2M\left(1 + \frac{M\bar{\gamma}^2}{2m}\right)}}\right) \\ &= Q\left(\frac{\lambda - M(1+\bar{\gamma})}{\sqrt{2M}}\right) \\ &= \tilde{P}_{d_{ND}}(\bar{\gamma}).\end{aligned} \tag{5.81}$$

[7] Again, this is a minor abuse of notation as $n = 1$ for receivers with no diversity.

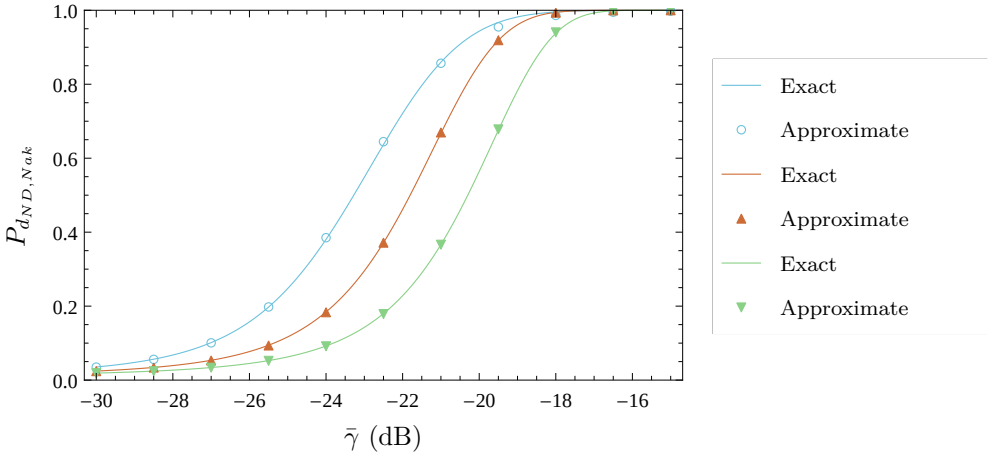

(a) A plot of the exact and approximate (large mn) probabilities of detection.

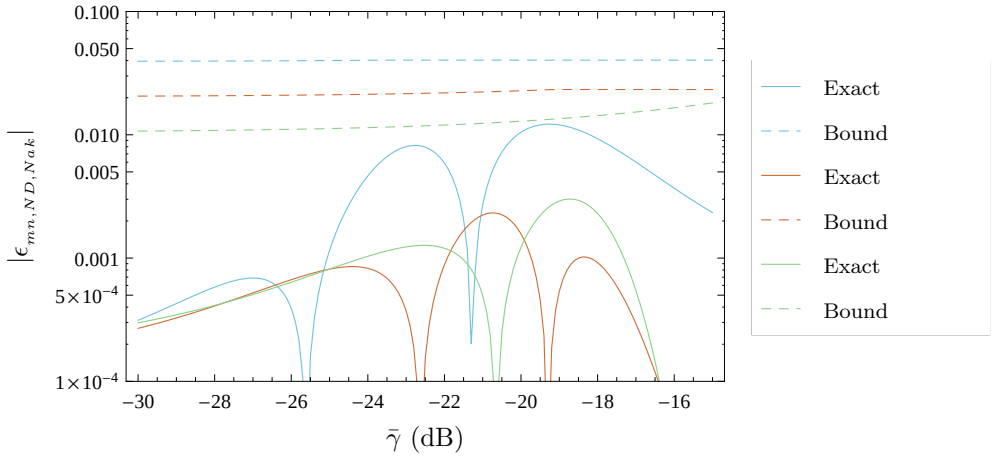

(b) A log-linear plot of the total approximation error, and its bound, for the trends shown in Figure 5.13(a).

Figure 5.13: Plots of the exact and approximate probabilities of detection, and the resulting approximation errors, for energy detectors with no diversity operating on Nakagami-m channels. The blue trends correspond to $M = 5 \times 10^5$ and $m = 11.48$, the red trends to $M = 2.5 \times 10^5$ and $m = 42.72$, while the green trends correspond to $M = 1.25 \times 10^5$ and $m = 161.30$. In each case, $P_{f_{ND}} = 0.01$.

5.3.2.2 Quantifying the approximation error

The total error resulting from the use of $\check{P}_{d_{X,Y}}$ to approximate $P_{d_{X,Y}}$, $\epsilon_{mn,X,Y}$, can be written as

$$\begin{aligned}\epsilon_{mn,X,Y} &= P_{d_{X,Y}} - \check{P}_{d_{X,Y}} \\ &= P_{d_{X,Y}} - \tilde{P}_{d_{X,Y}} + \tilde{P}_{d_{X,Y}} - \check{P}_{d_{X,Y}} \\ &= \epsilon_{tot,X,Y} + \tilde{P}_{d_{X,Y}} - \check{P}_{d_{X,Y}}. \end{aligned} \tag{5.82}$$

Thus, the quantity $\tilde{P}_{d_{ND,Nak}} - \check{P}_{d_{ND,Nak}}$ represents the additional error introduced through the use of (5.80). This error, which henceforth shall be denoted by $\epsilon_{\Gamma,X,Y}$, can be expanded as

$$\begin{aligned}\epsilon_{\Gamma,X,Y} &= \tilde{P}_{d_{X,Y}} - \check{P}_{d_{X,Y}} \\ &= \int_{-\infty}^{\infty} \tilde{P}_{d_X}(x)(f_{X,Y}(x) - \check{f}_{X,Y}(x))dx. \end{aligned} \tag{5.83}$$

Using the second mean value theorem [69, Equation 12.114], it can be shown that

$$\int_{-\infty}^{\infty} \tilde{P}_{d_X}(x)(f_{X,Y}(x) - \check{f}_{X,Y}(x))dx = \int_{\xi}^{\infty} (f_{X,Y}(x) - \check{f}_{X,Y}(x))dx, \tag{5.84}$$

for some $-\infty \leq \xi \leq \infty$. Thus, $|\epsilon_{\Gamma,X,Y}|$ can be bounded as

$$\begin{aligned}|\epsilon_{\Gamma,X,Y}| &= \left| \int_{\xi}^{\infty} (f_{X,Y}(x) - \check{f}_{X,Y}(x))dx \right| \\ &\leq \max_{\xi} \left| \int_{\xi}^{\infty} (f_{X,Y}(x) - \check{f}_{X,Y}(x))dx \right|. \end{aligned} \tag{5.85}$$

As, for each of the diversity types under consideration, $f_{X,Nak}(x)$ is the PDF of a gamma distributed random variable and $\check{f}_{X,Nak}(x)$ is its central limit theorem approximation, (5.85) can be further simplified to

$$\begin{aligned}|\epsilon_{\Gamma,X,Nak}| &\leq \max\left(\max_{\xi \leq 0} \left| 1 - Q\left(\frac{\frac{\xi}{\theta} - \eta}{\sqrt{\eta}} \right) \right|, \max_{\xi > 0} \left| \frac{\Gamma(\eta, \frac{\xi}{\theta})}{\Gamma(\eta)} - Q\left(\frac{\frac{\xi}{\theta} - \eta}{\sqrt{\eta}} \right) \right| \right) \\ &\leq \max_{\xi} \left| \epsilon_{\Gamma}\left(\eta, \frac{\xi}{\theta} \right) \right| \\ &\leq \max\left(Q\left(\sqrt{\eta}\right), \epsilon_{\Gamma,\infty}(\eta) \right), \end{aligned} \tag{5.86}$$

where η is the shape parameter of the gamma distribution defined by $f_{X,Nak}(x)$.

Therefore, the additional error resulting from the use of (5.80) over (5.15) is upper

bounded by

$$|\epsilon_{\Gamma,ND,Nak}| \leq \max|\epsilon_{\Gamma,ND,Nak}| \triangleq \max\left(Q\left(\sqrt{m}\right), \epsilon_{\Gamma,\infty}(m)\right), \tag{5.87}$$

and so the total error, with respect to the exact method, is bounded as

$$\begin{aligned}\max|\epsilon_{mn,ND,Nak}| &\leq \max|\epsilon_{tot,ND,Nak}| + \max|\epsilon_{\Gamma,ND,Nak}| \\ &\leq \max|\epsilon_{CLT,ND}| + \max|\epsilon_{SNR,ND,Nak}| + \max|\epsilon_{\Gamma,ND,Nak}|. \end{aligned}\tag{5.88}$$

Thus, the error resulting from the use of the approximation given in (5.80) can be bounded as the sum of the maximum errors resulting from the use of the central limit theorem, the low SNR approximation and the approximation in (5.74). Unfortunately, this means that the large mn approximation in (5.80) is only accurate in situations where all three errors are small. However, as such situations occur only when the number of samples is large, the signal to noise ratio is small and the m parameter is large, they correspond precisely to those situations where the low SNR approximation in (5.15) becomes complicated to use. Thus, the region of applicability of the large mn approximation naturally complements that of the low SNR approximation.

The bound in (5.88) is useful when bounding the maximum error resulting from the use of (5.80). For instance, using (5.88), the errors resulting from the use of (5.80) in approximating the detection probabilities in Figure 5.13(a) can be bounded as in Figure 5.13(b). As a consequence of (5.87) being a function of m only, the error bounds tend to significantly overestimate the magnitude of the errors across the entire range of signal to noise ratios.

5.3.3 Receivers with diversity

Large mn approximations for energy detectors with diversity reception can be derived in a similar manner to (5.80) and are given[8] in Table 5.1, along with their respective approximate PDFs, which can be derived using (5.74). Again, unlike the low SNR approximations in Section 5.2, each of the large mn approximations in Table 5.1 is valid for $mn \in \mathbb{R}^+$.

Noting that the shape parameter for each of the diversity types is equal to mn, it is not difficult to show that

$$\max|\epsilon_{\Gamma,X,Nak}| = \max\left(Q(\sqrt{mn}), \epsilon_{\Gamma,\infty}(mn)\right), \ X \in \{MRC, EGC, SLC\}, \tag{5.89}$$

[8]The results are not difficult to show and so, for brevity, their derivations are omitted. Noting that $\eta = mn$ and $\theta = \frac{\bar{\gamma}}{m}$ for MRC and SLC systems (recall from Section 3.3.6 that $f_{MRC,Nak}(x) = f_{SLC,Nak}(x)$) and that $\eta = mn$ and $\theta = \frac{\omega\bar{\gamma}}{mn}$ for EGC systems, the approximate PDFs can be derived using (5.74). The corresponding approximate detection probabilities then follow from Lemma 5.4.

Table 5.1: Large mn approximations for energy detectors with diversity reception operating on Nakagami-m channels.

X	$\check{f}_{X,Nak}(x)$	$\check{P}_{d_{X,Nak}}$
MRC	$\frac{1}{\bar{\gamma}}\sqrt{\frac{m}{2\pi n}}\exp\left[-\left(\frac{x-n\bar{\gamma}}{\sqrt{\frac{2n}{m}}\bar{\gamma}}\right)^2\right]$	$Q\left(\frac{\lambda - M(1+n\bar{\gamma})}{\sqrt{2M\left(1+\frac{M\bar{\gamma}^2 n}{2m}\right)}}\right)$
EGC	$\frac{1}{\omega\bar{\gamma}}\sqrt{\frac{mn}{2\pi}}\exp\left[-\left(\frac{x-\omega\bar{\gamma}}{\sqrt{\frac{2}{mn}}\omega\bar{\gamma}}\right)^2\right]$	$Q\left(\frac{\lambda - M(1+\omega\bar{\gamma})}{\sqrt{2M\left(1+\frac{M\bar{\gamma}^2\omega^2}{2mn}\right)}}\right)$
SLC	$\frac{1}{\bar{\gamma}}\sqrt{\frac{m}{2\pi n}}\exp\left[-\left(\frac{x-n\bar{\gamma}}{\sqrt{\frac{2n}{m}}\bar{\gamma}}\right)^2\right]$	$Q\left(\frac{\lambda - Mn(1+\bar{\gamma})}{\sqrt{2Mn\left(1+\frac{M\bar{\gamma}^2}{2m}\right)}}\right)$

and so the total approximation errors are bounded as

$$\max|\epsilon_{mn,X,Nak}| \leq \max|\epsilon_{tot,X,Nak}| + \max|\epsilon_{\Gamma,X,Nak}|,\ X \in \{MRC, EGC, SLC\}. \quad (5.90)$$

Using the large mn approximations in Table 5.1, the exact and approximate detection probabilities can be plotted as in Figure 5.14(a), while the bound in (5.90) can be used to bound the resulting errors, as shown in Figure 5.14(b). As can be seen, the proposed approximations are quite accurate across the entire range of signal to noise ratios although, again, the error bounds tend to significantly overestimate the magnitude of the errors.

The approximations can also be used to calculate the behaviour of the detection probabilities of diversity receivers as mn becomes large. Noting the approximation

$$\frac{\Gamma(m+\frac{1}{2})}{\Gamma(m)} \approx \sqrt{m}, \quad (5.91)$$

which becomes valid as m becomes large [68, Equation 5.11.12], (3.36) can be manipulated to show that

$$\omega \approx n, \quad (5.92)$$

as m becomes large. Using the appropriate formula from Table 5.1, it can then be

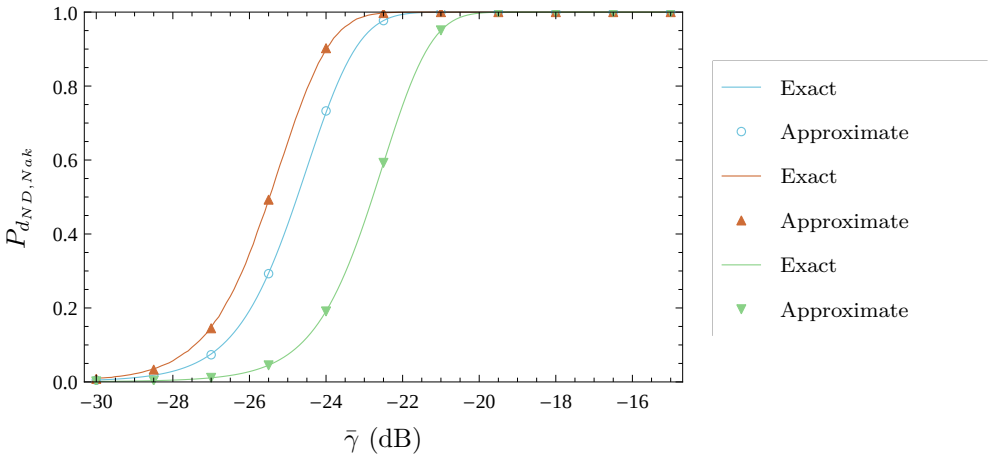

(a) A plot of the exact and approximate (large mn) probabilities of detection.

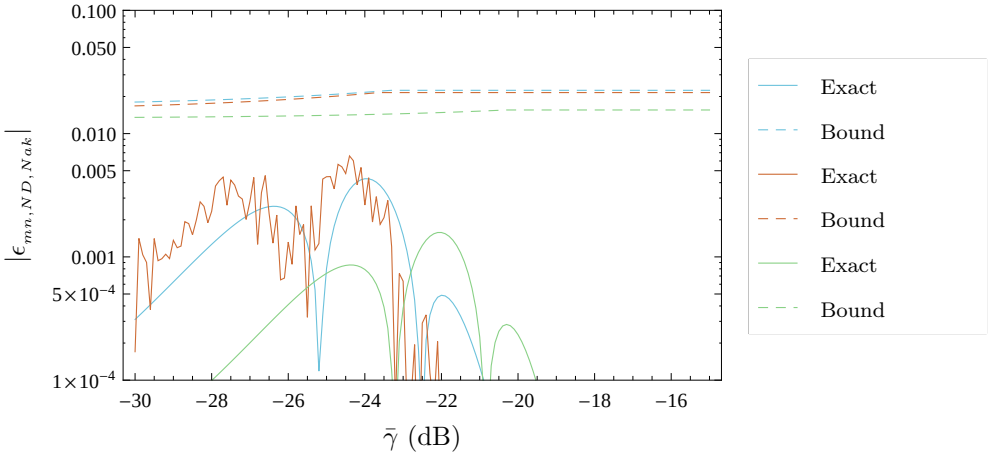

(b) A log-linear plot of the total approximation error, and its bound, for the trends shown in Figure 5.14(a). As the exact probability of detection in the EGC case was calculated numerically, the resulting error is less smooth.

Figure 5.14: Plots of the exact and approximate probabilities of detection, and the resulting approximation errors, for energy detectors with no diversity operating on Nakagami-m channels. The blue trends correspond to an MRC receiver operating on a Nakagami-m channel with $m = 12.5$, the red trends to an EGC receiver operating on a Nakagami-m channel with $m = 12.5$, while the green trends correspond to an SLC receiver operating on a Nakagami-m channel with $m = 10$. In each case, $M = 10^5$ and the probability of false alarm is 10^{-4}.

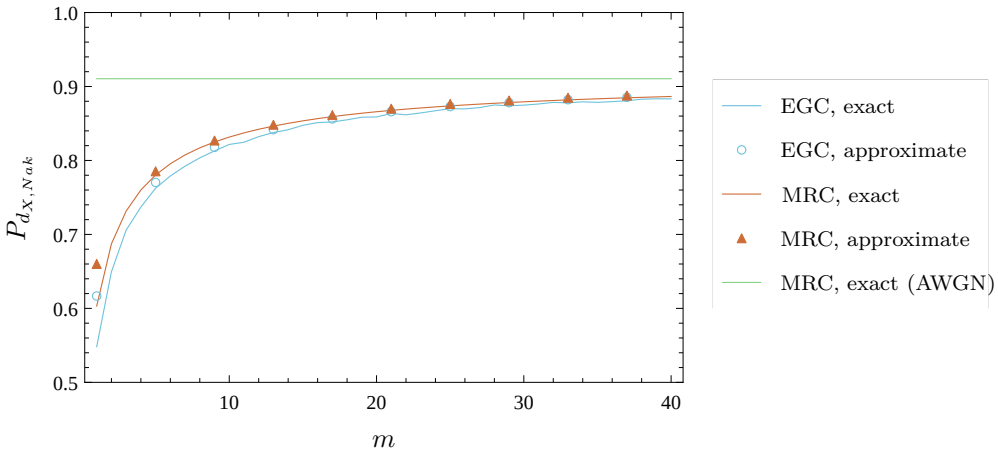

Figure 5.15: A plot of the convergence of the probabilities of detection of energy detectors with EGC and MRC diversity as the fading parameter increases. In each case, $M = 100000$, $P_{f_X} = 10^{-3}$, $\bar{\gamma} = -20\,\text{dB}$ and $n = 2$. As m becomes very large, the detection probabilities of both diversity receivers tend towards the detection probability of an energy detector with MRC diversity operating on an AWGN channel.

shown that

$$\check{P}_{d_{EGC,Nak}} \approx Q\left(\frac{\lambda - M(1+n\bar{\gamma})}{\sqrt{2M\left(1+\frac{M\bar{\gamma}^2 n}{2m}\right)}}\right) = \check{P}_{d_{MRC,Nak}}. \tag{5.93}$$

Thus, as m becomes large, the detection probability of energy detectors with EGC diversity becomes approximately equal to that of energy detectors with MRC diversity[9], as can be seen in Figure 5.15. This is interesting to note as MRC systems require prior (or estimated) knowledge of the channel coefficients, while EGC systems do not. Thus, for sufficiently large values of m, EGC diversity performs similarly to MRC diversity, and requires no additional information about the radio environment.

Using (5.93), the behaviour of both EGC and MRC systems as $m \to \infty$ can be described as

$$\begin{aligned}\lim_{m\to\infty} \check{P}_{d_{EGC,Nak}} = \lim_{m\to\infty} \check{P}_{d_{MRC,Nak}} &= \lim_{m\to\infty} Q\left(\frac{\lambda - M(1+n\bar{\gamma})}{\sqrt{2M\left(1+\frac{M\bar{\gamma}^2 n}{2m}\right)}}\right) \\ &= Q\left(\frac{\lambda - M(1+n\bar{\gamma})}{\sqrt{2M}}\right) \\ &= \tilde{P}_{d_{MRC}}(\bar{\gamma}).\end{aligned} \tag{5.94}$$

Thus, the performance of both diversity types tends towards the expected performance

[9]This can be demonstrated more generally by substituting (5.92) into (3.35) to give (3.33).

of an MRC receiver operating on an AWGN channel. This behaviour can also be seen in Figure 5.15.

5.3.4 Novel approximations for other system parameters

While the large mn approximations are useful for calculating the value of the detection probability in situations where mn is large, they are also in a simple form, similar to the approximations in Chapter 4. Consequently, it is possible to derive closed form approximations for quantities such as sample complexity, minimum signal to noise ratio and diversity gain, albeit with constrained regions of applicability.

5.3.4.1 Sample complexity

In a similar manner to Section 4.4.1, closed form approximations for the sample complexity of each diversity type[10] can be derived, as shown in Table 5.2. It is interesting to note that, for each diversity type, the relationship $M\bar{\gamma}^2 = k$ is once again apparent. As before, it should be noted that the approximations in Table 5.2 are only valid if the total approximation error is not large. Consequently, they are of most use when the signal to noise ratio is small, and the number of samples and the product of the fading parameter and the number of branches, mn, are both large.

The formulae in Table 5.2 are useful in approximating the sample complexity when the m parameter is large. For instance, if an energy detector with two branch MRC diversity, operating on a Nakagami-m channel with $m = 25$, has a probability of false alarm of 10^{-3} and a probability of missed detection of 10^{-2} at a signal to noise ratio of $-20\,\text{dB}$, using the appropriate formula from Table 5.2, it can be shown that $M_{MRC,Nak} \approx 190938$. Using more complex numerical methods, it can be shown that the precise number of samples required is 187938.

5.3.4.2 Minimum signal to noise ratio

Large mn approximations for the minimum signal to noise ratio of each diversity system can also be derived quite simply. For instance, given the sample complexity for SLC

[10] As the derivations of these are very similar to the derivation given in Section 4.4.1, they are omitted to avoid repetition.

Table 5.2: Large mn approximations for the sample complexity of energy detectors operating on Nakagami-m channels.

X	$\check{M}_{X,Nak}$
ND	$2\left(\frac{Q^{-1}\left(\hat{P}_{f_{ND}}\right)-\sqrt{1+\frac{Q^{-1}\left(\hat{P}_{f_{ND}}\right)^2-Q^{-1}\left(\check{P}_{d_{ND,Nak}}\right)^2}{m}}Q^{-1}\left(\check{P}_{d_{ND,Nak}}\right)}{\bar{\gamma}\left(1-\frac{Q^{-1}\left(\check{P}_{d_{ND,Nak}}\right)^2}{m}\right)}\right)^2$
MRC	$\frac{2}{n^2}\left(\frac{Q^{-1}\left(\hat{P}_{f_{MRC}}\right)-\sqrt{1+\frac{Q^{-1}\left(\hat{P}_{f_{MRC}}\right)^2-Q^{-1}\left(\check{P}_{d_{MRC,Nak}}\right)^2}{mn}}Q^{-1}\left(\check{P}_{d_{MRC,Nak}}\right)}{\bar{\gamma}\left(1-\frac{Q^{-1}\left(\check{P}_{d_{MRC,Nak}}\right)^2}{mn}\right)}\right)^2$
EGC	$2\left(\frac{Q^{-1}\left(\hat{P}_{f_{EGC}}\right)-\sqrt{1+\frac{Q^{-1}\left(\hat{P}_{f_{EGC}}\right)^2-Q^{-1}\left(\check{P}_{d_{EGC,Nak}}\right)^2}{mn}}Q^{-1}\left(\check{P}_{d_{EGC,Nak}}\right)}{\omega\bar{\gamma}\left(1-\frac{Q^{-1}\left(\check{P}_{d_{EGC,Nak}}\right)^2}{mn}\right)}\right)^2$
SLC	$\frac{2}{n}\left(\frac{Q^{-1}\left(\hat{P}_{f_{SLC}}\right)-\sqrt{1+\frac{Q^{-1}\left(\hat{P}_{f_{SLC}}\right)^2-Q^{-1}\left(\check{P}_{d_{SLC,Nak}}\right)^2}{mn}}Q^{-1}\left(\check{P}_{d_{SLC,Nak}}\right)}{\bar{\gamma}\left(1-\frac{Q^{-1}\left(\check{P}_{d_{SLC,Nak}}\right)^2}{mn}\right)}\right)^2$

systems in Table 5.2, it can be shown that

$$M = \frac{2}{n}\left(\frac{Q^{-1}\left(\hat{P}_{f_{SLC}}\right) - \sqrt{1 + \frac{Q^{-1}\left(\hat{P}_{f_{SLC}}\right)^2 - Q^{-1}\left(\check{P}_{d_{SLC,Nak}}\right)^2}{mn}}Q^{-1}\left(\check{P}_{d_{SLC,Nak}}\right)}{\bar{\gamma}\left(1 - \frac{Q^{-1}\left(\check{P}_{d_{SLC,Nak}}\right)^2}{mn}\right)}\right)^2$$

$$\therefore \bar{\gamma} = \sqrt{\frac{2}{Mn}}\left(\frac{Q^{-1}\left(\hat{P}_{f_{SLC}}\right) - \sqrt{1 + \frac{Q^{-1}\left(\hat{P}_{f_{SLC}}\right)^2 - Q^{-1}\left(\check{P}_{d_{SLC,Nak}}\right)^2}{mn}}Q^{-1}\left(\check{P}_{d_{SLC,Nak}}\right)}{\left(1 - \frac{Q^{-1}\left(\check{P}_{d_{SLC,Nak}}\right)^2}{mn}\right)}\right)$$

$$\triangleq \check{\gamma}_{min,SLC,Nak}, \tag{5.95}$$

where $\check{\gamma}_{min,SLC,Nak} \approx \gamma_{min,SLC,Nak}$ and $\gamma_{min,SLC,Nak}$ denotes the minimum signal to noise ratio of energy detectors with SLC diversity operating on Nakagami-m channels. Approximations for the other diversity types may be derived in a similar manner, and so are omitted for brevity.

The approximation is (5.95) can be quite useful in approximating the minimum signal to noise ratio detectable by an SLC system. For instance, if an energy detector with ten branch SLC diversity operates on a Nakagami-m channel with $m = 5$, $M = 100000$ and $P_{f_{SLC}} = P_{m_{SLC}} = 10^{-3}$, (5.95) can be used to show that $\gamma_{min,SLC,Nak} \approx -19.66\,\text{dB}$, while the use of a numerical method shows that the exact solution is $-19.82\,\text{dB}$.

5.3.4.3 Diversity gain

It is also possible to derive approximations for the diversity gain of MRC, EGC and SLC systems as mn becomes large. However, as the number of diversity branches in MRC and EGC systems is usually not large, large mn approximations for these systems are not of particular interest. In contrast, large numbers of branches are often required in SLC systems, particularly when they are used to model cooperative sensing networks. Thus, the discussion in this section focuses on SLC systems only.

Substituting (4.23) into $\check{P}_{d_{SLC,Nak}}$, and solving for n, it can be shown that

$$n \approx \left\lceil \frac{2}{M}\left(\frac{Q^{-1}(\hat{P}_{f_{SLC}}) - \sqrt{1 + \frac{M\bar{\gamma}^2}{2m}}Q^{-1}(\check{P}_{d_{SLC,Nak}})}{\bar{\gamma}}\right)^2\right\rceil \triangleq \check{n}_{SLC,Nak}, \tag{5.96}$$

where $\check{n}_{SLC,Nak} \approx n_{SLC,Nak}$, $n_{SLC,Nak}$ is the diversity gain for SLC systems operating on

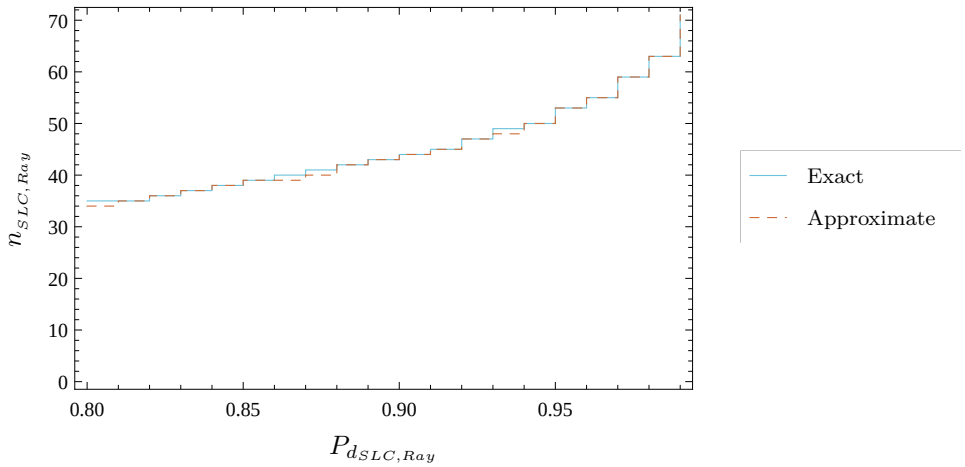

Figure 5.16: A plot of the exact (calculated numerically) and approximate (calculated using (5.96)) numbers of nodes required to ensure the given probability of detection when $P_{f_{SLC}} = 10^{-3}$ and $M = 10000$ in a Rayleigh fading channel with an average signal to noise ratio of $-20\,\text{dB}$.

Nakagami-m channels and the ceiling function, $\lceil \cdot \rceil$, has been applied to ensure that the value of $\check{n}_{SLC,Nak}$ is sufficiently large to guarantee that the specified operating conditions are met. Once again, (5.96) is only accurate if the total approximation error, given by (5.90), is small.

Figure 5.16 illustrates the exact (calculated numerically) and approximate (calculated using (5.96)) numbers of nodes required to ensure the given probability of detection is met when $P_{f_{SLC}} = 10^{-3}$ and $M = 10000$ in a Rayleigh fading channel with an average signal to noise ratio of $-20\,\text{dB}$. As can be seen, the approximation in (5.96) is quite accurate over the entire range of detection probabilities.

5.3.5 Discussion

In this section, simple, closed form approximations for the detection probabilities of energy detector diversity receivers were derived. These approximations are well suited to situations where the number of samples is large, the signal to noise ratio is small and the product of the m parameter and the number of diversity branches, mn, is large. Thus, they naturally complement the low SNR approximations presented in Section 5.2, which become more complicated to evaluate as mn becomes large. As a further benefit, the approximations are also valid for $mn \in \mathbb{R}^+$.

The accuracy of the large mn approximations was verified for certain situations of interest using numerical simulations. In each case, it was shown that the maximum total approximation error could be bounded as the sum of the maximum absolute error resulting from the use of the central limit theorem to approximate the detection probability in an AWGN channel, the maximum absolute error resulting from the use

of the low SNR approximation and the maximum absolute error resulting from the use of the central limit theorem approximation for the PDF of the signal to noise ratio at the output of the combiner. In many cases of interest, the derived bounds are useful. However, in some cases, the magnitude of the actual error can be significantly overestimated (for example, see Figure 5.13(b)). This can mostly be attributed to the bound for $\max|\epsilon_{\Gamma,X,Nak}|$, which decreases slowly with increasing mn and does not vary with $\bar{\gamma}$. However, while a tighter bound may be possible (one depending on $\bar{\gamma}$, say), it might not demonstrate the decrease in error with increasing values of mn, without which the large mn approximations would have no useful region of applicability.

The simple forms of the large mn approximations enabled the derivation of novel, closed form approximations for the sample complexity, minimum signal to noise ratio and, for SLC systems, the diversity gain in Nakagami-m channels. These approximations are accurate for the same conditions as the large mn approximations, and so are of most use in situations where the number of samples and the product of the m parameter and number of branches, mn, is large, and the signal to noise ratio is low. Numerical examples illustrated the usefulness of the approximations in several scenarios of interest. In each case, the accuracy of the approximations was verified through comparisons with exact results which, unlike the approximate results, had to be calculated using numerical methods. The approximations for SLC systems are of particular interest, as SLC diversity is often used to model cooperative spectrum sensing networks, where the number of nodes is typically large.

A central limit theorem approximation for the sum of i.i.d. gamma random variables was used in deriving the new approximations. It was subsequently found that the error resulting from the use of the approximation could be bounded using Theorem 4.1 which, to the best of the author's knowledge at the time of writing, is a novel result and so should have applications in much broader fields than just spectrum sensing.

5.4 Summary

In Section 5.1, several objectives for this chapter were outlined, namely: to derive accurate and computationally inexpensive approximations for the detection probabilities of energy detector diversity receivers operating on Nakagami-m channels; to derive error bounds for these approximations, so that their regions of applicability are clearly defined; and, finally, to derive further approximations enabling the analysis of several other parameters of interest.

To meet the first objective, two series of approximations for the detection probability in Nakagami-m channels were derived. The first series of approximations is appropriate for use in situations where the number of samples is large and the signal to noise ratio is small. As such constraints are often imposed in spectrum sensing, these approxi-

mations are particularly suited to the analysis of such systems. Furthermore, as the approximations are substantially less complicated to evaluate than any of the exact methods currently available in the literature, they are equally useful for both system analysis and low cost parameter optimisation in real time. However, the approximations become more complicated to evaluate as the product of the fading parameter and the number of diversity branches, mn, becomes large and, furthermore, they are valid for $mn \in \mathbb{N}^+$ only. Thus, a second series of approximations was derived, suited to situations where $mn \in \mathbb{R}^+$ and is large. As these approximations involve the computation of just a single Gaussian Q function, they are even simpler to evaluate than the low SNR approximations, although the resulting approximation error is, in general, larger. The approximations for the detection probability of EGC systems are particularly noteworthy as, previously, the only known way to evaluate this quantity involved the computation of multiple nested infinite series, which are difficult to compute, in general. However, it is now trivial to accurately approximate the detection probability in many scenarios of interest, regardless of the number of diversity branches.

To meet the second objective, error bounds were derived for each of the approximations for the detection probabilities. In particular, two bounds for the error resulting from the use of the low SNR simplification were derived, one of which is useful in situations where the signal to noise ratio is small, which is often the case in spectrum sensing, and the other which is useful when the number of samples is large, which is often the case when dealing with small signal to noise ratios and/or fading channels. Error bounds for the large mn series of detection probability approximations were also provided, and so the region of applicability of each is clear, although the bound can sometimes overestimate the actual error by a large amount. In deriving these bounds, it was necessary to derive a further bound for the error resulting from the application of the central limit theorem to sums of i.i.d. gamma random variables. As this result is quite general, it is likely to be of further use outside the area of spectrum sensing.

The relationships between other system parameters were also investigated. In a similar manner to AWGN channels, it was found that the product of the number of samples and the square of the average signal to noise ratio per branch is approximately constant when the former quantity is large and the latter is small, regardless of the diversity type. Thus, if the sample complexity is known for a given average signal to noise ratio, then the sample complexity can be inferred at a different average signal to noise ratio, or vice versa. The relationship between the sample complexities and sensitivities of different diversity architectures was also considered, and simple expressions were derived, enabling direct comparisons to be made between the operation of each. Under the constraint that mn is large, closed form approximations for the sample complexity and minimum signal to noise ratio were derived. While expressions were provided for each diversity type, it is likely that those relating to SLC diversity will be of most interest in practice, as the number of branches in these systems can often be large.

A closed form approximation for the diversity gain of SLC systems, valid for large mn, was also derived. In each case, the use of approximations led to the discovery of novel and interesting relationships that would be difficult to infer from any of the exact formulations available in the literature.

Box and Draper [100, p. 74] wrote that *all models are wrong; the practical question is how wrong do they have to be to not be useful*. In this chapter, the proposed models are *wrong*, in the sense that they are approximations, and so are generally inexact. However, by bounding the maximum error resulting from their use, the question of how wrong they are — essentially, how *useful* they are — is no longer difficult to answer. Furthermore, as the mathematical tools developed in this chapter are quite generally applicable, it is worth considering whether they can used to simplify other problems in a similar manner. Consequently, the following chapter concerns the extension of the approximation based approach to Rice fading channels.

Chapter 6

Multipath fading channel analysis II: Rice channels

This chapter focuses on approximations for the analysis of energy detector systems operating on Rice channels. In particular, computationally inexpensive approximations for the detection probabilities of such systems are derived under the constraint that the signal to noise is low or the number of samples is large, or both. These enable the further analysis of the behaviour of the sample complexity and minimum signal to noise ratio under similar constraints.

Under the additional restriction that the product of the fading parameter and the number of diversity branches is large, a second series of approximations for the detection probabilities is derived. These approximations have simple closed forms and enable the derivation of further closed form approximations for the sample complexity, minimum signal to noise ratio and diversity gain, in a similar manner to Section 5.3. In each case, error bounds are derived so that the region of applicability of the approximations is well defined. In course of the analysis, a novel theorem, describing the maximum error resulting from the use of the central limit theorem to approximate the distribution of noncentral chi square random variables, is derived for the special case where the noncentrality parameter is a multiple of the number of degrees of freedom.

6.1 Motivation

While the analysis of energy detector systems operating on Nakagami-m channels has received much attention in the literature, the analysis of their operation on Rice channels has received a far less extensive treatment. In the brief review conducted in Chapter 3 it was shown that, while four distinct, exact expressions for the detection probability are available in the no diversity case, only two expressions describing MRC systems are available, just one in the case of SLC systems, and none in case of EGC

systems[1]. Furthermore, as Digham et al.'s expression [11] for the detection probability in the no diversity case applies when $M = 2$ only, it is of limited use in practice. Of the remaining expressions, those derived by Herath et al. [53, 55] require the evaluation of derivatives on the order of $u = \frac{M}{2}$, and so are complicated to evaluate when the number of samples is large. Consequently, the only expressions likely to be of use in practice are those of Annamalai et al. [57–59] and Sun [61, 62]. However, as in the Nakagami-m channel case, these consist of infinite series, and require large numbers of terms to be evaluated in order to give an accurate result (recall Figure 3.4(d)). Thus, there is some motivation to consider less computationally intensive methods for evaluating the detection probability.

In the previous chapter, a series of useful approximations for the analysis of energy detector systems operating on Nakagami-m channels were derived. These approximations are not computationally intensive to evaluate, and so provide a simple and accurate alternative to the available exact methods. Furthermore, as the approximations have novel forms, they enable the derivation and inference of certain behaviours of various system parameters which, to the best of the author's knowledge, could not have been readily deduced from the available exact methods. It is natural, then, to ask whether a similar approach might yield equally interesting results in the case of Rice channels. As before, however, it must be ensured that the error resulting from the use of these approximations can be described easily, so that the region of applicability of each is clearly defined.

Therefore, the aims of this chapter are:

1. To derive accurate and computationally inexpensive approximations for the detection probabilities of energy detector systems operating on Rice channels.
2. To derive bounds on the error resulting from the use of these approximations, so that their regions of applicability are well defined.
3. To derive further approximations for the sample complexity, minimum signal to noise ratio and diversity gain, enabling a complete description of the sensor system.

As, to the best of the author's knowledge at the time of writing, such an approach has not been published before, the findings in this chapter are entirely novel.

6.2 Novel approximations for small signal to noise ratios

Approximations based on the low SNR approximation made in Section 5.2 shall be considered first. The use of the low SNR approximation is necessary as, to the best of

[1]No exact PDF for the signal to noise ratio at the output of an equal gain combiner is currently available.

the author's knowledge at the time of writing, the integral in (5.5) has no closed from solution when $f_{X,Y}(x)$ is given by any of the Rice channel PDFs discussed in Section 3.3. Consequently, the following analysis will make use of Lemmas 5.1, 5.2 and 5.3 in a similar manner to Chapter 5, but with some subtle differences, due to the variation in the formulations of the PDFs involved.

6.2.1 Receivers with no diversity

6.2.1.1 A novel approximation for the probability of detection

The probability of detection of energy detectors with no diversity operating on Rice channels may be approximated by substituting (3.30) into (5.8), that is

$$P_{d_{ND,Rice}} \approx \tilde{P}_{d_{ND,Rice}} = \int_0^\infty Q\left(\frac{\lambda - M(1+x)}{\sqrt{2M}}\right)\left(\frac{K+1}{\bar{\gamma}}\right) e^{-K-\frac{(K+1)x}{\bar{\gamma}}} \times I_0\left(2\sqrt{\frac{K(K+1)x}{\bar{\gamma}}}\right) dx, \tag{6.1}$$

where $I_n(z)$ is the modified Bessel function of the first kind, and is given [68, Equation 10.25.2] by

$$I_n(z) = \left(\frac{z}{2}\right)^n \sum_{l=0}^{\infty} \frac{\left(\frac{z}{2}\right)^{2l}}{l!\,\Gamma(n+l+1)}. \tag{6.2}$$

Substituting (6.2) into (6.1), it can be shown that

$$\begin{aligned}\tilde{P}_{d_{ND,Rice}} &= e^{-K}\sum_{l=0}^{\infty}\frac{K^l}{l!}\frac{1}{\Gamma(l+1)}\int_0^\infty Q\left(\frac{\lambda - M(1+x)}{\sqrt{2M}}\right) e^{-\frac{(K+1)x}{\bar{\gamma}}}\left(\frac{K+1}{\bar{\gamma}}\right)^{l+1} x^l dx \\ &= e^{-K}\sum_{l=0}^{\infty}\frac{K^l}{l!}\, F_{l+1}\left(\frac{\lambda - M}{\sqrt{2M}}, \sqrt{\frac{M}{2}}, \frac{K+1}{\bar{\gamma}}\right),\end{aligned} \tag{6.3}$$

where $F_k(a,b,c)$ is as defined in (5.11), and so Lemma 5.1 can be used to show that

$$\begin{aligned}\tilde{P}_{d_{ND,Rice}} = \hat{P}_{f_{ND}} &+ \frac{1}{2}\exp\left[-\frac{\frac{2(K+1)}{\bar{\gamma}}}{\sqrt{M}}\left(\frac{\lambda - M - \frac{K+1}{\bar{\gamma}}}{2\sqrt{M}}\right)\right] \\ &\times e^{-K}\sum_{l=0}^{\infty}\frac{K^l}{l!}\sum_{p=0}^{l}\left(\frac{\frac{2(K+1)}{\bar{\gamma}}}{\sqrt{M}}\right)^p i^p \operatorname{erfc}\left[-\left(\frac{\lambda - M - \frac{2(K+1)}{\bar{\gamma}}}{2\sqrt{M}}\right)\right].\end{aligned} \tag{6.4}$$

It interesting to note that, unlike (5.15), the approximation in (6.4) places no restriction on the values of the fading parameter. Thus, (6.4) is valid for $K \in \mathbb{R}_0^+$.

Using (6.4), it is possible to derive an approximation for the detection probability of an energy detector operating on a Rayleigh faded channel. As discussed in Section 2.2.4,

the Rice channel is equivalent to the Rayleigh channel when the fading parameter is equal to zero. Therefore, the detection probability in a Rayleigh channel can be approximated as

$$\begin{aligned} P_{d_{ND,Ray}} &\approx \tilde{P}_{d_{ND,Rice}}\Big|_{K=0} \\ &\approx \hat{P}_{f_{ND}} + \frac{1}{2}\exp\left[-\frac{\frac{2}{\bar{\gamma}}}{\sqrt{M}}\left(\frac{\lambda - M - \frac{1}{\bar{\gamma}}}{2\sqrt{M}}\right)\right]\operatorname{erfc}\left[-\left(\frac{\lambda - M - \frac{2}{\bar{\gamma}}}{2\sqrt{M}}\right)\right], \end{aligned} \tag{6.5}$$

which agrees with the approximation given in (5.16), that is

$$P_{d_{ND,Ray}} \approx \tilde{P}_{d_{ND,Rice}}\Big|_{K=0} = \tilde{P}_{d_{ND,Nak}}\Big|_{m=1} = \tilde{P}_{d_{ND,Ray}}. \tag{6.6}$$

Unfortunately, $\forall\, K > 0$, (6.4) has the form of an infinite series, which must be truncated in order for the detection probability to be computed. If the series is truncated at the point $l = N$, then (6.4) can be written as

$$\begin{aligned} \tilde{P}_{d_{ND,Rice}} = \hat{P}_{f_{ND}} &+ \frac{1}{2}\exp\left[-\frac{\frac{2(K+1)}{\bar{\gamma}}}{\sqrt{M}}\left(\frac{\lambda - M - \frac{K+1}{\bar{\gamma}}}{2\sqrt{M}}\right)\right]e^{-K}\sum_{l=0}^{N}\frac{K^l}{l!} \\ &\times \sum_{p=0}^{l}\left(\frac{\frac{2(K+1)}{\bar{\gamma}}}{\sqrt{M}}\right)^p i^p \operatorname{erfc}\left[-\left(\frac{\lambda - M - \frac{2(K+1)}{\bar{\gamma}}}{2\sqrt{M}}\right)\right] + \epsilon_{tr,ND}(N), \end{aligned} \tag{6.7}$$

where $\epsilon_{tr,X}(N)$ represents the truncation error for the diversity type X and, in the no diversity case, has the form

$$\epsilon_{tr,ND}(N) = e^{-K}\sum_{l=N+1}^{\infty}\frac{K^l}{l!}\left[F_{l+1}\left(\frac{\lambda - M}{\sqrt{2M}}, \sqrt{\frac{M}{2}}, \frac{K+1}{\bar{\gamma}}\right) - \hat{P}_{f_{ND}}\right], \tag{6.8}$$

where, for convenience, the notation has reverted to that of (6.3), prior to the application of Lemma 5.1.

Recalling the definition of $F_k(a, b, c)$ in (5.11), the first mean value theorem for infinite integrals [69, Equation 12.113] can be used to show that

$$\begin{aligned} F_k(a, b, c) &= Q(a - b\xi) \times \frac{1}{\Gamma(k)}\int_0^{\infty} e^{-cx}c^k x^{k-1}dx \\ &= Q(a - b\xi), \end{aligned} \tag{6.9}$$

for some $0 \leq \xi \leq \infty$, if $c > 0$ and $k \geq 1$. Consequently, if $b > 0$, $F_k(a, b, c)$ can be bounded as

$$F_k(a, b, c) \leq \max_{\xi \geq 0}\left[Q(a - b\xi)\right] = 1. \tag{6.10}$$

Substituting (6.10) into (6.8), the truncation error can be bounded as

$$\epsilon_{tr,ND}(N) \leq e^{-K} \sum_{l=N+1}^{\infty} \frac{K^l}{l!} \left(1 - \hat{P}_{f_{ND}}\right) = \left(1 - \frac{\Gamma(N+1,K)}{\Gamma(N+1)}\right) \left(1 - \hat{P}_{f_{ND}}\right), \quad (6.11)$$

where $\frac{\Gamma(n,z)}{\Gamma(n)}$ denotes the regularised incomplete gamma function of order n.

The bound in (6.11) is useful in determining the maximum error resulting from the truncation of (6.4) at a given point. Yet, determining the value of N required to ensure a specified truncation error is complicated, as the regularised incomplete gamma function has no known closed form inversion for its order parameter. However, the problem can be simplified by noting that

$$1 - \frac{\Gamma(N+1,K)}{\Gamma(N+1)} < 1 - Q\left(\frac{K-(N+1)}{\sqrt{N+1}}\right), \quad (6.12)$$

when $\frac{\Gamma(N+1,K)}{\Gamma(N+1)}$ is large. Conveniently, this condition corresponds precisely to situations where the truncation error is small, and so (6.11) can be approximated, for small values of $\epsilon_{tr,ND}(N)$, as

$$\epsilon_{tr,ND}(N) < \left[1 - Q\left(\frac{K-(N+1)}{\sqrt{N+1}}\right)\right] \left(1 - \hat{P}_{f_{ND}}\right). \quad (6.13)$$

It is interesting to note that, as N becomes large,

$$\frac{\Gamma(N+1,K)}{\Gamma(N+1)} \approx Q\left(\frac{K-(N+1)}{\sqrt{N+1}}\right), \quad (6.14)$$

and so (6.13) becomes equivalent to (6.11) under the same condition[2].

Using (6.13), it is not difficult to show that the value of N required to ensure that $\epsilon_{tr,ND}(N) \leq \epsilon_0(1 - \hat{P}_{f_{ND}}) \triangleq \max|\epsilon_{tr,ND}|$ is given by

$$N = \left\lceil K - 1 - \frac{Q^{-1}(1-\epsilon_0)}{\sqrt{2}} \left[\sqrt{\left(\frac{Q^{-1}(1-\epsilon_0)}{\sqrt{2}}\right)^2 + 2K} - \frac{Q^{-1}(1-\epsilon_0)}{\sqrt{2}}\right]\right\rceil. \quad (6.15)$$

While the inverse of the Gaussian Q function does not have an exact closed form itself, it is not difficult to accurately compute using a simple power series expansion [68, Section 7.17]. Furthermore, as the Gaussian Q function is a single variable function, while the regularised incomplete gamma function depends on two distinct parameters, look up tables for the inverse of the former require fewer entries than for the inverse of the latter. Thus, for certain applications, particularly where power or computation time is limited, the use of (6.15) may be preferable to (6.11).

However, while (6.15) is useful when $K > 0$, it does not account for the $K = 0$ case,

[2]This can be verified by noting that the error resulting from the approximation in (6.14) is equivalent to $\epsilon_{CLT}(N+1, 0, K)$. The result then follows from an application of Theorem 4.1.

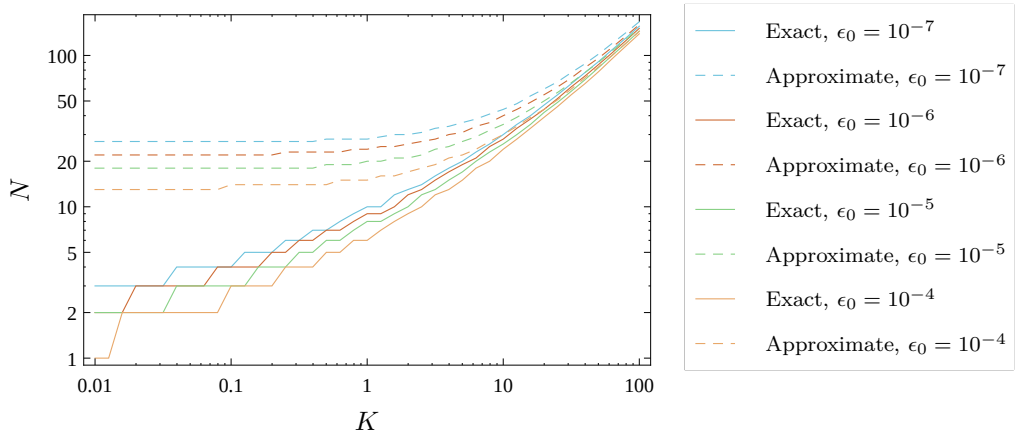

Figure 6.1: A log-log plot of the truncation point required to ensure that $\epsilon_{tr,ND}(N) \leq \epsilon_0(1 - \hat{P}_{f_{ND}})$. The exact results were calculated from (6.11) using a numerical root finding method, while the approximate results were computed directly from (6.16).

where no truncation is required (recall (6.5)). Consequently, this special case will be accounted for using the more general rule

$$N = \begin{cases} 0, & K = 0, \\ \left\lceil K - 1 - \frac{Q^{-1}(1-\epsilon_0)}{\sqrt{2}} \left[\sqrt{\left(\frac{Q^{-1}(1-\epsilon_0)}{\sqrt{2}} \right)^2 + 2K} - \frac{Q^{-1}(1-\epsilon_0)}{\sqrt{2}} \right] \right\rceil, & K > 0. \end{cases} \tag{6.16}$$

Figure 6.1 illustrates the exact and approximate number of terms required to ensure that $\epsilon_{tr,ND}(N) \leq \epsilon_0(1 - \hat{P}_{f_{ND}})$, for different values of ϵ_0. As can be seen, (6.16) bounds the required number of terms over the entire range of values of K quite well. In particular, for $K > 1$, the difference between the exact and the approximate methods is small, and decreases as N increases, as expected; for $K \leq 1$, the difference is larger, but the total number of terms required is small, and so the overestimation resulting from the use of (6.16) should not be problematic in practice.

Using, (6.16) it is possible to approximate the value of N required to ensure an arbitrary truncation error. For instance, if $\epsilon_{tr,ND}(N) \leq \max|\epsilon_{tr,ND}|$, then ϵ_0 can be calculated as

$$\epsilon_0 = \frac{\max|\epsilon_{tr,ND}|}{1 - \hat{P}_{f_{ND}}}, \tag{6.17}$$

and so, substituting (6.17) into (6.16), N can be calculated for arbitrary system parameters.

6.2.1.2 Quantifying the approximation error

If the truncation error is sufficiently small, then (6.7) may be accurately approximated as

$$\tilde{P}_{d_{ND,Rice}} \approx \hat{P}_{f_{ND}} + \frac{1}{2}\exp\left[-\frac{\frac{2(K+1)}{\bar{\gamma}}}{\sqrt{M}}\left(\frac{\lambda - M - \frac{K+1}{\bar{\gamma}}}{2\sqrt{M}}\right)\right] \times e^{-K}\sum_{l=0}^{N}\frac{K^l}{l!}\sum_{p=0}^{l}\left(\frac{\frac{2(K+1)}{\bar{\gamma}}}{\sqrt{M}}\right)^p i^p \operatorname{erfc}\left[-\left(\frac{\lambda - M - \frac{2(K+1)}{\bar{\gamma}}}{2\sqrt{M}}\right)\right]. \quad (6.18)$$

In a similar fashion to (5.20), it can be shown that the total error resulting from the use of (6.18), $\epsilon_{tot,ND,Rice}$, is bounded as

$$|\epsilon_{tot,ND,Rice}| \leq \max|\epsilon_{CLT,ND}| + |\epsilon_{SNR,ND,Rice}| + \epsilon_{tr,ND}(N). \quad (6.19)$$

Using Lemma 5.2, $|\epsilon_{SNR,ND,Rice}|$ can be bounded as

$$\begin{aligned}|\epsilon_{SNR,ND,Rice}| &\leq \frac{1}{\sqrt{2\pi e}}\int_{-\infty}^{\infty} x\ f_{ND,Rice}(x)\ dx \\ &\leq \frac{1}{\sqrt{2\pi e}}\int_{0}^{\infty} x\left(\frac{K+1}{\bar{\gamma}}\right)e^{-K-\frac{(K+1)x}{\bar{\gamma}}}I_0\left(2\sqrt{\frac{K(K+1)x}{\bar{\gamma}}}\right)\ dx. \quad (6.20)\end{aligned}$$

Using the substitution $u = \frac{2(K+1)x}{\bar{\gamma}}$, the right hand side of the inequality in (6.20) can be simplified as

$$\begin{aligned}&\frac{1}{\sqrt{2\pi e}}\int_{0}^{\infty} x\ \left(\frac{K+1}{\bar{\gamma}}\right)e^{-K-\frac{(K+1)x}{\bar{\gamma}}}I_0\left(2\sqrt{\frac{K(K+1)x}{\bar{\gamma}}}\right)\ dx \\ &\qquad = \frac{1}{\sqrt{2\pi e}}\frac{\bar{\gamma}}{2(K+1)}\int_{0}^{\infty}\frac{u}{2}\ e^{-K-\frac{u}{2}}I_0\left(\sqrt{2Ku}\right)\ du, \quad (6.21)\end{aligned}$$

As the integral on the right hand side of (6.21) is equivalent to the mean of the noncentral chi square distribution with two degrees of freedom and noncentrality parameter $2K$, (6.21) can be simplified to

$$|\epsilon_{SNR,ND,Rice}| \leq \frac{\bar{\gamma}}{\sqrt{2\pi e}}, \quad (6.22)$$

where the fact that the mean of the distribution is $2(K+1)$ has been used to simplify the result.

It is also possible to bound $|\epsilon_{SNR,ND,Rice}|$ using Lemma 5.3 as

$$|\epsilon_{SNR,ND,Rice}| \lessapprox \frac{1}{\sqrt{M\pi}}\max_x\left(x\ f_{ND,Rice}(x)\right). \quad (6.23)$$

Using (3.30), and expanding the modified Bessel function of the first kind therein using

(6.2), the product $x\ f_{ND,Rice}(x)$ can be written as

$$x\ f_{ND,Rice}(x) = e^{-K}\sum_{l=0}^{\infty}\frac{K^l}{l!}\left(\frac{(l+1)\bar{\gamma}}{K+1}\right)\left[\frac{1}{\Gamma(l+2)}\left(\frac{K+1}{\bar{\gamma}}\right)^{l+2}x^{l+1}e^{-\frac{(K+1)x}{\bar{\gamma}}}\right]. \quad (6.24)$$

In (6.24), the term in the square brackets is equivalent to the probability density function of the gamma distribution, with shape parameter, $l+2$, and scale parameter, $\frac{\bar{\gamma}}{K+1}$. As the gamma distribution PDF is maximised at its mode, in this case when $x = \frac{(l+1)\bar{\gamma}}{K+1}$, it is not difficult to show that

$$\max_x\left[\frac{1}{\Gamma(l+2)}\left(\frac{K+1}{\bar{\gamma}}\right)^{l+2}x^{l+1}e^{-\frac{(K+1)x}{\bar{\gamma}}}\right] = \left(\frac{K+1}{\bar{\gamma}}\right)\frac{\left(\frac{l+1}{e}\right)^{l+1}}{\Gamma(l+2)}. \quad (6.25)$$

Using (6.25), it can be shown that

$$\begin{aligned}\max_x\left(x\ f_{ND,Rice}(x)\right) &= e^{-K}\sum_{l=0}^{\infty}\frac{K^l}{l!}\left(\frac{(l+1)\bar{\gamma}}{K+1}\right)\\ &\quad\times\max_x\left[\frac{1}{\Gamma(l+2)}\left(\frac{K+1}{\bar{\gamma}}\right)^{l+2}x^{l+1}e^{-\frac{(K+1)x}{\bar{\gamma}}}\right]\\ &< e^{-K}\sum_{l=0}^{\infty}\frac{K^l}{l!}\left[\frac{\left(\frac{l+1}{e}\right)^{l+1}}{\Gamma(l+1)}\right]\\ &< \frac{e^{-K}}{\sqrt{2\pi}}\sum_{l=0}^{\infty}\frac{K^l}{l!}\sqrt{l+1}, \end{aligned} \quad (6.26)$$

where Stirling's inequality (recall (5.28)) has been used to simplify the result. Unfortunately, to the best of the author's knowledge at the time of writing, the series in (6.26) has no closed form. However, Jensen's inequality [101, Equation 3.8.2] can be used to further bound the result.

Jensen's inequality: If $\phi(x)$ is a concave function and $\sum_{i=0}^{\infty}p_i = 1$, then

$$\sum_{i=0}^{\infty}p_i\phi(x_i) \le \phi\left(\sum_{i=0}^{\infty}p_ix_i\right). \quad (6.27)$$

Noting that $\phi(x) = \sqrt{x}$ is a concave function and that, by definition,

$$e^{-x}\sum_{i=0}^{\infty}\frac{x^i}{i!} = 1,\ \forall\ x \ge 0, \quad (6.28)$$

Jensen's inequality can be applied to (6.26) to show that

$$\max_x\left(x\ f_{ND,Rice}(x)\right) < \frac{1}{\sqrt{2\pi}}\sqrt{e^{-K}\sum_{l=0}^{\infty}\frac{K^l}{l!}(l+1)} = \sqrt{\frac{K+1}{2\pi}}, \quad (6.29)$$

and so (6.23) can be simplified to

$$|\epsilon_{SNR,ND,Rice}| \lessapprox \frac{1}{\pi}\sqrt{\frac{K+1}{2M}}. \tag{6.30}$$

As before, both (6.22) and (6.30) can be summarised using the single expression

$$\max|\epsilon_{SNR,ND,Rice}| = \min\left(\frac{\bar{\gamma}}{\sqrt{2\pi e}}, \frac{1}{\pi}\sqrt{\frac{K+1}{2M}}\right), \tag{6.31}$$

where $\max|\epsilon_{SNR,ND,Rice}| \geq |\epsilon_{SNR,ND,Rice}|$. Consequently, the total approximation error can be bounded as

$$\max|\epsilon_{tot,ND,Rice}| = \max|\epsilon_{CLT,ND}| + \max|\epsilon_{SNR,ND,Rice}| + \max|\epsilon_{tr,ND}|, \tag{6.32}$$

where $\max|\epsilon_{tot,ND,Rice}| \geq |\epsilon_{tot,ND,Rice}|$. Figure 6.2(a) illustrates the exact (calculated numerically) and approximate (calculated using (6.18) with N chosen so that $\epsilon_{tr,ND}(N) \leq 10^{-6}$) probabilities of detection for some typical scenarios, while Figure 6.2(b) illustrates the resulting errors and their bounds, calculated using (6.32). As with the approximations for Nakagami-m channels, the bound for the total error tends to overestimate the actual total error by a greater amount when the signal to noise ratio is large. However, as small numbers of samples are usually sufficient to guarantee reliable sensing when the signal to noise is large, the exact expressions listed in Table 3.2 should not be difficult to evaluate in such situations, and so the use of approximations can be avoided altogether. Thus, while a further bound may better describe the behaviour of the error when the signal to noise ratio is large, it is likely to be of limited use in practice.

6.2.1.3 Novel approximations for other system parameters

Substituting (5.32) into (6.4), it can be shown that

$$\tilde{P}_{d_{ND,Rice}} = \hat{P}_{f_{ND}} + \frac{1}{2}\exp\left[-\frac{2(K+1)}{\sqrt{M\bar{\gamma}^2}}\left(\frac{Q^{-1}(\hat{P}_{f_{ND}})}{\sqrt{2}} - \frac{K+1}{2\sqrt{M\bar{\gamma}^2}}\right)\right] e^{-K}\sum_{l=0}^{\infty}\frac{K^l}{l!} \times \sum_{p=0}^{l}\left(\frac{2(K+1)}{\sqrt{M\bar{\gamma}^2}}\right)^p i^p \operatorname{erfc}\left[-\left(\frac{Q^{-1}(\hat{P}_{f_{ND}})}{\sqrt{2}} - \frac{K+1}{\sqrt{M\bar{\gamma}^2}}\right)\right]. \tag{6.33}$$

Thus, for given values of $\tilde{P}_{d_{ND,Rice}}$, $\hat{P}_{f_{ND}}$, and K, the product $M\bar{\gamma}^2$ must be constant, and so it can be inferred that the relationships given in (5.36) and (5.37) also hold for energy detectors with no diversity operating on Rice channels, provided that the approximation error is not large.

As in the AWGN and Nakagami-m cases, this relation can be quite useful in practice.

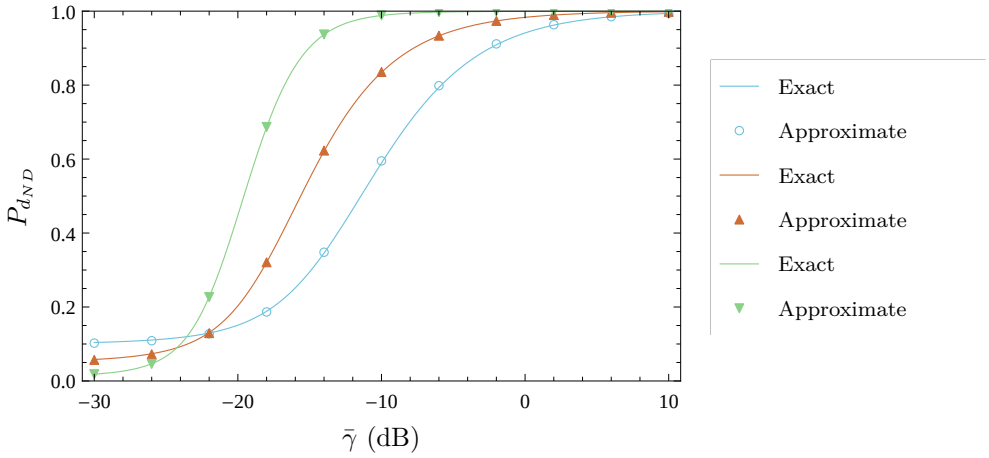

(a) A plot of the exact and approximate probabilities of detection.

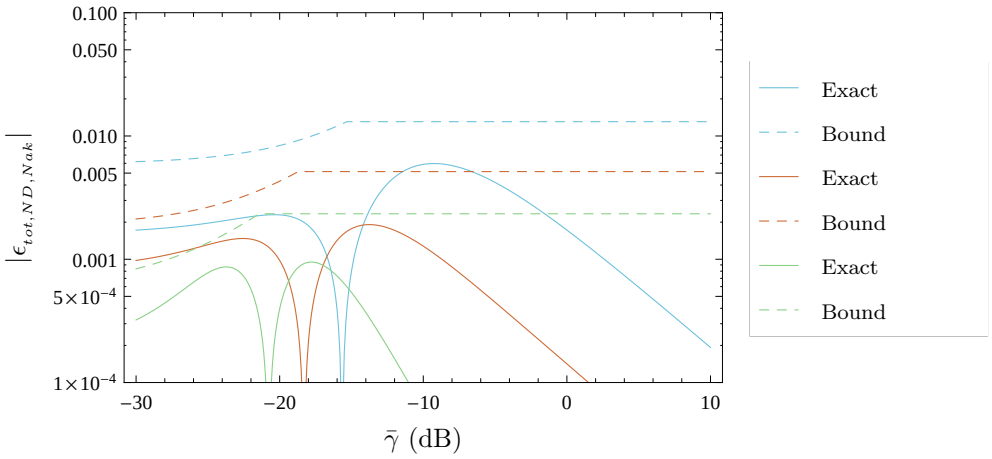

(b) A log-linear plot of the total approximation error, and its bound, for the trends shown in Figure 6.2(a).

Figure 6.2: Plots of the exact and approximate probabilities of detection, and the resulting approximation errors, for energy detectors with no diversity operating on Rice fading channels. The blue trends correspond to the scenario where $K = 0$, $M = 1000$ and $\hat{P}_{f_{ND}} = 0.1$, the red trends to the scenario where $K = 1.1$, $M = 10000$ and $\hat{P}_{f_{ND}} = 0.05$, and the green trends to the scenario where $K = 5$, $M = 100000$ and $\hat{P}_{f_{ND}} = 0.01$.

For instance, if an energy detector with no diversity, operating on a Rice faded channel with $K = 1.1$, requires 10000 samples to ensure that $\tilde{P}_{d_{ND,Rice}} = 0.9$ and $\hat{P}_{f_{ND}} = 0.05$ at a signal to noise ratio of $-7.78\,\text{dB}$, (5.36) can be used to show that, to ensure the same reliability at a signal to noise ratio of $-15.56\,\text{dB}$, 359895 samples are required. Using a numerical method, it can be shown that the precise number of additional samples required is 355210. Thus, the approximation overestimates the required number of samples by just 1.32%.

6.2.2 Receivers with MRC diversity

For maximal ratio combiner systems, the probability of detection in Rice channels can be approximated by substituting (3.34) into (5.8) to give

$$P_{d_{MRC,Rice}} \approx \tilde{P}_{d_{MRC,Rice}} = \int_0^\infty Q\left(\frac{\lambda - M(1+x)}{\sqrt{2M}}\right)\left(\frac{K+1}{\bar{\gamma}}\right)^{\frac{n+1}{2}}\left(\frac{x}{Kn}\right)^{\frac{n-1}{2}} \times e^{-Kn-\frac{(K+1)x}{\bar{\gamma}}} I_{n-1}\left(2\sqrt{\frac{Kn(K+1)x}{\bar{\gamma}}}\right) dx. \tag{6.34}$$

Expanding the modified Bessel function of the first kind using (6.2), it can be shown that (6.34) simplifies to

$$\begin{aligned}\tilde{P}_{d_{MRC,Rice}} &= e^{-Kn}\sum_{l=0}^{\infty}\frac{(Kn)^l}{l!}\,F_{l+n}\left(\frac{\lambda - M}{\sqrt{2M}}, \sqrt{\frac{M}{2}}, \frac{K+1}{\bar{\gamma}}\right) \\ &= \hat{P}_{f_{MRC}} + \frac{1}{2}\exp\left[-\frac{\frac{2(K+1)}{\bar{\gamma}}}{\sqrt{M}}\left(\frac{\lambda - M - \frac{K+1}{\bar{\gamma}}}{2\sqrt{M}}\right)\right] e^{-Kn}\sum_{l=0}^{\infty}\frac{(Kn)^l}{l!} \\ &\quad \times \sum_{p=0}^{l+n-1}\left(\frac{\frac{2(K+1)}{\bar{\gamma}}}{\sqrt{M}}\right)^p i^p\,\text{erfc}\left[-\left(\frac{\lambda - M - \frac{2(K+1)}{\bar{\gamma}}}{2\sqrt{M}}\right)\right].\end{aligned} \tag{6.35}$$

As the use of Lemma 5.1 in this instance does not place restrictions on the value of K, (6.35) is valid for $K \in \mathbb{R}_0^+$.

In a similar manner to (6.33), (6.35) can be used to show that the product $M\bar{\gamma}^2$ is constant for given values of $\tilde{P}_{d_{MRC,Rice}}$, $\hat{P}_{f_{MRC}}$, K and n, and so it can once again be inferred that the relationships in (5.36) and (5.37) hold, as long as the error resulting from the use of (6.35) is not large.

However, as (6.35) is in the form of an infinite series, it must be truncated before

computation. If the series is truncated at the point $l = N$, then the approximation

$$\tilde{P}_{d_{MRC,Rice}} \approx \hat{P}_{f_{MRC}} + \frac{1}{2}\exp\left[-\frac{\frac{2(K+1)}{\bar{\gamma}}}{\sqrt{M}}\left(\frac{\lambda - M - \frac{K+1}{\bar{\gamma}}}{2\sqrt{M}}\right)\right] e^{-Kn}\sum_{l=0}^{N}\frac{(Kn)^l}{l!} \times \sum_{p=0}^{l+n-1}\left(\frac{\frac{2(K+1)}{\bar{\gamma}}}{\sqrt{M}}\right)^p i^p \operatorname{erfc}\left[-\left(\frac{\lambda - M - \frac{2(K+1)}{\bar{\gamma}}}{2\sqrt{M}}\right)\right], \tag{6.36}$$

can be made, provided that the truncation error, $\epsilon_{tr,MRC}(N)$, is not large.

In a similar manner to (6.8), it can be shown that

$$\epsilon_{tr,MRC}(N) = e^{-Kn}\sum_{l=N+1}^{\infty}\frac{(Kn)^l}{l!}\left[F_{l+n}\left(\frac{\lambda - M}{\sqrt{2M}}, \sqrt{\frac{M}{2}}, \frac{K+1}{\bar{\gamma}}\right) - \hat{P}_{f_{MRC}}\right], \tag{6.37}$$

and so it follows that

$$\epsilon_{tr,MRC}(N) \leq \left(1 - \frac{\Gamma(N+1, Kn)}{\Gamma(N+1)}\right)(1 - \hat{P}_{f_{MRC}}) \triangleq \max|\epsilon_{tr,MRC}|. \tag{6.38}$$

Again, while (6.38) is useful for evaluating the maximum truncation error, numerical methods are required in order to solve for the number of terms necessary to ensure that $\epsilon_{tr,MRC}(N) \leq \epsilon_0(1 - \hat{P}_{f_{MRC}})$. However, in a similar manner to (6.16), the number of terms required can be approximated as

$$N = \begin{cases} 0, & K = 0, \\ \left\lceil Kn - 1 - \frac{Q^{-1}(1-\epsilon_0)}{\sqrt{2}}\left[\sqrt{\left(\frac{Q^{-1}(1-\epsilon_0)}{\sqrt{2}}\right)^2 + 2Kn} - \frac{Q^{-1}(1-\epsilon_0)}{\sqrt{2}}\right]\right\rceil, & K > 0. \end{cases} \tag{6.39}$$

Again, it is not difficult to show that (6.39) becomes equivalent to the numerical solution of (6.38) as N becomes large. Also, it is interesting to note that, where $K > 0$, more terms are required in order to ensure the same truncation error as in the no diversity case. This is a consequence of (6.38), which is equivalent to (6.11) only when $n = 1$. Thus, (6.36) always requires a larger value of N than (6.18) to ensure the same truncation error.

Figure 6.3(a) illustrates the exact (calculated numerically) and approximate (calculated using (6.36) with N chosen so that $\epsilon_{tr,MRC}(N) \leq 10^{-5}$) probabilities of detection for a typical two branch MRC receiver sensing scenario. As can be seen, the approximation is quite accurate over the entire range of signal to noise ratio values.

Noting that the mean of the distribution specified by $f_{MRC,Rice}(x)$ is $2n(K+1)$, the absolute value of the low SNR approximation error can be bounded, in a similar manner to (6.22), as

$$|\epsilon_{SNR,MRC,Rice}| \leq \frac{n\bar{\gamma}}{\sqrt{2\pi e}}, \tag{6.40}$$

while Lemma 5.3 provides the alternative bound

$$|\epsilon_{SNR,MRC,Rice}| \lessapprox \frac{1}{\sqrt{M\pi}} \max_x \left(x \; f_{MRC,Rice}(x) \right). \tag{6.41}$$

Recalling (6.29), it is not difficult to show that

$$\begin{aligned} \max_x \left(x \; f_{MRC,Rice}(x) \right) &= e^{-Kn} \sum_{l=0}^{\infty} \frac{(Kn)^l}{l!} \left(\frac{(l+n)\bar{\gamma}}{K+1} \right) \\ &\quad \times \max_x \left[\frac{x^{l+n}}{\Gamma(l+n+1)} \left(\frac{K+1}{\bar{\gamma}} \right)^{l+n+1} e^{-\frac{(K+1)x}{\bar{\gamma}}} \right] \\ &< \frac{e^{-Kn}}{\sqrt{2\pi}} \sum_{l=0}^{\infty} \frac{(Kn)^l}{l!} \sqrt{l+n}. \end{aligned} \tag{6.42}$$

Again, to the best of the author's knowledge at the time of writing, the infinite series in (6.42) has no closed form. However, Jensen's inequality can be applied to show that

$$\max_x \left(x \; f_{MRC,Rice}(x) \right) < \frac{1}{\sqrt{2\pi}} \sqrt{e^{-Kn} \sum_{l=0}^{\infty} \frac{(Kn)^l}{l!} (l+n)} = \sqrt{\frac{(K+1)n}{2\pi}}, \tag{6.43}$$

and so (6.41) can be simplified to

$$|\epsilon_{SNR,MRC,Rice}| \lessapprox \frac{1}{\pi} \sqrt{\frac{(K+1)n}{2M}}. \tag{6.44}$$

As before, both (6.40) and (6.44) can be described using a single expression, that is

$$\max |\epsilon_{SNR,MRC,Rice}| = \min \left(\frac{n\bar{\gamma}}{\sqrt{2\pi e}}, \frac{1}{\pi} \sqrt{\frac{(K+1)n}{2M}} \right), \tag{6.45}$$

where $\max |\epsilon_{SNR,MRC,Rice}| \geq |\epsilon_{SNR,MRC,Rice}|$.

Consequently, the total error resulting from the use of (6.36) can be bounded as

$$\max |\epsilon_{tot,MRC,Rice}| = \max |\epsilon_{CLT,MRC}| + \max |\epsilon_{SNR,MRC,Rice}| + \max |\epsilon_{tr,MRC}|, \tag{6.46}$$

where $\max |\epsilon_{tot,MRC,Rice}| \geq |\epsilon_{tot,MRC,Rice}|$. As can be seen in Figure 6.3(b), (6.46) describes the error quite well over the entire range of signal to noise ratios.

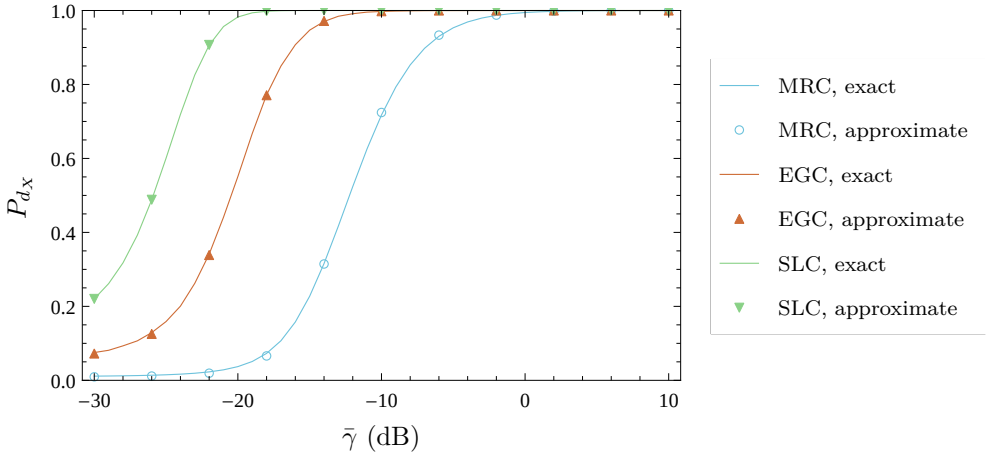

(a) A plot of the exact and approximate probabilities of detection.

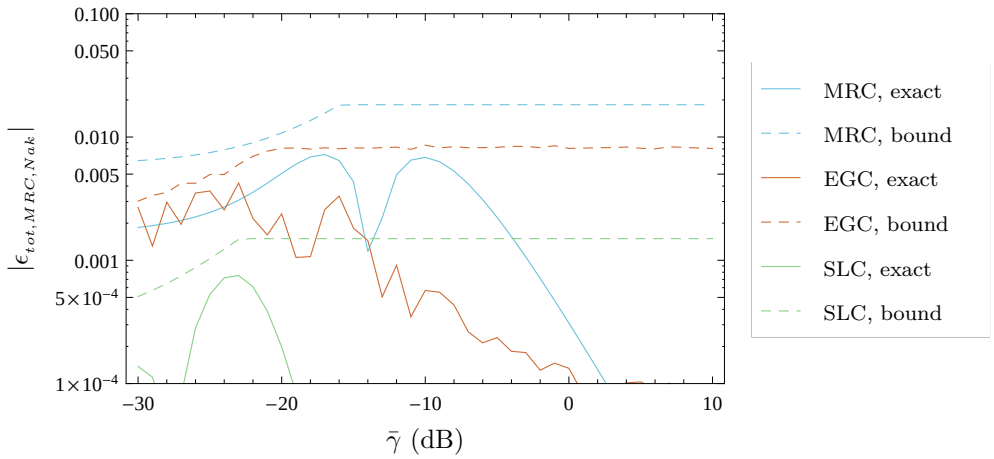

(b) A log-linear plot of the total approximation error, and its bound, for the trends shown in Figure 6.3(a).

Figure 6.3: Plots of the exact and approximate probabilities of detection, and the resulting approximation errors, for energy detector diversity receivers operating on Rice fading channels. The blue trends correspond to a two branch MRC receiver operating on a Rice channel with $K = 0.5$, $M = 1000$ and $\hat{P}_{f_{MRC}} = 0.1$; the red trends to a three branch EGC receiver operating on a Rice channel with $K = 1.5$, $M = 10000$ and $\hat{P}_{f_{EGC}} = 0.05$; and the green trends to a five branch SLC receiver operating on a Rice channel with $K = 2$, $M = 100000$ and $\hat{P}_{f_{SLC}} = 0.1$.

6.2.3 Receivers with EGC diversity

For equal gain combiner systems, the probability of detection in Rice channels can be approximated by substituting (3.37) into (5.8) to give

$$\begin{aligned}\tilde{P}_{d_{EGC,Rice}} &= \int_0^\infty Q\left(\frac{\lambda - M(1+x)}{\sqrt{2M}}\right)\left(\frac{K+1}{b\bar{\gamma}}\right)^{\frac{n+1}{2}}\left(\frac{ax}{Kn}\right)^{\frac{n-1}{2}} e^{-\frac{Kn}{a}-\frac{(K+1)x}{b\bar{\gamma}}} \\ &\qquad \times I_{n-1}\left(2\sqrt{\frac{Kn(K+1)x}{ab\bar{\gamma}}}\right)dx \\ &= e^{-\frac{Kn}{a}}\sum_{l=0}^{\infty}\frac{\left(\frac{Kn}{a}\right)^l}{l!}F_{l+n}\left(\frac{\lambda - M}{\sqrt{2M}}, \sqrt{\frac{M}{2}}, \frac{K+1}{b\bar{\gamma}}\right) \\ &\approx \hat{P}_{f_{EGC}} + \frac{1}{2}\exp\left[-\frac{\frac{2(K+1)}{b\bar{\gamma}}}{\sqrt{M}}\left(\frac{\lambda - M - \frac{K+1}{b\bar{\gamma}}}{2\sqrt{M}}\right)\right]e^{-\frac{Kn}{a}}\sum_{l=0}^{N}\frac{\left(\frac{Kn}{a}\right)^l}{l!} \\ &\qquad \times \sum_{p=0}^{l+n-1}\left(\frac{\frac{2(K+1)}{b\bar{\gamma}}}{\sqrt{M}}\right)^p i^p \operatorname{erfc}\left[-\left(\frac{\lambda - M - \frac{2(K+1)}{b\bar{\gamma}}}{2\sqrt{M}}\right)\right], \end{aligned} \tag{6.47}$$

where the resulting infinite series has been truncated at the point $l = N$, in a similar manner to (6.36). Again, as the use of Lemma 5.1 has not placed any restrictions on the values of K, (6.47) is valid for $K \in \mathbb{R}_0^+$.

Using (6.47), it can be shown that (5.36) and (5.37) also hold in the case of EGC systems operating on Rice channels, provided that the total approximation error is not large. This is an interesting result because it holds regardless of the available values of the constants a and b which, as can be seen in Table 3.5, are limited to $K \in \{1\,\text{dB}, 3\,\text{dB}, 5\,\text{dB}, 7\,\text{dB}\}$ and $n \in [2, 8]$.

As before, it is not difficult to show that the error resulting from the truncation of the series in (6.47) is bounded as

$$\epsilon_{tr,EGC}(N) \leq \left(1 - \frac{\Gamma(N+1, \frac{Kn}{a})}{\Gamma(N+1)}\right)(1 - \hat{P}_{f_{EGC}}) \triangleq \max|\epsilon_{tr,EGC}|, \tag{6.48}$$

and so the number of terms required to ensure that $\epsilon_{tr,EGC}(N) \leq \epsilon_0(1 - \hat{P}_{f_{EGC}})$ can be approximated, for small ϵ_0, as

$$N = \begin{cases} 0, & K = 0, \\ \left\lceil \frac{Kn}{a} - 1 - \frac{Q^{-1}(1-\epsilon_0)}{\sqrt{2}}\left[\sqrt{\left(\frac{Q^{-1}(1-\epsilon_0)}{\sqrt{2}}\right)^2 + \frac{2Kn}{a}} - \frac{Q^{-1}(1-\epsilon_0)}{\sqrt{2}}\right]\right\rceil, & K > 0. \end{cases} \tag{6.49}$$

Again, as N becomes larger, the value given by (6.49) becomes closer to the value resulting from the numerical solution of (6.48).

Figure 6.3(a) illustrates the exact (calculated numerically) and approximate (calculated using (6.47) with N chosen so that $\epsilon_{tr,EGC}(N) \leq 10^{-4}$) probabilities of detection for a typical three branch EGC receiver sensing scenario. As $K = 1.5$, the constants a and b are not given by Table 3.5. However, linear interpolation can be used to find the appropriate values. As can be seen, the approximation is quite accurate over the entire range of signal to noise ratio values, despite the use of interpolation to find appropriate values for a and b.

In deriving (6.47), Hu and Beaulieu's approximation for the probability density function of the signal to noise ratio at the equal gain combiner output [71] was used, and so the total approximation error cannot be bounded as in (6.46). Recalling (5.49), however, it is not difficult to show that

$$|\epsilon_{tot,EGC,Rice}| \leq \max |\epsilon_{CLT,EGC}| + |\epsilon_{SNR,EGC,Rice}| + |\epsilon_{PDF,EGC,Rice}| + \epsilon_{tr,EGC}(N), \quad (6.50)$$

where $|\epsilon_{PDF,EGC,Rice}|$ is given by

$$|\epsilon_{PDF,EGC,Rice}| = \left| \int_{-\infty}^{\infty} P_{d_{EGC}}(x) \left(f_{EGC,Rice}(x) - \hat{f}_{EGC,Rice}(x) \right) \, dx \right|. \quad (6.51)$$

Noting that the mean of the distribution defined by $\hat{f}_{EGC,Rice}(x)$ is $2n(\frac{K}{a} + 1)$, the absolute value of the low SNR approximation error can be bounded as

$$|\epsilon_{SNR,EGC,Rice}| \leq \left(\frac{\frac{K}{a} + 1}{K + 1} \right) \frac{nb\bar{\gamma}}{\sqrt{2\pi e}}, \quad (6.52)$$

and, in a similar manner to (6.42), it can be shown that

$$\max_x \left(x \hat{f}_{EGC,Rice}(x) \right) < \sqrt{\frac{(\frac{K}{a} + 1)n}{2\pi}}, \quad (6.53)$$

and so an alternative bound for the low SNR approximation error can be derived, using Lemma 5.3, as

$$|\epsilon_{SNR,EGC,Rice}| \lessapprox \frac{1}{\pi} \sqrt{\frac{(\frac{K}{a} + 1)n}{2M}}. \quad (6.54)$$

As before, both (6.52) and (6.54) can be described using the single expression

$$\max |\epsilon_{SNR,EGC,Rice}| = \min \left(\left(\frac{\frac{K}{a} + 1}{K + 1} \right) \frac{nb\bar{\gamma}}{\sqrt{2\pi e}}, \frac{1}{\pi} \sqrt{\frac{(\frac{K}{a} + 1)n}{2M}} \right), \quad (6.55)$$

where $\max |\epsilon_{SNR,EGC,Rice}| \geq |\epsilon_{SNR,EGC,Rice}|$.

As in (5.54), the error resulting from the use of Hu and Beaulieu's PDF approximation

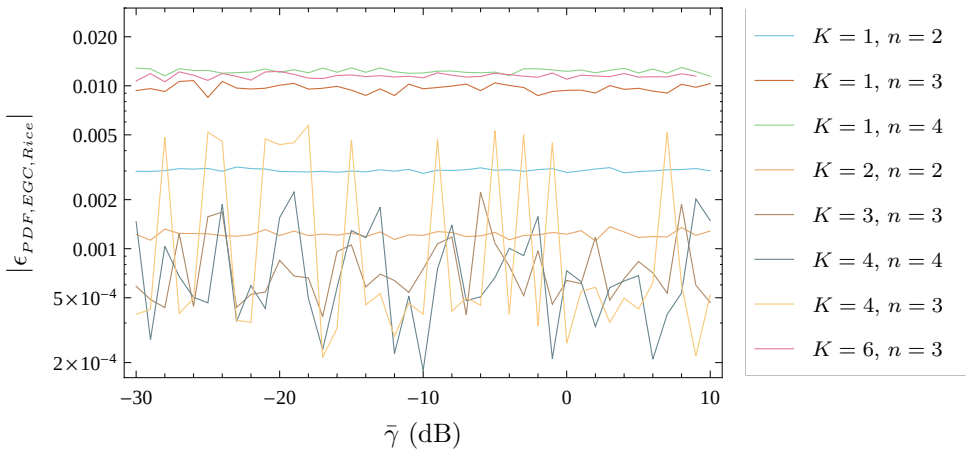

Figure 6.4: Plots of the error resulting from the use of Hu and Beaulieu's approximation for the probability density function of the signal to noise ratio at the output of an equal gain combiner operating on a Rice channel.

can be bounded using the second mean value theorem for infinite integrals, that is

$$\max|\epsilon_{PDF,EGC,Rice}| = \max_{\zeta}\left|\int_{\zeta}^{\infty}\left(f_{EGC,Rice}(x) - \hat{f}_{EGC,Rice}(x)\right)\,dx\right|, \tag{6.56}$$

where $\max|\epsilon_{PDF,EGC,Rice}| \geq |\epsilon_{PDF,EGC,Rice}|$. However, as $f_{EGC,Rice}(x)$ is not available in closed form, (6.56) must be computed numerically. Figure 6.4 illustrates the values of $\max|\epsilon_{PDF,EGC,Rice}|$ for various combinations of K and n. As can be seen, the resulting errors are quite small.

Using (6.50), (6.55) and (6.56), the total error resulting from the use of (6.47) can be bounded as

$$\begin{aligned}\max|\epsilon_{tot,EGC,Rice}| = {} & \max|\epsilon_{CLT,EGC}| + \max|\epsilon_{SNR,EGC,Rice}| \\ & + \max|\epsilon_{PDF,EGC,Rice}| + \max|\epsilon_{tr,EGC}|,\end{aligned} \tag{6.57}$$

where $\max|\epsilon_{tot,EGC,Rice}| \geq |\epsilon_{tot,EGC,Rice}|$. Figure 6.3(b) illustrates the use of (6.57) in bounding the error resulting from the use of approximations in Figure 6.3(a). In this case, as (6.57) relies on the bound in (6.56), it must also be computed numerically. Still, as can be seen, the bound describes the total error well across the entire range of signal to noise ratio values.

As Table 3.5 defines the values of a and b for $K \in \{1\,\text{dB}, 3\,\text{dB}, 5\,\text{dB}, 7\,\text{dB}\}$, interpolation is only possible when the value of the fading parameter falls within this range. Consequently, if $K < 1\,\text{dB}$ or $K > 7\,\text{dB}$, extrapolation must be relied upon, and there can be significant variation in the magnitudes of the results. This can be seen quite clearly in Figures 6.5(a) and 6.5(b), where the interpolated and extrapolated values of the parameters have been plotted as functions of the fading parameter. The problem

is less severe for $K < 1\,\text{dB}$, as the possible range of values of the fading parameter is limited to $K \in [0, 1.25)$, and so the magnitudes of the extrapolated constants are bounded[3]. However, for $K > 7\,\text{dB}$, and particularly as K becomes large, extrapolation can result in poor approximations for the values of the constants, and so $\epsilon_{PDF,EGC,Rice}$ becomes large.

One might expect that the problem can be solved by fitting additional values of a and b for $K < 1\,\text{dB}$ and $K > 7\,\text{dB}$. However, such a look up table could only describe a finite subset of the total range of possible values, as the fading parameter has no upper bound. Furthermore, as Hu and Beaulieu only consider EGC systems with up to eight diversity branches, extrapolation of the constants is also required for $n > 8$, with similar consequences. While many EGC systems have fewer than eight branches, it is possible that technological advances, decreasing implementation costs and/or demand may result in systems with larger numbers of branches in the future, and so the total number of points in any useful look up table would be very large.

The fitted parameters in Hu and Beaulieu's approximation also hinder comparisons between EGC and MRC systems in the manner of (5.57). Consider the scenario where an energy detector with MRC diversity operates on a Rice channel with $K = K_{MRC}$, while an energy detector with EGC diversity operates on a Rice channel with $K = K_{EGC} = aK_{MRC}$. Let the MRC system require $M = M_{MRC,Rice}$ samples to ensure certain decision probabilities are met at an average signal to noise ratio of $\bar{\gamma}_{MRC,Rice}$, and the EGC system require $M = M_{EGC,Rice}$ samples to meet the same decision probabilities at an average signal to noise ratio of $\bar{\gamma}_{EGC,Rice}$. Equating (6.35) and (6.47), it is not difficult to show that these conditions require that

$$M_{EGC,Rice}\bar{\gamma}^2_{EGC,Rice} \approx \left[\frac{1}{b}\left(\frac{K_{EGC}+1}{K_{MRC}+1}\right)\right]^2 M_{MRC,Rice}\bar{\gamma}^2_{MRC,Rice}, \tag{6.58}$$

provided that the total approximation errors resulting from the use of (6.35) and (6.47) are not large. However, using (6.58), it is only possible to compare the sample complexities of the architectures when they operate on Rice channels with differing fading parameters, and only then when the fading parameters are related as $K_{EGC} = aK_{MRC}$. Consequently, the result is likely to be of limited use in practice.

A preferable outcome, then, would be the development of a PDF approximation similar to (3.35) or, better again, the development of an exact closed form PDF, either of which would enable the derivation of an approximation for the detection probability free from fitted parameters. However, to the best of the author's knowledge at the time of writing, only approximate PDFs based on fitted parameters are available in the literature and, of these, Hu and Beaulieu's relies on the fewest number of fitted parameters. Furthermore, as an exact PDF has thus far eluded discovery in the simpler

[3]It is worth recalling that, when $K = 0$, the Rice channel becomes equivalent to a Rayleigh channel, and so (5.48) can be used instead of (6.47) in this instance.

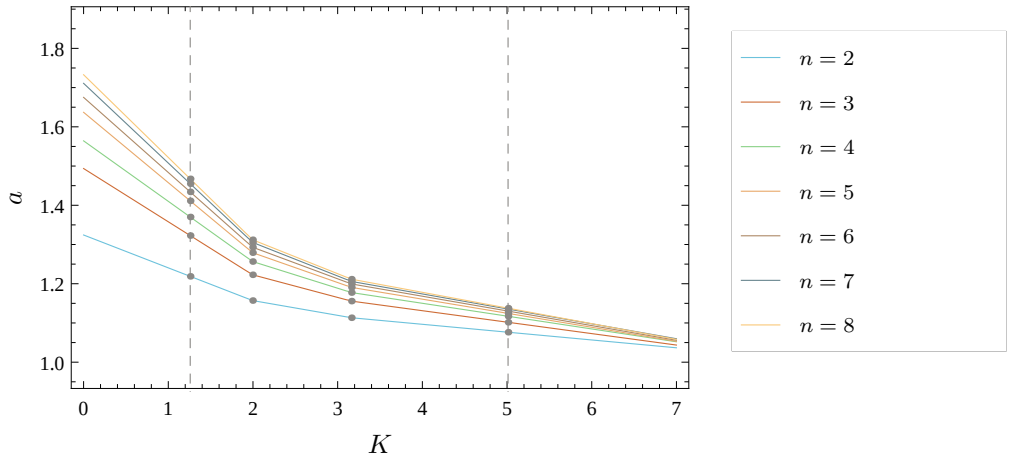

(a) Interpolated and extrapolated values of the a parameter.

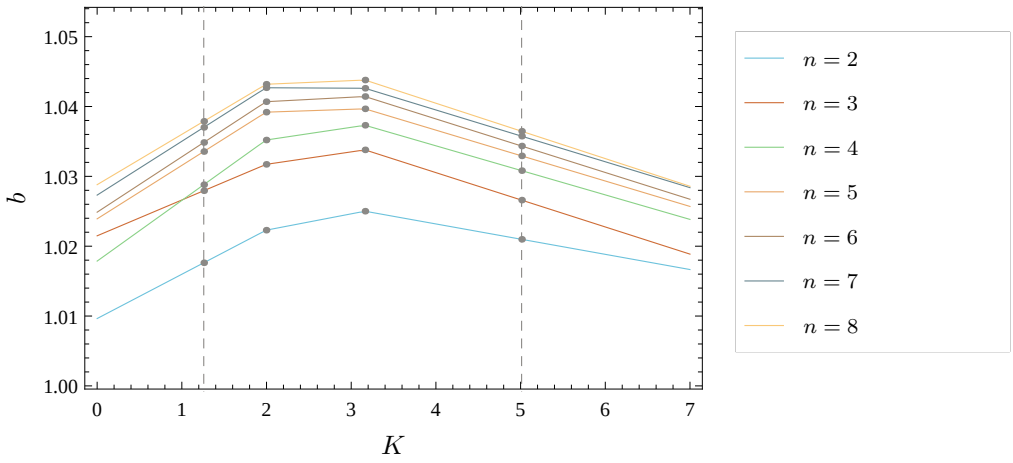

(b) Interpolated and extrapolated values of the b parameter.

Figure 6.5: Plots of the constants a and b, interpolated and extrapolated from the data in Table 3.5 (the values of K shown have been converted from their decibel units). The dashed lines indicate the range of values of K for which the data in in Table 3.5 is defined, while the point markers indicate the value of each data point therein.

case of the Nakagami-m channel (recall that Dharmawansa et al.'s expression for the PDF relies on a complicated series of nested infinite summations), it may continue to do so in the case of Rice channels for some time to come. Nevertheless, the approach outlined here is, in many cases of interest, accurate and useful and, to the best of the author's knowledge, the only manner in which the detection probability of energy detectors with EGC diversity operating on Rice channels can be computed without the use of numerical methods.

6.2.4 Receivers with SLC diversity

Finally, substituting (3.34) into (5.8), the probability of detection of square law combiner systems operating on Rice channels can be approximated as

$$\begin{aligned}\tilde{P}_{d_{SLC,Rice}} &= \int_0^\infty Q\left(\frac{\lambda - M(n+x)}{\sqrt{2Mn}}\right)\left(\frac{K+1}{\bar{\gamma}}\right)^{\frac{n+1}{2}}\left(\frac{x}{Kn}\right)^{\frac{n-1}{2}} \\ &\quad \times e^{-Kn-\frac{(K+1)x}{\bar{\gamma}}} I_{n-1}\left(2\sqrt{\frac{Kn(K+1)x}{\bar{\gamma}}}\right)dx \\ &= e^{-Kn}\sum_{l=0}^{\infty}\frac{(Kn)^l}{l!}F_{n+l}\left(\frac{\lambda - Mn}{\sqrt{2Mn}}, \sqrt{\frac{M}{2n}}, \frac{K+1}{\bar{\gamma}}\right) \\ &\approx \hat{P}_{f_{SLC}} + \frac{1}{2}\exp\left[-\frac{\frac{2(K+1)n}{\bar{\gamma}}}{\sqrt{Mn}}\left(\frac{\lambda - Mn - \frac{(K+1)n}{\bar{\gamma}}}{2\sqrt{Mn}}\right)\right] e^{-Kn}\sum_{l=0}^{N}\frac{(Kn)^l}{l!} \\ &\quad \times \sum_{p=0}^{l+n-1}\left(\frac{\frac{2(K+1)n}{\bar{\gamma}}}{\sqrt{Mn}}\right)^p i^p \operatorname{erfc}\left[-\left(\frac{\lambda - Mn - \frac{2(K+1)n}{\bar{\gamma}}}{2\sqrt{Mn}}\right)\right], \end{aligned} \tag{6.59}$$

where, once again, the resulting infinite series has been truncated after N terms. It should be noted that, as before, the use of Lemma 5.1 here places no restrictions on the value of K, and so (6.59) is valid for $K \in \mathbb{R}_0^+$.

Again, in a similar manner to (6.11), it can be shown that

$$\epsilon_{tr,SLC}(N) \leq \left(1 - \frac{\Gamma(N+1, Kn)}{\Gamma(N+1)}\right)(1 - \hat{P}_{f_{SLC}}) \triangleq \max|\epsilon_{tr,SLC}|. \tag{6.60}$$

As (6.60) is equivalent to (6.38), the number of terms required to ensure that $\epsilon_{tr,SLC}(N) \leq \epsilon_0(1 - \hat{P}_{f_{SLC}})$ can be approximated using (6.39).

Figure 6.3(a) illustrates the exact (calculated numerically) and approximate (calculated using (6.59) with N chosen so that $\epsilon_{tr,SLC}(N) \leq 10^{-6}$) probabilities of detection for a typical five branch SLC receiver sensing scenario. As can be seen, the approximation is quite accurate over the entire range of signal to noise ratio values.

Noting that $f_{SLC,Rice}(x) = f_{MRC,Rice}(x)$, it is not difficult to show that the low SNR

approximation error is bounded as

$$\max|\epsilon_{SNR,SLC,Rice}| = \left(\frac{\bar{\gamma}}{\sqrt{2\pi e}}, \frac{1}{\pi}\sqrt{\frac{K+1}{2M}}\right), \tag{6.61}$$

where $\max|\epsilon_{SNR,SLC,Rice}| \geq |\epsilon_{SNR,SLC,Rice}|$, and so the total error resulting from the use of (6.59) can be bounded as

$$\max|\epsilon_{tot,SLC,Rice}| = \max|\epsilon_{CLT,SLC}| + \max|\epsilon_{SNR,SLC,Rice}| + \max|\epsilon_{tr,SLC}|, \tag{6.62}$$

where $\max|\epsilon_{tot,SLC,Rice}| \geq |\epsilon_{tot,SLC,Rice}|$. Figure 6.3(b) illustrates the bound given in (6.62). The exact approximation error, calculated using the data shown in Figure 6.3(a), is also shown for comparison, and it is clear that it is well described by the derived bound across the entire range of signal to noise ratio values.

Provided that the error in (6.62) is not large, (6.59) can be used to show that the relationships in (5.36) and (5.37) also hold for energy detectors with SLC diversity. Consequently, they hold for each diversity type in AWGN, Rayleigh, Nakagami-m and Rice channels.

Furthermore, (6.36) and (6.59) can be used to relate the sample complexity of MRC and SLC systems, provided that both systems have the same number of diversity branches. Consider the scenario where energy detectors with n branch MRC and SLC diversity operate on Rice channels with fading parameter K. The MRC system requires $M_{MRC,Rice}$ samples to ensure certain decision probabilities are met when the average signal to noise ratio is given by $\bar{\gamma}_{MRC,Rice}$, while the SLC system requires $M_{SLC,Rice}$ samples to ensure the same decision probabilities at an average signal to noise ratio of $\bar{\gamma}_{SLC,Rice}$. Equating (6.36) and (6.59), it is not difficult to show that

$$M_{SLC,Rice}\bar{\gamma}^2_{SLC,Rice} \approx nM_{MRC,Rice}\bar{\gamma}^2_{MRC,Rice}, \tag{6.63}$$

provided that the total approximation errors resulting from the use of (6.36) and (6.59) are not large. It is interesting to note that (6.63) is an equivalent result to (5.65), and can also be shown to hold in AWGN channels, when the signal to noise ratio is small, using the formulae in Table 4.1. Thus, again, the same behaviour can be observed in AWGN, Rayleigh, Nakagami-m and Rice channels.

The approximation in (6.63) can be useful when comparing the performance of SLC receivers to MRC receivers. For instance, if an energy detector with five branch MRC diversity, operating on a Rice channel with $K = \frac{1}{2}$, requires 10000 samples to ensure that $P_{d_{MRC,Rice}} = 0.999$ and $P_{f_{MRC}} = 0.01$ when the average signal to noise ratio is $-12.84\,\text{dB}$, (6.63) can be used to show that a five branch SLC receiver requires 40000 additional samples in order to achieve the same performance. Again, using an numerical method, it can be shown that the precise number of additional samples required is 38608

— a small difference.

Unfortunately, however, such useful insights into the relationship between EGC and SLC systems are not readily apparent. Consider the scenario where an energy detector with EGC diversity operates on a Rice channel with $K = K_{EGC}$ while an energy detector with SLC diversity operates on a Rice channel with $K = K_{SLC}$. If the EGC system requires $M_{EGC,Rice}$ samples to ensure certain decision probabilities are met when the average signal to noise ratio is given by $\bar{\gamma}_{EGC,Rice}$ and the SLC system requires $M_{SLC,Rice}$ samples to ensure the same decision probabilities at an average signal to noise ratio of $\bar{\gamma}_{SLC,Rice}$, it can be shown that

$$M_{SLC,Rice}\bar{\gamma}^2_{SLC,Rice} \approx \left[b\left(\frac{K_{SLC}+1}{K_{EGC}+1}\right)\right]^2 nM_{EGC,Rice}\bar{\gamma}^2_{EGC,Rice}, \tag{6.64}$$

provided that the total approximation errors resulting from the use of (6.47) and (6.59) are not large. However, again, due to the fitted parameters in Hu and Beaulieu's PDF approximation, (6.64) only holds in the restrictive circumstance when $K_{EGC} = aK_{SLC}$, and so is of limited use in practice.

6.2.5 Discussion

6.2.5.1 Computational complexity

Perhaps unsurprisingly, the low SNR approximations derived in this chapter are similar in form to the low SNR approximations derived in Chapter 5. However, there is a key difference between the two, as those relating to Rice channels consist of an infinite series which must be truncated in order for the detection probability to be computed. Consequently, the analysis of the complexity of these approximations is not as simple as in Section 5.2.5.1.

However, the problem is not intractable. By letting the truncation error be proportional to the sum of the errors resulting from the use of the central limit theorem and the low SNR approximation, it can be ensured that its value becomes negligibly small with respect to the total approximation error, facilitating a comparison in the vein of Section 5.2.5.1. To see this, for $X \in \{\text{ND, MRC, SLC}\}$, let $\max|\epsilon_{tr,X}| = \varepsilon\left(\max|\epsilon_{CLT,X}| + \max|\epsilon_{SNR,X,Rice}|\right)$ so that

$$\max|\epsilon_{tot,X,Rice}| = (1+\varepsilon)\left(\max|\epsilon_{CLT,X}| + \max|\epsilon_{SNR,X,Rice}|\right). \tag{6.65}$$

By choosing a suitably small value of ε, it can be ensured that the truncation error does not dominate the value of the total error, and so the exact and approximate methods can be compared directly, as in Section 5.2.5.1, by calculating the truncation point required to give $\epsilon^T_{X,Rice} \leq \max|\epsilon_{tot,X,Rice}|$ for each diversity type.

Some example results, for the case where $\varepsilon = 0.001$, are shown in Figures 6.6(a)–6.6(c). As can be seen, when the number of samples is small, the exact methods require fewer numbers of terms to be computed than the low SNR approximations while, for large numbers of samples, the reverse is true. However, it is also clear that the truncation points are much greater for the exact methods than for the approximate methods[4], and so the former require significantly more terms to be computed as the number of samples becomes large.

Yet, as before, it is not simply the number of terms that must be computed that determines which method is more computationally demanding, but rather the combination of the number of terms and the complexity of each. While the exact and approximate expressions for the detection probabilities in Rice channels are more complicated than in the Nakagami-m case, they again consist of weighted sums of regularised incomplete gamma functions, in the case of the exact expressions, and weighted sums of the repeated integral of the complementary error function, in the case of the approximate methods. However, using the recurrence relations in (5.13), the repeated integral of the complementary error function can be expressed as in (5.67), and so the weighted sums of the repeated integral of the complementary error function can be expressed as weighted sums of the exponential and complementary error functions. As noted previously, the regularised incomplete gamma function is known to be more difficult to compute to a specified degree of precision than these functions. Consequently, in situations where larger numbers of regularised incomplete gamma functions than complementary error functions must be computed, the low SNR approximations presented in this chapter are preferable to the exact methods given in Chapter 3, if the total error resulting from their use is equal. As this is clearly the case when the number of samples is large, from Figures 6.6(a)–6.6(c), it can be concluded that the derived approximations are less computationally intensive to evaluate in such scenarios.

However, it should be noted that, for each diversity type, N increases with the product of the fading parameter and the number of diversity branches, Kn, and so it may be necessary to compute large numbers of terms in scenarios where this product is large, in order to ensure that the truncation error is acceptably small. Consequently, the low SNR approximations may only be useful in scenarios where the values of the fading parameter and the number of diversity branches are small to moderate. However, this is often the case in practice, and so the approximations derived here should be quite generally applicable.

[4]The increase in the value of the required truncation point for the low SNR approximations is due to the constraint imposed in (6.65), as $\max|\epsilon_{CLT,X}|$ and $\max|\epsilon_{SNR,X,Rice}|$ decrease with increasing values of M.

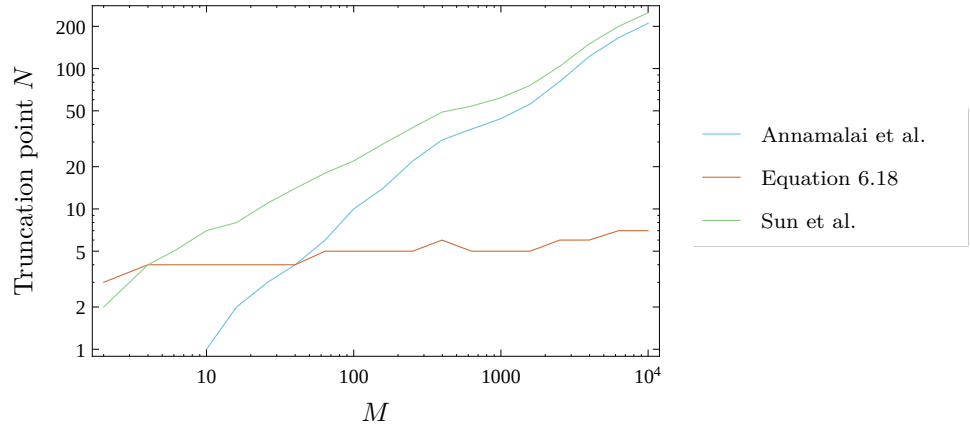

(a) Truncation points required for the analysis of systems with no diversity.

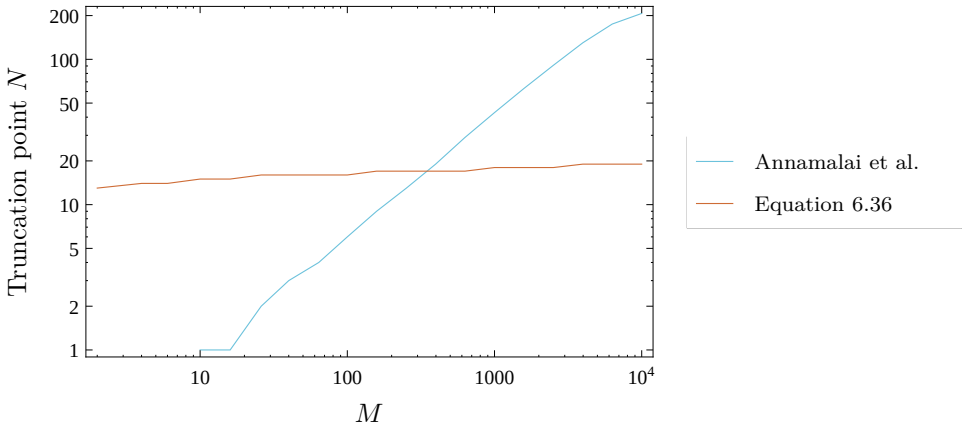

(b) Truncation points required for the analysis of MRC systems.

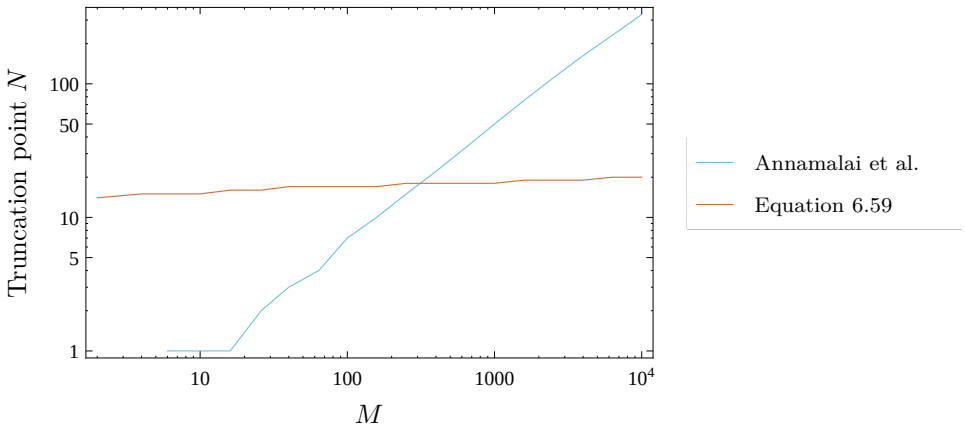

(c) Truncation points required for the analysis of SLC systems.

Figure 6.6: Log-log plots of the truncation points required to give $\epsilon^{T}_{X,Rice} \leq \max|\epsilon_{tot,X,Rice}| = 1.001\left(\max|\epsilon_{CLT,X}| + \max|\epsilon_{SNR,X,Rice}|\right)$ as functions of the number of samples. The conditions in each case match those used to generate Figure 3.4(d).

6.2.5.2 Accuracy / region of applicability

The low SNR approximations derived in this chapter principally depend on two assumptions: that the detection probability for each diversity type can be approximated as in Table 4.1 and that, when the signal to noise ratio is small, these approximations can be further simplified using (5.6). Conveniently, these are the same assumptions that the low SNR approximations for Nakagami-m channels depend upon, and so the resulting error can be quantified in a similar way.

As in the Nakagami-m case, two bounds for the error resulting from the use of the low SNR approximation were derived. The first bound demonstrates that the error is proportional to the average signal to noise ratio per branch at the receiver. Thus, the low SNR approximation error decreases as the signal to noise ratio becomes smaller. The second bound demonstrates that the low SNR approximation error is inversely proportional to the square root of the number of samples. Thus, the low SNR approximation error decreases as the number of samples increases. Consequently, the derived approximations for the detection probabilities are quite accurate when the signal to noise ratio is small, which is often the case in spectrum sensing applications, or when the number of samples is large, which is often the case if reliable detection is to be ensured in multipath fading channels. In particular, when the signal to noise ratio is small, the derived bounds demonstrate that the total approximation error is comparable in size to the error resulting from the use of the central limit theorem to approximate the decision probabilities, and so the derived approximations are comparable in accuracy to the approximations given in Table 4.1 in such situations.

Unfortunately, the derived approximations for the detection probabilities consist of infinite series, which must be truncated for computational purposes. However, it was demonstrated that the number of terms necessary to ensure a given truncation error is independent of both the signal to noise ratio and the number of samples, and only varies with the fading parameter and number of diversity branches. Consequently, for finite K, the truncation error can be made arbitrarily small by increasing the number of terms to be computed. Of course, for large values of K, the number of terms required may become quite large itself, and so there is some motivation to consider alternative methods of approximation suitable for use in such situations.

Finally, while the approximation for the detection probability of energy detectors with EGC diversity is useful in many scenarios of interest, its use is limited to situations where K and n are such that the constants a and b are given by Table 3.5, or can be accurately interpolated or extrapolated from the values therein. While additional values of a and b may be fitted to extend the range of the approximation, the approach is, in general, a limited one as the fading parameter and number of diversity branches are unbounded. If an alternative approximation for the PDF of the signal to noise ratio at

Table 6.1: Numbers of samples required to ensure that the specified decision probabilities are met under the given channel conditions.

X	n	$P_{m_{X,Rice}}$	P_{f_X}	K	$\bar{\gamma}$	M
ND	—	0.05	0.05	0.5	-10 dB	174285
MRC	3	0.001	0.001	1.2	-15 dB	318005
EGC	4	0.005	0.01	2.5	-20 dB	175934
SLC	5	0.001	0.001	3.4	-25 dB	5917287

the EGC output, free from fitted parameters, were available, it may be possible to derive a more generally applicable approximation for the detection probability. However, to the best of the author's knowledge at the time of writing, no such approximations are currently available, and so this may be of interest in future research.

6.2.5.3 Approximations for other system parameters

Using the derived approximations for the detection probabilities, it was possible to infer certain behaviours of system parameters that were not clear from the available exact expressions in Chapter 3. Of most general interest is the fact that, for given decision probabilities, when the number of samples is large and the signal to noise ratio is small, the product of the former with the square of the latter is approximately constant. Interestingly, this is precisely the same behaviour that was observed in the case of AWGN and Nakagami-m channels. Consequently, if the value of the number of samples required to ensure given decision probabilities at a certain signal to noise ratio is known, the number of samples required to ensure the same decision probabilities at a different signal to noise ratio can easily, and accurately, be approximated for each of the diversity architectures and channel types considered. As a corollary, the minimum signal to noise ratio can be similarly approximated, for a given number of samples, if the minimum signal to noise ratio at a different number of samples is known. Figure 6.7 illustrates the power of these approximations given just the data in Table 6.1. As can be seen, the approximation in (5.36) is quite accurate across the entire range of signal to noise ratios, even when the signal to noise ratio is large.

It was also possible to relate the sample complexities of energy detectors with MRC and SLC diversity operating on Rice channels, again under the condition that the number of samples is large and the signal to noise ratio is small. Specifically, it was shown that, if both systems have n diversity branches, then the SLC system requires approximately n times the number of samples than the MRC system in order to ensure the same decision probabilities are met. Again, it is interesting to note that this is the same behaviour that was observed in the case of AWGN and Nakagami-m channels. While similar comparisons can be made between the sample complexities of EGC and MRC and EGC and SLC systems, they are of limited use due to constraints imposed by the

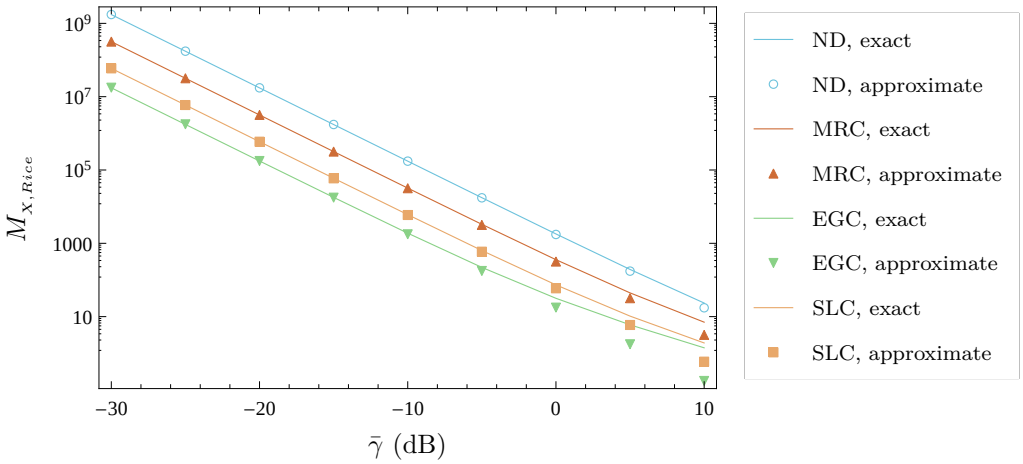

Figure 6.7: A log-log plot of the numbers of samples required to ensure the operating conditions specified in Table 6.1 for the specified diversity types.

use of Hu and Beaulieu's PDF approximation.

6.3 Novel approximations for small signal to noise ratios and large Kn

While the low SNR approximations derived in Section 6.2 provide an accurate and, in many cases of interest, convenient method by which to compute the detection probabilities of energy detector systems operating on Rice channels, they require a larger computational effort to evaluate when the product of the fading parameter and the number of diversity branches, Kn, is large. Thus, there is some motivation to consider alternative approximations, more suited to such situations, in the manner of Section 5.3.

6.3.1 New approximations for the detection probabilities

Using (4.9), it can be shown that the PDF of the noncentral chi square distribution with k degrees of freedom and noncentrality parameter s, $f_{\chi_k^2(s)}(x)$, has the central limit theorem approximation

$$f_{\chi_k^2(s)}(x) = \frac{d}{dx}\left(P[\chi_k^2(s) \leq x]\right) \approx \frac{d}{dx}\left[1 - Q\left(\frac{x-(k+s)}{\sqrt{2(k+2s)}}\right)\right] \triangleq \check{f}_{\chi_k^2(s)}(x), \qquad (6.66)$$

as k becomes large. Simplifying the right hand side of (6.66), it is not difficult to show that the approximate noncentral chi square PDF can be written as

$$\check{f}_{\chi^2_k(s)}(x) = \frac{1}{\sqrt{2\pi}} \frac{1}{\sqrt{2(k+2s)}} \exp\left[-\left(\frac{x-(k+s)}{2\sqrt{k+2s}} \right)^2 \right], \ \forall x. \tag{6.67}$$

Thus, the PDFs of noncentral chi square distributed random variables can be approximated as k becomes large.

Consider the noncentral chi square random variable, Y, which has $2n$ degrees of freedom and noncentrality parameter equal to $\frac{2Kn}{a}$. The probability density function of Y [102, Equation 2.44] can be written as

$$f_{\chi^2_k(s)}(y)\Big|_{k=2n, s=\frac{2Kn}{a}} = \begin{cases} 0, & y < 0, \\ \frac{1}{2} \left(\frac{ay}{2Kn} \right)^{\frac{n-1}{2}} e^{-\frac{Kn}{a} - \frac{y}{2}} I_{n-1}\left(\sqrt{\frac{2Kny}{a}} \right), & y \geq 0. \end{cases} \tag{6.68}$$

Letting $y = \frac{2(K+1)x}{b\bar{\gamma}}$ in (6.68), and scaling appropriately, results in (3.37). Consequently, the PDF of the signal to noise ratio at the equal gain combiner output can be approximated by letting $k = 2n$ and $s = \frac{2Kn}{a}$ in (6.67) and applying a similar transform. Thus, it is not difficult to show that

$$\check{f}_{\chi^2_k(s)}(y)\Big|_{k=2n, s=\frac{2Kn}{a}} = \frac{1}{\sqrt{2\pi}} \frac{1}{2\sqrt{n(1+\frac{2K}{a})}} \exp\left[-\left(\frac{y - 2n(1+\frac{K}{a})}{2\sqrt{2n(1+\frac{2K}{a})}} \right)^2 \right]. \tag{6.69}$$

Letting $y = \frac{2(K+1)x}{b\bar{\gamma}}$ in (6.69), and again scaling the result appropriately, results in $\check{f}_{EGC,Rice}(x)$, given in Table 6.2, where $\hat{f}_{EGC,Rice}(x) \approx \check{f}_{EGC,Rice}(x)$ as n becomes large. Noting that

$$\hat{f}_{EGC,Rice}(x)\Big|_{a=1,b=1} = f_{MRC,Rice}(x) = f_{SLC,Rice}(x), \tag{6.70}$$

and

$$f_{MRC,Rice}(x)\Big|_{n=1} = f_{ND,Rice}(x), \tag{6.71}$$

approximations for the PDFs of the other diversity types can be derived directly from $\check{f}_{EGC,Rice}(x)$ and are also given in Table 6.2.

Using these approximate PDFs, it is possible to derive new approximations for the detection probabilities of each diversity receiver in a similar manner to Section 5.3. For instance, in the EGC case, the probability of detection can be approximated by

X	$\check{f}_{X,Rice}(x)$	$\check{P}_{d_{X,Rice}}$
ND	$\frac{1}{\sqrt{2\pi}}\left(\frac{1}{\left(\frac{\bar{\gamma}}{K+1}\right)\sqrt{2K+1}}\right)\exp\left[-\left(\frac{x-\bar{\gamma}}{\left(\frac{\bar{\gamma}}{K+1}\right)\sqrt{2(2K+1)}}\right)^2\right]$	$Q\left(\frac{\lambda - M(1+\bar{\gamma})}{\sqrt{2M\left(1+\frac{M}{2}\left(\frac{\bar{\gamma}}{K+1}\right)^2(2K+1)\right)}}\right)$
MRC	$\frac{1}{\sqrt{2\pi}}\left(\frac{1}{\left(\frac{\bar{\gamma}}{K+1}\right)\sqrt{n(2K+1)}}\right)\exp\left[-\left(\frac{x-n\bar{\gamma}}{\left(\frac{\bar{\gamma}}{K+1}\right)\sqrt{2n(2K+1)}}\right)^2\right]$	$Q\left(\frac{\lambda - M(1+n\bar{\gamma})}{\sqrt{2M\left(1+\frac{Mn}{2}\left(\frac{\bar{\gamma}}{K+1}\right)^2(2K+1)\right)}}\right)$
EGC	$\frac{1}{\sqrt{2\pi}}\left(\frac{1}{\left(\frac{b\bar{\gamma}}{K+1}\right)\sqrt{n(2K+1)}}\right)\exp\left[-\left(\frac{x-nb\bar{\gamma}\left(\frac{\frac{K}{a}+1}{K+1}\right)}{\left(\frac{b\bar{\gamma}}{K+1}\right)\sqrt{2n(\frac{2K}{a}+1)}}\right)^2\right]$	$Q\left(\frac{\lambda - M\left(1+nb\bar{\gamma}\left(\frac{\frac{K}{a}+1}{K+1}\right)\right)}{\sqrt{2M\left(1+\frac{Mn}{2}\left(\frac{b\bar{\gamma}}{K+1}\right)^2\left(\frac{2K}{a}+1\right)\right)}}\right)$
SLC	$\frac{1}{\sqrt{2\pi}}\left(\frac{1}{\left(\frac{\bar{\gamma}}{K+1}\right)\sqrt{n(2K+1)}}\right)\exp\left[-\left(\frac{x-n\bar{\gamma}}{\left(\frac{\bar{\gamma}}{K+1}\right)\sqrt{2n(2K+1)}}\right)^2\right]$	$Q\left(\frac{\lambda - Mn(1+\bar{\gamma})}{\sqrt{2Mn\left(1+\frac{M}{2}\left(\frac{\bar{\gamma}}{K+1}\right)^2(2K+1)\right)}}\right)$

Table 6.2: Large Kn approximations for energy detector systems operating on Rice channels.

substituting (5.6) and $\check{f}_{EGC,Rice}(x)$ into (5.1) to give

$$\begin{aligned}\check{P}_{d_{EGC,Rice}} &= \frac{1}{\sqrt{2\pi}}\left(\frac{1}{\left(\frac{b\bar{\gamma}}{K+1}\right)\sqrt{n(\frac{2K}{a}+1)}}\right) \\ &\quad\times\int_{-\infty}^{\infty} Q\left(\frac{\lambda - M(1+x)}{\sqrt{2M}}\right)\exp\left[-\left(\frac{x - nb\bar{\gamma}\left(\frac{\frac{K}{a}+1}{K+1}\right)}{\left(\frac{b\bar{\gamma}}{K+1}\right)\sqrt{2n(\frac{2K}{a}+1)}}\right)^2\right]dx. \\ &= Q\left(\frac{\lambda - M\left(1+nb\bar{\gamma}\left(\frac{\frac{K}{a}+1}{K+1}\right)\right)}{\sqrt{2M\left(1+\frac{Mn}{2}\left(\frac{b\bar{\gamma}}{K+1}\right)^2\left(\frac{2K}{a}+1\right)\right)}}\right), \end{aligned} \tag{6.72}$$

where the result follows from an application of Lemma 5.4. Expressions for the detection probabilities of the other diversity types can be derived similarly, and a complete listing in given in Table 6.2.

The error resulting from the use of these approximations can be written as

$$\begin{aligned} P_{X,Rice} - \check{P}_{d_{X,Rice}} &= P_{X,Rice} - \hat{P}_{X,Rice} + \hat{P}_{X,Rice} - \check{P}_{d_{X,Rice}} \\ &= \epsilon_{tot,X,Rice} + \epsilon_{Kn,X}, \end{aligned} \tag{6.73}$$

where $\epsilon_{Kn,X} = \hat{P}_{X,Rice} - \check{P}_{d_{X,Rice}}$ and represents the additional error, with respect to the low SNR approximations, resulting from the use of the approximations in Table 6.2. Using the second mean value theorem for infinite integrals [69, Equation 12.114], $\epsilon_{Kn,X}$ can be expanded as

$$\begin{aligned} \epsilon_{Kn,X} &= \int_{-\infty}^{\infty} \tilde{P}_{d_X}(x)\left(f_{X,Rice}(x) - \check{f}_{X,Rice}(x)\right)dx \\ &= \int_{\xi}^{\infty}\left(f_{X,Rice}(x) - \check{f}_{X,Rice}(x)\right)dx \\ \implies \max|\epsilon_{Kn,X}| &= \max_{\xi}\left|\int_{\xi}^{\infty}\left(f_{X,Rice}(x) - \check{f}_{X,Rice}(x)\right)dx\right|, \end{aligned} \tag{6.74}$$

for some $-\infty \leq \xi \leq \infty$. As the PDFs of the signal to noise ratio for each diversity type follow a noncentral chi square distribution, (6.74) can be further simplified using Theorem 4.1. Given that the distribution has two degrees of freedom in the no diversity case, and $2n$ degrees of freedom otherwise,

$$\max|\epsilon_{Kn,X}| = \max\left(Q\left(\sqrt{n}\right), \epsilon_{\infty}(2n)\right), \tag{6.75}$$

where $n = 1$ in the no diversity case. However, the bounds defined by (6.75) are problematic as they are constant with respect to K and, therefore, cannot be used to

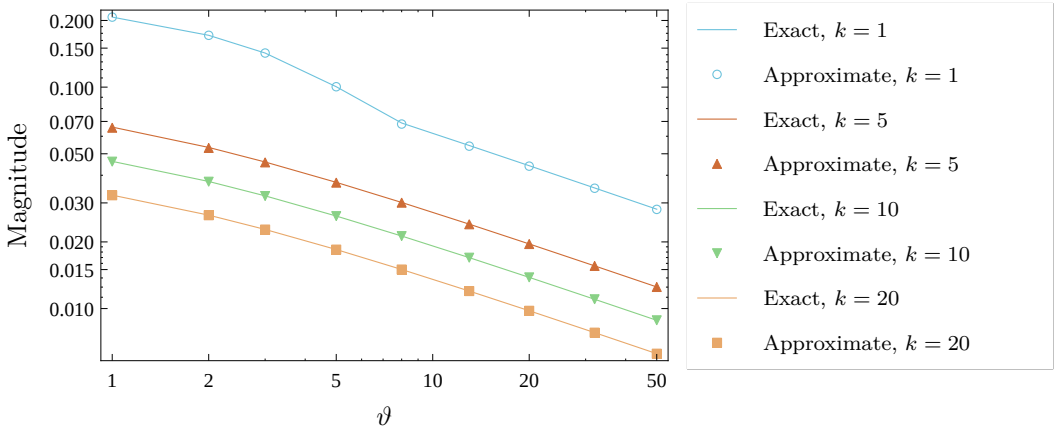

Figure 6.8: A log-log plot of $\max_x |\epsilon_{CLT}(k, k\vartheta, x)|$ and the bound given in Theorem 6.1 for different values of k.

demonstrate that $\max |\epsilon_{Kn,X}|$ decreases as K becomes larger.

While this is an inconvenient result, the problem is by no means intractable. Theorem 4.1 provides a bound which is a function of the number of degrees of freedom only. Instead, a bound which is a function of the noncentrality parameter is required. This can be realised through the use of Theorem 6.1, which is stated below and proved in Appendix A.6.

> **Theorem 6.1:** For the central limit theorem approximation in (4.9), if the number of degrees of freedom is finite, and the noncentrality parameter is related to the number of degrees of freedom as $s = k\vartheta$, where $\vartheta \in \mathbb{R}^+$, then the maximum absolute error resulting from the use of the approximation, with respect to the location parameter only, $\max_x |\epsilon_{CLT}(k, k\vartheta, x)|$, is given by
>
> $$\max_x |\epsilon_{CLT}(k, k\vartheta, x)| = \max\left(Q\left(\frac{k(1+\vartheta)}{\sqrt{2k(1+2\vartheta)}}\right), \epsilon_{\infty,\vartheta}(k)\right), \tag{6.76}$$
>
> where
>
> $$\epsilon_{\infty,\vartheta}(k, \vartheta) \approx Q_{\frac{k}{2}}\left(\sqrt{k\vartheta}, \sqrt{k(1+\vartheta)}\right) - \frac{1}{2}, \tag{6.77}$$
>
> as ϑ becomes large.

The bound given in Theorem 6.1 is illustrated in Figure 6.8, along with the actual maximum error, which has been calculated numerically. As can be seen, in each case, the derived bound describes the value of the actual error very well. Consequently, Theorem 6.1 can be used to derive new bounds for $|\epsilon_{Kn,X}|$.

Using the values of k and s given in Section 3.3, and noting that the noncentrality

parameter has the form $s = k\vartheta$, where ϑ is independent of k, in each case, it is not difficult to show that

$$\max|\epsilon_{Kn,ND}| = \max\left(Q\left(\frac{1+K}{\sqrt{1+2K}}\right), \epsilon_{\infty,\vartheta}(2,K)\right), \tag{6.78}$$

$$\max|\epsilon_{Kn,MRC}| = \max|\epsilon_{Kn,SLC}| = \max\left(Q\left(\frac{n(1+K)}{\sqrt{n(1+2K)}}\right), \epsilon_{\infty,\vartheta}(2n,K)\right), \tag{6.79}$$

$$\max|\epsilon_{Kn,EGC}| = \max\left(Q\left(\frac{n(1+\frac{K}{a})}{\sqrt{n(1+\frac{2K}{a})}}\right), \epsilon_{\infty,\vartheta}\left(2n,\frac{K}{a}\right)\right). \tag{6.80}$$

Using these new bounds, it is possible to demonstrate that the value of the error decreases with increasing values of both K and n. Figure 6.9(a) illustrates the exact and approximate detection probabilities in some typical scenarios. As can be seen, while the approximations are not accurate for small values of K (e.g. $K \leq 10$), they become increasingly accurate as K becomes larger, a property which is demonstrated quite well by the derived error bounds, as can be seen in Figure 6.9(b).

Unfortunately, the approximation for the detection probability of EGC receivers given in Table 6.2 is of limited use as the values of a and b are defined for $K \in \{1\,\text{dB}, 3\,\text{dB}, 5\,\text{dB}, 7\,\text{dB}\}$ and $n \in [2,8]$ only. One solution would be to extend Hu and Beaulieu's approximation for larger values of K and n, but again the approach is a limited one as K is unbounded and so any useful look up table would be very large and, also, incomplete. Therefore, a preferable solution would be the development of an exact PDF or, at the very least, an approximation free from fitted parameters. However, it is known that the problem is a difficult one [70, 71, 73]. Nevertheless, it may be of interest in future research.

6.3.2 Novel approximations for other system parameters

6.3.2.1 Sample complexity

Using a similar method to that in Section 4.4.1, it is not difficult to verify that the approximations given in Table 6.3 are accurate when either the signal to noise ratio is low or the number of samples is large and when the fading parameter and number of nodes are large. Figure 6.10 illustrates a typical use case for these. As can be seen, the exact sample complexities of MRC and SLC receivers operating on Rice channels can be approximated quite well as n becomes larger (in this case, for $n \geq 4$), without the use of numerical methods.

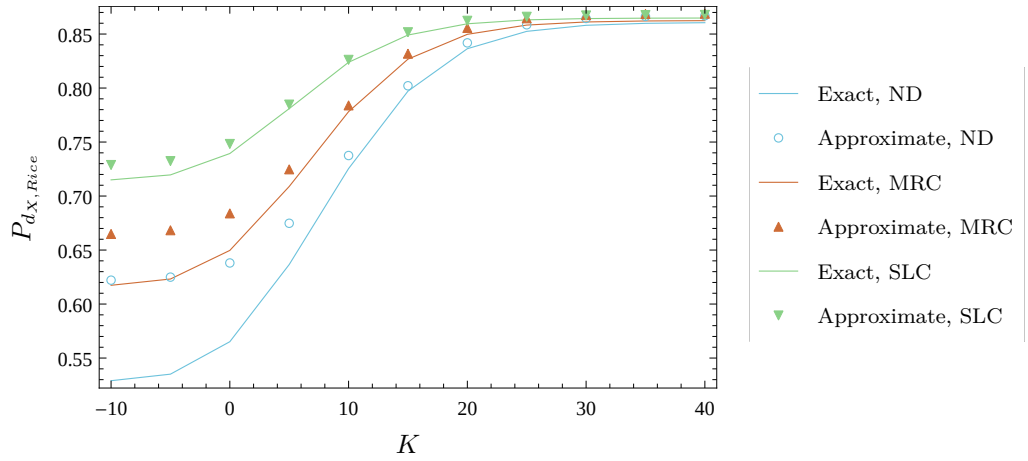

(a) A plot of the exact and approximate (large Kn) probabilities of detection.

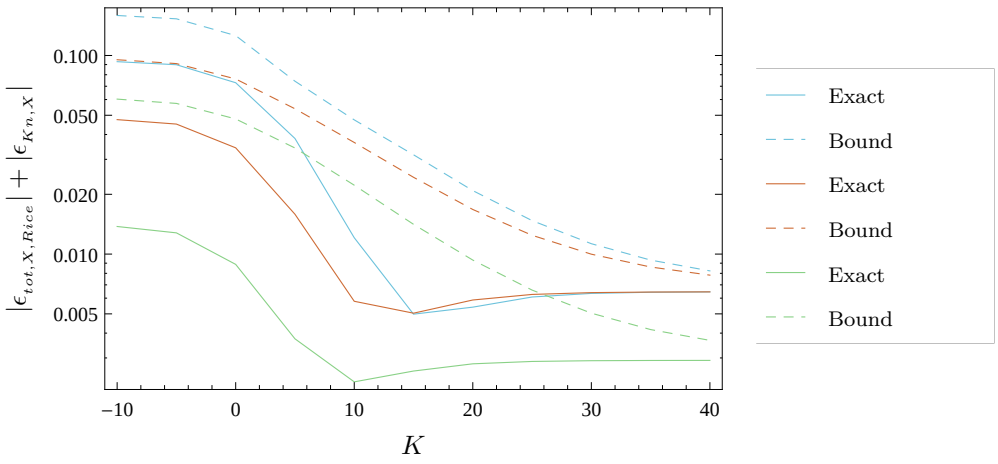

(b) A log-linear plot of the total approximation error, and its bound, for the trends shown in Figure 6.9(a).

Figure 6.9: Plots of the exact and approximate probabilities of detection, and the resulting approximation errors, for energy detectors operating on Rice channels. The blue trends correspond to an energy detector with no diversity operating on a channel with $\bar{\gamma} = -14\,\text{dB}$; the red trends to an energy detector with two branch MRC diversity operating on a channel with $\bar{\gamma} = -17\,\text{dB}$; while the green trends correspond to an energy detector with five branch SLC diversity operating on a channel with $\bar{\gamma} = -17.5\,\text{dB}$. In each case, $M = 10000$, $P_{f_X} = 0.01$ and N is such that $\max|\epsilon_{tr,X}| = 10^{-6}$.

6.3.2.2 Minimum signal to noise ratio

Closed form approximations for the minimum signal to noise ratio can be derived directly from the expressions in Table 6.3 by noting that $\check{M}_{X,Rice}$ is inversely proportional to $\bar{\gamma}^2$ in each case. For instance, for receivers with SLC diversity, it can be shown that

$$\bar{\gamma}_{SLC,Rice} \approx \sqrt{\frac{2}{Mn}} \left(\frac{Q^{-1}\left(\hat{P}_{f_{SLC}}\right) - \sqrt{1 + \frac{Q^{-1}\left(\hat{P}_{f_{SLC}}\right)^2 - Q^{-1}\left(\check{P}_{d_{SLC,Rice}}\right)^2}{\frac{n(K+1)^2}{2K+1}}} Q^{-1}\left(\check{P}_{d_{SLC,Rice}}\right)}{\left(1 - \frac{Q^{-1}\left(\check{P}_{d_{SLC,Rice}}\right)^2}{\frac{n(K+1)^2}{2K+1}}\right)} \right). \quad (6.81)$$

Similar approximations can be shown to hold for the other diversity types.

6.3.2.3 Diversity gain

Finally, using the expressions in Table 6.3, closed form approximations can also be derived for the diversity gain. However, as the number of branches in EGC systems and MRC systems is typically small, and the approximations in Table 6.3 are valid for large Kn only, the diversity gain of SLC systems is likely to be of practical interest. It is not difficult to show that

$$\check{n}_{SLC,Nak} = \left\lceil \frac{2}{M} \left(\frac{Q^{-1}(\hat{P}_{f_{SLC}}) - \sqrt{1 + \frac{M\bar{\gamma}^2}{\frac{2(K+1)^2}{2K+1}}} Q^{-1}(\check{P}_{d_{SLC,Nak}})}{\bar{\gamma}} \right)^2 \right\rceil, \quad (6.82)$$

where the ceiling function has been used to ensure that the resulting number of nodes is always sufficiently large so that the conditions specified in the right hand side of (6.82) are met.

In a similar manner to (5.96), (6.82) can be used to accurately approximate the diversity gain in many situations of interest. Figure 6.11 illustrates the exact (calculated numerically) and approximate (evaluated directly using (6.82)) number of nodes required to achieve the given probability of detection in a typical sensing scenario. As can be seen, the approximation is quite accurate over the entire range of detection probabilities.

6.3.3 Discussion

The closed form approximations derived in this section enable the fast and accurate evaluation of the detection probabilities of energy detector systems in scenarios where the low SNR series of approximations, derived in Section 6.2, require large numbers of terms to be computed. Consequently, their region of applicability, though limited, naturally complements the region of applicability of the low SNR approximations.

Table 6.3: Large mn approximations for the sample complexity of energy detectors operating on Rice channels.

X	$\check{M}_{X,Rice}$
ND	$2\left(\frac{Q^{-1}\left(\hat{P}_{f_{ND}}\right)-\sqrt{1+\frac{Q^{-1}\left(\hat{P}_{f_{ND}}\right)^2-Q^{-1}\left(\check{P}_{d_{ND,Rice}}\right)^2}{\frac{(K+1)^2}{2K+1}}}Q^{-1}\left(\check{P}_{d_{ND,Rice}}\right)}{\bar{\gamma}\left(1-\frac{Q^{-1}\left(\check{P}_{d_{ND,Rice}}\right)^2}{\frac{(K+1)^2}{2K+1}}\right)}\right)^2$
MRC	$\frac{2}{n^2}\left(\frac{Q^{-1}\left(\hat{P}_{f_{MRC}}\right)-\sqrt{1+\frac{Q^{-1}\left(\hat{P}_{f_{MRC}}\right)^2-Q^{-1}\left(\check{P}_{d_{MRC,Rice}}\right)^2}{\frac{n(K+1)^2}{2K+1}}}Q^{-1}\left(\check{P}_{d_{MRC,Rice}}\right)}{\bar{\gamma}\left(1-\frac{Q^{-1}\left(\check{P}_{d_{MRC,Rice}}\right)^2}{\frac{n(K+1)^2}{2K+1}}\right)}\right)^2$
EGC	$2\left(\frac{Q^{-1}\left(\hat{P}_{f_{EGC}}\right)-\sqrt{1+\frac{Q^{-1}\left(\hat{P}_{f_{EGC}}\right)^2-Q^{-1}\left(\check{P}_{d_{EGC,Rice}}\right)^2}{\frac{n\left(\frac{K}{a}+1\right)^2}{2K+1}}}Q^{-1}\left(\check{P}_{d_{EGC,Rice}}\right)}{b\left(\frac{\frac{K}{a}+1}{K+1}\right)\bar{\gamma}\left(1-\frac{Q^{-1}\left(\check{P}_{d_{EGC,Rice}}\right)^2}{\frac{n\left(\frac{K}{a}+1\right)^2}{2K+1}}\right)}\right)^2$
SLC	$\frac{2}{n}\left(\frac{Q^{-1}\left(\hat{P}_{f_{SLC}}\right)-\sqrt{1+\frac{Q^{-1}\left(\hat{P}_{f_{SLC}}\right)^2-Q^{-1}\left(\check{P}_{d_{SLC,Rice}}\right)^2}{\frac{n(K+1)^2}{2K+1}}}Q^{-1}\left(\check{P}_{d_{SLC,Rice}}\right)}{\bar{\gamma}\left(1-\frac{Q^{-1}\left(\check{P}_{d_{SLC,Rice}}\right)^2}{\frac{n(K+1)^2}{2K+1}}\right)}\right)^2$

The simple forms of the large Kn approximations enabled the derivation of further closed form approximations for certain system parameters of interest, such as sample complexity, minimum signal to noise ratio and diversity gain. Again, these approximations are valid for large Kn only, but in such situations allow the use of numerical methods to be avoided. As in the Nakagami-m case, these approximations are likely to be of much more use in the analysis of SLC diversity systems, where the number of diversity branches may be large, than for systems with no diversity, where there is just one diversity branch, or EGC or MRC diversity, where the number of diversity branches is typically small. In particular, in the case of cooperative spectrum sensing, where SLC diversity can be used to describe the operation of cooperative systems with uncompressed decisions, the derived approximations could save a large computational effort, if the size of the network is large.

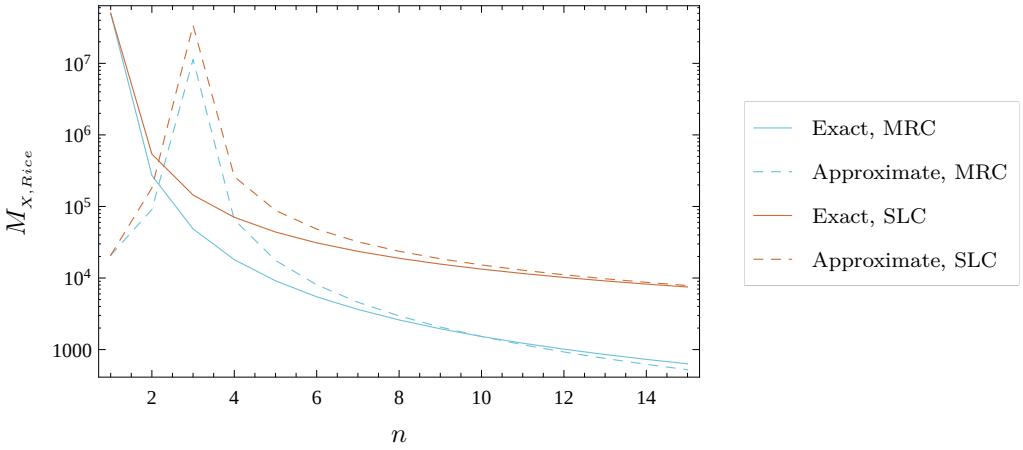

Figure 6.10: A log plot of the sample complexities of MRC and SLC receivers operating on Rice channels with $K = 5$ and $\bar{\gamma} = -15\,\text{dB}$. In both cases, $P_f = 0.001$ and $P_m = 0.001$.

Finally, in deriving the large Kn approximations, it was necessary to derive a bound on the error resulting from the use of the central limit theorem approximation for noncentral chi square random variables, which is described in Theorem 6.1. To the best of the author's knowledge at the time of writing, this result is novel and, as it is quite generally applicable, it is likely to have further uses beyond the analysis of energy detection.

6.4 Summary

At the beginning of this chapter, several goals were listed, namely: to derive accurate and computationally inexpensive approximations for the detection probabilities of energy detector systems operating on Rice channels; to derive bounds for the errors resulting from these approximations, so that their regions of applicability are well defined; and finally, to derive further approximations for other system parameters of interest, such as sample complexity, minimum signal to noise ratio and diversity gain.

As the low SNR approximation approach worked well in the analysis of Nakagami-m channels, its use was extended for the case of Rice channels. While this resulted in infinite series based approximations for the detection probabilities in each case, it was possible to show that these series could be truncated with a very small loss in accuracy when the product of the fading parameter and the number of diversity branches, Kn, was small to moderate. Furthermore, unlike the low SNR approximations in Chapter 5, which are valid for $m \in \mathbb{N}^+$ only, the approximations derived in this chapter are valid for $K \in \mathbb{R}_0^+$. Consequently, in many practical scenarios of interest, if the resulting approximation error is acceptable, the use of the low SNR approximations is preferable to the exact methods given in Chapter 3 as the computational effort required to eval-

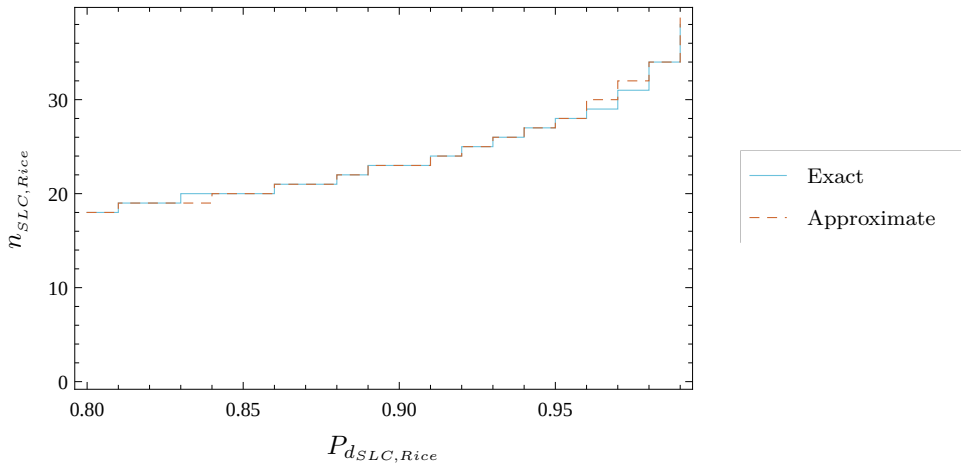

Figure 6.11: Exact (calculated numerically) and approximate (calculated using (6.82)) number of nodes required to ensure the given probabilities of detection in a centralised cooperative network operating on a Rice channel, with $K = 1$, $\bar{\gamma} = -20\,\text{dB}$, $P_{f_{SLC}} = 10^{-3}$ and $M = 20000$.

uate them is, in general, smaller. When Kn is very large, it is possible that the low SNR approximations may involve greater computational effort than the exact methods. However, in such circumstances, the large Kn series of approximations can be used instead, as the additional error is likely to be very small. Consequently, in many situations of interest, the derived approximations can be used to reduce the computational effort involved in evaluating the exact values of the detection probabilities, with a very small decrease in accuracy.

Approximations for the detection probability of energy detectors with EGC diversity were also derived. To the best of the author's knowledge at the time of writing, these are the only methods by which numerical evaluation of the detection probability can be avoided. However, their regions of applicability are limited by the their dependence on fitted parameters, which are defined only for a small number of scenarios. While it is possible to fit additional parameters, and therefore extend the regions of applicability of the approximations, the approach is, in general, a limited one as the fitted parameters depend upon the fading parameter, which is unbounded. A preferable solution would be the development of an exact PDF for the signal to noise ratio at the equal gain combiner output, although this has thus far eluded discovery. Therefore, a more fruitful line of inquiry may be the derivation of an approximate PDF, free from fitted parameters, and accurate across the entire range of values of K and n. While this lies beyond the scope of the work in this thesis, it may be of interest in future research.

Using the lemmas given in Chapter 5, it was not difficult to derive simple bounds on the errors resulting from the use of the detection probability approximations. However, in some cases, some additional effort was required. In particular, the use of Jensen's inequality enabled the derivation of a simple closed form expression for the maximum

error resulting from the use of the low SNR approximation, while it was necessary to derive a further bound on the error resulting from the use of central limit theorem approximations to the noncentral chi square distribution (recall Theorem 6.1) in order to verify the accuracy of the large Kn approximation. Using these error bounds, it was possible to verify the accuracy of the derived approximations in many cases of interest. Consequently, it was possible to verify that the product of the number of samples and the square of the signal to noise ratio is approximately constant for each diversity type, under the constraint that either the signal to noise ratio is low or that the number of samples is large. Under the further constraint that Kn is large, it was possible to derive closed form approximations for the sample complexity and diversity gain of energy detector systems. An approximation for the diversity gain of SLC systems was also derived, under similar constraints.

The application of approximations has simplified the analysis of energy detector systems operating on Rice channels quite significantly. Where, previously, computationally intensive expressions had to be evaluated, there are now simple and accurate alternatives. Similarly, in certain cases where numerical methods had to be relied upon (in the calculation of sample complexity, for example), it is now possible to directly compute the desired result.

Chapter 7

Conclusions and future work

7.1 Summary of contributions

The aim of this thesis was to explore the use of approximations in the analysis of energy detector systems, with a view to reducing the complexity involved in evaluating their performance, specifically in relation to their potential use as spectrum sensing devices. Four different hardware architectures were considered, consisting of single antenna systems — that is, those with no diversity — and multiple antenna systems, with MRC, EGC and SLC diversity. The operation of these systems was considered for four different channel types — AWGN, Rayleigh, Nakagami-m and Rice — which are of most widespread use in the literature. While previous research had uncovered exact expressions describing the operation of energy detector systems in some of these scenarios, the use of such formulae can be problematic due to the large number of computations required to achieve acceptably small truncation errors when the number of samples is large, which is often the case in spectrum sensing scenarios or when reliable detection is to be ensured. To this end, a number of specific contributions were made:

1. Inspired by Urkowitz's approximations for the decision probabilities of energy detectors with no diversity operating on AWGN channels, simple, novel, closed form approximations were derived for the decision probabilities of energy detectors with diversity reception operating on AWGN channels.

   The approximations are based on the Gaussian Q function, and so evaluation of the regularised incomplete gamma function, which is known to be more difficult to compute, and the Marcum Q_m function, which is known to be difficult to compute in general, can be avoided. Furthermore, as the Gaussian Q function is a univariate function, while the regularised incomplete gamma function is a bivariate function and the Marcum Q_m function is a trivariate function, the derived approximations are also attractive from an implementation perspective, requiring a much smaller look up table than available exact methods.

Error bounds were provided for the approximations (including Urkowitz's original approximations), so that the region of applicability of each is clearly defined. The bounds are tight, simple to compute, and demonstrate that the derived approximations are particularly suited to the analysis of spectrum sensing systems, as the error resulting from their use is inversely proportional to the square root of the number of samples, which is usually large in such scenarios. Consequently, the widespread use of Urkowitz's approximations in the literature [10, 13, 19–21, 43, 46, 64–67, 89–97] can be validated for specific numbers of samples, and clear guidelines for their future use have been established.

2. Novel, closed form approximations for the detection probabilities of energy detector systems operating on Rayleigh and Nakagami-m channels were derived, enabling the fast and accurate computation of the detection probabilities in many situations of interest, and particularly in spectrum sensing scenarios. The approximations offer an attractive alternative to the existing exact methods, which are not in a closed form, requiring the truncation of infinite series for their computation. In particular, the approximation for the detection probability of energy detectors with EGC diversity is, to the best of the author's knowledge at the time of writing, the only method by which this quantity can be computed without the use of complicated numerical methods when the number of diversity branches is greater than two.

   In each case, the approximations consist of a summation of a finite number of weighted repeated integrals of the complementary error function. As the number of terms involved in the summation operation is equal to the product of the fading parameter and the number of diversity branches, mn, and the repeated integral of the complementary error function can be computed using a simple recurrence relation (recall (5.13)), the approximations are simple to compute in a wide variety of scenarios.

   Again, bounds were provided in order to quantify the error resulting from the use of the approximations, so that the region of applicability of each is clearly defined. The bounds are tight, simple to compute and demonstrate that the derived approximations are well suited to the analysis of spectrum sensing, as the resulting error is proportional to the signal to noise ratio, which is often small in such scenarios, and inversely proportional to the square root of the number of samples, which is often large. The bounds can also be applied to quantify the error resulting from similar approximations in the literature [65–67, 95–97].

3. Novel approximations for the detection probabilities of energy detector systems operating on Rice channels were derived. These approximations enable the fast and accurate calculation of the detection probabilities in many situations of interest, particularly in spectrum sensing scenarios, where the existing exact methods

become difficult to compute. To the best of the author's knowledge at the time of writing, the approximation for the detection probability of energy detectors with EGC diversity, though of limited applicability, is the only method by which this quantity can be computed without the use of numerical integration.

In each case, the approximations consist of a summation of weighted repeated integrals of the complementary error function. As the summations involve infinitely many terms, truncations must be applied in order to compute the values of the detection probabilities. However, it was demonstrated that the number of terms required to ensure a given truncation error is independent of the number of samples, signal to noise ratio and values of the decision probabilities, and depends only on the product of the fading parameter and the number of diversity branches, Kn. Consequently, the derived approximations often require fewer computations than existing exact expressions, which also consist of infinite series, but require an increasing number of terms to be evaluated as the number of samples becomes large.

Once again, bounds were provided so that the error resulting from the use of the approximations can easily be quantified and so that the region of applicability of each is readily apparent. These bounds are tight, simple to compute and demonstrate that the error is proportional to the signal to noise ratio and inversely proportional to the square root of the number of samples, making the approximations particularly appropriate for use in spectrum sensing type applications.

4. Novel approximations for the detection probabilities of energy detector systems operating on Rayleigh, Nakagami-m and Rice channels were also derived for the scenarios where the product of the fading parameter and the number of diversity branches is large. These approximations are less generally applicable than the low SNR series of approximations, but naturally complement their region of applicability. Again, simple bounds for the error resulting from the use of these approximations were derived, so that their regions of applicability are well defined.

5. Several novel approximations for other system parameters were also derived. Perhaps the most generally applicable of these is the fact that, for given energy detector system (ND, MRC, EGC or SLC) operating on a given channel model (AWGN, Rayleigh, Nakagami-m or Rice) ensuring certain target decision probabilities, the product of the number of samples and the square of the signal to noise ratio is approximately constant, either when the former quantity is large or the latter is small. Thus, if the number of samples required to ensure target decision probabilities in a given channel type at a specific signal to noise ratio is known, the number of samples required to ensure the same decision probabilities at a different signal to noise ratio, given the same channel conditions, can easily

be calculated. This enables the fast and accurate approximation of the sample complexity for a given minimum signal to noise ratio based on prior knowledge of the sample complexity for a different minimum signal to noise ratio and vice versa (recall Figure 6.7).

Additionally, approximations for the sample complexity, minimum signal to noise ratio and diversity gain of energy detectors operating on AWGN channels were derived. An expression describing the effect of altering the number of branches on the detection probability for an energy detector with MRC operating on Rayleigh or Nakagami-m channels was also derived, and interesting and useful comparisons between the sample complexities and receiver sensitivities of energy detectors with MRC, EGC and SLC diversity, in the case of Nakagami-m channels, and energy detectors with MRC and SLC diversity, in the case of Rice channels, were made.

Further approximations for the sample complexity, minimum signal to noise ratio and diversity gain of energy detectors operating on Rayleigh, Nakagami-m and Rice channels were also derived, under the constraint that the product of the fading parameter and the number of diversity branches is large.

In addition, a number of more general contributions were made:

1. A novel bound on the error resulting from the application of the central limit theorem to chi square, noncentral chi square and gamma distributed random variables was derived. The bound describes the maximum distance between the cumulative distribution functions of the given distributions and their normal approximations, is in a simple, closed form and is much tighter than existing Berry-Esseen type bounds.

2. A novel alternative bound on the error resulting from the application of the central limit theorem to noncentral chi square random variables, where the noncentrality parameter is a multiple of the number of degrees of freedom, was derived. This bound describes the maximum distance between the cumulative distribution functions of the noncentral chi square and normal distributions and is in a relatively simple, closed form.

7.2 Recommendations for future work

The work in this thesis has the potential to be extended in a number of ways:

1. The low SNR series of approximations for energy detector systems operating on Nakagami-m channels are only valid where $mn \in \mathbb{N}^+$. As these approximations are quite useful, one obvious generalisation is to the case where $mn \in \mathbb{R}^+$. However, this would require an alternative integral identity to Lemma 5.1, which may lead to more complicated, albeit general, forms.

2. The derivation of an approximation for the PDF of the sum of i.i.d. Rice distributed random variables, free from fitted parameters, would not only enable the derivation of more generally applicable approximations describing the behaviour of energy detectors with EGC diversity operating on Rice faded channels, but also facilitate the more general analysis of EGC diversity in Rice channels (the calculation of outage probability, for instance). To the best of the author's knowledge at the time of writing, only approximations which rely on fitted parameters are available in the literature. However, an approach similar to Nakagami's approximation for the distribution of a sum of i.i.d. Nakagami-m distributed random variables may yield some success.

3. The derivation of exact closed form PDFs for sums of i.i.d. Rayleigh, Nakagami-m and Rice random variables would enable the tractable analysis of EGC diversity in the context of energy detection and also in the broader context of digital communications. Approaches in recent years have yielded some interesting but verbose results, which are not attractive from a computational perspective, and so do not facilitate tractable analysis in general. However, these are likely to be difficult problems.

4. One of the primary assumptions made in this work is that the noise uncertainty problem can be overcome via noise power estimation techniques. While this may be a valid assumption in many cases, an extension of the derived approximations to include its effects will yield a more generally applicable model. López-Benítez and Casadevall [103] have already considered low SNR type approximations for the case of uniformly distributed noise power uncertainty, to which the error bounds given in Theorem 4.1 and Lemmas 5.2 and 5.3 could be applied, but their model does not account for the noise power estimation technique proposed by Mariani et al. [43], and so some further analytical work would be required in order to produce a satisfactorily general model.

5. A further assumption made in this work is that the received signals on each diversity branch are independent, identically distributed and uncorrelated. Again, while this assumption is valid in many cases (recall that, in many cases, the effects of correlation can be mitigated through appropriate antenna spacing), it is not true in general, and the extension of the approximation approach to include its effects may yield interesting and useful new results. Furthermore, as the exact formulations available in the literature suffer from similar drawbacks to those discussed in Section 3.3, there is some motivation to consider such an approach.

   For instance, Banjade et al. [63] derived exact expressions for energy detectors with SLC diversity operating on Nakagami-m channels. However, their approach is similar to that of Herath et al., and so their results also require the evaluation of high order derivatives, which may not be practical in many circumstances.

Similarly, Annamalai et al. [57] considered the effects of independent and non-identically distributed Nakagami-m fading for energy detectors with MRC and SLC diversity, but again their results consist of complicated infinite series, which must be truncated in order to be computed.

Using the expression for the PDF of the sum of gamma random variables derived by Ansari et al. [104], it should be possible to extend the low SNR series of approximations derived here to the cases of i.n.d. and correlated Nakagami-m fading. While the PDF derived by Ansari et al. depends on the Meijer G function, which is difficult to evaluate in general, it can be manipulated into a significantly simpler form in the case of i.n.d. Rayleigh fading [104, Equation 13], which allows a direct application of Lemma 5.1. The resulting expression consists of a series with n terms, each term being a weighted repeated integral of the complementary error function, and so should be significantly easier to evaluate than the existing exact methods. Some additional work would be required in order to extend the analysis to the case of correlated Rayleigh fading (Ansari et al. outline how this can be done), and further work again for the cases of i.n.d. and correlated Nakagami-m fading, but the approach appears promising. Moschopoulos [105] and Alouini et al. [106] also consider sums of i.n.d. and correlated gamma random variables, respectively, although their formulations depend on infinite series, and so may cause any resulting approximation to be difficult to evaluate.

6. The methods developed during the course of this work could also be applied to simplify the analysis of energy detection under various other channel models, such as the log-normal shadow fading channel, the Weibull fading channel or composite multipath / shadowing models, which are more appropriate for use in certain circumstances than the Rayleigh, Nakagami-m or Rice channel models [14, p. 19–34]. More general models, such as the generalised κ-μ [107] or α-μ [108] models may also be of interest.

   As the theorems and lemmas derived in the course of this work are general (for instance, Lemma 5.3 can be applied to any signal to noise ratio distribution), the extension of the low SNR approximations to other channel models should not prove too difficult, although some alteration of the integral identity in Lemma 5.1 will be required to account for the variations in the formulations of the PDFs involved.

7.3 Concluding remarks

If Rosenblueth and Wiener's assertion is correct — that no substantial part of the universe is so simple that it can be understood without abstraction — then the use of approximations in the modelling of any physical process is a necessity, if a deep

level of understanding is to be attained. However, without defining their regions of applicability, approximations cannot be relied upon in general. In this thesis, these ideas were applied directly to the analysis of energy detector systems, and the results have been fruitful: where complication once existed, there is now simplicity or, at the very least, a reduced level of complication; however, every effort has been made to ensure that, where abstractions have been used, the resulting loss in broad detail has only served to focus on finer details which had, until now, been obscure. The trade off between abstraction and generality is perhaps best summed up by Box and Draper, who wrote that *all models are wrong, but some are useful*. It is hoped that the methodology followed throughout the course of this work has been faithful to this proposition.

Appendix A

Proofs of theorems and lemmas

A.1 Proof of Theorem 4.1

From (4.11), it can be seen that the error resulting from the use of the central limit theorem has differing representations[1] for $x \leq 0$ than for $x > 0$. Therefore, the maximum value of $|\epsilon_{CLT}(k, s, x)|$, with respect to s and x, is given by

$$\max_{s,x} |\epsilon_{CLT}(k, s, x)| = \max \left(\max_{s,x \leq 0} |\epsilon_{CLT}(k, s, x)|, \max_{s,x>0} |\epsilon_{CLT}(k, s, x)| \right). \tag{A.1}$$

Thus, in order to bound the maximum error $\forall\ x$, the maximum values for $x \leq 0$ and $x > 0$ must be determined individually.

Maximum value for $x \leq 0$

Using (4.11), it can be shown that

$$\begin{aligned} \max_{s,x \leq 0} |\epsilon_{CLT}(k, s, x)| &= \max_{s,x \leq 0} \left| 1 - Q\left(\frac{x - (k+s)}{\sqrt{2(k+2s)}} \right) \right| \\ &= \max_{s,x \leq 0} \left[1 - Q\left(\frac{x - (k+s)}{\sqrt{2(k+2s)}} \right) \right], \end{aligned} \tag{A.2}$$

where the simplification comes from the fact that, by definition, $Q(z) \leq 1\ \forall\ z$.

As the Gaussian Q function is a monotonically decreasing function, and x is constrained to be less than or equal to zero, the maximisation of (A.2) with respect to x is satisfied

[1] Again, it should be noted that, in practice, x is never less than zero. The special treatment of this case here is purely for mathematical completeness.

when $x = 0$, and so

$$\begin{aligned}\max_{s,x\leq 0} |\epsilon_{CLT}(k,s,x)| &= \max_{s}\left[1 - Q\left(\frac{-k-s}{\sqrt{2(k+2s)}}\right)\right] \\ &= \max_{s}\left[Q\left(\frac{k+s}{\sqrt{2(k+2s)}}\right)\right]. \end{aligned} \tag{A.3}$$

Similarly, because the Gaussian Q function is a monotonically decreasing function, the maximisation with respect to s in (A.3) is equivalent to the minimisation of the argument to the Q function, that is

$$\max_{s}\left[Q\left(\frac{k+s}{\sqrt{2(k+2s)}}\right)\right] = Q\left[\min_{s}\left(\frac{k+s}{\sqrt{2(k+2s)}}\right)\right]. \tag{A.4}$$

It can easily be shown that $\frac{k+s}{\sqrt{2(k+2s)}}$ is minimised when $s = 0$, and so

$$\max_{s,x\leq 0} |\epsilon_{CLT}(k,s,x)| = Q\left(\sqrt{\tfrac{k}{2}}\right). \tag{A.5}$$

Maximum value for $x > 0$

While the maximisation of $|\epsilon_{CLT}(k,s,x)|$ is quite simple when $x \leq 0$, it becomes significantly more complicated when $x > 0$ as the Marcum Q_m function must be used to represent the complementary CDF of the noncentral chi square distribution. For a given value of k, the critical points of $\epsilon_{CLT}(k,s,x)$, (s_0, x_0), may be found using the first partial derivative test [68, Equation 1.5.19], that is

$$\frac{\delta}{\delta s}\left[\epsilon_{CLT}(k,s,x)\right]\Big|_{s=s_0,x=x_0} = 0, \tag{A.6}$$

$$\frac{\delta}{\delta x}\left[\epsilon_{CLT}(k,s,x)\right]\Big|_{s=s_0,x=x_0} = 0. \tag{A.7}$$

Letting $k = 2\nu$ in (4.11), it can be shown, without loss of generality, that

$$\epsilon_{CLT}(2\nu,s,x) = Q_\nu(\sqrt{s},\sqrt{x}) - Q\left(\frac{x-(2\nu+s)}{2\sqrt{\nu+s}}\right). \tag{A.8}$$

The partial derivative of $\epsilon_{CLT}(2\nu,s,x)$ with respect to s is given by

$$\frac{\delta}{\delta s}\left[\epsilon_{CLT}(2\nu,s,x)\right] = \frac{1}{2}\left(e^{-\frac{s}{2}-\frac{x}{2}}\left(\frac{x}{s}\right)^{\frac{\nu}{2}} I_\nu\left(\sqrt{sx}\right) - \frac{(s+x)e^{-\frac{(x-(2\nu+s))^2}{8(\nu+s)}}}{2\sqrt{2\pi}(\nu+s)^{3/2}}\right), \tag{A.9}$$

where $I_n(z)$ is the modified Bessel function of the first kind [68, Equation 10.25.2]. Combining (A.9) with (A.6) gives the condition

$$e^{-\frac{(x_0-(2\nu+s_0))^2}{8(\nu+s_0)}} = \frac{2\sqrt{2\pi}(\nu+s_0)^{\frac{3}{2}}}{(s_0+x_0)}\left(e^{-\frac{s_0}{2}-\frac{x_0}{2}}\left(\frac{x_0}{s_0}\right)^{\frac{\nu}{2}} I_\nu\left(\sqrt{s_0x_0}\right)\right). \tag{A.10}$$

Similarly, the partial derivative of $\epsilon_{CLT}(2\nu, s, x)$ with respect to x is given by

$$\frac{\delta}{\delta x}\left[\epsilon_{CLT}(2\nu,s,x)\right] = \frac{1}{2}\left(\frac{e^{-\frac{(x-(2\nu+s))^2}{8(\nu+s)}}}{\sqrt{2\pi(\nu+s)}} - e^{-\frac{s}{2}-\frac{x}{2}}\left(\frac{x}{s}\right)^{\frac{\nu-1}{2}} I_{\nu-1}\left(\sqrt{sx}\right)\right), \tag{A.11}$$

which, when combined with (A.7), can be shown to give the condition

$$e^{-\frac{(x_0-(2\nu+s_0))^2}{8(\nu+s_0)}} = \sqrt{2\pi(\nu+s_0)}\left(e^{-\frac{s_0}{2}-\frac{x_0}{2}}\left(\frac{x_0}{s_0}\right)^{\frac{\nu-1}{2}} I_{\nu-1}\left(\sqrt{s_0x_0}\right)\right). \tag{A.12}$$

Combining (A.10) and (A.12), and simplifying, leads to the condition

$$2(\nu+s_0)\sqrt{x_0}\; I_\nu(\sqrt{s_0x_0}) = (s_0+x_0)\sqrt{s_0}\; I_{\nu-1}(\sqrt{s_0x_0}). \tag{A.13}$$

Letting $s_0 = 0$ is a satisfactory solution of (A.13), but is by no means guaranteed to be the only solution[2], and so may not always produce a maximum. However, for large values of ν or, equivalently, for large values of k, the problem can be simplified.

For large orders, the modified Bessel function of the first kind may be approximated [68, Equation 10.41.1] as

$$I_n(z) \approx \hat{I}_n(z) = \frac{1}{\sqrt{2\pi n}}\left(\frac{ez}{2n}\right)^n. \tag{A.14}$$

The approximation is illustrated for different values of n and z in Figure A.1.

The following identity [68, Equation 4.4.17], which is valid for large n and is illustrated in Figure A.2, is also useful:

$$\left(\frac{n-1}{n}\right)^n \approx \frac{1}{e}. \tag{A.15}$$

Using (A.14) and (A.15), (A.13) can be simplified to

$$(\nu+s_0)(\sqrt{s_0})^\nu(\sqrt{x_0})^{\nu+1} = \sqrt{\nu(\nu-1)}(s_0+x_0)(\sqrt{s_0})^\nu(\sqrt{x_0})^{\nu-1}, \tag{A.16}$$

for large values of ν. Thus, (A.16) is equivalent to (A.13) when ν is large.

Assuming that $\nu \geq 2$, (A.16) admits three unique solutions. Two of these are immedi-

[2]For instance, (A.13) is also satisfied when $s_0 \to \infty$ for arbitrary $0 \leq x_0 < \infty$ and when $x_0 \to \infty$ for arbitrary $0 \leq s_0 < \infty$. However these solutions are trivial as $\epsilon(k, s_0, x_0) = 0$ in both cases.

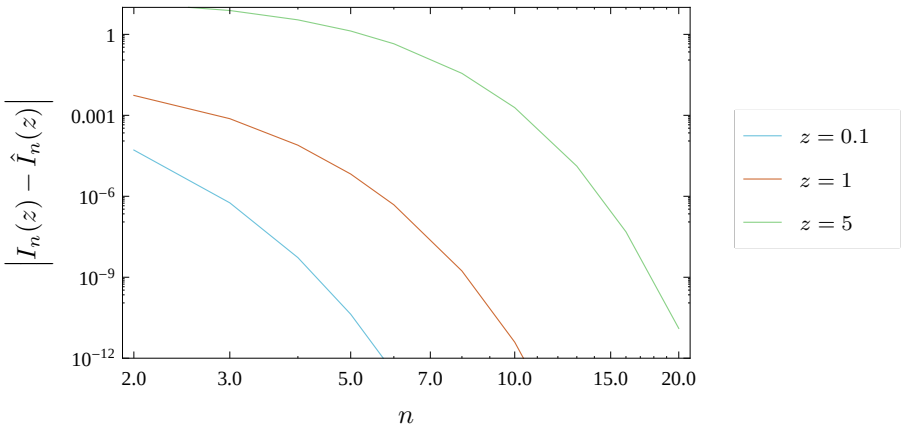

Figure A.1: A log-log plot of the absolute value of the error resulting from the approximation for the modified Bessel function of the first kind, defined in (A.14), for different values of z.

ately clear: $s_0 = 0$ and $x_0 = 0$; the third can be found by cancelling the common terms (which lead to the solutions $s_0 = 0$ and $x_0 = 0$) on both sides of (A.16) to give

$$x_0 = \frac{\sqrt{\nu(\nu-1)}s_0}{\nu + s_0 - \sqrt{\nu(\nu-1)}}. \tag{A.17}$$

For large values of ν, (A.17) simplifies to

$$x_0 \approx \nu. \tag{A.18}$$

Using (A.6), it can be shown that, for the solution $x_0 = 0$, the only value of s_0 that satisfies both first partial derivative tests, as ν becomes large, is $s_0 \to \infty$ which, as noted previously, is a trivial solution. Similarly, it can be shown that, if $x_0 = \nu$, then (A.6) requires that $s_0 \to \infty$ when ν is large, and so $x_0 = \nu$ is a further trivial solution.

The value of x_0 corresponding to $s_0 = 0$ can be found using the identity [68, Equation 10.30.1]

$$\lim_{s_0 \to 0} \left(\left(\frac{x_0}{s_0} \right)^{\frac{\nu-1}{2}} I_{\nu-1}\left(\sqrt{s_0 x_0}\right) \right) = \frac{\left(\frac{x_0}{2}\right)^{\nu-1}}{\Gamma(\nu)}, \tag{A.19}$$

where $\Gamma(n)$ represents the gamma function. Using (A.19), it can be shown that the first partial derivative test, with respect to x, reduces to the condition

$$\frac{e^{-\frac{x_0}{2}} \left(\frac{x_0}{2}\right)^{\nu-1}}{\Gamma(\nu)} = \frac{e^{-\frac{(x_0-2\nu)^2}{8\nu}}}{\sqrt{2\pi\nu}}, \tag{A.20}$$

which can be solved for x_0 using a numerical method, but admits the solution $x_0 \approx 2\nu$ for large values of ν. This can easily be shown by letting $x_0 \approx 2\nu$ in (A.20) to give the

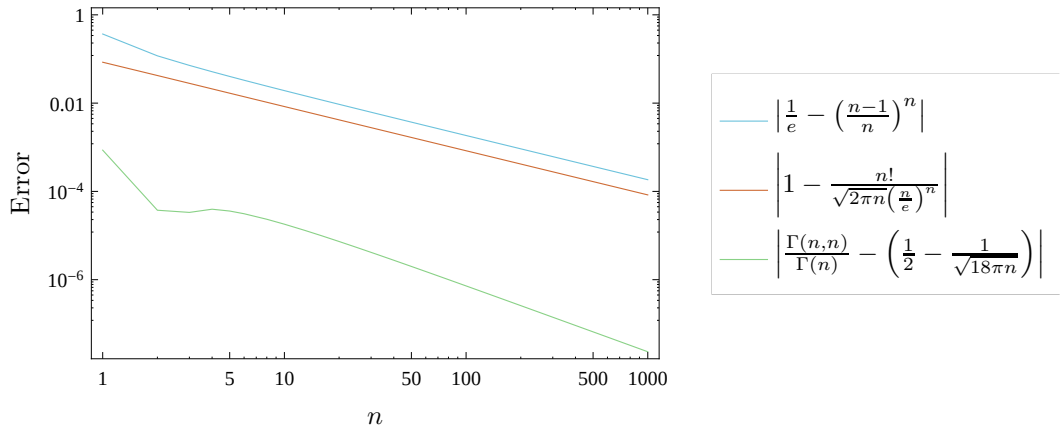

Figure A.2: A log-log plot of the absolute value of the error resulting from the approximation for the reciprocal of the exponential function (blue) given in (A.15), Stirling's approximation (red) given in (A.22), and the regularised incomplete gamma function approximation (green) given in (A.25).

condition

$$\frac{\nu!}{\sqrt{2\pi\nu}\left(\frac{\nu}{e}\right)^\nu} \approx 1, \tag{A.21}$$

which is guaranteed from the limit of Stirling's approximation [68, Equation 5.11.3], that is

$$\lim_{n\to\infty} \frac{n!}{\sqrt{2\pi n}\left(\frac{n}{e}\right)^n} = 1, \tag{A.22}$$

as illustrated in Figure A.2. Consequently, (A.21) is satisfied for large values of ν and so the only non-trivial critical points for large ν are $(s_0, x_0) = (0, 2\nu)$.

Substituting $(s, x) = (0, 2\nu)$ into (A.8), it can be shown that

$$\epsilon_{CLT}(2\nu, 0, 2\nu) = \frac{\Gamma(\nu,\nu)}{\Gamma(\nu)} - \frac{1}{2}. \tag{A.23}$$

For large values of n, $\frac{\Gamma(n,n)}{\Gamma(n)}$ can be approximated [68, Equation 8.11.12] as

$$\frac{\Gamma(n,n)}{\Gamma(n)} \approx \frac{\left(\frac{n}{e}\right)^n\sqrt{2\pi n}}{n!}\left(\frac{1}{2}-\frac{1}{\sqrt{18\pi n}}\right), \tag{A.24}$$

which can be simplified using (A.22) as

$$\frac{\Gamma(n,n)}{\Gamma(n)} \approx \frac{1}{2}-\frac{1}{\sqrt{18\pi n}}, \tag{A.25}$$

an illustration of which is shown in Figure A.2.

Consequently, (A.23) can be written as

$$\epsilon_{CLT}(2\nu, 0, 2\nu) \approx -\frac{1}{\sqrt{18\pi\nu}}, \tag{A.26}$$

as ν becomes large, which suggests that the sign of the error with maximum magnitude is negative and $(s, x) = (0, 2\nu)$ results in a minimum.

The second partial derivative test [68, Equations 1.5.20 and 1.5.21] can be used to show that this intuition is correct. The test states that the critical points (s_0, x_0) result in a local minimum if

$$\begin{aligned} D_1(2\nu, s_0, x_0) = & \left.\frac{\delta^2}{\delta x^2}\left[\epsilon_{CLT}(2\nu, s, x)\right]\right|_{s=s_0, x=x_0} \\ & > 0, \end{aligned} \tag{A.27}$$

$$\begin{aligned} D_2(2\nu, s_0, x_0) = & \left.\frac{\delta^2}{\delta x^2}\left[\epsilon_{CLT}(2\nu, s, x)\right]\right|_{s=s_0, x=x_0} \left.\frac{\delta^2}{\delta s^2}\left[\epsilon_{CLT}(2\nu, s, x)\right]\right|_{s=s_0, x=x_0} \\ & - \left.\left(\frac{\delta^2}{\delta x \delta s}\left[\epsilon_{CLT}(2\nu, s, x)\right]\right)^2\right|_{s=s_0, x=x_0} \\ & > 0. \end{aligned} \tag{A.28}$$

For $(s_0, x_0) = (0, 2\nu)$, the second order partial derivatives in (A.27) and (A.28) can easily be derived from (A.9) and (A.11) to show that

$$D_1(2\nu, 0, 2\nu) = \frac{1}{4\nu}\frac{\left(\frac{\nu}{e}\right)^\nu}{\nu!}, \tag{A.29}$$

$$D_2(2\nu, 0, 2\nu) = \frac{1}{8\nu^2}\frac{\left(\frac{\nu}{e}\right)^\nu}{\nu!}\left(\frac{1}{\sqrt{2\pi\nu}} - \frac{\left(\frac{\nu}{e}\right)^\nu}{2(n+1)\Gamma(\nu)}\right) - \frac{1}{32\pi\nu^3}, \tag{A.30}$$

both of which can be shown to be positive for $\nu \geq 1$. Figure A.3 illustrates the values of $D_1(2\nu, 0, 2\nu)$ and $D_2(2\nu, 0, 2\nu)$ for increasing values of $k = 2\nu \geq 2$.

Furthermore, as $(s_0, x_0) = (0, 2\nu)$ and $(s_0, x_0) = (\infty, \nu)$ are the only critical points as ν becomes large, and because $(s_0, x_0) = (\infty, \nu)$ results in $\epsilon_{CLT}(2\nu, s, x) = 0$, the points $(s_0, x_0) = (0, 2\nu)$ must produce a global minimum, and so, for large $\nu = \frac{k}{2}$,

$$\min_{s,x>0}(\epsilon_{CLT}(2\nu, s, x)) \approx -\frac{1}{\sqrt{18\pi\nu}}, \tag{A.31}$$

or, equivalently,

$$\max_{s,x>0}|\epsilon_{CLT}(k, s, x)| \approx \frac{1}{\sqrt{9\pi k}}. \tag{A.32}$$

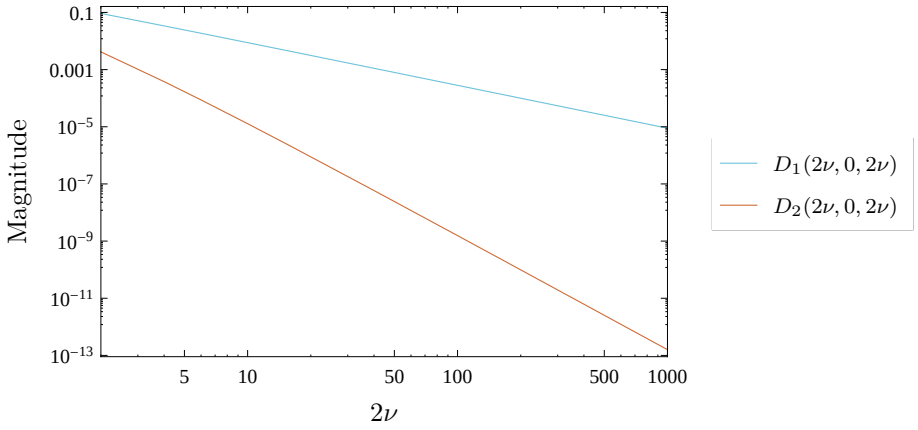

Figure A.3: A log-log plot of the second partial derivative tests specified in (A.27) and (A.28), as functions of $k = 2\nu$.

Finally, substituting (A.5) and (A.32) into (A.1) gives the desired result:

$$\max_{s,x} |\epsilon_{CLT}(k, s, x)| = \max\left(Q\left(\sqrt{\tfrac{k}{2}}\right), \epsilon_\infty(k)\right), \qquad \square \tag{A.33}$$

where, for convenience, $\epsilon_\infty(k) \triangleq \max_{s,x>0} |\epsilon_{CLT}(k, s, x)|$.

A.2 Proof of Lemma 5.1

By definition [49, Equation 26.2.3], the Gaussian Q function is related to the error function as

$$Q(x) = \frac{1}{2}\left[1 - \operatorname{erf}\left(\frac{x}{\sqrt{2}}\right)\right], \tag{A.34}$$

and so (5.11) can be written as

$$\begin{aligned} F_k(a, b, c) &= \frac{1}{2\,\Gamma(k)} \int_0^\infty \left[1 - \operatorname{erf}\left(\frac{a - bx}{\sqrt{2}}\right)\right] e^{-cx} c^k x^{k-1} dx \\ &= \frac{1}{2\,\Gamma(k)} \int_0^\infty e^{-cx} c^k x^{k-1} dx - \frac{1}{2\,\Gamma(k)} \int_0^\infty \operatorname{erf}\left(\frac{a - bx}{\sqrt{2}}\right) e^{-cx} c^k x^{k-1} dx \\ &= \frac{1}{2} - \frac{1}{2\,\Gamma(k)} \int_0^\infty \operatorname{erf}\left(\frac{a - bx}{\sqrt{2}}\right) e^{-cx} c^k x^{k-1} dx, \end{aligned} \tag{A.35}$$

where the last line has been simplified using the identity [69, Equation 3.351-3]

$$\frac{1}{\Gamma(k)} \int_0^\infty e^{-cx} c^k x^{k-1} dx = 1, \quad c > 0. \tag{A.36}$$

Changing the variable of integration in (A.35) to $y = cx$, $F_k(a, b, c)$ can be written as

$$\begin{aligned} F_k(a,b,c) &= \frac{1}{2} - \frac{1}{2\ \Gamma(k)} \int_0^\infty \operatorname{erf}\left(\frac{a - \frac{by}{c}}{\sqrt{2}}\right) e^{-y} y^{k-1} dy \\ &= \frac{1}{2} - \frac{(-1)^{k-1}}{2\ \Gamma(k)} \frac{d^{k-1}}{dt^{k-1}} \left[\int_0^\infty e^{-ty} \operatorname{erf}\left(\frac{a - \frac{by}{c}}{\sqrt{2}}\right) dy\right]\Bigg|_{t=1}. \end{aligned} \tag{A.37}$$

Now, letting $z = y - \frac{ac}{b}$, and changing limits appropriately, (A.37) can be written as

$$F_k(a,b,c) = \frac{1}{2} + \frac{(-1)^{k-1}}{2\ \Gamma(k)} \frac{d^{k-1}}{dt^{k-1}} \left[e^{-\frac{act}{b}} \int_{-\frac{ac}{b}}^\infty e^{-tz} \operatorname{erf}\left(\frac{bz}{\sqrt{2}c}\right) dz\right]\Bigg|_{t=1}. \tag{A.38}$$

Using the integral identity [49, Equation 7.4.36]

$$\int e^{-tz} \operatorname{erf}\left(\frac{bz}{\sqrt{2}c}\right)\ dz = \frac{1}{t}\left[e^{\frac{(ct)^2}{2b^2}} \operatorname{erf}\left(\frac{bz}{\sqrt{2}c} + \frac{ct}{\sqrt{2}b}\right) - e^{-tz} \operatorname{erf}\left(\frac{bz}{\sqrt{2}c}\right)\right], \tag{A.39}$$

it can be shown that (A.38) simplifies to

$$F_k(a,b,c) = \frac{1}{2} + \frac{(-1)^{k-1}}{2\ \Gamma(k)} \frac{d^{k-1}}{dt^{k-1}} \left[\frac{e^{-\frac{a^2}{2}} e^{\left(\frac{a - \frac{ct}{b}}{\sqrt{2}}\right)^2} \left[1 + \operatorname{erf}\left(\frac{a - \frac{ct}{b}}{\sqrt{2}}\right)\right]}{t} - \frac{\operatorname{erf}\left(\frac{a}{\sqrt{2}}\right)}{t}\right]\Bigg|_{t=1}, \tag{A.40}$$

which is equivalent to the form given by Atapattu et al. [66].

However, this can be further simplified by noting that

$$\frac{d^n}{dt^n}\left[\frac{1}{t}\right]\Bigg|_{t=1} = \frac{n!}{(-1)^n}, \tag{A.41}$$

and so (A.40) can be written as

$$\begin{aligned} F_k(a,b,c) &= \frac{1}{2}\left[1 - \operatorname{erf}\left(\frac{a}{\sqrt{2}}\right)\right] + \frac{e^{-\frac{a^2}{2}}}{2} \frac{(-1)^{k-1}}{\Gamma(k)} \sum_{p=0}^{k-1} \binom{k-1}{p} \frac{d^{k-1-p}}{dt^{k-1-p}} \left[\frac{1}{t}\right]\Bigg|_{t=1} \\ &\quad \times \frac{d^p}{dt^p}\left[e^{\left(\frac{a - \frac{ct}{b}}{\sqrt{2}}\right)^2} \left[1 + \operatorname{erf}\left(\frac{a - \frac{ct}{b}}{\sqrt{2}}\right)\right]\right]\Bigg|_{t=1} \\ &= Q(a) + \frac{e^{-\frac{a^2}{2}}}{2} \sum_{p=0}^{k-1} \frac{(-1)^p}{p!} \frac{d^p}{dt^p}\left[e^{\left(\frac{a - \frac{ct}{b}}{\sqrt{2}}\right)^2} \left[1 + \operatorname{erf}\left(\frac{a - \frac{ct}{b}}{\sqrt{2}}\right)\right]\right]\Bigg|_{t=1}, \end{aligned} \tag{A.42}$$

where Leibniz's formula [68, Equation 1.4.12] has been used to expand the derivative in the first line, and (A.34) and (A.41) to simplify the second line.

Finally, using the identity [68, Equation 7.18.4]

$$\frac{d^n}{dz^n}\left(e^{z^2}\,\mathrm{erfc}(z)\right) = (-1)^n\ 2^n\ n!\ e^{z^2}\ \mathrm{i}^n\,\mathrm{erfc}(z), \tag{A.43}$$

and the composite function derivative rule [69, Equation 0.430-1], (A.42) can be simplified to

$$F_k(a,b,c) = Q(a) + \frac{e^{\frac{c^2}{2b^2}-\frac{ac}{b}}}{2}\sum_{p=0}^{k-1}\left(\frac{\sqrt{2}c}{b}\right)^p \mathrm{i}^p\,\mathrm{erfc}\left(\frac{\frac{c}{b}-a}{\sqrt{2}}\right). \qquad \square \tag{A.44}$$

A.3 Proof of Lemma 5.2

Using (5.9), $|\epsilon_{SNR,X,Y}|$ can be written as

$$\begin{aligned}|\epsilon_{SNR,X,Y}| &= \left|\int_{-\infty}^{\infty}\epsilon_{SNR,X}(x)\ f_{X,Y}(x)\ dx\right| \\ &\leq \int_{-\infty}^{\infty}|\epsilon_{SNR,X}(x)||f_{X,Y}(x)|\ dx \\ &\leq \int_{-\infty}^{\infty}|\epsilon_{SNR,X}(x)|\ f_{X,Y}(x)\ dx,\end{aligned} \tag{A.45}$$

where the fact that, because $f_{X,Y}(x)$ is a probability density function, $f_{X,Y}(x) \geq 0\ \forall\ x$, has been used to simplify the notation.

The following identity, which is proved next in this appendix, is useful:

$$|\epsilon_{SNR,X}(\gamma_X)| \leq \frac{1}{\sqrt{2\pi e}}\cdot\frac{\gamma_X}{N_X}. \tag{A.46}$$

Using (A.46), (A.45) can be simplified to

$$|\epsilon_{SNR,X,Y}| \leq \frac{1}{\sqrt{2\pi e}}\cdot\frac{1}{N_X}\int_{-\infty}^{\infty} x\ f_{X,Y}(x)\ dx, \qquad \square \tag{A.47}$$

which completes the proof.

Proof of (A.46)

Substituting (5.3) and (5.6) into (5.7), it can be shown that

$$\epsilon_{SNR,X}(\gamma_X) = Q\left(\frac{\lambda - M(N_X+\gamma_X)}{\sqrt{2M(N_X+2\gamma_X)}}\right) - Q\left(\frac{\lambda - M(N_X+\gamma_X)}{\sqrt{2MN_X}}\right). \tag{A.48}$$

For given values of M, N_X and γ_X, the critical points of $\epsilon_{SNR,X}(\gamma_X)$ may be found using the first partial derivative test [68, Equation 1.5.19], that is

$$\frac{\delta}{\delta\lambda}\Big[\epsilon_{SNR,X}(\gamma_X)\Big]\Big|_{\lambda=\lambda_0} = 0. \tag{A.49}$$

Differentiating $\epsilon_{SNR,X}(\gamma_X)$ with respect to λ, using (A.49), and simplifying, leads to the condition

$$\lambda_0^2 - 2M(N_X+\gamma_X)\lambda_0 + M^2(N_X+\gamma_X)^2 - \tfrac{MN_X}{\gamma_X}(N_X+2\gamma_X)\log\left(1+\tfrac{2\gamma_X}{N_X}\right) = 0, \tag{A.50}$$

which is in the form of a quadratic equation, and has the solutions

$$\lambda_0 = M(N_X+\gamma_X) \pm \sqrt{\frac{MN_X}{\gamma_X}(N_X+2\gamma_X)\log\left(1+\frac{2\gamma_X}{N_X}\right)}. \tag{A.51}$$

Using the second derivative test [68, Equation 1.5.20], it can be shown that the smaller value of λ_0 produces a minimum, while the larger value results in a maximum. However, the absolute value of the error is the same using either solution. This can easily be shown by substituting (A.51) into (A.48) and taking the absolute value of both sides to give

$$\left|\epsilon_{SNR,X}(\gamma_X)\right|\Big|_{\lambda=\lambda_0} = \left|Q\left(\sqrt{\frac{N_X\log\left(1+\frac{2\gamma_X}{N_X}\right)}{2\gamma_X}}\right) - Q\left(\sqrt{\frac{(N_X+2\gamma_X)\log\left(1+\frac{2\gamma_X}{N_X}\right)}{2\gamma_X}}\right)\right|, \tag{A.52}$$

and so it can be concluded that either value of λ_0 maximises the absolute value of the error.

Letting $x = \frac{2\gamma_X}{N_X}$, (A.52) can be written as

$$|g(x)| = \left|Q\left(\sqrt{\frac{\log(1+x)}{x}}\right) - Q\left(\sqrt{\frac{(1+x)\log(1+x)}{x}}\right)\right|, \tag{A.53}$$

which is a concave function of x, as illustrated in Figure A.4, and so can be bounded using a first order Taylor series approximation about $x = 0$.

The Taylor expansion [69, Equation 0.318-1] of $g(x)$ about $x = 0$ can be written as

$$\begin{aligned} g(x) &= \sum_{k=0}^{\infty}\frac{x^k}{k!}g^{(k)}(0) \\ &= g(0) + xg^{(1)}(0) + \sum_{k=2}^{\infty}\frac{x^k}{k!}g^{(k)}(0) \\ &= \frac{x}{\sqrt{8\pi e}} + \sum_{k=2}^{\infty}\frac{x^k}{k!}g^{(k)}(0), \end{aligned} \tag{A.54}$$

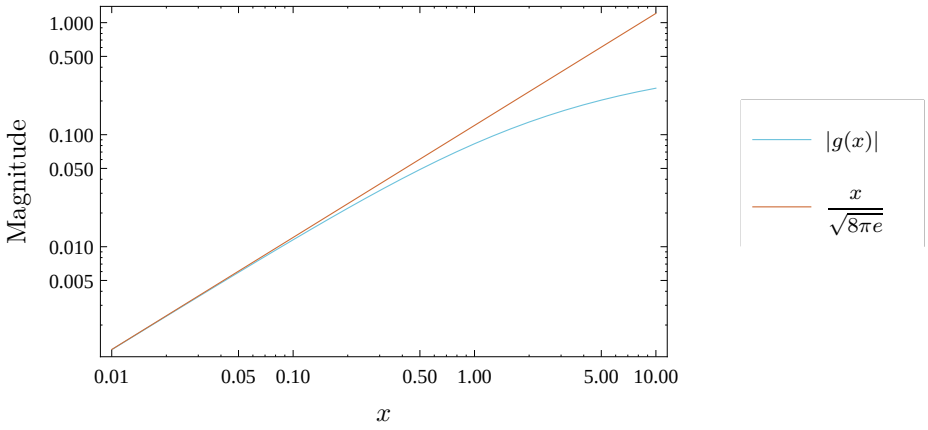

Figure A.4: A log-log plot of the maximum error and the bound proposed in (A.55).

where the fact that $\lim_{x\to 0} g(x) = 0$ has been used to simplify the result.

Discarding the higher order terms in (A.54) and evaluating at the point $x = \frac{2\gamma_X}{N_X}$ gives the desired result:

$$\left| g\left(\frac{2\gamma_X}{N_X}\right)\right| = \left|\epsilon_{SNR,X}(\gamma_X)\right|_{\lambda=\lambda_0} \leq \frac{\gamma_X}{\sqrt{2\pi e}\ N_X}, \quad \gamma_X \geq 0, \qquad \square \tag{A.55}$$

where equality holds as $\gamma_X \to 0$, as shown in Figure A.4.

A.4 Proof of Lemma 5.3

Using (5.9), $\epsilon_{SNR,X,Y}$ can be written as

$$\begin{aligned}\epsilon_{SNR,X,Y} &= \int_{-\infty}^{\gamma_0} \epsilon_{SNR,X}(x)\ f_{X,Y}(x)\ dx + \int_{\gamma_0}^{\infty} \epsilon_{SNR,X}(x)\ f_{X,Y}(x)\ dx \\ &= \epsilon^{+}_{SNR,X,Y} - \epsilon^{-}_{SNR,X,Y},\end{aligned} \tag{A.56}$$

where $\gamma_0 = \frac{\lambda - MN_X}{M}$, N_X is as given in (5.4) and, for convenience, $\epsilon^{+}_{SNR,X,Y} = \int_{-\infty}^{\gamma_0} \epsilon_{SNR,X}(x)\ f_{X,Y}(x)\ dx$ and $\epsilon^{-}_{SNR,X,Y} = -\int_{\gamma_0}^{\infty} \epsilon_{SNR,X}(x)\ f_{X,Y}(x)\ dx$.

Using (5.3) and (5.6), it can be shown that $\epsilon_{SNR,X}(\gamma_X)$ has the property

$$\epsilon_{SNR,X}(\gamma_X) \begin{cases} > 0 & \gamma_X < \gamma_0 \\ = 0 & \gamma_X = \gamma_0 \\ < 0 & \gamma_X > \gamma_0, \end{cases} \tag{A.57}$$

and so $\epsilon^{+}_{SNR,X,Y}$ and $\epsilon^{-}_{SNR,X,Y}$ are strictly non-negative. Consequently, $|\epsilon_{SNR,X,Y}|$ can be

bounded as

$$\begin{aligned} |\epsilon_{SNR,X,Y}| &= \left|\epsilon^{+}_{SNR,X,Y} - \epsilon^{-}_{SNR,X,Y}\right| \\ &\leq \max\left(\epsilon^{+}_{SNR,X,Y}, \epsilon^{-}_{SNR,X,Y}\right). \end{aligned} \tag{A.58}$$

The following relation, which is proved later in this appendix, is useful:

$$|\epsilon_{SNR,X}(\gamma_X)| \leq \frac{|\phi_X(\gamma_X)|}{\sqrt{2\pi}} \left(\frac{\gamma_X}{N_X}\right) \exp\left(-\frac{\phi_X^2(\gamma_X)}{2\left(1+\frac{2\gamma_X}{N_X}\right)}\right), \tag{A.59}$$

where

$$\phi_X(\gamma_X) = \frac{\lambda - M(N_X+\gamma_X)}{\sqrt{2MN_X}}. \tag{A.60}$$

Using (A.59), and noting that $\phi(x) \geq 0$ for $x \in (-\infty, \gamma_0]$, $\epsilon^{+}_{SNR,X,Y}$ can be bounded as

$$\begin{aligned} \epsilon^{+}_{SNR,X,Y} &\leq \frac{1}{\sqrt{2\pi}} \cdot \frac{1}{N_X} \int_{-\infty}^{\gamma_0} \phi_X(x)\ x\ \exp\left(-\frac{\phi_X^2(x)}{2\left(1+\frac{2x}{N_X}\right)}\right)\ f_{X,Y}(x)\ dx \\ &\leq \max_x\left(x\ f_{X,Y}(x)\right) \frac{1}{\sqrt{2\pi}} \cdot \frac{1}{N_X} \int_{-\infty}^{\gamma_0} \phi_X(x)\ \exp\left(-\frac{\phi_X^2(x)}{2\left(1+\frac{2x}{N_X}\right)}\right)\ dx, \end{aligned} \tag{A.61}$$

where the first mean value theorem for infinite integrals [69, Equation 12.113] has been used to simplify the result, and the notation $\max_x(g(x))$ indicates the maximum value of the function $g(x)$ for $x \in (-\infty, \infty)$.

To the best of the author's knowledge at the time of writing, the integral in (A.61) cannot be evaluated symbolically due to the $\frac{2x}{N_X}$ term in the denominator of the argument to the exponential function. Thus, the following simplification is made:

$$g_X(x) = \exp\left(-\frac{\phi_X^2(x)}{2\left(1+\frac{2x}{N_X}\right)}\right) \approx \hat{g}_X(x) = \exp\left(-\frac{\phi_X^2(x)}{2}\right). \tag{A.62}$$

While (A.62) is valid near $x = \gamma_0$ (recall that $\phi_X(\gamma_0) = 0$), it is less accurate for moderate deviations of x from γ_0, as can be seen in Figure A.5. Still, the difference is usually not large, and decreases as $x \to \pm\infty$. Consequently, $\hat{g}_X(x)$ can be used to approximate $g_X(x)$ in (A.61), and so $\epsilon^{+}_{SNR,X,Y}$ can be written as

$$\epsilon^{+}_{SNR,X,Y} \lessapprox \max_x\left(x\ f_{X,Y}(x)\right) \frac{1}{\sqrt{2\pi}} \cdot \frac{1}{N_X} \int_{-\infty}^{\gamma_0} \phi_X(x)\ \exp\left(-\frac{\phi_X^2(x)}{2}\right)\ dx, \tag{A.63}$$

where $\lessapprox$ indicates that the left hand side of the equation is less than, or approximately equal to, the right hand side, and is a consequence of the fact that $\hat{g}_X(x) \leq g_X(x)$, which disagrees with the direction of the inequality in (A.61).

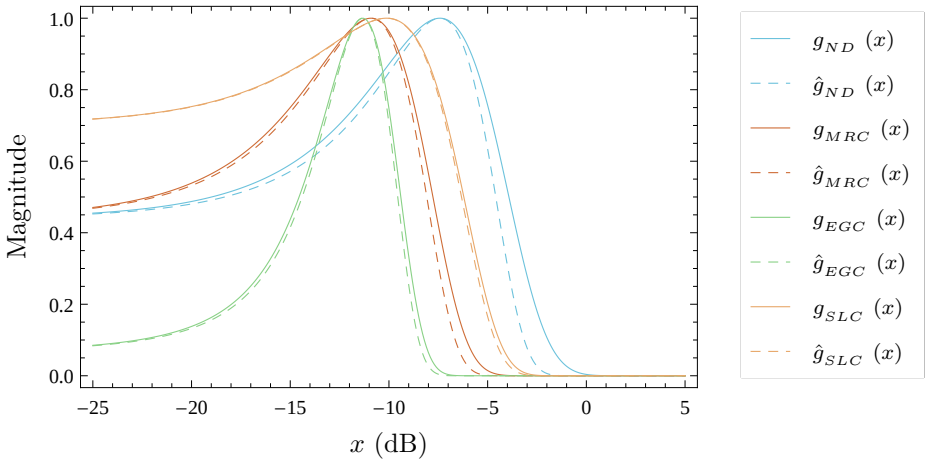

Figure A.5: A plot of the exact and approximate functions in (A.62), for some typical system parameters. In the no diversity case, $M = 100$ and $\hat{P}_{f_{ND}} = 0.1$; in the MRC diversity case, $n = 2$, $M = 500$, and $\hat{P}_{f_{MRC}} = 0.1$; in the EGC diversity case, $n = 3$, $M = 2000$, and $\hat{P}_{f_{EGC}} = 0.01$; and in the SLC diversity case, $n = 5$, $M = 750$, and $\hat{P}_{f_{SLC}} = 0.2$.

Changing the variable of integration to $u = \phi_{_X}(x)$, and noting that $\phi_{_X}(\gamma_0) = 0$, the integral in (A.63) can be written as

$$\begin{aligned}\int_{-\infty}^{\gamma_0} \phi_{_X}(x)\ \exp\left(-\frac{\phi_{_X}^2(x)}{2}\right)\ dx &= \sqrt{\frac{2N_{_X}}{M}}\int_0^{\infty} u e^{-\frac{u^2}{2}}\ du \\ &= \sqrt{\frac{2N_{_X}}{M}},\end{aligned} \tag{A.64}$$

where the integral identity $\int_0^{\infty} x e^{-\frac{x^2}{2}}\ dx = 1$ [69, Equation 3.321-4] has been used to simplify the result.

Using (A.64), (A.63) can be written as

$$\epsilon^{+}_{_{SNR,X,Y}} \lessapprox \frac{1}{\sqrt{MN_{_X}\pi}} \max_x \left(x\ f_{_{X,Y}}(x)\right). \tag{A.65}$$

Similarly, noting that $\phi(x) \leq 0$ for $x \in [\gamma_0, \infty)$, $\epsilon^{-}_{_{SNR,X,Y}}$ can be bounded as

$$\begin{aligned}\epsilon^{-}_{_{SNR,X,Y}} &\leq -\frac{1}{\sqrt{2\pi}} \cdot \frac{1}{N_{_X}} \int_{\gamma_0}^{\infty} \phi_{_X}(x)\ x\ \exp\left(-\frac{\phi_{_X}^2(x)}{2\left(1+\frac{2x}{N_{_X}}\right)}\right)\ f_{_{X,Y}}(x)\ dx \\ &\lessapprox -\max_x \left(x\ f_{_{X,Y}}(x)\right) \frac{1}{\sqrt{2\pi}} \cdot \frac{1}{N_{_X}} \int_{\gamma_0}^{\infty} \phi_{_X}(x)\ \exp\left(-\frac{\phi_{_X}^2(x)}{2}\right)\ dx.\end{aligned} \tag{A.66}$$

Once again changing the variable of integration to $u = \phi_{_X}(x)$, the integral in (A.66)

can be written as

$$\int_{\gamma_0}^{\infty} \phi_X(x)\ \exp\left(-\frac{\phi_X^2(x)}{2}\right)\ dx = \sqrt{\frac{2N_X}{M}} \int_{-\infty}^{0} u e^{-\frac{u^2}{2}}\ du$$
$$= -\sqrt{\frac{2N_X}{M}}, \tag{A.67}$$

and so $\epsilon^{-}_{SNR,X,Y}$ can be bounded as

$$\epsilon^{-}_{SNR,X,Y} \lessapprox \frac{1}{\sqrt{MN_X\pi}} \max_x \left(x\ f_{X,Y}(x)\right). \tag{A.68}$$

As both $\epsilon^{+}_{SNR,X,Y}$ and $\epsilon^{-}_{SNR,X,Y}$ are approximately bounded by the same function, (A.58) can be simplified to

$$|\epsilon_{SNR,X,Y}| \lessapprox \frac{1}{\sqrt{MN_X\pi}} \max_x \left(x\ f_{X,Y}(x)\right), \qquad \square \tag{A.69}$$

which completes the proof.

Proof of (A.59)

The Taylor series expansion [69, Equation 0.318-1] of $Q(x)$ about $x = \varphi$ is given by

$$Q(x) = \sum_{k=0}^{\infty} \frac{(x-\varphi)^k}{k!} \frac{d^k}{dz^k} \left[Q(z)\right]\Big|_{z=\varphi}. \tag{A.70}$$

Using (A.70), it can be shown that, for $c \geq 0$,

$$Q\left(\frac{\varphi}{\sqrt{1+c}}\right) = \sum_{k=0}^{\infty} \frac{\varphi^k}{k!} \left(\frac{1}{\sqrt{1+c}} - 1\right)^k \frac{d^k}{dz^k} \left[Q(z)\right]\Big|_{z=\varphi}.$$
$$= Q(\varphi) + R, \tag{A.71}$$

where the remainder, R, can be written in Lagrange form [69, Equation 0.317-3], with $z_0 = \varphi + \theta\left(\frac{\varphi}{\sqrt{1+c}} - \varphi\right)$, as

$$R = \varphi\left(\frac{1}{\sqrt{1+c}} - 1\right) \frac{d}{dz} \left[Q(z)\right]\Big|_{z=z_0}$$
$$= \frac{\varphi}{\sqrt{2\pi}} \left(1 - \frac{1}{\sqrt{1+c}}\right) \exp\left[-\frac{\varphi^2}{2}\left(1 - \theta\left(1 - \frac{1}{\sqrt{1+c}}\right)\right)^2\right], \tag{A.72}$$

where equality holds for some $\theta \in (0,1)$.

The argument to the exponential function in (A.72) can be written in the simplified form $-\eta\ (1-\theta\zeta)^2$, where $\eta = \frac{\varphi^2}{2} > 0$, and $\zeta = 1 - \frac{1}{\sqrt{1+c}}$. As $c \geq 0$, $0 \leq \zeta \leq 1$, and so the quantity $1 - \theta\zeta$ is minimised as $\theta \to 1$, as illustrated in Figure A.6. Thus, the

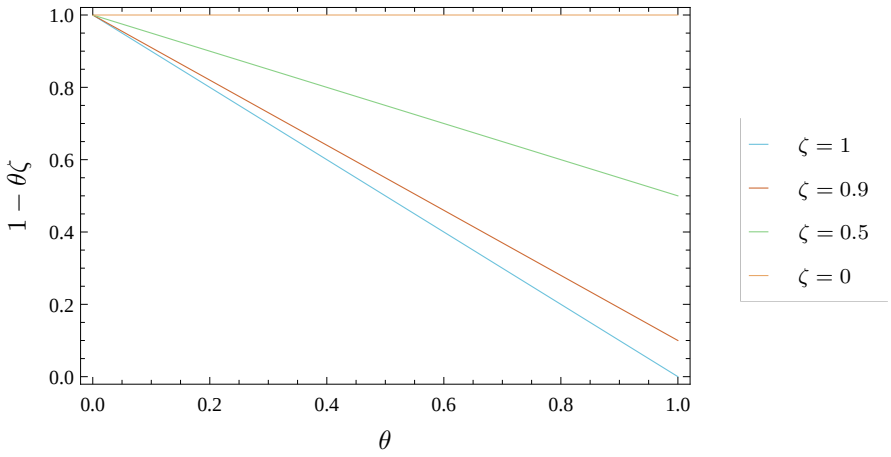

Figure A.6: A plot of the quantity $1-\theta\zeta$, as a function of θ, for $0 \leq \zeta \leq 1$.

exponential function in (A.72) can be bounded as

$$\exp\left(-\eta\,(1-\theta\zeta)^2\right) \leq \exp\left(-\eta\,(1-\zeta)^2\right). \tag{A.73}$$

Similarly, the quantity $1-\frac{1}{\sqrt{1+c}}$ can be bounded as

$$\begin{aligned} 1-\frac{1}{\sqrt{1+c}} &\leq 1-\frac{1}{\sqrt{1+c+\frac{c^2}{4}}} \\ &\leq 1-\frac{1}{1+\frac{c}{2}} \\ &\leq \frac{\frac{c}{2}}{1+\frac{c}{2}} \\ &\leq \frac{c}{2}. \end{aligned} \tag{A.74}$$

Using (A.72), (A.73) and (A.74), $|R|$ can be bounded as

$$\begin{aligned} |R| &= \frac{|\varphi|}{\sqrt{2\pi}}\left(1-\frac{1}{\sqrt{1+c}}\right)\exp\left[-\frac{\varphi^2}{2}\left(1-\theta\left(1-\frac{1}{\sqrt{1+c}}\right)\right)^2\right] \\ &\leq \frac{|\varphi|}{\sqrt{2\pi}}\left(\frac{c}{2}\right)\exp\left(-\frac{\varphi^2}{2\,(1+c)}\right). \end{aligned} \tag{A.75}$$

Returning to (A.71), it can be shown that

$$\begin{aligned} Q\left(\frac{\varphi}{\sqrt{1+c}}\right) &= Q(\varphi)+R \\ \left|Q\left(\frac{\varphi}{\sqrt{1+c}}\right)-Q(\varphi)\right| &= |R| \\ \implies \left|Q\left(\frac{\varphi}{\sqrt{1+c}}\right)-Q(\varphi)\right| &\leq \frac{|\varphi|}{\sqrt{2\pi}}\left(\frac{c}{2}\right)\exp\left(-\frac{\varphi^2}{2(1+c)}\right). \end{aligned} \tag{A.76}$$

Letting $\varphi = \phi_X(\gamma_X)$ and $c = \frac{2\gamma_X}{N_X}$ in (A.76) completes the proof.

Additional remarks

Using (A.75) and noting that $1 - \frac{1}{\sqrt{1+c}} \leq 1$, $|R|$ can also be bounded as

$$\begin{aligned} |R| &\leq \frac{|\varphi|}{\sqrt{2\pi}} \exp\left[-\frac{\varphi^2}{2(1+c)}\right] \\ &\lessapprox \frac{|\varphi|}{\sqrt{2\pi}} \exp\left[-\frac{\varphi^2}{2}\right], \end{aligned} \tag{A.77}$$

which attains a maximum when $\varphi = 1$, and so (A.77) can be written as

$$|R| \lessapprox \frac{1}{\sqrt{2\pi e}}. \tag{A.78}$$

Using (5.9) and (A.78), $\epsilon_{SNR,X,Y}$ can be written as

$$\begin{aligned} \epsilon_{SNR,X,Y} &= \int_{-\infty}^{\infty} \epsilon_{SNR,X}(x)\ f_{X,Y}(x)\ dx \\ &\lessapprox \frac{1}{\sqrt{2\pi e}} \int_{-\infty}^{\infty} f_{X,Y}(x)\ dx \\ &\lessapprox \frac{1}{\sqrt{2\pi e}} \approx 0.24, \end{aligned} \tag{A.79}$$

where the fact that $f_{X,Y}(x)$ is a probability density function, and so $\int_{-\infty}^{\infty} f_{X,Y}(x)\ dx = 1$, has been used to simplify the result.

Equation A.79 is not particularly useful as a bound because of its large value, but it does serve to illustrate that $\epsilon_{SNR,X,Y}$ has a finite upper limit or, put more simply, that there is no combination of system parameters that cause $\epsilon_{SNR,X,Y} \to \infty$. The bound given by (A.69) does not imply such a constraint, and for particular combinations of inputs may result in a value larger than $\frac{1}{\sqrt{2\pi e}}$.

A.5 Proof of Lemma 5.4

First, the substitution $\sqrt{p}y = \frac{x-s}{t}$, $p > 0$, should be made in (5.77). Noting that the change in the variable of integration does not affect the limits, but that $dx = t\sqrt{p}dy$,

$G(q,r,s,t)$ can be written as

$$\begin{aligned} G(q,r,s,t) &= t\sqrt{p}\int_{-\infty}^{\infty} Q\left(q-rs-rt\sqrt{p}y\right)e^{-py^2}dy \\ &= \frac{t\sqrt{p}}{2}\int_{-\infty}^{\infty}\left[1-\operatorname{erf}\left(\frac{q-rs-rt\sqrt{p}y}{\sqrt{2}}\right)\right]e^{-py^2}dy \\ &= \frac{t\sqrt{p}}{2}\int_{-\infty}^{\infty}e^{-py^2}dy - \frac{t\sqrt{p}}{2}\int_{-\infty}^{\infty}\operatorname{erf}\left(\frac{q-rs-rt\sqrt{p}y}{\sqrt{2}}\right)e^{-py^2}dy, \end{aligned} \tag{A.80}$$

where the definition of the Gaussian Q function has been used to simplify the result.

The first integral in (A.80) can be further simplified as

$$\begin{aligned} \int_{-\infty}^{\infty}e^{-py^2}dy &= \int_{-\infty}^{0}e^{-py^2}dy + \int_{0}^{\infty}e^{-py^2}dy \\ &= -\int_{\infty}^{0}e^{-py^2}dy + \int_{0}^{\infty}e^{-py^2}dy \\ &= 2\int_{0}^{\infty}e^{-py^2}dy \\ &= 2\times\frac{1}{2}\sqrt{\frac{\pi}{p}} \\ &= \sqrt{\frac{\pi}{p}}, \end{aligned} \tag{A.81}$$

where the integral identity given in [69, Equation 3.3213] has been used to simplify the result.

The second integral in (A.80) can be simplified, using [69, Equation 8.2591], as

$$\int_{-\infty}^{\infty}\operatorname{erf}\left(\frac{q-rs-rt\sqrt{p}y}{\sqrt{2}}\right)e^{-py^2}dy = \sqrt{\frac{\pi}{p}}\operatorname{erf}\left(\frac{q-rs}{\sqrt{2+r^2t^2}}\right). \tag{A.82}$$

Substituting (A.81) and (A.82) into (A.80), it is not difficult to show that

$$\begin{aligned} G(q,r,s,t) &= t\sqrt{\pi}\times\frac{1}{2}\left[1-\operatorname{erf}\left(\frac{q-rs}{\sqrt{2+r^2t^2}}\right)\right] \\ &= t\sqrt{\pi}Q\left(\frac{q-rs}{\sqrt{1+\frac{r^2t^2}{2}}}\right), \qquad \square \end{aligned} \tag{A.83}$$

where the definition of the Gaussian Q function has again been used to simplify the result.

A.6 Proof of Theorem 6.1

Recalling (4.11), the error resulting from the use of (4.9) has differing representations for $x \leq 0$ and $x > 0$. Therefore, when $s = k\vartheta$, its maximum absolute value, with

respect to x, is given by

$$\max_x |\epsilon_{CLT}(k, k\vartheta, x)| = \max\left(\max_{x\leq 0} |\epsilon_{CLT}(k, k\vartheta, x)|, \max_{x>0} |\epsilon_{CLT}(k, k\vartheta, x)|\right). \tag{A.84}$$

While the formulation in (A.84) is similar to (A.1), the fact that k is large can no longer be exploited, and so the maximum absolute error for the individual cases where $x \leq 0$ and $x > 0$ must be determined before the absolute error over the entire range of values of x can be bounded.

Maximum value for $x \leq 0$

When $x \leq 0$,

$$\max_{x\leq 0} |\epsilon_{CLT}(k, k\vartheta, x)| = \max_{x\leq 0}\left[1 - Q\left(\frac{x - k(1+\vartheta)}{\sqrt{2k(1+2\vartheta)}}\right)\right], \tag{A.85}$$

as in (A.2). Noting that the Gaussian Q function is monotonically decreasing, the maximisation in (A.85) is satisfied when the argument to the Q function is maximised. As the range of values of x is constrained, this occurs when $x = 0$, and so

$$\begin{aligned}\max_{x\leq 0} |\epsilon_{CLT}(k, k\vartheta, x)| &= 1 - Q\left(\frac{-k(1+\vartheta)}{\sqrt{2k(1+2\vartheta)}}\right) \\ &= Q\left(\frac{k(1+\vartheta)}{\sqrt{2k(1+2\vartheta)}}\right).\end{aligned} \tag{A.86}$$

Maximum value for $x > 0$

The maximisation of $\epsilon_{CLT}(k, k\vartheta, x)$ is more difficult when $x > 0$. As a first step, the critical points of $\epsilon_{CLT}(k, k\vartheta, x)$ can be determined using the first derivative test [68, Section 1.4 (iii)], that is

$$\frac{d}{dx}\left[\epsilon_{CLT}(k, k\vartheta, x)\right]\Big|_{x=x_0} = 0. \tag{A.87}$$

In a similar fashion to (A.12), it is not difficult to show that (A.87) is satisfied by

$$e^{-\frac{(x_0 - 2\nu(1+\vartheta))^2}{8\nu(1+2\vartheta)}} = \sqrt{2\pi\nu(1+2\vartheta)}e^{-\vartheta\nu - \frac{x_0}{2}}\left(\frac{x_0}{2\vartheta\nu}\right)^{\frac{\nu-1}{2}} I_{\nu-1}\left(\sqrt{2\vartheta\nu x_0}\right), \tag{A.88}$$

where, once again, $\nu = \frac{k}{2}$ for convenience.

While (A.88) precisely describes the condition necessary to maximise $\epsilon_{CLT}(2\nu, 2\vartheta\nu, x)$ when $x > 0$, determining the exact value of x_0 required is complicated due to the presence of the modified Bessel function of the first kind. However, it can be shown

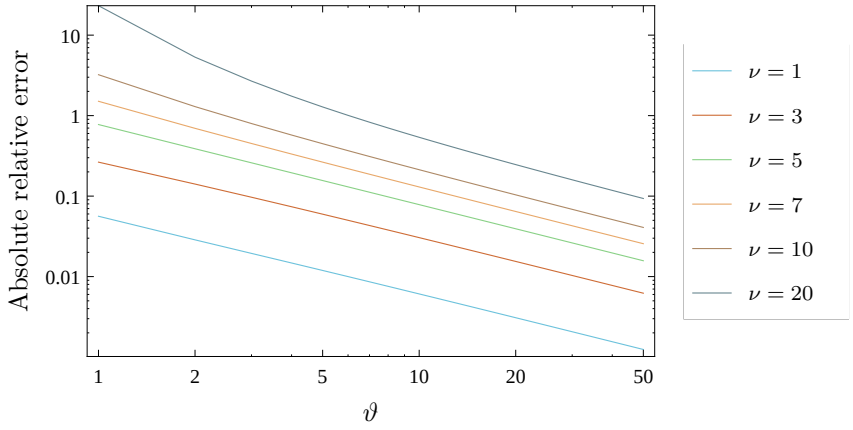

Figure A.7: A plot of the absolute relative error resulting from the use of the approximation given in (A.90).

that $x_0 \approx 2\nu(1+\vartheta)$ as ϑ becomes large. To see this, consider the approximation

$$I_n(z) \approx \tilde{I}_n(z) = \frac{e^z}{\sqrt{2\pi z}}, \tag{A.89}$$

which is valid when z becomes large relative to n [68, Equation 10.30.4]. Letting $n = \nu - 1$ and $z = 2\nu\sqrt{\vartheta(1+\vartheta)}$ in (A.89) results in the further approximation

$$I_{\nu-1}\left(2\nu\sqrt{\vartheta(1+\vartheta)}\right) \approx \frac{e^{2\nu\sqrt{\vartheta(1+\vartheta)}}}{\sqrt{4\pi\nu\sqrt{\vartheta(1+\vartheta)}}}, \tag{A.90}$$

as ϑ becomes large relative to ν. Figure A.7 illustrates the relative error resulting from the use of the approximation in (A.90) for various values of ν and ϑ.

Letting $x_0 = 2\nu(1+\vartheta)$ in (A.88) gives the condition

$$1 = \sqrt{2\pi\nu(1+2\vartheta)}e^{-\nu(1+2\vartheta)}\left(\frac{1+\vartheta}{\vartheta}\right)^{\frac{\nu-1}{2}} I_{\nu-1}\left(2\nu\sqrt{\vartheta(1+\vartheta)}\right). \tag{A.91}$$

The approximation in (A.90) can be applied to simplify this condition to

$$\begin{aligned} 1 = &\left(\frac{1+4\vartheta+4\vartheta^2}{4\vartheta+4\vartheta^2}\right)^{\frac{1}{4}}\left(\frac{1+\vartheta}{\vartheta}\right)^{\frac{\nu-1}{2}} \\ &\times \exp\left[-\nu\sqrt{4\vartheta+4\vartheta^2}\left(\sqrt{\frac{1+4\vartheta+4\vartheta^2}{4\vartheta+4\vartheta^2}}-1\right)\right], \end{aligned} \tag{A.92}$$

which holds approximately, for large values of ϑ, as

$$\lim_{\vartheta\to\infty}\left(\frac{1+4\vartheta+4\vartheta^2}{4\vartheta+4\vartheta^2}\right)=1, \tag{A.93}$$

$$\lim_{\vartheta\to\infty}\left(\frac{1+\vartheta}{\vartheta}\right)=1. \tag{A.94}$$

Consequently, it can be concluded that $x_0 \approx 2\nu(1+\vartheta)$ as ϑ becomes large. The second derivative test can be applied to verify that this value of x_0 produces a maximum, and so

$$\max_{x>0}|\epsilon_{CLT}(k,k\vartheta,x)| \triangleq \epsilon_{\infty,\vartheta}(k) \approx Q_\nu\left(\sqrt{k\vartheta},\sqrt{k(1+\vartheta)}\right)-\frac{1}{2}, \tag{A.95}$$

as ϑ becomes large and so, using (A.84) and (A.86), it can be shown that

$$\max|\epsilon_{CLT}(k,k\vartheta,x)| = \max\left(Q\left(\frac{k(1+\vartheta)}{\sqrt{2k(1+2\vartheta)}}\right),\epsilon_{\infty,\vartheta}(k)\right). \qquad \square \tag{A.96}$$

Notation

$\cap$	The set intersection operator.
$\cup$	The set union operator.
$\square$	*quod erat demonstrandum* (QED).
$\mathbb{E}[X]$	The expected value of the random variable X.
$\mathbb{N}^+$	The set of positive integers.
$P[A]$	The probability of the event A occurring.
$P[A \mid B]$	The probability of the event A occurring, given that the event B has already occurred.
$\mathbb{R}^+$	The set of positive real numbers.
$\mathbb{R}_0^+$	The set of non-negative real numbers.
$\mathrm{Var}[X]$	The variance of the random variable X.

Abbreviations

AWGN additive white Gaussian noise

BPSK binary phase shift keying

CDF cumulative distribution function

DSA dynamic spectrum access

DTV digital television

EGC equal gain combiner

ENP estimated noise power

ERG European Regulators Group

FCC Federal Communications Commission

FFT fast Fourier transform

FPGA field programmable gate array

GPS Global Positioning System

IEEE Institute of Electrical and Electronics Engineers

i.i.d. independent and identically distributed

i.n.d. independent and non-identically distributed

IRCSET The Irish Research Council for Science, Education and Technology

LOS line of sight

LRT likelihood ratio test

MRC maximal ratio combiner

ND no diversity

NTIA National Telecommunications and Information Administration

OFDM orthogonal frequency-division multiplexing

PDF probability density function

PMF	probability mass function
PWM	pulse width modulation
QED	quod erat demonstrandum
QoS	quality of service
QPSK	quadrature phase shift keying
RF	radio frequency
ROC	receiver operating characteristic
SLC	square law combiner
SNR	signal to noise ratio
UWB	ultra wideband
WRAN	wireless regional area network

Bibliography

[1] Federal Communications Commission. FCC spectrum inventory table. Technical report, 1996. URL http://www.fcc.gov/oet/info/database/spectrum/spinvtbl.pdf.

[2] Federal Communications Commission. FCC adopts rules for unlicensed use of television white spaces. Technical report, November 2008. URL http://hraunfoss.fcc.gov/edocs_public/attachmatch/FCC-08-260A1.pdf.

[3] National Telecommunications and Information Administration. NTIA frequency allocation chart. Technical report, 2003. URL http://www.ntia.doc.gov/osmhome/allochrt.pdf.

[4] European Regulators Group. ERG complementary report on possible bottlenecks in mobile access. Technical report, 2006. URL http://www.irg.eu/streaming/erg_06_45_b_complementary_report_on_possible_bottlenecks_in_mobile_access.pdf?contentId=543425&field=ATTACHED_FILE.

[5] M.A. McHenry, D. McCloskey, D. Roberson, and J.T. MacDonald. Spectrum occupancy measurements: Chicago, Illinois. Technical report, Shared Spectrum Company, December 2005. URL http://www.sharedspectrum.com/wp-content/uploads/NSF_Chicago_2005-11_measurements_v12.pdf.

[6] Tugba Erpek, Karl Steadman, and David Jones. Spectrum occupancy measurements: Dublin, Ireland. Technical report, Shared Spectrum Company, November 2007. URL http://www.sharedspectrum.com/wp-content/uploads/Ireland_Spectrum_Occupancy_Measurements_v2.pdf.

[7] M.A. McHenry and K. Steadman. Spectrum occupancy measurements: Riverbend Park, Great Falls, Virginia. Technical Report 1, Shared Spectrum Company, August 2005. URL http://www.sharedspectrum.com/wp-content/uploads/1_NSF_Riverbend_Park_Report.pdf.

[8] H. Harada, Y. Alemseged, S. Filin, M. Riegel, M. Gundlach, O. Holland, B. Bochow, M. Ariyoshi, and L. Grande. IEEE dynamic spectrum access networks standards committee. *IEEE Communications Magazine*, 51(3):104–111, 2013.

ISSN 0163-6804. doi: 10.1109/MCOM.2013.6476873. URL `http://ieeexplore.ieee.org/xpl/articleDetails.jsp?arnumber=6476873`.

[9] T. Yücek and H. Arslan. A survey of spectrum sensing algorithms for cognitive radio applications. *IEEE Communications Surveys & Tutorials*, 11(1):116–130, 2009. ISSN 1553-877X. doi: 10.1109/SURV.2009.090109. URL `http://ieeexplore.ieee.org/xpls/abs_all.jsp?arnumber=4796930`.

[10] H. Tang. Some physical layer issues of wide-band cognitive radio systems. In *Proceedings of the First IEEE International Symposium on New Frontiers in Dynamic Spectrum Access Networks (DySPAN)*, pages 151–159, Baltimore, MD, USA, 2005. doi: 10.1109/DYSPAN.2005.1542630. URL `http://ieeexplore.ieee.org/xpls/abs_all.jsp?arnumber=1542630`.

[11] F.F. Digham, M.S. Alouini, and M.K. Simon. On the energy detection of unknown signals over fading channels. In *Proceedings of the IEEE International Conference on Communications (ICC)*, volume 5, pages 3575–3579. IEEE, May 2003. ISBN 0-7803-7802-4. doi: 10.1109/ICC.2003.1204119. URL `http://ieeexplore.ieee.org/xpls/abs_all.jsp?arnumber=1204119`.

[12] Yonghong Zeng and Ying-Chang Liang. Eigenvalue-based spectrum sensing algorithms for cognitive radio. *IEEE Transactions on Communications*, 57(6):1784–1793, 2009. ISSN 0090-6778. doi: 10.1109/TCOMM.2009.06.070402. URL `http://ieeexplore.ieee.org/xpl/articleDetails.jsp?arnumber=5089517`.

[13] H. Urkowitz. Energy detection of unknown deterministic signals. *Proceedings of the IEEE*, 55(4):523–531, April 1967. ISSN 0018-9219. doi: 10.1109/PROC.1967.5573. URL `http://ieeexplore.ieee.org/xpls/abs_all.jsp?arnumber=1447503`.

[14] Marvin K. Simon and Mohamed-Slim Alouini. *Digital communication over fading channels*. John Wiley & Sons, 2nd edition, 2005. ISBN 9780471649533.

[15] D.G. Brennan. Linear diversity combining techniques. *Proceedings of the IEEE*, 91(2):331–356, February 2003. ISSN 0018-9219. doi: 10.1109/JPROC.2002.808163. URL `http://ieeexplore.ieee.org/xpls/abs_all.jsp?arnumber=1182067`.

[16] V.A. Aalo. Performance of maximal-ratio diversity systems in a correlated Nakagami-fading environment. *IEEE Transactions on Communications*, 43(8):2360–2369, August 1995. ISSN 0090-6778. doi: 10.1109/26.403769. URL `http://ieeexplore.ieee.org/xpl/articleDetails.jsp?arnumber=403769`.

[17] S. Chaudhari, J. Lunden, V. Koivunen, and H.V. Poor. Cooperative sensing with imperfect reporting channels: Hard decisions or soft decisions? *IEEE Transactions on Signal Processing*, 60(1):18–28, January 2012. ISSN 1053-

587X. doi: 10.1109/TSP.2011.2170978. URL `http://ieeexplore.ieee.org/xpls/abs_all.jsp?arnumber=6036191`.

[18] Donagh Horgan and Colin C. Murphy. On the convergence of the chi square and noncentral chi square distributions to the normal distribution. *IEEE Communications Letters*, 17(12):2233–2236, December 2013. ISSN 1089-7798. doi: 10.1109/LCOMM.2013.111113.131879. URL `http://ieeexplore.ieee.org/xpl/articleDetails.jsp?arnumber=6663749`.

[19] Donagh Horgan and Colin C. Murphy. Fast and accurate approximations for the analysis of energy detection in Nakagami-m channels. *IEEE Communications Letters*, 17(1):83–86, January 2013. ISSN 1089-7798. doi: 10.1109/LCOMM.2012.111612.121964. URL `http://ieeexplore.ieee.org/xpls/abs_all.jsp?arnumber=6355939`.

[20] Donagh Horgan and Colin C. Murphy. Implementation issues for optimized hard decision energy detector-based cooperative spectrum sensing. In *Proceedings of the 4th International Conference on Cognitive Radio and Advanced Spectrum Management (CogART)*, Barcelona, Spain, 2011. ACM. ISBN 978-1-4503-0912-7. doi: 10.1145/2093256.2093264. URL `http://doi.acm.org/10.1145/2093256.2093264`.

[21] Donagh Horgan and Colin C. Murphy. Performance limits of cooperative energy detection in fading environments. In *Proceedings of the 4th International Conference on Cognitive Radio and Advanced Spectrum Management (CogART)*, Barcelona, Spain, 2011. ACM. ISBN 978-1-4503-0912-7. doi: 10.1145/2093256.2093274. URL `http://doi.acm.org/10.1145/2093256.2093274`.

[22] Donagh Horgan and Colin C. Murphy. Voting rule optimisation for double threshold energy detector-based cognitive radio networks. In *Proceedings of the 4th International Conference on Signal Processing and Communication Systems (ICSPCS)*, page 1–8, Gold Coast, Australia, 2010. doi: 10.1109/ICSPCS.2010.5709679. URL `http://ieeexplore.ieee.org/xpls/abs_all.jsp?arnumber=5709679`.

[23] Arturo Rosenblueth and Norbert Wiener. The role of models in science. *Philosophy of Science*, 12(4):316–321, October 1945. ISSN 0031-8248. doi: 10.2307/184253. URL `http://www.jstor.org/stable/184253`.

[24] A. Leon-Garcia. *Probability, statistics, and random processes for electrical engineering*. Pearson/Prentice Hall, 3rd edition, 2008. ISBN 9780131471221.

[25] Simon S. Haykin. *Adaptive filter theory*. Prentice Hall, 3rd edition, 1996. ISBN 9780133227604.

[26] John G. Proakis and Masoud Salehi. *Digital Communications*. McGraw-Hill Higher Education, New York, January 2008. ISBN 9780071263788.

[27] W.A. Gardner. Signal interception: a unifying theoretical framework for feature detection. *IEEE Transactions on Communications*, 36(8):897–906, August 1988. ISSN 0090-6778. doi: 10.1109/26.3769. URL `http://ieeexplore.ieee.org/xpls/abs_all.jsp?arnumber=3769`.

[28] D. Cabric, S.M. Mishra, and R.W. Brodersen. Implementation issues in spectrum sensing for cognitive radios. In *Conference Record of the Thirty-Eighth Asilomar Conference on Signals, Systems and Computers*, volume 1, pages 772–776. IEEE, November 2004. ISBN 0-7803-8622-1. doi: 10.1109/ACSSC.2004.1399240. URL `http://ieeexplore.ieee.org/xpls/abs_all.jsp?arnumber=1399240`.

[29] Mahsa Derakhshani, Tho Le-Ngoc, and Masoumeh Nasiri-Kenari. Efficient cooperative cyclostationary spectrum sensing in cognitive radios at low SNR regimes. *IEEE Transactions on Wireless Communications*, 10(11):3754–3764, November 2011. ISSN 1536-1276. doi: 10.1109/TWC.2011.080611.101580. URL `http://ieeexplore.ieee.org/xpls/abs_all.jsp?arnumber=6021438`.

[30] V. Turunen, M. Kosunen, A. Huttunen, S. Kallioinen, P. Ikonen, A. Parssinen, and J. Ryynanen. Implementation of cyclostationary feature detector for cognitive radios. In *Proceedings of the 4^{th} International Conference on Cognitive Radio Oriented Wireless Networks and Communications (CROWNCOM)*, page 1–4, Hanover, Germany, 2009. doi: 10.1109/CROWNCOM.2009.5188993. URL `http://ieeexplore.ieee.org/xpls/abs_all.jsp?arnumber=5188993`.

[31] A. Fehske, J. Gaeddert, and J.H. Reed. A new approach to signal classification using spectral correlation and neural networks. In *Proceedings of the First IEEE International Symposium on New Frontiers in Dynamic Spectrum Access Networks (DySPAN)*, page 144–150, Baltimore, MD, USA, 2005. doi: 10.1109/DYSPAN.2005.1542629. URL `http://ieeexplore.ieee.org/xpls/abs_all.jsp?arnumber=1542629`.

[32] P.D. Sutton, J. Lotze, K.E. Nolan, and L.E. Doyle. Cyclostationary signature detection in multipath Rayleigh fading environments. In *Proceedings of the 2^{nd} International Conference on Cognitive Radio Oriented Wireless Networks and Communications (CROWNCOM)*, pages 408–413, Orlando, FL, USA, August 2007. doi: 10.1109/CROWNCOM.2007.4549833. URL `http://ieeexplore.ieee.org/xpls/abs_all.jsp?arnumber=4549833`.

[33] S. Haykin. Cognitive radio: brain-empowered wireless communications. *IEEE Journal on Selected Areas in Communications*, 23(2):201–220, 2005. ISSN 0733-8716. doi: 10.1109/JSAC.2004.839380. URL `http://ieeexplore.ieee.org/xpls/abs_all.jsp?arnumber=1391031`.

[34] Zhi Tian and G.B. Giannakis. A wavelet approach to wideband spectrum sensing for cognitive radios. In *Proceedings of the 1st International Conference on Cognitive Radio Oriented Wireless Networks and Communications (CROWNCOM)*, pages 1–5, Mykonos Island, June 2006. doi: 10.1109/CROWNCOM.2006.363459. URL `http://ieeexplore.ieee.org/xpls/abs_all.jsp?arnumber=4211139`.

[35] Z. Chair and P.K. Varshney. Optimal data fusion in multiple sensor detection systems. *IEEE Transactions on Aerospace and Electronic Systems*, AES-22(1): 98–101, January 1986. ISSN 0018-9251. doi: 10.1109/TAES.1986.310699. URL `http://ieeexplore.ieee.org/xpls/abs_all.jsp?arnumber=4104179`.

[36] Chunhua Sun, Wei Zhang, and K.B. Letaief. Cooperative spectrum sensing for cognitive radios under bandwidth constraints. In *Proceedings of the Wireless Communications and Networking Conference (WCNC)*, pages 1–5, Kowloon, 2007. ISBN 1525-3511. doi: 10.1109/WCNC.2007.6. URL `http://ieeexplore.ieee.org/xpls/abs_all.jsp?arnumber=4224251`.

[37] E. Drakopoulos and C.C. Lee. Optimum multisensor fusion of correlated local decisions. *IEEE Transactions on Aerospace and Electronic Systems*, 27(4):593–606, July 1991. ISSN 0018-9251. doi: 10.1109/7.85032. URL `http://ieeexplore.ieee.org/xpls/abs_all.jsp?arnumber=85032`.

[38] G.L. Grisdale, J.G. Morris, and D.S. Palmer. Fading of long-distance radio signals and a comparison of space- and polarization-diversity reception in the 6-18Mc/s range. *Proceedings of the IEE - Part B: Radio and Electronic Engineering*, 104 (13):39–51, 1957. doi: 10.1049/pi-b-1.1957.0112. URL `http://ieeexplore.ieee.org/xpls/abs_all.jsp?arnumber=5243398`.

[39] A. Ghasemi and E.S. Sousa. Asymptotic performance of collaborative spectrum sensing under correlated log-normal shadowing. *IEEE Communications Letters*, 11(1):34–36, January 2007. ISSN 1089-7798. doi: 10.1109/LCOMM.2007.060662. URL `http://ieeexplore.ieee.org/xpls/abs_all.jsp?arnumber=4114218`.

[40] M. Gudmundson. Correlation model for shadow fading in mobile radio systems. *Electronics Letters*, 27(23):2145–2146, November 1991. ISSN 0013-5194. doi: 10.1049/el:19911328. URL `http://digital-library.theiet.org/content/journals/10.1049/el_19911328`.

[41] Gordon L. Stüber. *Principles of Mobile Communication*. Springer, 3rd edition, September 2011. ISBN 9781461403630.

[42] Jun Ma, Guodong Zhao, and Ye Li. Soft combination and detection for cooperative spectrum sensing in cognitive radio networks. *IEEE Transactions on Wireless Communications*, 7(11):4502–4507, 2008. doi: 10.1109/T-WC.2008.070941. URL `http://ieeexplore.ieee.org/xpls/abs_all.jsp?arnumber=4686831`.

[43] A. Mariani, A. Giorgetti, and M. Chiani. Effects of noise power estimation on energy detection for cognitive radio applications. *IEEE Transactions on Communications*, 59(12):3410–3420, December 2011. ISSN 0090-6778. doi: 10.1109/TCOMM.2011.102011.100708. URL `http://ieeexplore.ieee.org/xpls/abs_all.jsp?arnumber=6068200`.

[44] A. Sonnenschein and P.M. Fishman. Limitations on the detectability of spread-spectrum signals. In *Proceedings of the IEEE Military Communications Conference (MILCOM)*, pages 364–369, Boston, MA, USA, 1989. doi: 10.1109/MILCOM.1989.103955. URL `http://ieeexplore.ieee.org/xpls/abs_all.jsp?arnumber=103955`.

[45] A. Sonnenschein and P.M. Fishman. Radiometric detection of spread-spectrum signals in noise of uncertain power. *IEEE Transactions on Aerospace and Electronic Systems*, 28(3):654–660, 1992. doi: 10.1109/7.256287. URL `http://ieeexplore.ieee.org/xpls/abs_all.jsp?arnumber=256287`.

[46] R. Tandra and A. Sahai. SNR walls for signal detection. *IEEE Journal of Selected Topics in Signal Processing*, 2(1):4–17, 2008. ISSN 1932-4553. doi: 10.1109/JSTSP.2007.914879. URL `http://ieeexplore.ieee.org/xpls/abs_all.jsp?arnumber=4453895`.

[47] R. Tandra and A. Sahai. Noise calibration, delay coherence and SNR walls for signal detection. In *Proceedings of the 3rd IEEE Symposium on New Frontiers in Dynamic Spectrum Access Networks (DySPAN)*, pages 1–11, Chicago, IL, USA, 2008. doi: 10.1109/DYSPAN.2008.42. URL `http://ieeexplore.ieee.org/xpls/abs_all.jsp?arnumber=4658253`.

[48] D.A. Hill and E.B. Felstead. Laboratory performance of spread spectrum detectors. *IEE Proceedings - Communications*, 142(4):243–249, 1995. ISSN 1350-2425. doi: 10.1049/ip-com:19952059. URL `http://digital-library.theiet.org/content/journals/10.1049/ip-com_19952059`.

[49] Milton Abramowitz and Irene A. Stegun. *Handbook of mathematical functions with formulas, graphs, and mathematical tables*. U.S. Government Print Office, 10th edition, 1972. ISBN 9780318117300.

[50] F.F. Digham, M.S. Alouini, and M.K. Simon. On the energy detection of unknown signals over fading channels. *IEEE Transactions on Communications*, 55(1):21–24, January 2007. ISSN 0090-6778. doi: 10.1109/TCOMM.2006.887483. URL `http://ieeexplore.ieee.org/xpls/abs_all.jsp?arnumber=4063501`.

[51] A. Nuttall. Some integrals involving the Q_m function. *IEEE Transactions on Information Theory*, 21(1):95–96, January 1975. ISSN 0018-9448. doi: 10.1109/TIT.1975.1055327. URL `http://ieeexplore.ieee.org/xpls/abs_all.jsp?arnumber=1055327`.

[52] S.P. Herath, N. Rajatheva, and C. Tellambura. Unified approach for energy detection of unknown deterministic signal in cognitive radio over fading channels. In *Proceedings of the IEEE International Conference on Communications Workshops (ICC Workshops)*, pages 1–5, Dresden, Germany, June 2009. IEEE. ISBN 978-1-4244-3437-4. doi: 10.1109/ICCW.2009.5208031. URL `http://ieeexplore.ieee.org/xpls/abs_all.jsp?arnumber=5208031`.

[53] S.P. Herath, N. Rajatheva, and C. Tellambura. Energy detection of unknown signals in fading and diversity reception. *IEEE Transactions on Communications*, 59(9):2443–2453, September 2011. ISSN 0090-6778. doi: 10.1109/TCOMM.2011.071111.090349. URL `http://ieeexplore.ieee.org/xpls/abs_all.jsp?arnumber=5958751`.

[54] V.I. Kostylev. Energy detection of a signal with random amplitude. In *Proceedings of the IEEE International Conference on Communications (ICC)*, volume 3, pages 1606–1610. IEEE, 2002. ISBN 0-7803-7400-2. doi: 10.1109/ICC.2002.997120. URL `http://ieeexplore.ieee.org/xpls/abs_all.jsp?arnumber=997120`.

[55] S.P. Herath. *Spectrum sensing in cognitive radio - fading, diversity and user cooperation*. Masters thesis, Asian Institute of Technology, 2009. URL `http://www.ece.mcgill.ca/~hsanje/downloads/ThesisReport.pdf`.

[56] S.P. Herath and N. Rajatheva. Analysis of equal gain combining in energy detection for cognitive radio over Nakagami channels. In *Proceedings of the Global Telecommunications Conference (GLOBECOM)*, pages 1–5, New Orleans, LO, USA, November 2008. IEEE. ISBN 978-1-4244-2324-8. doi: 10.1109/GLOCOM.2008.ECP.570. URL `http://ieeexplore.ieee.org/xpls/abs_all.jsp?arnumber=4698345`.

[57] A. Annamalai, O. Olabiyi, S. Alam, O. Odejide, and D. Vaman. Unified analysis of energy detection of unknown signals over generalized fading channels. In *Proceedings of the 7th International Wireless Communications and Mobile Computing Conference (IWCMC)*, pages 636–641, Istanbul, July 2011. IEEE. ISBN 978-1-4244-9539-9. doi: 10.1109/IWCMC.2011.5982620. URL `http://ieeexplore.ieee.org/xpls/abs_all.jsp?arnumber=5982620`.

[58] O. Olabiyi and A. Annamalai. Further results on the performance of energy detector over generalized fading channels. In *Proceedings of the IEEE 22nd International Symposium on Personal Indoor and Mobile Radio Communications (PIMRC)*, pages 604–608, Toronto, ON, Canada, September 2011. doi: 10.1109/PIMRC.2011.6140033. URL `http://ieeexplore.ieee.org/xpls/abs_all.jsp?arnumber=6140033`.

[59] O. Olabiyi and A. Annamalai. Closed-form approximation of the energy detection

performance over generalized fading channels. In *Proceedings of the 14th ACM international conference on modeling, analysis and simulation of wireless and mobile systems (MSWiM)*, page 257–260, Miami Beach, FL, USA, 2011. ACM. ISBN 978-1-4503-0898-4. doi: 10.1145/2068897.2068942. URL `https://dl.acm.org/citation.cfm?id=2068942`.

[60] O. Olabiyi, S. Alam, O. Odejide, and A. Annamalai. Further results on the energy detection of unknown deterministic signals over generalized fading channel. In *Proceedings of the IEEE Global Telecommunications Conference Workshops (GLOBECOM Workshops)*, pages 908–912, Houston, TX, USA, December 2011. doi: 10.1109/GLOCOMW.2011.6162589. URL `http://ieeexplore.ieee.org/xpls/abs_all.jsp?arnumber=6162589`.

[61] Hongjian Sun, A. Nallanathan, Jing Jiang, and Cheng-Xiang Wang. Cooperative spectrum sensing with diversity reception in cognitive radios. In *Proceedings of the 6th International ICST Conference on Communications and Networking in China (CHINACOM)*, pages 216–220, Harbin, August 2011. doi: 10.1109/ChinaCom.2011.6158151. URL `http://ieeexplore.ieee.org/xpls/abs_all.jsp?arnumber=6158151`.

[62] Hongjian Sun. *Collaborative spectrum sensing in cognitive radio networks*. PhD thesis, University of Edinburgh, 2011. URL `http://www.era.lib.ed.ac.uk/bitstream/1842/4879/1/Sun2011.pdf`.

[63] V.R.S. Banjade, N. Rajatheva, and C. Tellambura. Performance analysis of energy detection with multiple correlated antenna cognitive radio in Nakagami-m fading. *IEEE Communications Letters*, 16(4):502–505, 2012. ISSN 1089-7798. doi: 10.1109/LCOMM.2012.020212.112541. URL `http://ieeexplore.ieee.org/xpl/articleDetails.jsp?arnumber=6150658`.

[64] Amir Ghasemi and Elvino S. Sousa. Spectrum sensing in cognitive radio networks: the cooperation-processing tradeoff. *Wireless Communications and Mobile Computing*, 7(9):1049–1060, 2007. ISSN 1530-8677. doi: 10.1002/wcm.480. URL `http://onlinelibrary.wiley.com/doi/10.1002/wcm.480/abstract`.

[65] Miguel López-Benítez and Fernando Casadevall. Versatile, accurate, and analytically tractable approximation for the Gaussian Q-function. *IEEE Transactions on Communications*, 59(4):917–922, April 2011. ISSN 0090-6778. doi: 10.1109/TCOMM.2011.012711.100105. URL `http://ieeexplore.ieee.org/xpls/abs_all.jsp?arnumber=5706433`.

[66] S. Atapattu, C. Tellambura, and Hai Jiang. Spectrum sensing in low SNR: diversity combining and cooperative communications. In *Proceedings of the 6th IEEE International Conference on Industrial and Information Systems (ICIIS)*,

pages 13–17, Kandy, 2011. doi: 10.1109/ICIINFS.2011.6038032. URL http://ieeexplore.ieee.org/xpls/abs_all.jsp?arnumber=6038032.

[67] S. Atapattu, C. Tellambura, and Hai Jiang. Spectrum sensing via energy detector in low SNR. In *Proceedings of the IEEE International Conference on Communications (ICC)*, pages 1–5, Kyoto, 2011. doi: 10.1109/icc.2011.5963316. URL http://ieeexplore.ieee.org/xpls/abs_all.jsp?arnumber=5963316.

[68] Frank W.J. Olver, Daniel W. Lozier, Ronald F. Boisvert, and Charles W. Clark. *NIST Handbook of Mathematical Functions*. Cambridge University Press, May 2010. ISBN 9780521140638.

[69] I.S. Gradshteyn and I.M. Ryzhik. *Table of integrals, series and products*. Academic Press, 7th edition, February 2007. ISBN 9780123736376.

[70] Saralees Nadarajah. A review of results on sums of random variables. *Acta Applicandae Mathematicae*, 103(2):131–140, 2008. ISSN 0167-8019. doi: 10.1007/s10440-008-9224-4. URL http://link.springer.com/article/10.1007/s10440-008-9224-4.

[71] J. Hu and N.C. Beaulieu. Accurate simple closed-form approximations to Rayleigh sum distributions and densities. *IEEE Communications Letters*, 9(2):109–111, 2005. ISSN 1089-7798. doi: 10.1109/LCOMM.2005.02003. URL http://ieeexplore.ieee.org/xpl/articleDetails.jsp?arnumber=1388722.

[72] M. Nakagami. The m-distribution - a general formula of intensity distribution of rapid fading. *Statistical Method of Radio Propagation*, pages 3–36, 1960.

[73] J.A. López-Salcedo. Simple closed-form approximation to Ricean sum distributions. *IEEE Signal Processing Letters*, 16(3):153–155, March 2009. ISSN 1070-9908. doi: 10.1109/LSP.2008.2012223. URL http://ieeexplore.ieee.org/xpls/abs_all.jsp?arnumber=4781943.

[74] P. Dharmawansa, N. Rajatheva, and K. Ahmed. On the distribution of the sum of Nakagami-m random variables. *IEEE Transactions on Communications*, 55(7):1407–1416, July 2007. ISSN 0090-6778. doi: 10.1109/TCOMM.2007.900621. URL http://ieeexplore.ieee.org/xpl/articleDetails.jsp?arnumber=4273691.

[75] M.A. Rahman and H. Harada. New exact closed-form PDF of the sum of Nakagami-m random variables with applications. *IEEE Transactions on Communications*, 59(2):395–401, February 2011. ISSN 0090-6778. doi: 10.1109/TCOMM.2010.112310.090212. URL http://ieeexplore.ieee.org/xpls/abs_all.jsp?arnumber=5654629.

[76] A.A. Abu-Dayya and N.C. Beaulieu. Microdiversity on Rician fading channels. *IEEE Transactions on Communications*, 42(6):2258–2267, 1994. ISSN 0090-6778.

doi: 10.1109/26.293677. URL http://ieeexplore.ieee.org/xpls/abs_all.jsp?arnumber=293677.

[77] Mark H. Holmes. *Introduction to Numerical Methods in Differential Equations*. Springer, 2007. ISBN 9780387308913.

[78] Mantsika Matooane. Parallel systems in symbolic and algebraic computation. Technical report, University of Cambridge, University of Cambridge Computer Laboratory, Cambridge, United Kingdom, June 2002. URL http://www.cl.cam.ac.uk/techreports/UCAM-CL-TR-537.pdf.

[79] S. Shellhammer. Spectrum sensing in IEEE 802.22. In *Proceedings of the IAPR Workshop on Cognitive Information Processing*, Santorini, Greece, June 2008. EURASIP. URL http://www.eurasip.org/Proceedings/Ext/CIP2008/papers/1569094657.pdf.

[80] Steve Shellhammer, Victor Tawil, Gerald Chouinard, Max Muterspaugh, and Monisha Ghosh. Spectrum sensing simulation model, IEEE 802.22-06/0028r10, September 2006. URL http://www.ieee802.org/22/Meeting_documents/2006_Sept/22-06-0028-10-0000-Spectrum-Sensing-Simulation-Model.doc.

[81] Serge Winitzki. Computing the incomplete gamma function to arbitrary precision. In *Computational Science and Its Applications*, volume 2667 of *Lecture Notes in Computer Science*, pages 968–968. Springer Berlin / Heidelberg, 2003. ISBN 978-3-540-40155-1. URL http://link.springer.com/chapter/10.1007/3-540-44839-X_83.

[82] P. Cantrell and A. Ojha. Comparison of generalized Q-function algorithms. *IEEE Transactions on Information Theory*, 33(4):591–596, 1987. ISSN 0018-9448. doi: 10.1109/TIT.1987.1057323. URL http://ieeexplore.ieee.org/xpl/articleDetails.jsp?arnumber=1057323.

[83] D.A. Shnidman. The calculation of the probability of detection and the generalized Marcum Q-function. *IEEE Transactions on Information Theory*, 35(2):389–400, 1989. ISSN 0018-9448. doi: 10.1109/18.32133. URL http://ieeexplore.ieee.org/xpl/articleDetails.jsp?arnumber=32133.

[84] C.W. Helstrom. Computing the generalized Marcum Q-function. *IEEE Transactions on Information Theory*, 38(4):1422–1428, 1992. ISSN 0018-9448. doi: 10.1109/18.144731. URL http://ieeexplore.ieee.org/xpl/articleDetails.jsp?arnumber=144731.

[85] Yin Sun, Á. Baricz, and Shidong Zhou. On the monotonicity, log-concavity, and tight bounds of the generalized Marcum and Nuttall Q-functions. *IEEE Transactions on Information Theory*, 56(3):1166–1186, 2010. ISSN 0018-9448.

doi: 10.1109/TIT.2009.2039048. URL http://ieeexplore.ieee.org/xpl/articleDetails.jsp?arnumber=5429099.

[86] Andrew C. Berry. The accuracy of the Gaussian approximation to the sum of independent variates. *Transactions of the American Mathematical Society*, 49(1): 122–136, January 1941. ISSN 0002-9947. doi: 10.2307/1990053. URL http://www.jstor.org/stable/1990053.

[87] C.G. Esseen. A moment inequality with an application to the central limit theorem. *Skandinavisk Aktuarie Tidskrift*, (39):160–170, 1956.

[88] Victor Korolev and Irina Shevtsova. An improvement of the Berry-Esseen inequality with applications to Poisson and mixed Poisson random sums. *Scandinavian Actuarial Journal*, (2):81–105, 2012. ISSN 0346-1238. doi: 10.1080/03461238.2010.485370. URL http://www.tandfonline.com/doi/abs/10.1080/03461238.2010.485370.

[89] S.M. Mishra, A. Sahai, and R.W. Brodersen. Cooperative sensing among cognitive radios. In *Proceedings of the IEEE International Conference on Communications (ICC)*, volume 4, pages 1658–1663, Istanbul, Turkey, June 2006. IEEE. ISBN 1-4244-0355-3. doi: 10.1109/ICC.2006.254957. URL http://ieeexplore.ieee.org/xpl/articleDetails.jsp?arnumber=4024390.

[90] Jun Ma and Ye Li. Soft combination and detection for cooperative spectrum sensing in cognitive radio networks. In *Proceedings of the IEEE Global Telecommunications Conference (GLOBECOM)*, pages 3139–3143, Washington, DC, USA, 2007. URL http://ieeexplore.ieee.org/xpl/articleDetails.jsp?arnumber=4411504.

[91] Zhi Quan, Shuguang Cui, and A.H. Sayed. Optimal linear cooperation for spectrum sensing in cognitive radio networks. *IEEE Journal of Selected Topics in Signal Processing*, 2(1):28–40, 2008. ISSN 1932-4553. doi: 10.1109/JSTSP.2007.914882. URL http://ieeexplore.ieee.org/xpl/articleDetails.jsp?arnumber=4453893.

[92] Wei Lin and Qinyu Zhang. A design of energy detector in cognitive radio under noise uncertainty. In *Proceedings of the 11th IEEE Singapore International Conference on Communication Systems (ICCS)*, pages 213–217, Guangzhou, 2008. URL http://ieeexplore.ieee.org/xpl/articleDetails.jsp?arnumber=4737174.

[93] Sungtae Kim, Jemin Lee, Hano Wang, and Daesik Hong. Sensing performance of energy detector with correlated multiple antennas. *IEEE Signal Processing Letters*, 16(8):671–674, 2009. ISSN 1070-9908. doi: 10.1109/LSP.2009.2021381. URL http://ieeexplore.ieee.org/xpl/articleDetails.jsp?arnumber=4838820.

[94] Gui-Cai Yu, Yu-Bin Shao, Hua Long, and Guang-Xin Yue. Dynamic threshold based spectrum detection in cognitive radio systems. In *Proceedings of the 5th International Conference on Wireless Communications, Networking and Mobile Computing (WiCom)*, pages 1–4, Beijing, 2009. URL `http://ieeexplore.ieee.org/xpl/articleDetails.jsp?arnumber=5301508`.

[95] Miguel López-Benítez, Fernando Casadevall, and Corrado Martella. Performance of spectrum sensing for cognitive radio based on field measurements of various radio technologies. In *Proceedings of the European Wireless Conference*, pages 969–977, Lucca, 2010. doi: 10.1109/EW.2010.5483510. URL `http://ieeexplore.ieee.org/xpl/articleDetails.jsp?arnumber=5483510`.

[96] Miguel López-Benítez. *Spectrum Usage Models for the Analysis, Design and Simulation of Cognitive Radio Networks*. PhD thesis, Universitat Politècnica de Catalunya, Barcelona, May 2011. URL `http://www.lopezbenitez.es/thesis/PhDThesis_LopezBenitez.pdf`.

[97] Miguel López-Benítez and Fernando Casadevall. Improved energy detection spectrum sensing for cognitive radio. *IET Communications*, 6(8):785–796, 2012. ISSN 1751-8628. doi: 10.1049/iet-com.2010.0571. URL `http://ieeexplore.ieee.org/lpdocs/epic03/wrapper.htm?arnumber=6231121`.

[98] Amir Ghasemi and Elvino S. Sousa. Opportunistic spectrum access in fading channels through collaborative sensing. *Journal of Communications*, 2(2), March 2007. ISSN 1796-2021. doi: 10.4304/jcm.2.2.71-82. URL `http://www.ojs.academypublisher.com/index.php/jcm/article/viewArticle/02027182`.

[99] J.M. Borwein and P.B. Borwein. On the complexity of familiar functions and numbers. *SIAM Review*, 30(4):589–601, December 1988. ISSN 0036-1445. URL `http://epubs.siam.org/doi/abs/10.1137/1030134`.

[100] George E.P. Box and Norman Richard Draper. *Empirical model-building and response surfaces*. Wiley, January 1987. ISBN 9780471810339.

[101] G.H. Hardy, J.E. Littlewood, and G. Pólya. *Inequalities*. Cambridge University Press, 1934.

[102] Marvin K. Simon. *Probability Distributions Involving Gaussian Random Variables: A Handbook for Engineers and Scientists*. Springer, 2006. ISBN 9780387476940.

[103] Miguel López-Benítez and Fernando Casadevall. Signal uncertainty in spectrum sensing for cognitive radio. *IEEE Transactions on Communications*, 61(4):1231–1241, 2013. ISSN 0090-6778. doi: 10.1109/TCOMM.2013.021413.110807. URL `http://ieeexplore.ieee.org/xpl/articleDetails.jsp?arnumber=6466335`.

[104] I.S. Ansari, F. Yilmaz, Mohamed-Slim Alouini, and O. Kucur. On the sum

of gamma random variates with application to the performance of maximal ratio combining over Nakagami-m fading channels. In *Proceedings of the 13th IEEE International Workshop on Signal Processing Advances in Wireless Communications (SPAWC)*, pages 394–398, Cesme, 2012. doi: 10.1109/SPAWC.2012.6292935. URL `http://ieeexplore.ieee.org/xpl/articleDetails.jsp?arnumber=6292935`.

[105] P.G. Moschopoulos. The distribution of the sum of independent gamma random variables. *Annals of the Institute of Statistical Mathematics*, 37(1):541–544, 1985. URL `http://www.springerlink.com/index/pdf/10.1007/BF02481123`.

[106] Mohamed-Slim Alouini, A. Abdi, and Mostafa Kaveh. Sum of gamma variates and performance of wireless communication systems over Nakagami-fading channels. *IEEE Transactions on Vehicular Technology*, 50(6):1471–1480, 2001. ISSN 0018-9545. doi: 10.1109/25.966578. URL `http://ieeexplore.ieee.org/xpl/articleDetails.jsp?arnumber=966578`.

[107] M.D. Yacoub. The κ-μ distribution: a general fading distribution. In *Proceedings of the 54th IEEE Vehicular Technology Conference (VTC)*, volume 3, pages 1427–1431, Atlantic City, NJ, USA, 2001. doi: 10.1109/VTC.2001.956432. URL `http://ieeexplore.ieee.org/xpl/articleDetails.jsp?arnumber=956432`.

[108] M.D. Yacoub. The α-μ distribution: A physical fading model for the Stacy d istribution. *IEEE Transactions on Vehicular Technology*, 56(1):27–34, 2007. ISSN 0018-9545. doi: 10.1109/TVT.2006.883753. URL `http://ieeexplore.ieee.org/xpl/articleDetails.jsp?arnumber=4067122`.